EXPERIMENTAL AND COMPUTATIONAL INVESTIGATIONS FOR THE DEVELOPMENT OF INTRA-AORTIC BALLOON PUMP THERAPY

A thesis submitted to Brunel University

for the degree of

Doctor of Philosophy

By

Gianpaolo Bruti

Institute for Bioengineering, Brunel University, London

December 2015

Declaration of authenticity

I hereby declare that the work presented in this thesis is my own.

Gianpaolo Bruti.

Acknowledgement

The whole work presented in this thesis would not have been possible without the help of my supervisor, Dr. Ashraf Khir, who carefully guided me from the research proposal till the last days of my PhD, and gave me the opportunity of attending prestigious conferences in the UK and abroad.

Nonetheless other people contributed in the development of the work here described: Dr. Quan Long, Prof. Colin Clark and Dr. Christina Kolyva suggestions have been precious and contributed in the development of my skills in the field of bioengineering and science.

Important contributions also come from Prof. Kim Parker, who patiently listened to the presentation of my investigations when I was less experienced than I am now, and from Alessandra and Francesco, who friendly welcome the huge amount of my first questions on different medical, scientific and engineering issues involved with my project. Mrs Jenny Kume and Mr. Roger Paton have been not less important in providing me all the possible help in the organisation of my PhD and in technical issues.

I am also deeply grateful for the people who made this path more than a professional, but a personal experience. From the first days in this University till nowadays a high number of Italian friends enjoyed working days, nights out and dinners with me. Nevertheless all my friends from all over the world highly contributed in widening my mind and horizon, and I hope I will not loose them as time goes by and while I will probably be in another part of the globe.

A very special person, my wife Ning, deserves a particular mention for sharing with me big part of this experience, always pushing me to move up my limits and spending time with me especially during the most critical moments.

I want to finally thank my family, for supporting me in all my choices, particularly the one to move far from them. I hope the future will push us closer.

Abstract

Heart failure (HF) is a widely prevalent state in developing countries, especially among people over 65, with percentages up to 10% of the population in the US. In all developed countries the expenditure related to congestive heart failure consists of a high percentage of the total health care expenditure, reaching 60% in the UK (1991 [1]). One of the main strategies for dealing with HF is the use of cardiac assist devices. Among these the most widely used device is the Intra-Aortic balloon pump (IABP).

The IABP has as the main aims to increase coronary flow during inflation, and decrease end diastolic pressure and ventricular afterload during deflation. The device was introduced for the first time into clinical practice over 40 years ago, but open issues still remain with the performance of the device. In fact, both inflation and deflation effectiveness are compromised when the balloon operates at an angle to the horizontal, which is often the operating position of the device in intensive care units.

The main aim of the work described in this thesis is to investigate the IABP in order to improve the efficacy of this therapy, in terms of IAB design and IABP timing effectiveness. For this purpose the balloon was first filmed in an experimental set-up to visualize its wall-motion with a high speed camera. The results of this investigation were the input for the development of different designs of balloon, tested at horizontal and angled positions. Both, inflation and deflation effectiveness were augmented using different shaped balloons in an experimental set-up characterized by static pressure as well as in one characterized by physiological pressure waveform. The improved performance was associated to an improved clinical outcome on a PV diagram.

In addition different pumps and pump settings were studied in an experimental set-up, characterized by physiological aortic pressure waveform, in order to estimate the influence of different pump manufacturers and triggers on the performance of the device. In this case one of the pumps (Teleflex), with the new technology for pressure measurement via a fibre optic sensor, showed to best trigger the IAB after inflation onset, while the highest number of assisted beats was obtained when this pump was set on electrocardiogram (ECG) triggering.

Nonetheless a first development of multi-dimensional computational model of the IAB counterpulsation was realized with the aim of establishing the effect of this therapy on relevant areas, such as aortic root, and in order to have an insight on the 3-D flow field in the surrounding of IAB: these information can be crucial for the optimisation of the balloon's shape.

In conclusion, the key finding was that a change in balloon shape influences both, inflation and deflation mechanics at horizontal and semi-recumbent positions, and this strategy can be used for maximising the IABP clinical benefits. With the aid of the computational model it will be possible to further develop the already tested balloon different shapes. Not less important, IABP therapy was demonstrated to be crucially influenced by the pump setting and mode (triggering inflation and deflation onsets), hence the clinical operator is addressed to change the pump mode of operation according to the patient's condition to maximise the potential benefit of this therapy.

TABLE OF CONTENTS

(Please note: The headings down to the 3rd level are not shown below)

List of Figures

List of tables

Nomenclature

0D (zero-dimensional)

0D ts (time step for zero-dimensional domain)

3D (three-dimensional)

3D ts (time step for three dimensional domain)

α (frequency parameter)

AF (assistance frequency)

C (conductor)

CHF (congestive heart failure)

CRT (cardiac re-synchronization therapy)

CO (cardiac output)

CV (coefficient of variation)

D (aortic diameter)

DAQ (data acquisition)

DoI (Time between onset of inflation to onset of deflation, inflation duration)

DPTI (diastolic pressure time index)

ECG (electrocardiogram)

EDP (End diastolic pressure)

EDPVR (End diastolic pressure-volume relationship)

EES (End systolic elastance)

ESPVR (End systolic pressure-volume relationship)

EVR (endocardial viability ratio)

EW (external work)

f (heart rate frequency)

FOS (fibre optic sensor)

g (gravitational acceleration)

HF (heart failure)

HR (heart rate)

IAB (intra-aortic balloon)

IABP (intra-aortic balloon pump)

ICU (intensive care unit)

IsDe (Time between onset of inflation to end of deflation)

L (inductance)

LVAD (left ventricular assist device)

NHLBI (National heart, lung and blood institute)

ODEs (ordinary differential equations)

p (statistical significance)

Pao (aortic pressure)

PLV (left ventricular pressure)

PPd (deflation pressure pulse)

PPi (inflation pressure pulse)

R (resistance)

Ratio (Ratio of missed beats over total number of beats)

Re (Reynolds number)

RMS (Root mean square)

RpIs (Time between R-wave (peak of QRS) to onset of inflation)

RpSp (Time between R-wave (peak of QRS) to peak systolic pressure)

pdbdAUTO (Datascope IABP working with Datascope IAB and automatic settings)

pdbdFOS (Datascope IABP working with Datascope IAB, FOS and automatic settings)

pdbdSEMIECG (Datascope IABP working with Datascope IAB and semi-automatic settings)

pdbtAUTO (Datascope IABP working with Teleflex IAB and automatic settings)

pdbtSEMITRA (Datascope IABP working with Teleflex IAB and semi-automatic settings)

ptbdAUTO (Teleflex IABP working with Datascope IAB and automatic settings)

ptbtAUTO (Teleflex IABP working with Teleflex IAB and automatic settings)

ptbtECG (Teleflex IABP working with Teleflex IAB, ECG trigger and automatic settings)

ptbtFOS (Teleflex IABP working with Teleflex IAB, FOS trigger and automatic settings)

Ps (static pressure)

PV loop (pressure – volume loop)

STTI (systolic tension time index)

SV (stroke volume)

TAH (total artificial heart)

TDD (tapered decreasing in diameter from IAB base to tip)

TID (tapered increasing in diameter from IAB base to tip)

$\mathbf{ts_i}$ (iteration time step)

VLV (volume left ventricle)

Vn (nominal IAB volume)

VS (volume suctioned from upstream the balloon)

VU (volume displaced upstream the balloon)
VUTVd (VS divided by Vn)
VUTVi (VU divided by V)

Chapter 1 Background

1.1 The cardiovascular system

The main function of the cardiovascular system is to provide oxygen and nutrients to the body and to remove waste products from tissues, through a network constituted by different sized vessels and through the pumping activity of the myocardial muscle. This tree is characterized by a regulatory system providing support to all the organs and parts of the body in requirement to their needs. The heart is the centre of the cardiovascular system [2], as represented in Figure 1-1. During rest it is able to pump approximately 5 litres per minute of blood around the system. In particular the left ventricle provides oxygenated blood to the system by pumping it firstly into the ascending aorta through the aortic valve, which sits between the aorta and the ventricle to impose unidirectional flow. From here the blood flows into the coronary arteries, providing oxygen and nutrients to the heart, as well as into the aortic arch, thoracic aorta and finally abdominal aorta. The aorta and its branches carry the blood throughout the systemic circulation [2]. The coronary arteries are vital for carrying blood within the wall of the heart, allowing the diffusion of nutrients through all layers of cells constituting the heart tissue. The coronary circulation is hence comprised of a number of vessels that pierce the myocardium, bedewing the whole volume of the heart. The pumping activity of the ventricle determines the cardiac cycle pattern, which can be divided into two main phases: systole and diastole. During systole the ventricle contracts increasing the pressure of the blood inside the chamber until it becomes higher than the one in the ascending aorta causing the aortic valve to open and delivering blood towards the systemic circulation. In diastole the ventricular muscle relaxes resulting in the pressure within the chamber to drop and the aortic valve to close. This cycle results in the pressure within the ascending aorta to constitute a waveform characterized by a maximum during systole, called systolic peak, and a minimum immediately before systole, called end diastolic pressure (EDP).

Figure 1-2 depicts the pressure on both, ventricle and ascending aorta during the cardiac cycle [119]. Coronary flow is at its maximum during diastole, since, although the pressure is smaller compared to the systolic phase, the impedance of the coronary vessels is markedly smaller, because of the relaxation of the myocardial muscle. For this reason the mean diastolic pressure assumes particular importance. A representation of the coronary flow during the cardiac cycle is presented in Figure 1-3, according to Gregg et al., whereby measurements were taken of canines at rest, exercise and recovery [4].

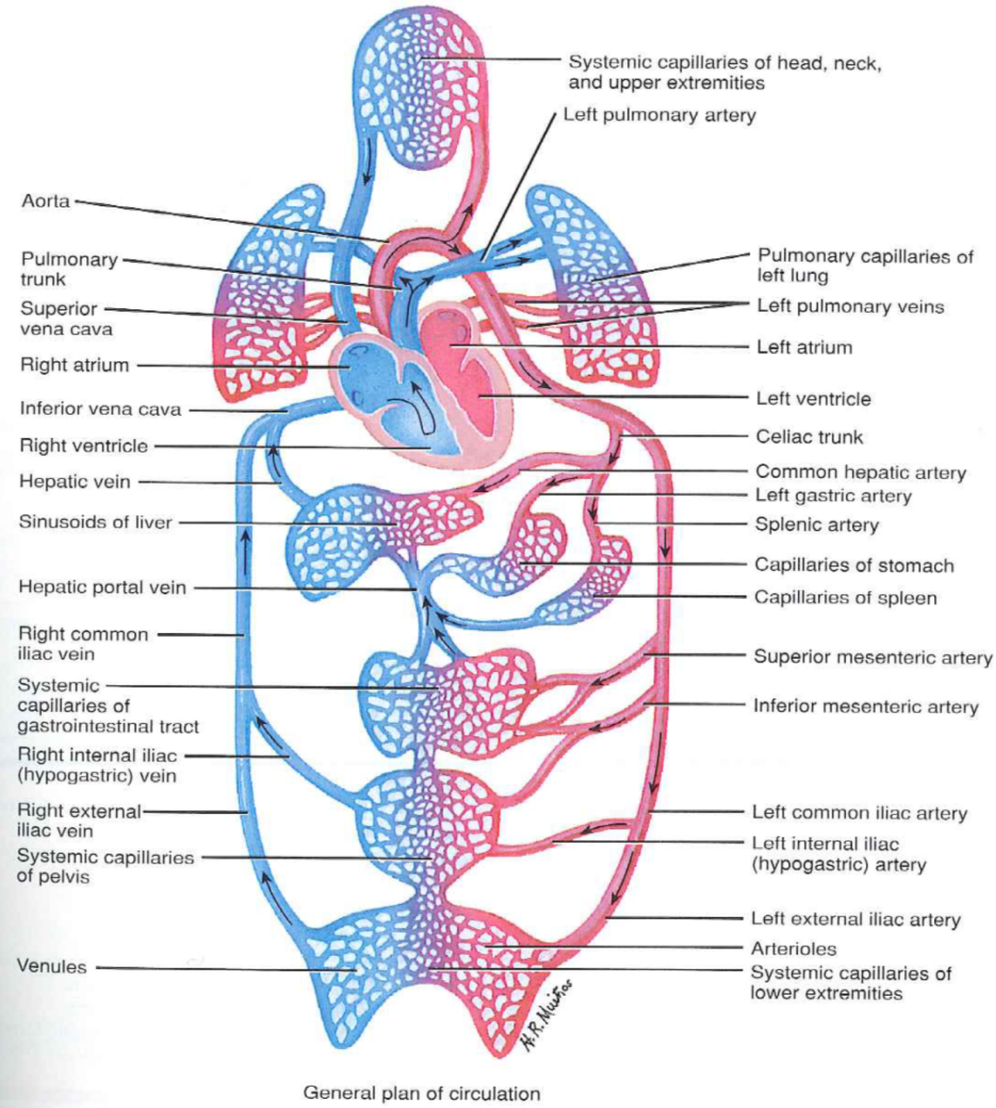

Figure 1-1: *Schematic representation of the human cardiovascular system. The path followed by the circulation is indicated by the arrows, oxygenated blood is indicated in red and de-oxygenated blood in blue. The heart represents the centre of the whole system and pushes the blood both, towards the system (left heart, red) and towards the pulmonary circulation (right heart, blue) (taken from Tortora et al.[2]).*

t (s)

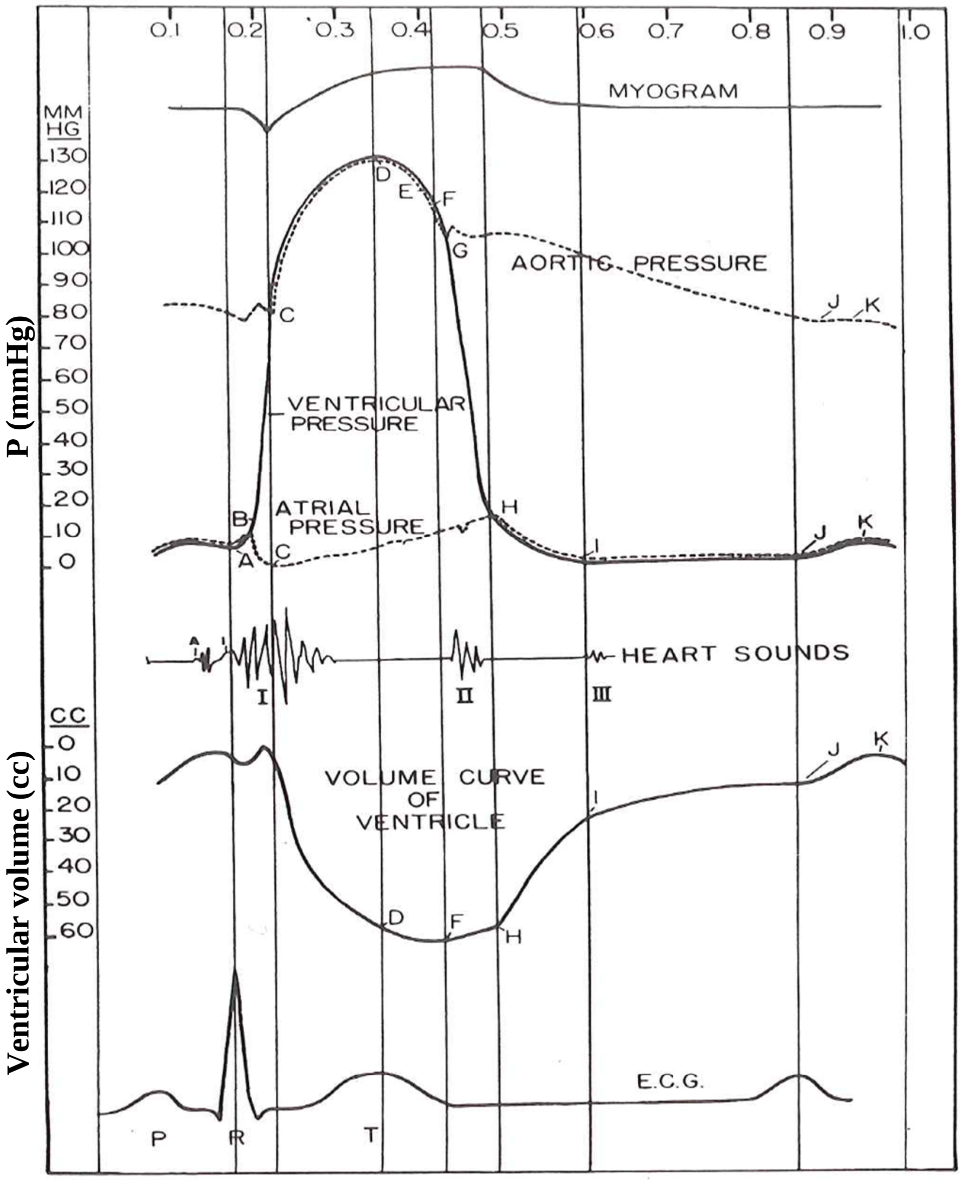

Figure 1-2: *The graph represents a typical human electrocardiogram, on the bottom, left ventricular, aortic and left atrial pressures, on the top, and left ventricular volume, on the centre, during one cardiac cycle. Myogram and heart sounds during the cardiac cycle are also represented. Systole is defined by phases A-C, representing isovolumic ventricular contraction, C-D, maximal ejection phase and D-F, reduced ejection phase. Diastole is defined by phases F-G, time of closure of aortic valve, G-H, isometric relaxation, H-I, rapid filling, I-J, diastasis, and J-K-A, atrial filling (taken from Sagawa et al.[119]).*

An important estimation of the activity of the heart is provided by the cardiac output (CO), which indicates the volume of blood ejected from the ventricle into the aorta each minute. The quantification of this parameter is given by the value of the stroke volume (SV), corresponding to the volume ejected by the ventricle for each heart-beat, and by the heart rate (HR), which is the number of cardiac cycles in one minute. Cardiac output is hence calculated as the product of SV and HR. The stroke volume SV depends on three main parameters [2]: preload, the stretch on the heart before it contracts, contractility, indicating the strength of contraction of the myocardial fibres, and afterload, corresponding to the pressure that must be exceeded in order for the ventricle to eject blood [2], also called end diastolic pressure. Each of the described parameters is crucial in addressing pathological or normal working conditions of the heart.

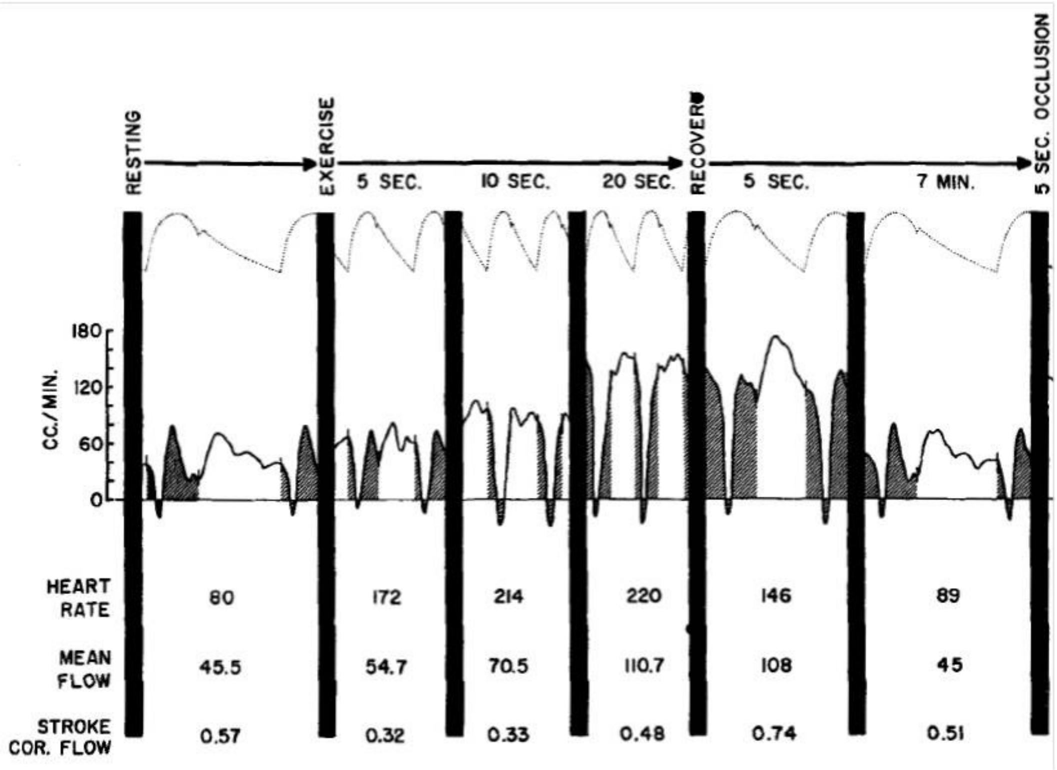

Figure 1-3: *Aortic pressure waveform (dashed line, above) and coronary blood flow through left circumflex artery (solid line, below) are indicated in conditions of rest, exercise and recovery, as measured in dog (taken from Gregg et al.[4]).*

1.2 The clinical problem: heart failure

Heart failure (HF) is a condition in which a problem with the structure or function of the heart impairs its ability to supply sufficient blood flow to satisfy the body requirements. The main causes of HF are summarized as hypertension, heart valves disease, myocardial infarction and other forms of ischemic heart disease, cardiomyopathy.

In developing countries, around 2% of adults suffer from HF, but in those over the age of 65, this percentage increases to 6-10%. In USA the estimated prevalence in adults (from 20 years old) is 5,300,000, and data from the National heart, lung and blood institute (NHLBI) Framigham heart study indicate that HF incidence approaches 10 per 1,000 population after the age of 65 (according to Medtech insight 550,000 new cases occurring annually). In Western Europe approximately 6.5 million people currently suffer from HF (14 million people considering all of Europe). Prevalence at each age increased between two periods surveyed (1976-80, 1988-91), according to USA National health and nutrition examination survey. This increasing prevalence, hospitalisations and deaths have made HF a major chronic condition: 875,000 USA hospitalisations are due to HF implementing it as the most common diagnosis in patients aged 65 years and older [5].

In Figure 1-4, the graph shows the costs for some of the most developed countries, compared to the total health care expenditure.

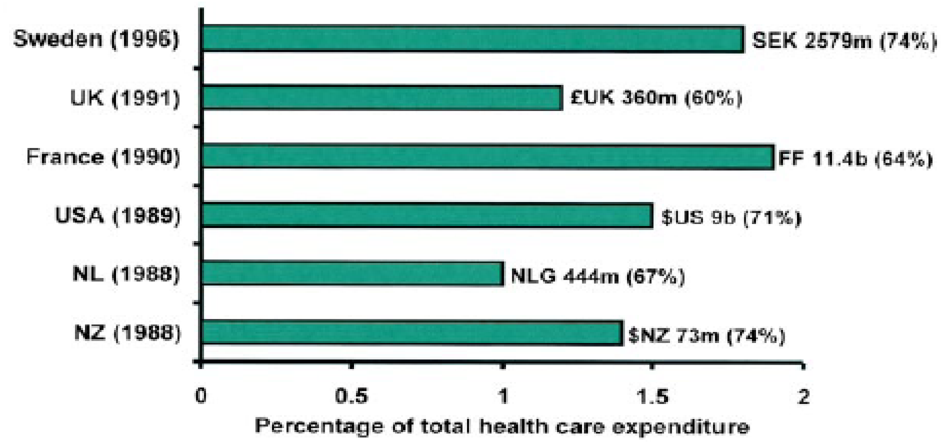

***Figure 1-4**: Percentage of total health care expenditure for HF in more developed countries (taken from Bundkirchen et al.[1]).*

The incidence of congestive heart failure continues to escalate worldwide, taxing health care systems. Current accepted regimens have provided some success;

however, most patients show progression of their disease. Because of this trend, research continues to explore therapies directed to a stabilisation of the disease and hopefully to improve the downward spiral.

Main treatments for HF are the following:

- Drugs; which is by definition the least invasive type of therapy, but not the most effective. 70% of patients are treated with this therapy, both, less severe heart failure cases and too severe cases who would not benefit (or be too risky) from other more invasive approaches. Obviously all patients, independently from the treatment, are continuously treated with drugs, even if drugs are not the sole therapy;
- Surgery only; such as surgical left ventricular remodelling and heart transplantation which are the most invasive approaches, only for patient in a very late stage of HF (Congestive Heart Failure, CHF);
- Lifestyle;
- Devices; mainly consisting of: mesh-like constraint devices; stents; left ventricular assistant devices (LVAD); cardiac resynchronization therapy (CRT); implantable defibrillators. Rhythm treatment, or electronic treatments, even very diffused like those using CRT approach, are not suitable for all HF patient populations and have a limited efficacy for the treatments of most severe cases. VAD implants are, on the other side, very invasive techniques, only for patients at a very late stage of HF (CHF).

It is deducible from the above scenery that to date there are no therapies which are completely effective in treating HF, and it remains a syndrome associated with high morbidity and mortality [6]. As stated by De Souza et al.[6], “the treatment of patients presenting severe heart failure, and particularly left ventricle failure, remains one of the most challenging situations in contemporary medicine”. Particularly the replication of the heart’s (or of a portion of the heart’s) function is a challenge to a bioengineer’s skill, whereby it is viewed as a functional pump, essential for human functions.

1.3 Left ventricular assist devices (LVAD)

LVAD are currently used as a temporary or permanent aid or replacement to the ventricular function, according to the device design and category. Originally in the 1960s the only therapeutic tool available was conservative medical therapy based on high doses of positive inotropic agents, vasopressors and diuretics [6].

The main devices clinically used for temporary or permanent heart recovery can be summarized into rotary, pulsatile or counter-pulsatile pumps. The latter one refers to IABPs. Among the rotary pumps are included the axial flow pumps: they ensure the movement of the fluid through a screw or some blades placed inside a tube, pushing the fluid into the desired direction. The presence of blades inside the tube ensures the one-directional flow of the fluid. Alimentation to the pump would be provided by an external battery, which is currently difficult to include inside the human body, as the instrument needs to be recharged. Indeed the newer technologies are targeting the possibility of charging up the battery through wireless systems. Wires connecting the pump to the rest of the device are designed to be biocompatible and to allow the skin ingrowth, in order to avoid any possibility of infection. However, modern VAD control systems are compact, allowing patients to carry them around without particular difficulty. Early active rehabilitation in patients implanted with LVAD improves their condition, favourably impacts the clinical course while they await heart transplantation, and also improves post-transplant recovery. LVADs can provide a temporary circulatory support in patients with HF, restoring normal hemodynamic and vital organ perfusion, even in cases of complete myocardial pump failure. The aid of an LVAD has beneficial effect on long-term outcomes by reducing ventricular strain and improving the remodelling of an acute failing ventricle [7]. There is also need of exercise therapy, important to improve the quality of life of patients with LVADs [8].

One of the most widely used LVAD in the group of axial flow pumps is the ‘Impella recover system’ (IRS, TexasHeart), shown in Figure 1-5. The IRS is a micro-axial pump sucking oxygenated blood from the left ventricular cavity, and injecting it into the ascending aorta. The intra-cardiac axial flow pump contains a rotor that is driven by an electrical motor and has an inflow cannula. The pump is purged with a solution of heparin, in order to prevent thrombus formation, and is inserted through the aortic valve into the left ventricle, providing an output flow of up to 2.5 L/min [9]. However, the device is contraindicated in patients with severe peripheral vascular disease or in patients with a mechanical aortic valve or a calcified aortic valve, and introduces an increased risk of infection[10].

Another type of rotary pump is the centrifugal flow pump. One example is the TandemHeart, depicted in Figure 1-6. In this case the LVAD is a left atrial to femoral bypass system that can provide rapid circulatory support and resolution for pulmonary edema and deranged metabolism within hours of patients undergoing cardiac shock. The system utilizes a drainage cannula placed via a trans-septal puncture into the left atrium to aspirate oxygenated blood, which is then injected by means of a centrifugal pump, placed externally to the patient, into the femoral artery, establishing the bypass [9]. The pump is able to generate up to 4 L/min flow and is characterized by low heat generation, haemolysis and emboli formation [11]. The TandemHeart pump can be used for up to 14 days [6].

Pulsatile pumps replicate the function of the whole myocardium, substituting both, right and left ventricles. Some examples of clinically used pulsatile pumps follow. The SynCardia Temporary (Syncardia) consists of 2 separate blood pumps that are pneumatically driven and generate pulsatile blood flow, as indicated in Figure 1-7 [12]. Each of the two pumps is constituted by a rigid plastic shell containing mechanical valves and a polyurethane diaphragm separating the blood sac from the air sac [13]. Each sac’s maximum volume, which equals their maximum stroke volume, is 70 cc. The air sacs are connected through a percutaneous driveline to a source of compressed air [14]. Differently the Abiomed AbioCor implantable replacement heart (IRH), shown in Figure 1-8, is based on one titanium shell containing 2 pumping chambers. The IRH also includes 4 tri-leaflet valves (2 in each pump) and diaphragms made by polyurethane resistant to calcification [13].

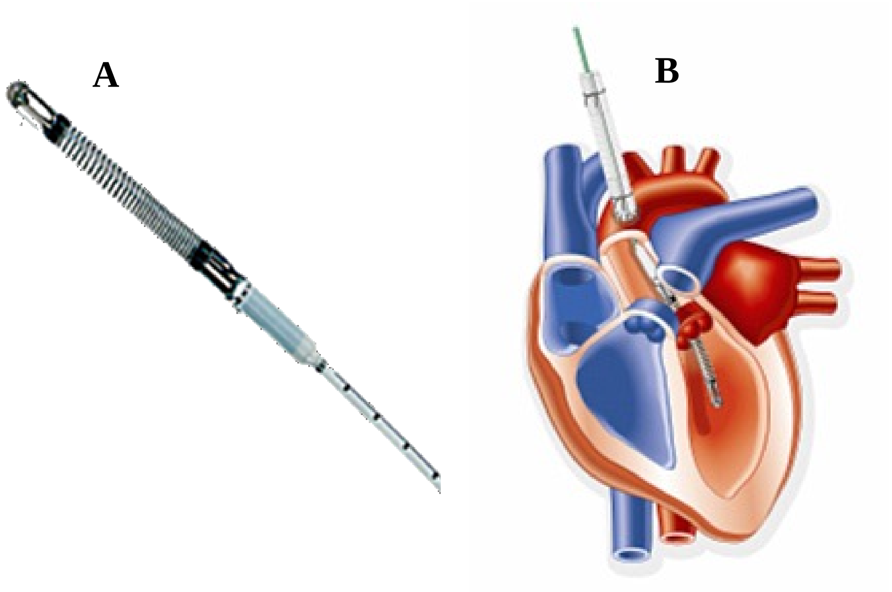

Figure 1-5: *The Impella recovery system (A), and its placement between the ventricle and the aorta (B), are represented in the figure (http://texasheart.org/Research/Devices/impella.cfm, accessed on 22/04/2014).*

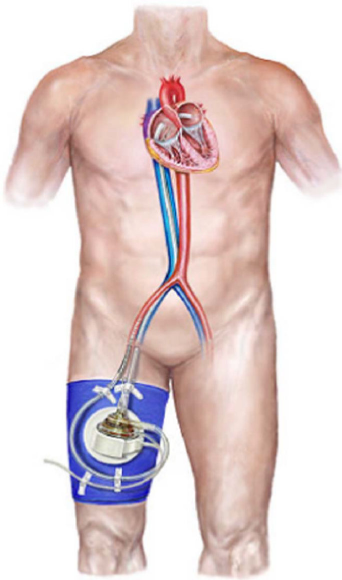

Figure 1-6: *The figure shows the placement of the TandemHeart LVAD. The pump is placed externally on the human body, and is connected to the left atrium on one side and on the left femoral artery on the other side, working as a bypass providing circulatory support (taken from Ng et al.*[15]*).*

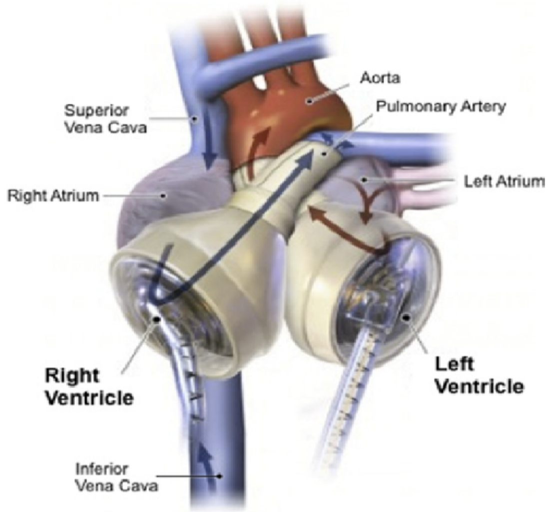

Figure 1-7: *The SynCardia total artificial heart, positioned physiologically with connections to the aortic root, pulmonary artery and atrial chambers (taken from Gaitan et al.*[12]*).*

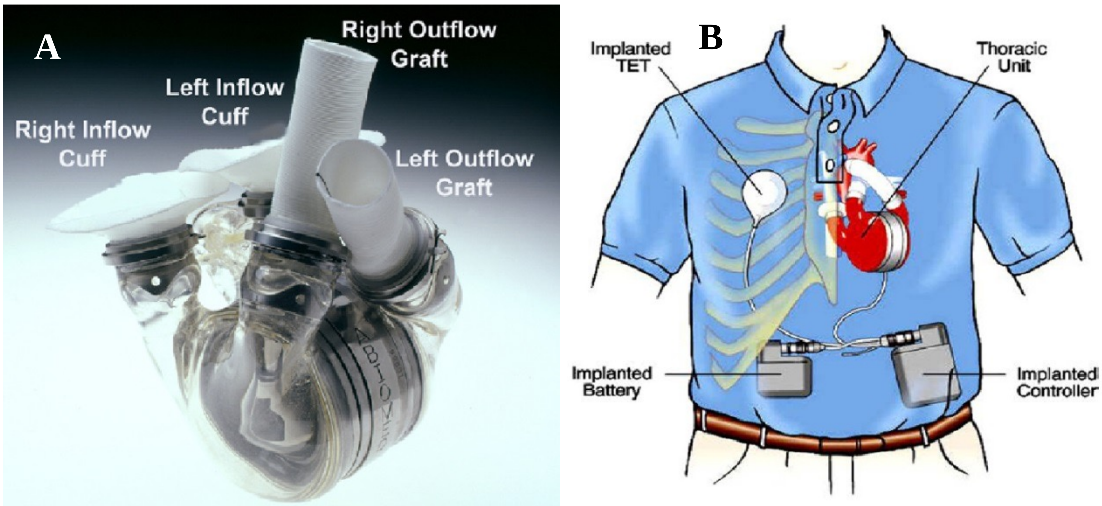

Figure 1-8: *The Abiomed Abiocor TAH and its physiological position within the human body are above described, A and B respectively (taken from Gaitan et al.*[12]*).*

In this case pulsatile blood flow is generated through an electro-hydraulic system: a fluid is pressurized by a centrifugal pump and pushes against the membranes of left and right ventricles, being directed alternatively from one to another by a switching valve changing the direction of the fluid, at a frequency ranging from 75 to 150 bpm [16]. The energy source for both switching valve and centrifugal pump is transcutaneous and consists of an implanted coil and an external coil, avoiding the use of a percutaneous driveline.

Both latest described artificial hearts showed an increase in survival for patients compared to those who underwent transplants without the use of a device (in case of SynCardia) or without the use of any other device (in case of Abiomed AbioCor IRH)[12]. Nevertheless future improvements are likely to rely on the use of wireless technology which would avoid any percutaneous driveline, as it is the case of Abiomed AbioCor IRH. Continuous-flow pumps do not require any volume compensation, and in this case a transcutaneous energy transfer system would be totally implantable and sealed.

Finally, aid to the ventricular function can also be provided through the use of a counter-pulsatile pump, or Intra-aortic balloon pump. The device, introduced in the following paragraph, will be discussed in more detail in the rest of this Chapter.

1.4 Introduction to Intra-Aortic Balloon Pump (IABP)

The Intra-aortic balloon pump (IABP) is a mechanical device widely used as a circulatory assist device for temporary mechanical assistance of the failing myocardium. The IABP aims at decreasing ventricular afterload and increasing coronary blood flow, therefore resulting in an increased oxygen delivery to the myocardium. The decrease in ventricular afterload is instead aiming at reducing ventricular work.

The device has been introduced to clinical practice in the 1960s. Its first application was in 1968 in patients developing cardiac shock [17]. The intra-aortic balloon was introduced by Moulopoulos et al. in 1962 [18]. The first clinical data regarding IABP therapy were reported in 1968 by Kantrowitz et al. [17]. In 1980, the insertion technique of the intra-aortic balloon (IAB) was amended by Bregman et al. [19] and is now the most favoured insertion technique in clinical practice. Currently the IABP is the most widely used cardiac assist device because of its low cost, easy insertion technique and handling [6].

1.4.1 IABP indications

The IABP is generally used [20] in cases where:

- Ischemia or heart failure due to coronary artery disease occurs prior to coronary revascularization [20];
- Acute myocardial infarction occurs before cardiac catheterization [21];
- Adjunctive therapy in the case of coronary angioplasty [22];

- High-risk percutaneous trans-luminal coronary angioplasty [23];
- Failed angioplasty [24];
- Left main coronary artery stenosis [25];
- Myocardial infarction with cardiogenic shock, combined with revascularisation procedures [26];
- Support before cardiac transplantation [27].

1.4.2 IABP Contra-indications

IABP is contraindicated for severe peripheral vascular disease, aortic aneurysm, aortic regurgitation, active bleeding, contraindications to anticoagulation, and severe thrombocytopenia [28]. Moreover IABP is associated with a wide variety of complications, the most common being bleeding, systemic embolization, limb ischemia, and amputation. Additionally, IABP may result in infection, as it is an indwelling catheter, and may be associated with inadequate inflation, or inadequate diastolic augmentation [29]. Furthermore the balloon might develop a mechanical failure and rupture, which could be characterized by a dramatic break, highlighted by the presence of blood on the IAB catheter, or by a pinhole allowing constant flow of Helium to escape the balloon chamber, with critical results [20], since Helium emboli could form and obstruct brain or other organs arteries.

However, the severity of complications currently encountered is less devastating than those reported in the 1970s [20]. In 1993 Tatar et al. [30] reported a decreased incidence of vascular complications associated with the use of sheath-less catheters. In any case IABP use is not without risks and it is necessary for the practitioner to determine whether IABP application is necessary by evaluating the risks associated with its use on a case by case basis and comparing them with the hypothetical benefit associated to the use of the device.

1.4.3 IABP Counterpulsation principle

The Intra-aortic balloon (IAB) actively inflates in early diastole, immediately after aortic valve closure, aiming at increasing blood flow towards the coronary arteries, and deflates in late diastole, just before systole and aortic valve opening, aiming at reducing left ventricular afterload resistance. The balloon inflation and deflation pattern is controlled by a computer linked to either an Electrocardiogram

(ECG) or a pressure source signal, as already mentioned. The working principle for the IABP is schematized in Figure 1-9.

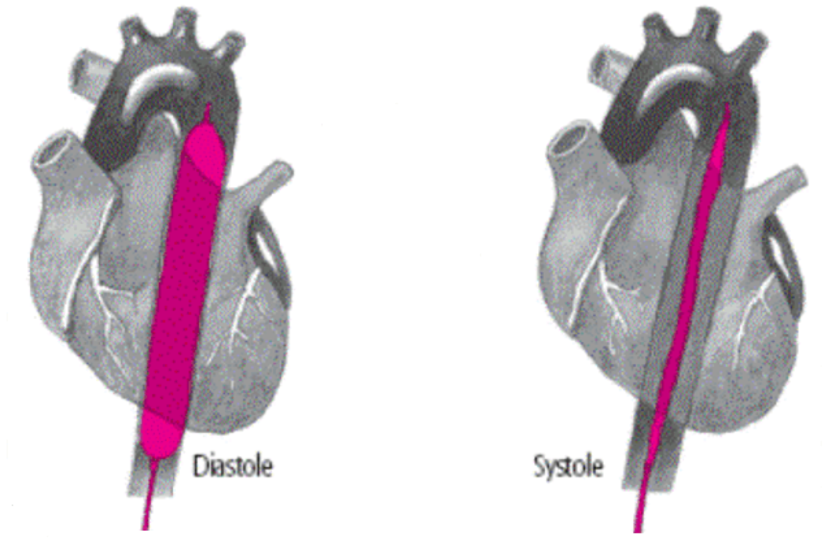

Figure 1-9*: The pictures represent the working principle of the IABP, which is inflated during diastole and deflated during systole* [31].

A typical pressure waveform with and without the activation of the IABP is shown in Figure 1-10 for providing a physical understanding of the hemodynamic changes associated to the use of the device. The increase in diastolic pressure translates as an increased driving pressure for the blood flow in the coronaries, while the decrease in end diastolic pressure implies a lower ventricular afterload which can be linked to a decrease in ventricular work.

The hemodynamic consequences due to the inflation, during diastole, and deflation, just before systole, actions of the IABP are primarily associated with decreases in heart rate, left ventricular end diastolic pressure, mean left atrial pressure, left ventricular afterload and myocardial oxygen consumption. The metabolic effects result in an improvement in the cardiac energy balance by increasing oxygen supply to the myocardium and by reducing cardiac oxygen demand [32].

In fact one of the indices used for testing IABP effectiveness is the endocardial viability ratio (EVR) [33], obtained by dividing diastolic pressure time index (DPTI) by systolic tension time index (STTI), both indicated in Figure 1-10**.**

DPTI indicates the oxygen supply to the myocardium, STTI is linked to the myocardial oxygen demand [33].

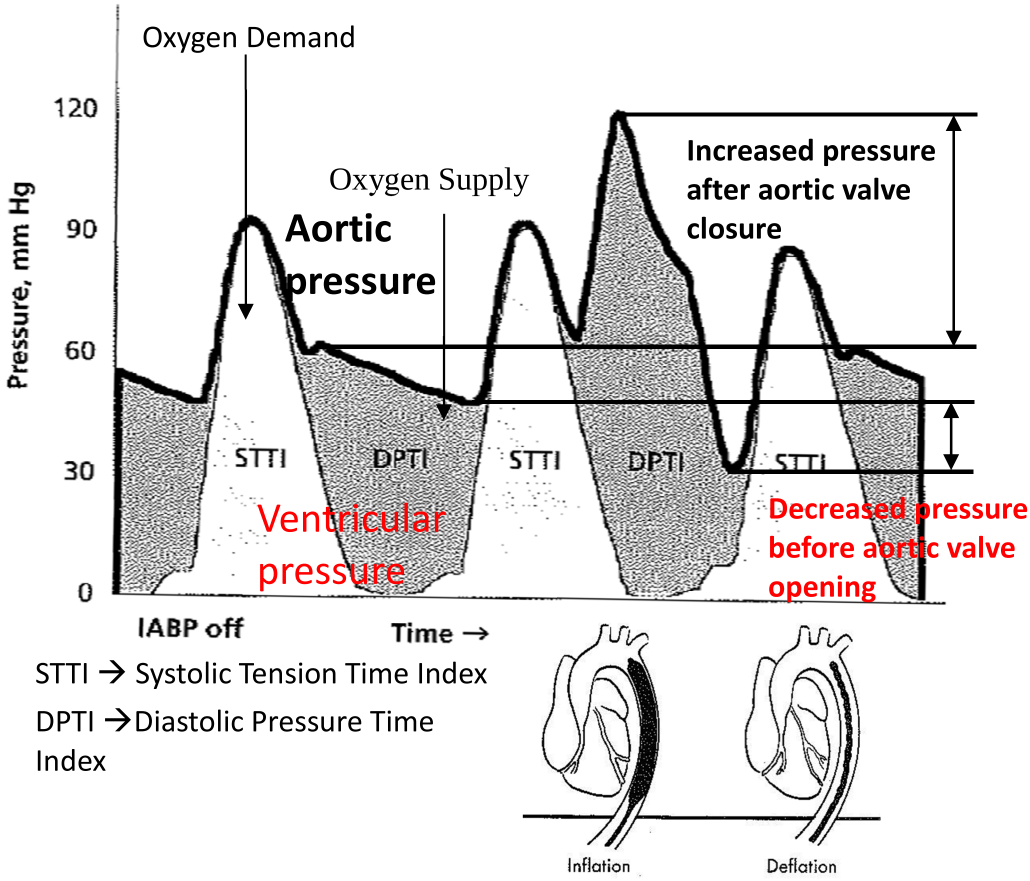

Figure 1-10: The graph represents the pressure waveforms associated with the aorta and left ventricle with and without the activation of the IABP. As described, the counterpulsation of the device during inflation causes an increase in DPTI, linked to oxygen supply to the myocardium, and, during deflation, to a decrease in STTI, linked to myocardium oxygen demand.

1.4.4 IABP therapy

The device consists of an inflatable cylindrical polyethylene balloon (depicted in Figure 1-11) generally inserted through the femoral artery, passed into the descending thoracic aorta, and placed, ideally, 1–2 cm below the origin of the left subclavian artery and above the renal artery branches [9]. Once the IAB is in place its position is confirmed by fluoroscopy or chest X-ray. The procedure is indicated in Figure 1-12.

Figure 1-11: *The Intra-aortic balloon (IAB) [IAB catheter for pediatrics by Tokai medical products]*

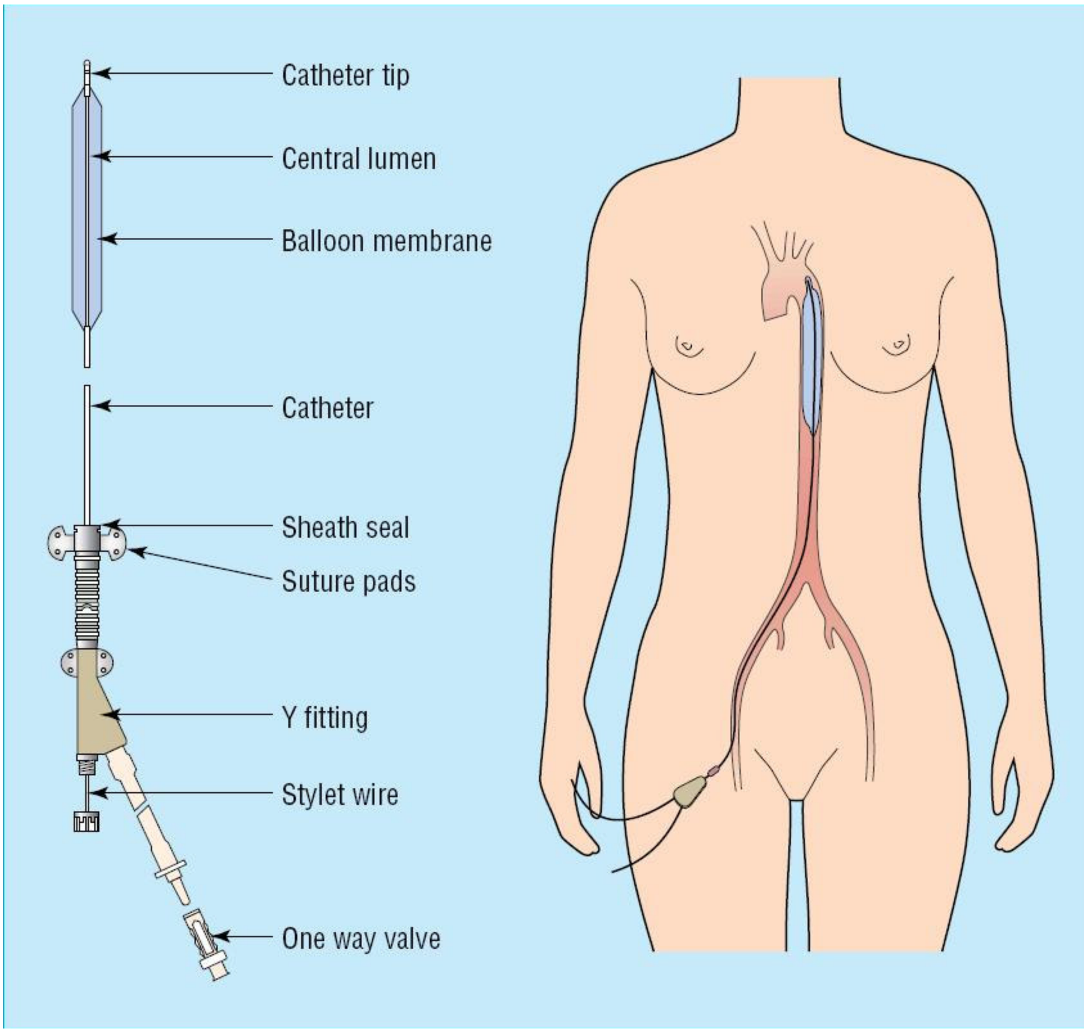

Figure 1-12: *Insertion and positioning of the Intra-aortic balloon (IAB) (taken from Ducas et al.*[34]*).*

The balloon is connected through a catheter to an external pump (as shown in Figure 1-13 A) shuttling Helium gas within the pierced internal catheter in the portion corresponding to the IAB membrane, resulting in the Helium filling up the balloon chamber. Helium is used because its low viscosity allows it to travel quickly through the long connecting tube, and has a lower risk of causing a harmful embolism in case of balloon membrane rupture, since the partial pressure of Helium in the blood is smaller compared to other gases such as, for instance, oxygen.

The pump mainly consists of a computer controlling the shuttling of Helium gas through the IAB catheter, a Helium bottle as a reserve of gas and a console which allows to control the relevant parameters related to the operation of IAB counterpulsation (different according to the pump model and brand). The most important parameters are listed as follows:

- assistance frequency, which regulates the ratio of heart beats assisted by the IABP;
- augmentation volume, referring to the volume of Helium gas to be pumped into the IAB;
- mode of signal selection, generally automatic, indicating that the computer will control the selection of signal and timings automatically, or manually (operator), enabling the operator to set source signal and inflation/deflation onset;
- source signal, upon which the computer selects the algorithm controlling shuttling of Helium gas (just in case of manual mode);
- inflation and deflation onset, regulating the onset of these two phases of counterpulsation, which will be described more in depth in the following paragraph.

The computer controlling the pump (and hence the IAB) can be linked to the ECG signal or aortic pressure signal at the tip of the balloon, or both. The console provides a display showing the main information regarding the working condition of the IAB and the main hemodynamic parameters, as indicated in Figure 1-13 B.

A

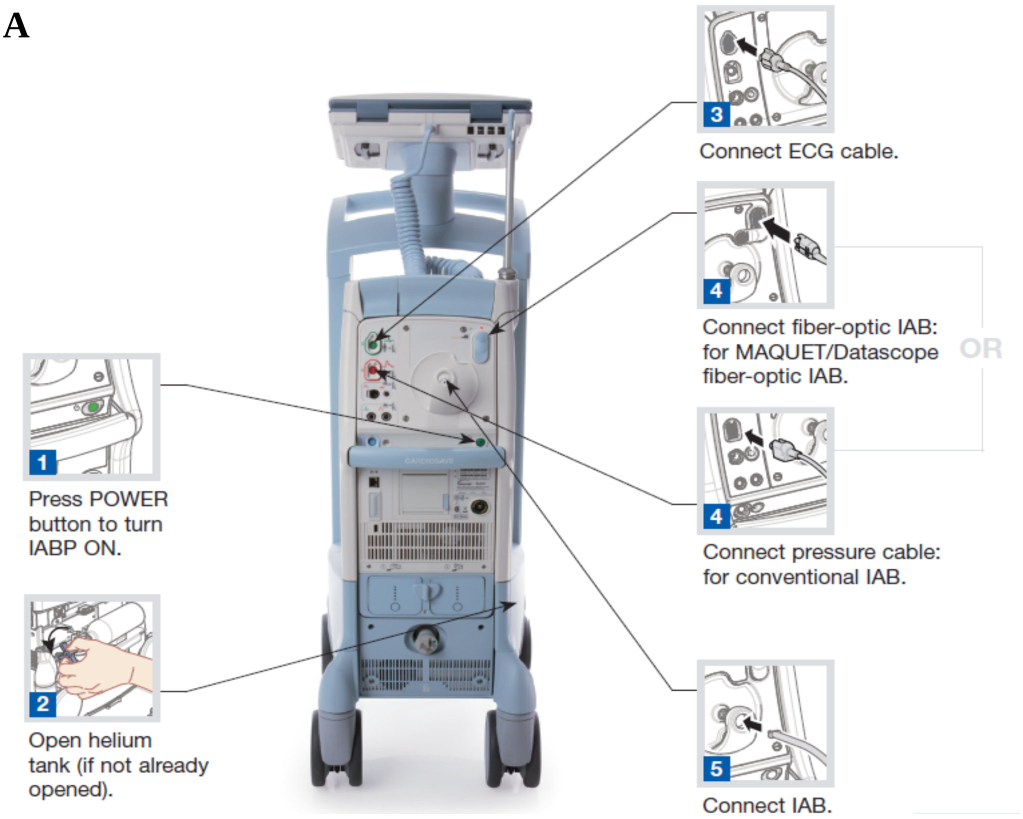

B

Figure 1-13*: A commercial Intra-Aortic balloon pump (IABP) (A), which controls the balloon counterpulsation, and its display (B), showing the most relevant hemodynamic parameters and IAB internal pressure, augmentation volume and assisting frequency (http://ca.maquet.com/products/iab-pumps/cs300/applications/, accessed on 22/04/2014).*

1.4.5 The importance of IABP correct timing

The onset of balloon inflation, its duration and the onset of balloon deflation affect the performance of the IAB and the related hemodynamic changes. Plummer et al. state that “accurate timing of balloon inflation and deflation is imperative for effective, maximum augmentation”[35]. For an accurate indication of IABP timing the aortic root pressure waveforms should be taken as a reference [35]. Aiming for an optimal diastolic pressure augmentation, the inflation of the balloon should begin immediately after the closure of the aortic valve. To obtain a maximised decrease in end diastolic pressure, linked to the lower heart’s demand for oxygen, the deflation of the IAB should progress fast and just before aortic valve opening. Consequently one of the manufacturer’s suggestions is that the timings of inflation and deflation should be adjusted by the operator by setting IABP assistance at a frequency of 1:2, observing both assisted and unassisted beats and targeting maximum diastolic augmentation and minimum end diastolic pressure [35].

In 1992 Barnea et al. [36] developed an automatic control for IABP pumping. The algorithm [36] is based on the maximization of mean diastolic pressure (effect of inflation) and minimisation of peak systolic pressure (effect of deflation) and can be used for reducing the attention required from the operator [36]. In 2013 Khir [37] reported that, while it is possible to control onsets of inflation and deflation, the effects of balloon inflation and deflation at the aortic root, which is the site of interest, depend on other parameters, such as Helium travelling speed and pressure wave-speed in the aortic arch. For an optimal therapeutic benefit, the delays between triggering time and actual balloon inflation/deflation, followed by the compression/decompression wave arrival times at the aortic root should be taken into account [37].

Inflation and deflation time errors can still be clinically observed and compromise the therapeutic benefit of IABP therapy. Overall incorrect timings can be categorized as following:

- Early inflation, compromising the stroke volume and constituting an impedance to blood flow towards the systemic circulation;
- Late inflation, compromising the benefit of balloon inflation in terms of diastolic pressure augmentation and mean diastolic pressure;

- Early deflation, affecting both medium diastolic pressure, which most likely will be decreased, and end diastolic pressure, since before systolic ejection there would be time for the pressure to rise;
- Late deflation, inducing the balloon to constitute a higher impedance in the early part of systole and increasing the ventricular afterload.

Schreuder et al. [38] studied the effects of an early inflation and late deflation, which one would say were the two most detrimental inflation/deflation onsets, on stroke volume and left ventricular mechanical dyssynchrony, defined as the percentage of left ventricular segments changing in volume in opposite direction or not showing changes at all in respect to the total ventricular volume change. The tests, carried out on 15 patients, showed that an early inflation causes a decrease in stroke volume and an increase in systolic dyssynchrony [38], while a late deflation induces an increase in stroke volume but at a price of an increased systolic work, as observed from the pressure-volume curve corresponding to this situation.

1.4.6 Considerations on IABP efficacy

An important tool for addressing the efficacy of IABP therapy on recovering the left ventricular heart function is the pressure-volume relationship (PV loop) tracked during the cardiac cycle. This representation of pressure and volume changes in the ventricular chamber can highlight whether the cardiac function has been impaired and if a therapy of cardiac release is successful in improving cardiac function or not. In fact different arterial pressures and ventricular volumes during contraction impact on the relationship between mechanical energy imparted to the blood and total chemical energy consumed [119], hence on the efficacy of the cardiac pump.

1.4.6.1 The PV loop

The working conditions imposed to the ventricle before and after the onset of ventricular contraction are called preload and afterload: based on these two parameters the pump function can be evaluated. The ventricular pressure volume diagram enables to have an evaluation of these working conditions, preload and afterload, and consequently of the pumping activity of the heart.

The pressure-volume diagram is represented in Figure 1-14: point a (preload) shows pressure and volume at which the ventricle starts contracting. Subsequently the mitral valve closes and, due to ventricle contraction, the pressure rises without a change in ventricular volume. This is called isovolumetric period and is represented by the vertical line a-b. Point b indicates when ventricular pressure exceeds the aortic blood pressure, thus pushing the aortic valve to open. Due to the aortic valve opening, the ventricle ejects blood: in this phase pressure rises mildly compared to the previous phase. Segment b-c represents this ejection phase, with the total volume of blood ejected called stroke volume. At the end of this phase, both ventricular and aortic pressure starts diminishing due to the contractile process of the myocardium reaching and passing its peak. The muscular fibres still contract, but in a lower degree. Shortly afterwards the aortic valve closes. End of ejection and closure of aortic valve is represented by point c. Subsequently ventricle undergoes to isovolumetric relaxation (segment c-d), corresponding to steep decrease in ventricular pressure with no change in its volume. When the pressure falls below the atrial pressure the mitral valve opens (point d), and blood fills up the relaxing ventricular chamber (segment d-a). The area indicated as EW, external work, in the Figure, represents the energy delivered to the blood through the contraction of the ventricle.

Figure 1-14 shows different pressure-volume trajectories. Through connecting the end diastolic points (points c) and end systolic points (points a) it is possible to obtain the end diastolic pressure-volume relationship (EDPVR) and end systolic pressure-volume relationship (ESPVR), respectively. These curves indicate the properties of the contracted ventricle and relaxed ventricle, respectively.

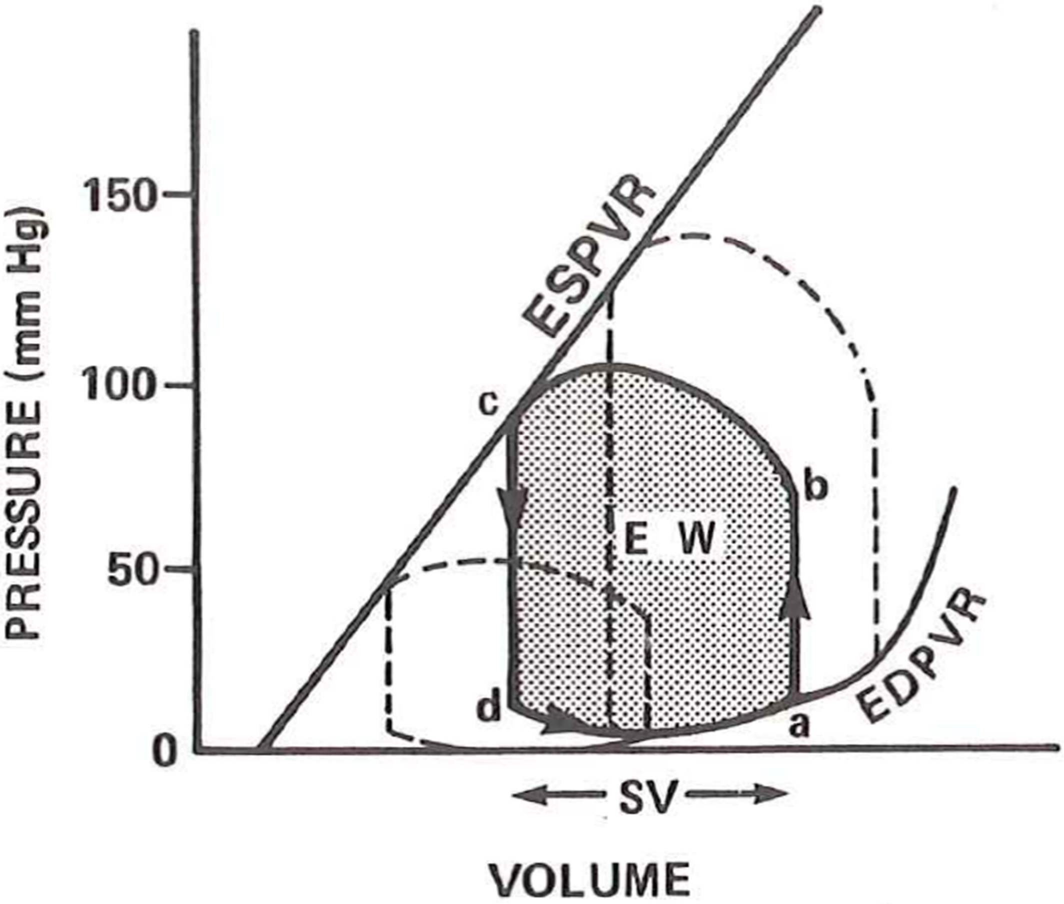

Figure 1-14: *Above represented the ventricular pressure-volume relationship as described by Sagawa et al. [119]. On the ordinate the ventricular cavity pressure, and on the abscissa the ventricular volume. EDPVR and ESPVR are end-diastolic pressure-volume relationship and end systolic pressure-volume relationship, respectively. EW indicates the external work of contraction of the ventricle, and SV represents the stroke volume, calculated as the difference between ventricular volume in the segment ab and the one in the segment dc [119].*

Through the pressure-volume diagram it is possible to visualize the effects on ventricular function of preload or inotropic state (contractility of ventricular fibres). This is represented in Figure 1-15, where A-C represents diastolic filling, after a drop in pressure A-B due to ventricular relaxation, C-D represents isovolumetric contraction, and D-F represents ventricular ejection (divided in D-E, rapid ejection, and E-F, deceleration of blood outflow). The volume displaced between D and F is the stroke volume, and F-A represents isovolumetric relaxation. At point A the mitral valve opens and blood flows into the ventricle, which reaches its end diastolic volume according to the venous return and to the preload, as highlighted in Figure 1-15. Due to Frank-Starling mechanism the increase in volume resulting in point C to move to C' and C'' is related to an increased stroke volume. Differently a higher contractility or inotropic effect would produce a greater force and a greater emptying of the ventricle, with consequent smaller residual volume, resulting in point F to move to F' and F'' (Figure 1-15) [120].

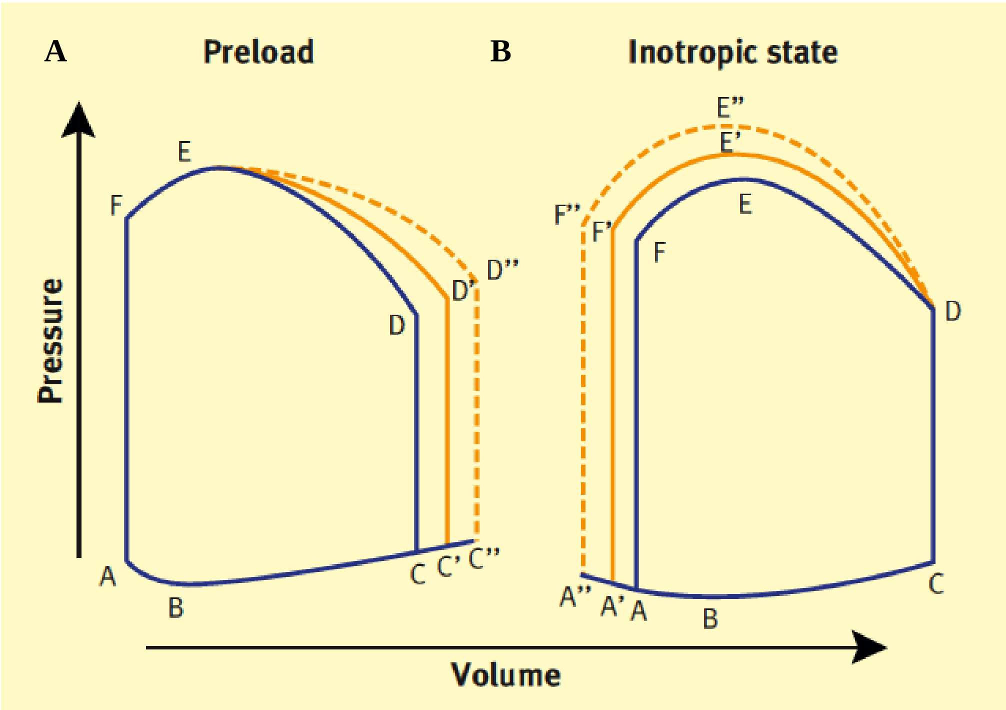

Figure 1-15*: Above, from Kirkman [120], a representation of pressure-volume relathionship characterizing the ventricles. In A) it is represented the effect of change in preload: point C moves to C' and C''with increasing preload because of an increased blood inflow into the ventricular chamber. In B) it is indicated instead the effect of a change in inotropic state, that is the contractility of the ventricle: points C and D do not move (afterload and preload are the same), while point F moves to F' and F'' with increasing contractility, resulting in an increased stroke volume and in a decreased ventricular residual volume.*

1.1.1.1.1. Intrinsic and extrinsic regulation of heart and effect on PV loop

Stroke volume depends on the arterial afterload, depending on both mechanical characteristics of the arterial system and on cardiac contraction.

The cardiac contraction is regulated by two main mechanisms, one intrinsic to cardiac muscle and one, extrinsic, mediated by nervous and hormonal control of the heart.

The intrinsic mechanism is called, as mentioned, Frank-Starling mechanism, and relates the maximal force that can be produced by a muscle fibre and its length immediately before contraction, called preload. It was demonstrated that, in a range of preload, with increasing preload force of contraction increases. This translates, on the PV loop in Figure 1-15 A, as a shift of point C towards the right-top, as already shown, and results in an increased stroke volume, since point F does not move. This mainly depends on the fact that the ventricular muscle fibres are oriented as a spring: the most dilated the fibres, the highest the force of the contraction. Through this mechanism, the ventricle can answer intrinsically to an increased venous return with a higher stroke volume.

Extrinsic regulation depends instead on sympathetic nervous system, which can act on myocardial force contraction. This means then that a change in ventricular muscle contractility can be obtained also without changes in preload and afterload. The result would be a different rise in pressure in case of sympathetic nervous system action, hence the point of maximum pressure, E, moves towards the top, and the point F, indicating the value of blood in the left ventricle at the end of systole, moves towards the left, as already indicated in Figure 1-15 B.

1.1.1.1.2. PV loop in case of heart failure

Three types of heart failures can be distinguished in relation to impaired conditions of the ventricle [119]:

- Systolic and diastolic ventricular functions physiological, with increased workload on the heart, due to the need of higher stroke volume or to ejection of blood against a high afterload (type 1);
- Decreased systolic function of the heart, resulting in decreased ability of the heart to develop pressure or eject blood (type 2);

- Diastolic function of the heart, resulting in inadequate diastolic ventricular filling (type 3).

Figure 1-16 shows four different PV loops, two representing type 1 failure, 1-16 A related to volume overload and 1-16 B to pressure overload, one representing type 2 failure, 1-16 C related to restriction to filling, and one representing type 3 failure, 1-16 D related to loss of contractility.

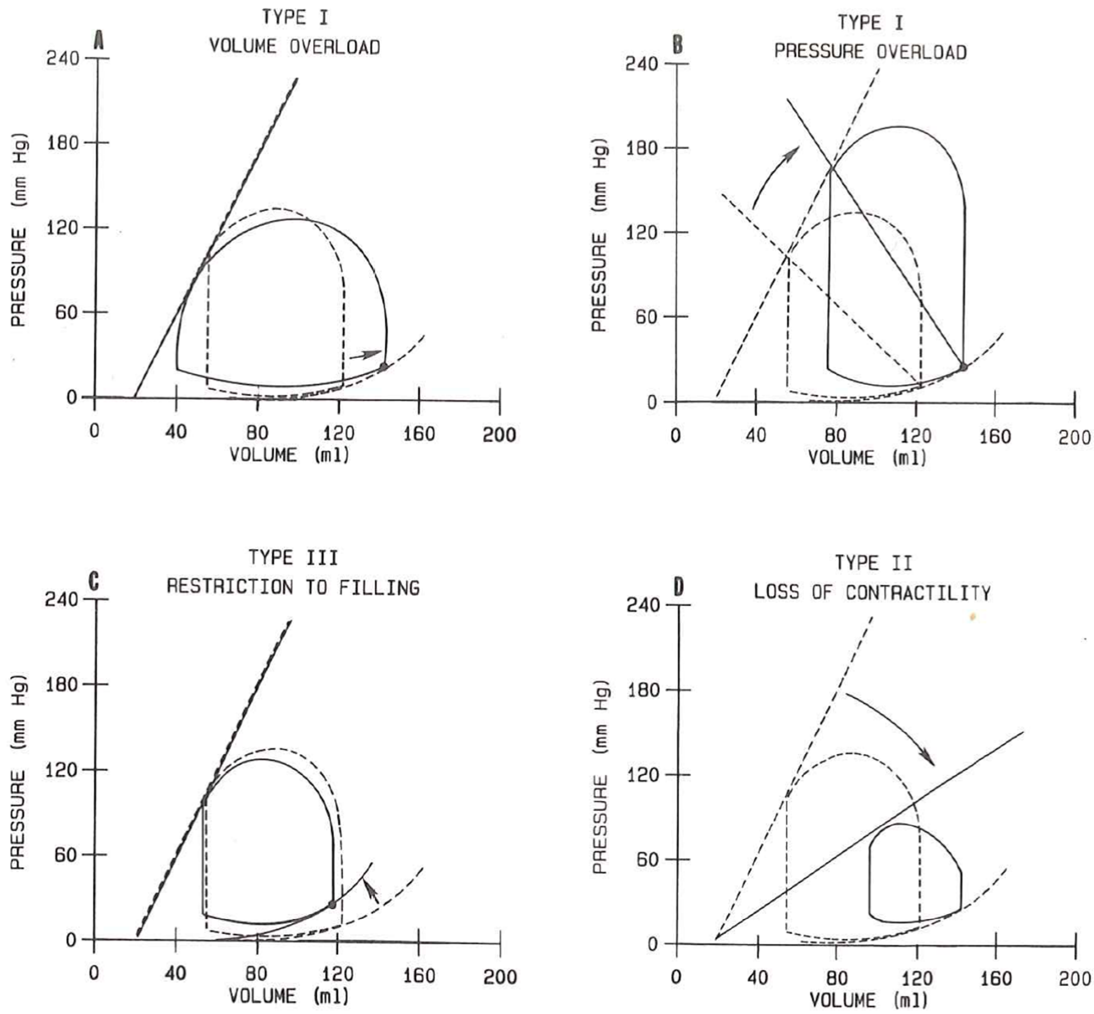

Figure 1-16:*PV loop diagrams representing the three main types of heart failures (solid line PV loops) compared with a physiological PV loop (dashed line PV loops). A) PV loop in case of type 1 failure due to volume overload; B) PV loop in case of type 1 failure due to pressure overload; C) PV loop in case of type 2 failure due to restriction to filling; D) PV loop in case of type 3 failure due to loss of contractility.*

1.4.6.2 Application of PV loop on IABP therapy

The graph (Figure 1-14) reporting ventricular pressure and volume throughout cardiac cycle can highlight information on ventricle working conditions and consequently address issues related to increased afterload or abnormal stroke volume and ventricle volume conditions. As already described, IABP therapy aims at reducing aortic pressure just before systolic phase by removing volume from the aorta, hence reducing afterload for the next left ventricular ejection. This can result in the left ventricle ejecting a greater stroke volume at a lower pressure working level [121].

The PV loop shown in Figure 1-16 B is related to a type 1 heart failure due to pressure overload, and presents an increased end diastolic pressure. This is normally due to pathological conditions such as systemic hypertension or aortic stenosis, and IABP therapy can be beneficial particularly for this condition. Left ventricular volume and end diastolic pressure have been demonstrated to decrease in patients treated with IABP, whereas cardiac output, ejection fraction and coronary flow may increase [122, 60].

Schreuder et al. [121] conducted a study focusing on establishing the effect of IABP inflation and deflation timing errors on the ventricular function, through means of left ventricular PV loop. Pressure and volume were measured through a cardiac function analyser which uses a conductance catheter to measure ventricular volumes, based on measuring time-varying electrical conductance of 5 to 7 ventricular blood segments, delineated by selected catheter electrodes. It was shown that if correctly used IABP produces immediate and physiological effects (Figure 1-17) within the first 4 beats. Inflation augments aortic diastolic pressure and reduces left ventricular end-systolic pressure and volume, improving stroke volume and reducing left ventricular stroke work.

Not only Schreuder al. [121], but also Barnea et al. [36, 96] and Cheung et al. [69] concluded that afterload reduction was the primary mechanism by which IABP improved left ventricular performance immediately because metabolic effects due to possible changes in coronary flow and cardiovascular compensatory reflexes can be excluded in this time frame.

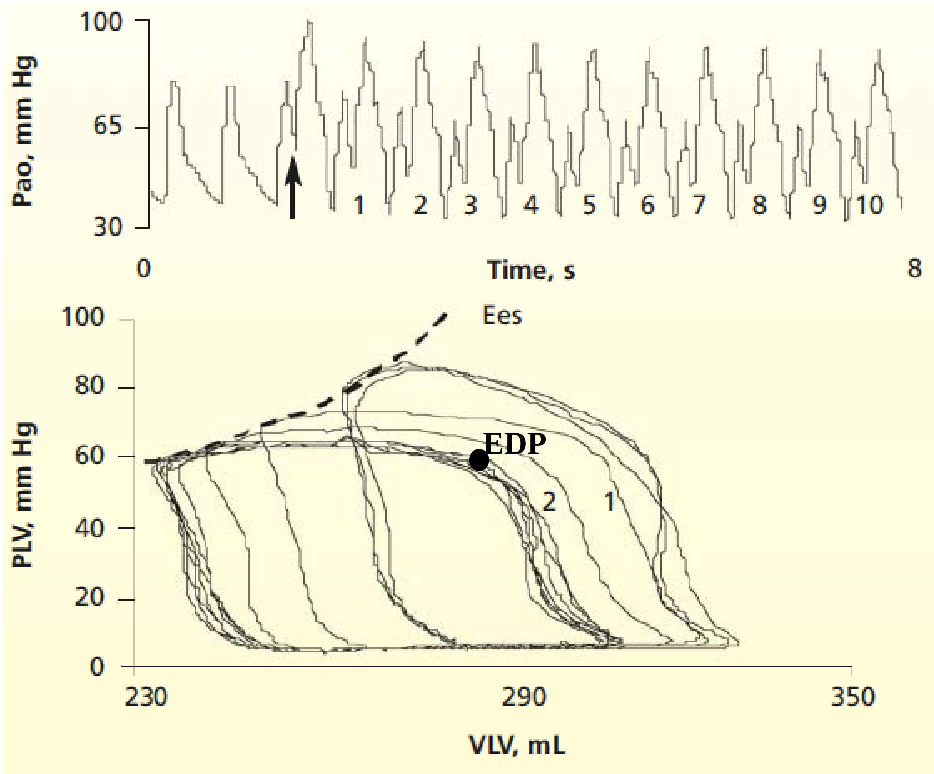

Figure 1-17: *PV loop and arterial pressure (Pao) show the immediate and beneficial effect of a properly used intra-aortic balloon counterpulsation on left ventricular function. The effect of the intra-aortic balloon pump is seen on the first beat of counterpulsation (1) and has reached its full effect within 4 beats. The shift of the pressure-volume loop down and to the left indicates a reduction in left ventricular work, whereas a widening of the pressure-volume loop indicates an increase in stroke volume [121]. The point EDP represent the end diastolic pressure, reduced in case IABP is counterpulsating.*

Furthermore it can be noticed that IABP therapy is related to a different effect on the stroke volume according to the contractility state of the ventricular muscle, represented by the dashed line with slope end-systolic elastance (Ees), in Figure 1-17. Schreuder et al. [121] concluded then that the largest increase in stroke volume due to IABP therapy occurs in patients with lowest contractile state, because this would be associated to a less steep Ees slope.

Errors in IABP timing, discussed in the previous paragraph, can introduce serious effects on the working condition of the left ventricle. These are in fact enhanced by the PV loop, which relates the non optimal IABP inflation and deflation onsets to the working conditions of the left ventricle. Examples are indicated in Figure 1-18 and 1-19, in relation to early inflation and late deflation visible effects on the PV loop. An abrupt increase in left ventricular afterload, as a result from increased aortic impedance, induced premature closure of the aortic valve and impaired left ventricular ejection with decreased stroke volume. In the second case late deflation caused increased end-diastolic aortic pressure and aortic impedance: this error first increased left ventricular afterload during early ejection, and afterwards reduced afterload due to IAB deflation. From the graph it is also possible to observe an increase in end diastolic pressure and decrease in ventricular stroke volume in case of early inflation, and an increased stroke volume in case of late deflation.

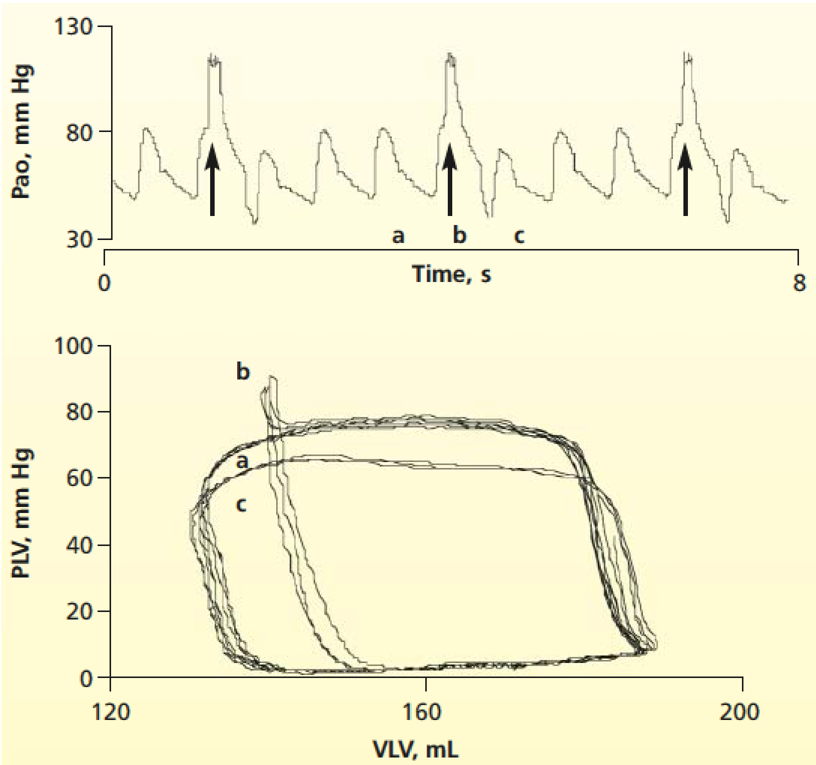

***Figure 1-18**: Effect of early inflation (arrows) of the intra-aortic balloon on PV loop and aortic pressure (Pao). The effect of early inflation (b) is shown on the pressure-volume loop by premature closure of the aortic valve (a) and reduced stroke volume (c)* [121].

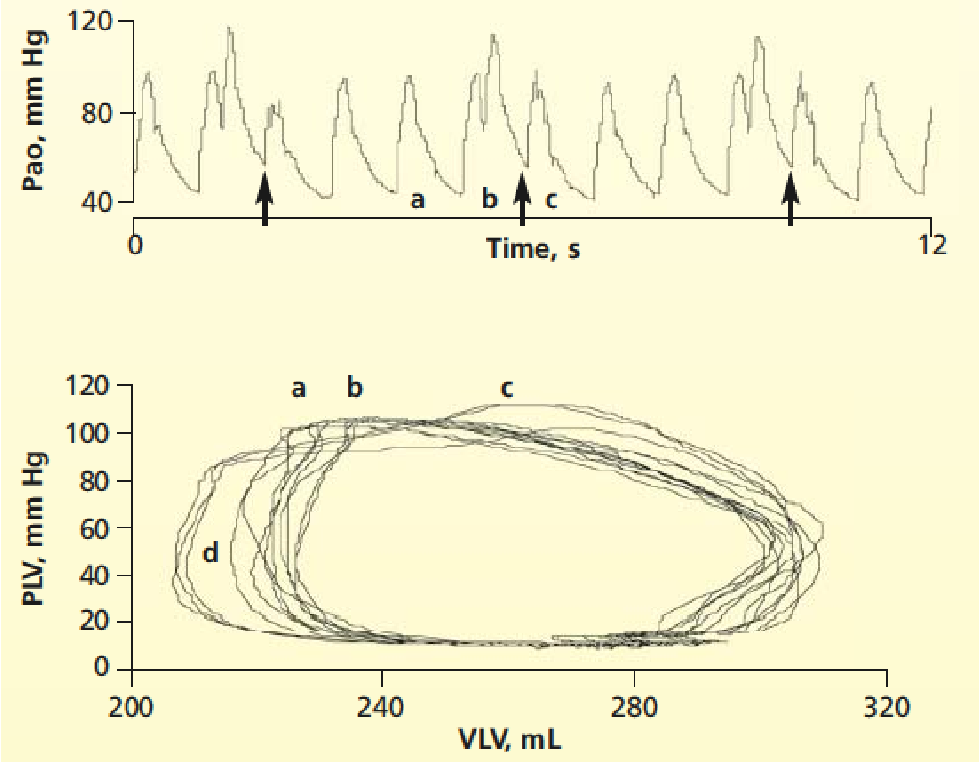

***Figure 1-19**: PV loop and arterial pressure (Pao). Late deflation is shown by arrows on the Pao waveform. Late deflation has a 2-part effect. First, the aortic valve opening pressure is elevated (c on the PLV plot), increasing myocardial oxygen demand at the end of isovolumetric contraction. However, active deflation of the intra-aortic balloon pump during systolic ejection reduces left ventricular work. The effect on stroke volume varies: stroke volume can increase slightly (d on the PLV plot), or consistently (d on the PLV plot), demonstrating that the hemodynamic impact of late deflation on stroke volume is variable.*

The PV loop can hence indicate whether IABP therapy is inducing a positive or negative effect on the ventricular function, allowing visualization of the effects of correct IABP timing in a range of patients with different heart diseases and ventricular contractilities and demonstrating a different increase in stroke volume in relation to different ventricular muscle contractilities. In addition the PV loop can show the quantitative effect of an error in IABP timing, as early inflation or late deflation, on the ventricular functions: indeed it highlights an impairment in left ventricular ejection and relaxation due to afterload increase during the second part of ejection, for early inflation, and increased stroke volume due to increase in afterload during early ejection and rapid afterload decrease during late ejection, for late deflation. Chapter 5 will relate to part of the features of the PV loop to enhance the positive effect of the developed and analysed IAB amended designs.

1.5 Changes in IAB technology

For maximizing the potential benefits of the IABP technique a variety of amendments to the IAB design have been studied by researchers in the past years. An amendment on IAB internal catheter design was developed by Skinner et al. [39] , with no changes on the design of the balloon. The modification was performed to maximize the balloon blood displacement towards the coronary circulation. The catheter within the IAB chamber was tapered from the bottom towards the tip, for the gas velocity to increase and dynamic filling pressure to be lower at IAB tip: this would result in the balloon to start inflating from the base to the tip.

In 1968, Brown et al [40] after initial encouraging results from previous studies [41], aimed at increasing coronary blood flow and decreasing left ventricular afterload through the design of a double chamber balloon, consisting in a top chamber placed in the ascending aorta followed by a rear chamber located in the descending aorta, as depicted in Figure 1-20. This balloon was compared with a standard balloon on 12 dogs in both normal condition and, afterward, with induced hypotension. By comparison the double balloon produced a 50% greater improvement in the measured indices of successful ventricular assistance such as systolic pressure reduction, aortic mean diastolic pressure elevation and ratio of circumflex coronary flow to tension-time index.

Later on, in 1972, Robert T. Jones [42], reviewed hemodynamic phenomena arising in connection with the use of artificial blood pumping devices. He described the potential advantage of a multi-chambered balloon in order to avoid the "trapping phenomena" which appeared in their simulation model, according to which the IAB would inflate first at both ends occluding the mock aorta and the passage of blood towards both directions.

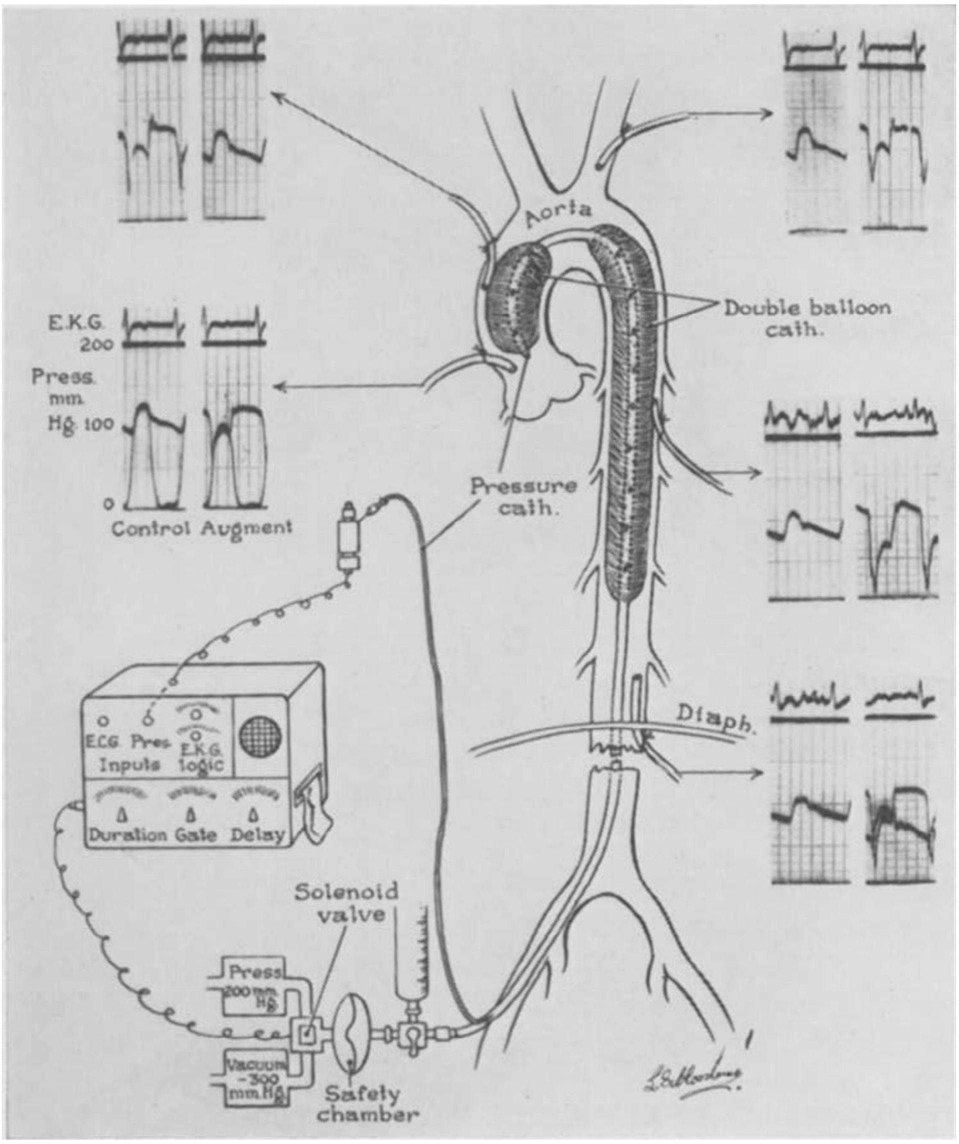

Figure 1-20: *The amended Intra-aortic balloon (IAB) introduced by Brown et al. is depicted above. It consisted of two chambers, the top one positioned just above the aortic root and the bottom one placed in the descending aortic tract (taken from Tatar et al.*[40]*).*

However practical studies focusing on this concept were conducted by first Buckley et al. [43] and Bregman et al. [44,45], and then Bai et al. [46]. This last work, through both computational simulations and experimental physical tests, presented an improved performance of a multi-chamber balloon (shown in Figure 1-21). One, two and three chambered balloons were tested computationally by using a compartment model and physical tests were conducted on single and dual chambered balloons produced in the researcher's laboratory. Simulations showed that dual and three chambered balloons induce a higher benefit to the mean diastolic pressure, coronary blood flow and end diastolic pressure, due to inflation which started at the rear chamber and progressed towards the top, with deflation moving in the other direction.

Also, the computational study investigated the effect of each chamber volume in relation to the total balloon volume and of each chamber radius, observing that for optimized results the rear chambers should be associated to smaller volume and higher radius. Physical tests confirmed the results of the simulations and suggest that an optimally controlled and structured multi-chambered balloon may have applications in IABP clinical treatment [46]. Unfortunately clinical tests on patients are lacking and the differently designed balloon has not yet been introduced to the IABP market.

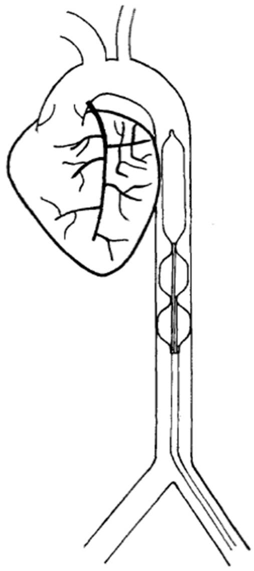

Figure 1-21*: Bai et al. tested a multi-chamber IAB, represented above, consisting of two chambers or three chambers whose filling could be controlled selectively, placed in the descending aorta (taken from Bai et al.*[46]*).*

Anstadt et al. [47] considered that a further benefit in IABP therapy could be achieved by placing a valve distally to the balloon, to avoid retrograde flow, inducing an optimal systolic unloading during balloon deflation. This type of IABP has been tested both ‘in vitro’ and on animals. In the former case the most affected parameter was the displacement of volume from the aortic root and upstream circulation during balloon deflation, which was twice higher in case of the valve endowed balloon compared to the standard balloon. In the latter case, instead, the presence of the valve showed to markedly affect the femoral pressure, and induced an effective benefit to the peripheral circulation caudal to the balloon. Following the authors suggestion the use of a valve in the tip of the IAB in order to reduce retrograde flow also during balloon inflation, would maximize the flow towards the aortic root and coronary arteries. Images of the IAB with distal valve on the top end and on the bottom end, the so-called umbrella balloon, are indicated in Figure 1-22.

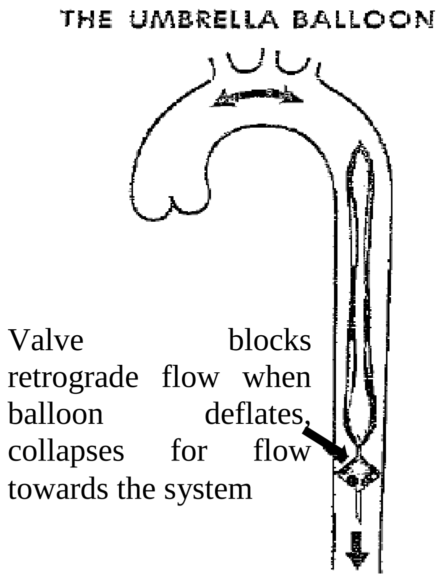

Figure 1-22*: The umbrella balloon, placed in the descending aorta, is shown above. The valve placed on the bottom of the IAB aims at containing the flow from the systemic circulation in order to improve the effectiveness of the balloon deflation (taken from Anstadt et al.*[47]*).*

After several attempts [48-50], the latest study focusing on comparing IAB counterpulsation on the ascending and descending aorta, in 2000, was led by Meyns et al. [51]. They reported a study focused on animal testing of an ascending aortic balloon (ICS), placed in a position similar to the one of the balloon designed by Brown et al. in 1968, comparing the results with the standard descending aortic balloon pump (IABP). The differently shaped balloon is shown in Figure 1-23.

Both balloons have undergone animal testing on sheep, whereby coronary flow was reduced by 50% to simulate stenosis, and data of diastolic augmentation, myocardial blood flow and cerebral and peripheral organ perfusion were collected. The ICS balloon induced a significantly higher peak diastolic aortic augmentation compared to the IABP and an increased myocardial blood perfusion, with no significant change in cerebral perfusion or peripheral organ perfusion. However the degree of complication caused by vascular access and dislodged plaques in the ascending aorta is not yet available, and with no further studies involving humans being conducted, the ICS has not as of yet been delivered on the market.

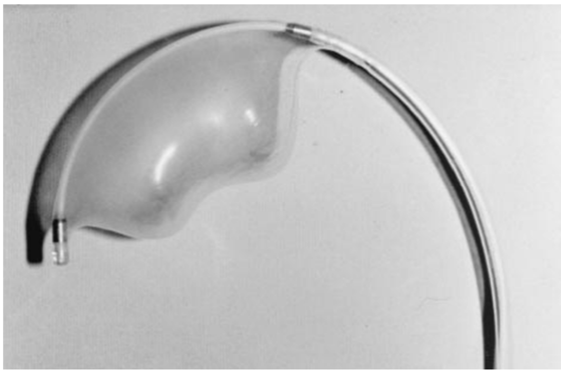

***Figure 1-23**: Above shown the differently shaped IAB designed and tested by Meyns et al.. The positioning of the IAB is equally unconventional as it is placed, as the shape itself suggests, in the aortic arch (taken from Meyns et al.[51]).*

A radically different design has been proposed by Bian and Downey [52], who compared a standard IABP with an enhanced one (EIABP), presenting one further inflatable balloon connected to the arterial circulation by a catheter passing axially through the internal standard IAB, as shown in Figure 1-24, inducing further augmentation in diastolic pressure and increased systolic unloading. The test studied the two systems on six adult dogs, and discovered improved performance of the amended balloon, compared to both standard IABP therapy and no treatment condition. In most of the analyzed cases concerning heart rate, peak of left ventricular pressure and systolic aortic pressure decreased and diastolic aortic pressure and coronary blood flow increased when the EIABP was used instead of the IABP [52] (2002). No in vivo studies have been published and the EIABP is not available on the market.

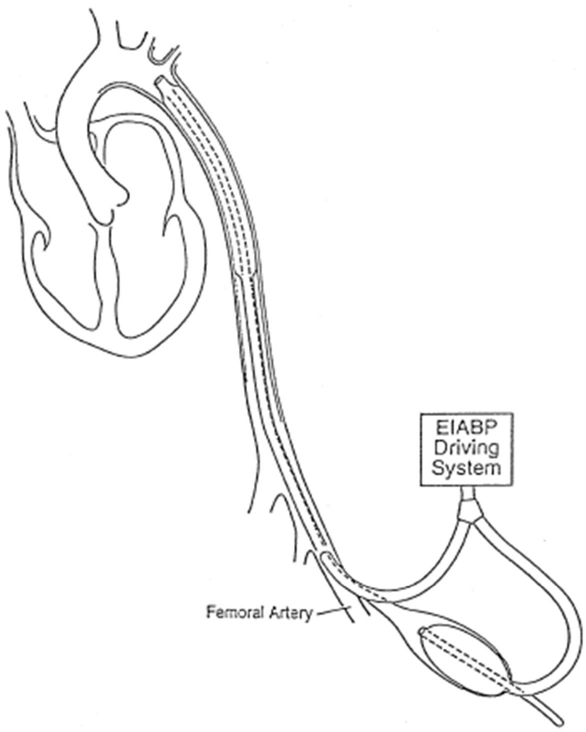

Figure 1-24: *A representation of the EIABP. The IAB is provided with a further external balloon which could further augment the aortic pressure due to its counterpulsation* [52].

1.6 IAB pump technology

A schematic representation of the IAB pump is shown in Figure 1-25, with related working mechanism. The pump is connected through cable and one-way valves to both, balloon and Helium box: it induces IAB inflation through pushing, and induces IAB deflation through reaching the original configuration [33].

As already mentioned above, the pressure signal can be used as a trigger for balloon inflation and deflation, implicating a time calculation based on the pressure waveform. The pressure is measured either through a fluid filled catheter that passes through the IAB and interfaces by an open-end with the fluid within the aorta, or through a fibre-optic sensor placed on the tip of the balloon. The latter has been introduced recently in order to improve the quality of pressure measurements and to avoid the delay of the tracked pressure due to water filling up the cable connecting pump and balloon.

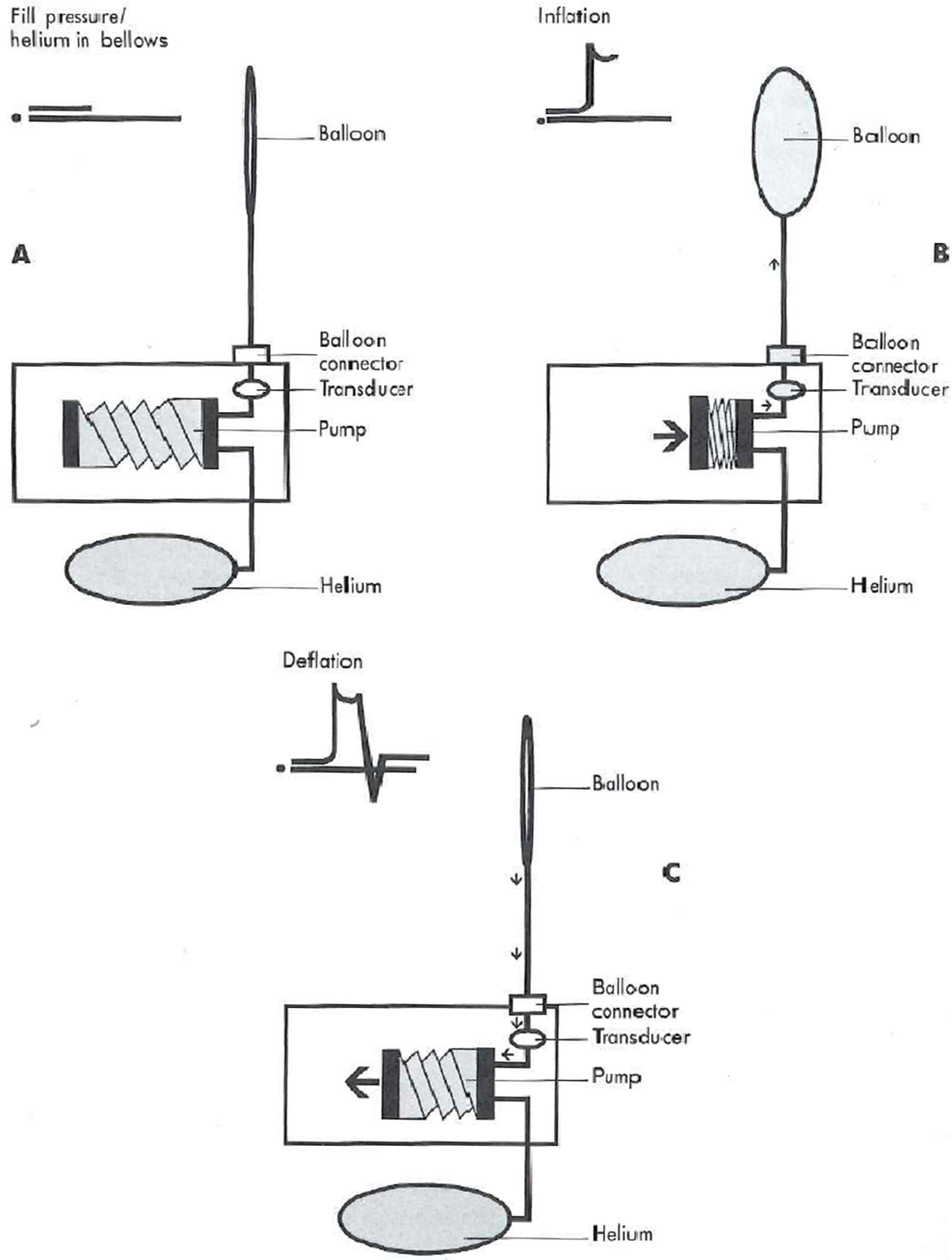

Figure 1-25*: The working mechanism of the pump inflating and deflating the IAB: A) pump at the starting configuration, with corresponding static pressure measured by the transducer. B) pump inflating the balloon and the related step in pressure, while in C the pump withdraws Helium from the IAB chamber, hence provoking a decrease in pressure (taken from Quaal et al.[33], 1993).*

The inflation/deflation pattern imposed on the balloon from the pump depends on two main parameters: source signals available and setting imposed. All pumps generally present two main setting options:

- **Manual**: the operator can choose among all available source signals, and is able to set inflation and deflation onset expressed to a certain reference point;
- **Automatic**: the pump itself selects automatically the best signal, chosen according to the signals available and to their quality, and the inflation and deflation onset, also selected according to the nature of the signal for a maximization of the benefit and also for ensuring a safe counterpulsation therapy.

Moreover once the setting is selected, and the source signal is chosen, different algorithms can command the inflation/deflation pattern associated to the IABP. This generally depends on the features of the source signal, and can be summarized into two main groups:

- **Safe counterpulsation**: in case of atrial fibrillation or highly irregular ECG, typical for patients operated with IABP, the safest algorithm is selected, triggering deflation onset based on systolic pressure rise, with the aim of ensuring balloon deflation during systole;
- **Benefit optimization**: in case of regular ECG this option targets the maximization of IABP benefit, calculating the duration of inflation based on the frequency of previous heart beats.

A comparison study (experimental or ‘in vivo’) analysing the advantages and disadvantages of these settings on different pumps and different ECGs has not been reported yet and will be described in Chapter 6.

1.7 Comparison between IABP and LVADs

Thiele et al. [53] compared the TandemHeart with the IABP. The primary end-point of the cardiac power index, calculated by Williams et al. [54] as the product of cardiac index and mean arterial pressure, was more effectively improved by the TandemHeart compared with the IABP support, and led to improved renal function. On the other side, complications like severe bleeding and limb ischemia were encountered more frequently after TandemHeart support, whereas the 30-day mortality was similar to the one shown by IABP therapy. So the authors concluded that hemodynamic and metabolic parameters could be reversed more successfully by the TandemHeart than by standard treatment with IABP, but more complications were encountered with TandemHeart, maybe because of the highly invasive nature of the procedure and the extracorporeal support [53].

Also Burkhoff et al. [55] compared the safety and efficacy of these two devices; The TandemHeart achieved significant increases in cardiac output, and mean arterial blood pressure, which was associated with considerably greater decreases in pulmonary capillary wedge pressure. On the other side IABP showed a slightly lower 30-day mortality compared to the TandemHeart, even if the frequency of severe adverse events occurring in patients with the TandemHeart is 130% against 120% for patients with IABP device.

Seyfarth et al. [56] compared the Impella device (LVAD) with the IABP to evaluate the hypothesis that the Impella provides better hemodynamic support in patients with cardiac shock caused by myocardial infarction. Hemodynamic improvements after 30 minutes from implantation were greater in patients with the Impella than in patients with the IABP. The same result is achieved for the mean arterial pressure and diastolic arterial pressure. The authors also measured organ dysfunction and after a period of 30 days results were similar for both cases, as was the 30-day mortality. Patients with the IABP showed better outcomes related to adverse effects such as need for transfusion of red blood cells, worsening of renal function and haemolysis.

Moreover one further study, PROTECT II, led by O’Neill et al. [57], aimed at analysing the 30-day incidence of major adverse events in case of the Impella 2.5 (n = 226) and the IABP (n = 226) were used for support in 452 symptomatic patients with complex 3-vessel disease or unprotected left main coronary artery disease. The outcome was a statistically non-significant difference between IABP or Impella 2.5 hemodynamic support, even though improved outcomes were observed in case of patients supported with the Impella 2.5 after 90 days.

1.8 Current gaps with IABP therapy

Even though many different studies have been conducted on the IABP, some of which have been indicated in the above paragraph, the design of the IAB has not undergone marked change throughout the latest 40 years since its introduction to the market. One important consideration for IABP counterpulsation performance concerns the position of the balloon. Most patients using the IABP are nursed at a semi-recumbent position to avoid respiratory complications [58], [59] and to further stimulate atrial emptying. Specifically Lorente et al.[59] suggested that the position of the patient should never be minor that 10°. Khir et al. [63] however reported a reduction in the benefits of the therapy when the IABP is operated at an angle to the horizontal. In fact both inflation and deflation phases have shown to be compromised in case of a semi-recumbent position. Kolyva et al. [61] examined the volume displacement by the IAB inflation towards the coronary circulation in a mock circulation and in patients. She concluded that the volume displaced towards the coronary circulation consists of a significant fraction of baseline coronary flow, and consequently that a balloon that can displace more volume towards the ascending aorta during inflation or not be affected by the operating angle would be advantageous and highly desirable. On the other hand the evidence of a decreased end diastolic pressure in the case of IAB therapy suggests, as stated before, a decreased myocardial oxygen consumption, hence also in this case reducing the influence of angle on IAB deflation performance would be markedly beneficial. Nonetheless previous studies [62],[63] concentrated more on inflation and did not focus on deflation phase. Information in the literature regarding the loss in balloon performance during deflation is then incomplete or not investigated.

While several studies on IAB aimed at a deeper understanding of the mechanics involved with the use of the device [42],[64],[65],[66],[63], the information available is still not clear and complete on the inflation and deflation mechanisms and dynamics, as well as the fluid dynamics in the surroundings of the IAB during its movements. Further details are thus required and may highlight the rationale for new designs using a different shape or technology of the IAB.

Furthermore, as described before, balloon inflation and deflation onset influences importantly the performance of the IAB and consequently the hemodynamic parameters. Hence it is important that these timings are properly set also taking into account the delays between the onset command and the actual balloon inflation and deflation. Especially in case of arrhythmia and high heart rate, as present for many of the patients undergoing IABP treatment, if balloon inflation and deflation are not controlled adequately the hemodynamic results could be critical.

1.9 Aims of the thesis

The main aim of the work presented in this thesis is to improve the efficacy and clinical outcome of the IABP therapy through experimental investigations. Specifically the objectives through which the aim of the work is met are as follows:

- Understanding of the mechanics associated with balloon inflation and deflation, both at a horizontal and at an angled position. The objective is to obtain a scientific explanation providing reasons to the loss in inflation and deflation benefits of the IABP at a semi-recumbent position.
- Investigate the effects of different balloon's shapes, developed for maintaining IAB performance at an angle, on pressure waveform and, through extending the results found, to the patient clinical condition. Both standard cylindrical and tapered balloons are tested experimentally in the same conditions resembling different patients' posture from horizontal to angle of 45°, and a simplified theoretical approach is provided in support of the experimental results found.
- Investigate balloon timing and effectiveness through a comparison study between different settings on two pumps currently on the market in response to different regular and irregular ECGs, to address the appropriate clinical use of the IABP for patients characterized by different pathological conditions.

In addition a pilot computational model was developed for providing an insight on the flow and pressure distribution around the balloon and of the counterpulsation effect on the main segments of the arterial tree, which could be used for investigating different IAB shapes.

1.10 Thesis outlook

Chapter 2: General experimental methodology

This chapter provides information on the accuracy and calibration of the experimental equipment used, and on the statistics used for the analysis of the results presented in the experimental studies (Chapter 3, 4, 5, 6).

Chapter 3: Measurements of Intra-Aortic Balloon (IAB) wall movements during inflation and deflation: Effects of angulation

This chapter introduces the visualization study of the IABP, performing both balloon wall movements and pressure measurements along the IAB, at a horizontal and angled position, to obtain a scientific rationale to the loss in inflation and deflation benefits of the IABP, at a semi-recumbent position.

[This work was published by “Artificial Organs”: Bruti G., Kolyva C., Pepper J.R., Khir A.W. Measurements of Intra-Aortic Balloon (IAB) wall movement during inflation and deflation: Effects of angulation. *Artif Organs*. 2015.]

Chapter 4: Changes in Intra-aortic balloon shape induce changes in IAB performance

New tapered balloons are tested together with a standard one, under the same conditions, resembling different patients’ posture from horizontal to an angle of 45°. The main parameters of interest for comparing the IABs are the volume displaced upstream over total balloon volume and the deflation pressure pulse.

[This work was published by “Artificial Organs”: Khir AW, Bruti G. Intra-aortic balloon shape change: Effects on volume displacement during inflation and deflation. *Artif Organs*. 2013.]

Chapter 5: Experimental study of novel shaped balloons for improved performance on a physiological test-bed

As a further step for investigating the effect of balloon shape changes on IABP benefits 6 different shapes of the balloon, with a cylindrical and a tapered portion, are compared with the standard one in a test-bed characterised by a physiological pressure waveform.

Chapter 6: Influence of pump setting modes on IAB inflation and deflation timings in an experimental set-up

In this chapter the effect of using different pumps and different pump settings are related to changes in pressure waveform characteristics, with the aim of defining a better configuration (pump and setting) for the optimization of IABP benefits.

Chapter 7: Multi-dimensional computational study for simulating balloon inflation and deflation in a physiological system

The developed multi-dimensional model for the study of the fluid-dynamics associated with the counterpulsation therapy is described and results are presented and compared with 'in vivo' measured data.

Chapter 8: General discussion

The main findings related to the conducted experimental and computational studies are summarized and discussed, underlying their importance and the implications on the clinical environment.

Chapter 9: Conclusions and future steps

The final chapter contains the last considerations and discuss the met targets described above, addressing further works to reinforce the obtained results in the light of a next clinical application.

Chapter 2 General experimental methodology

Throughout the experimental studies presented in this work (Chapters 3, 4, 5, 6), several instruments and measuring devices were used for assessing the fluid-dynamics associated to the counterpulsation of the IABP. This paragraph aims at providing information on the accuracy of the instrumentation used, by presenting their calibration data and repeatability of the measurements obtained.

2.1 Experimental equipment accuracy

2.1.1 Pressure transducers and flow probes calibration and accuracy

All pressure transducers and flow probes used in the experimental studies (Chapters 3, 4, 5, 6) have been calibrated before each use, in order to ensure the accuracy of the measurements and to verify the linearity of the relationship between the measurements from the equipment and the actual pressure and flow values. Below are reported calibration lines for all pressure transducers and flow probes used throughout the experiments.

All flow probes were calibrated using the timed collection technique at 15 different flow rates to obtain the calibration equation for the flow probe. The pressure transducers were calibrated using the column of fluid method at 4 different pressures, recorded to obtain the calibration equation for each transducer. Both flow and pressure were calibrated in a physiological range of human aorta. Flow probes have been calibrated through a higher number of measurements, compared to pressure transducer, because of a higher variability in measurement for any given flow.

Typical calibration lines are provided in Figure 2-1, for pressure transducers, and in Figure 2-2, for flow probes. For all the calibration lines presented, the R-squared value is higher than 0.99, demonstrating the excellent reliability of the measurements from the instrumentation used.

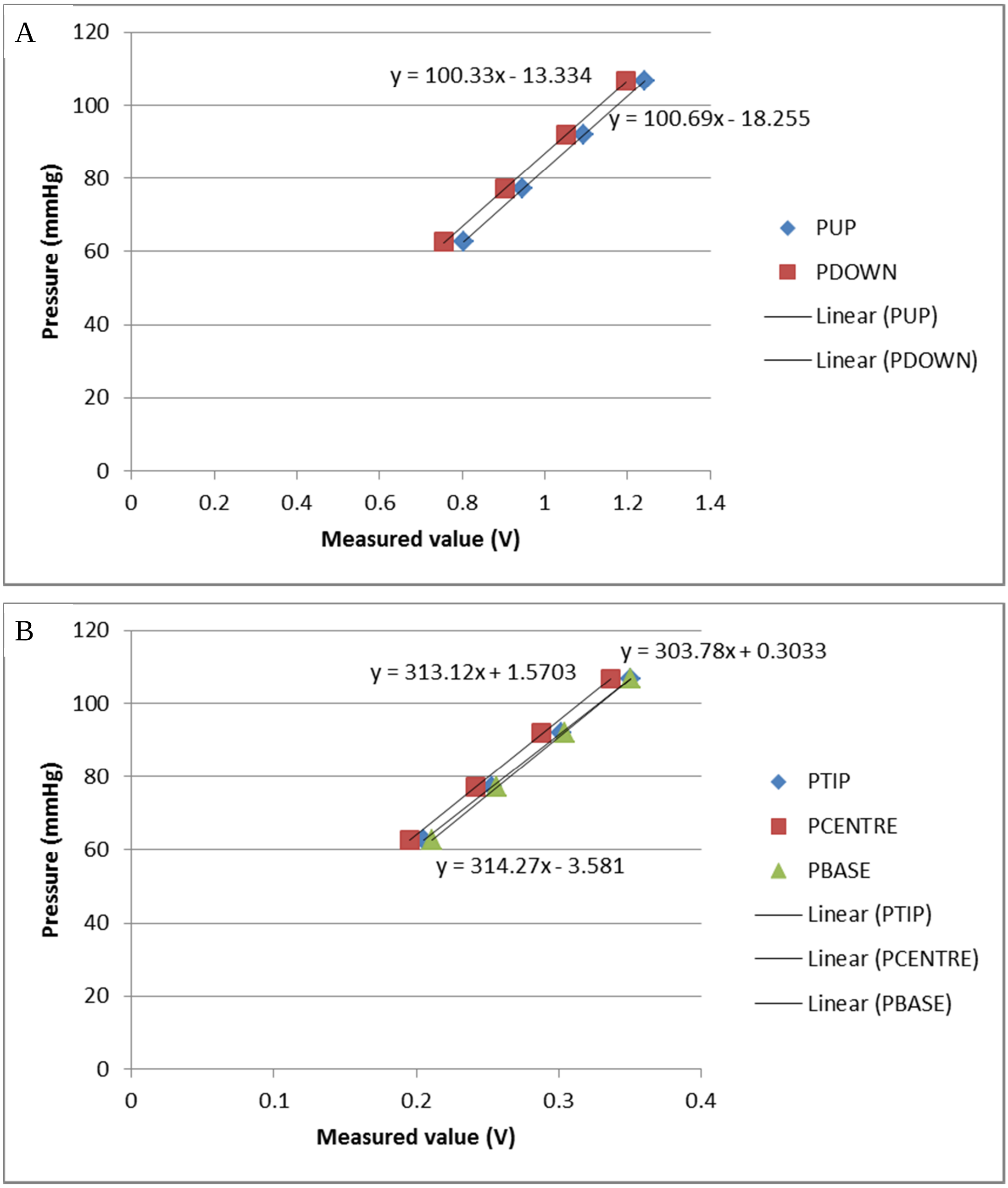

***Figure 2-1**: Pressure transducers calibration. A) calibration of single transducer pressure catheters (PUP and PDWON); B) calibration of a three transducers pressure catheter (PTIP, PCENTRE and PBASE).*

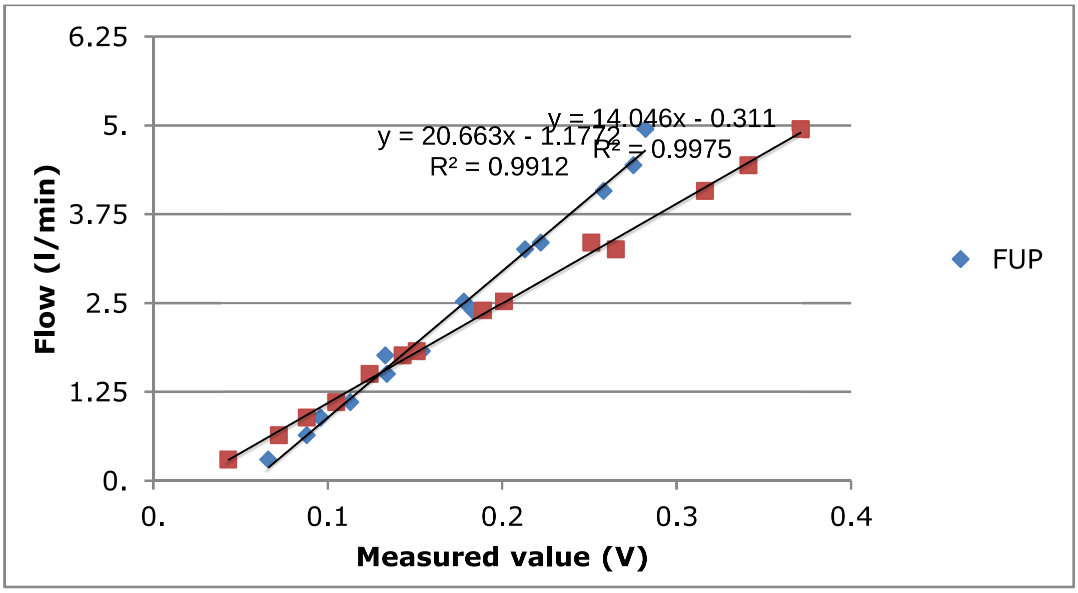

***Figure 2-2**: Flow probes (FUP and FDOWN) calibration shows an R^2 value higher than 0.99.*

Furthermore pressure transducer and flow probe measurements repeatability was verified through comparing different IABP beats measured in identical set-up and conditions. Results are presented in Figure 2-3, for both pressure and flow.

A

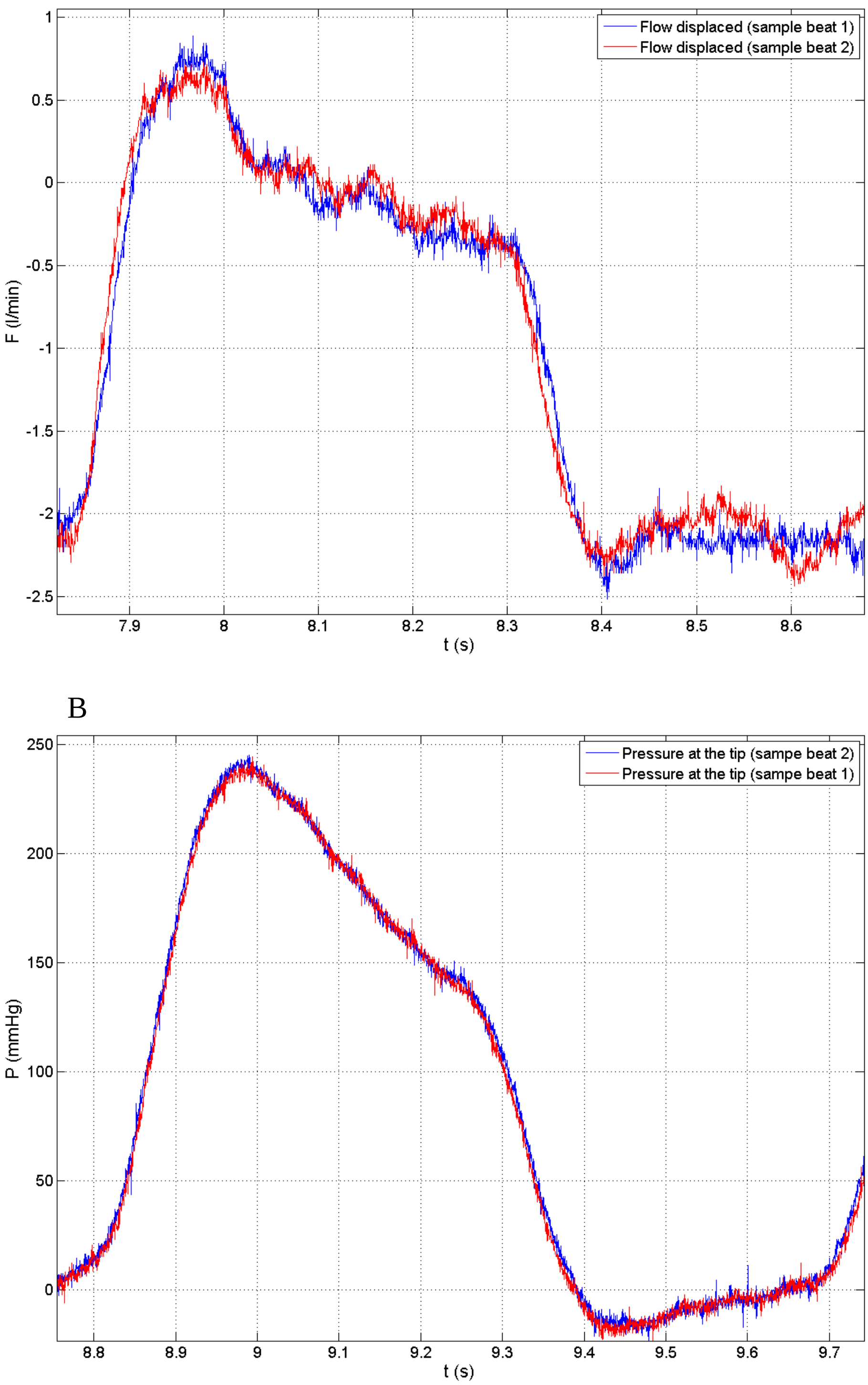

Figure 2-3: *A) Measured flow and B) measured pressure during two IABP beats pulsating in the same set-up. Both flow and pressure measurements show good repeatability for the two IABP beats analysed.*

2.1.2 IAB diameter calibration and accuracy

IAB diameter measurement (Chapter 3) accuracy depends on the calibration accuracy and on the resolution of the images captured by high speed camera during IABP pulsation. The calibration was performed through the measurement of a reference known diameter and by taking into account the effect of light refraction through the silicone rubber tube filled up with water, where the recorded IAB pulsated. This second factor was quantified through recording and measuring the size of a rigid object of known dimension. The correction factor for the refraction of the light in this set-up was 1.08.

To further verify the accuracy of the refraction coefficient calculated, it was measured the size of objects characterized by different known dimensions within the silicone rubber tube filled up with water. In this way it was possible to highlight the difference in light refraction for any IAB configuration: deflated, partially inflated or totally inflated. The diameters of the three objects were as follows:

A = 19.10 mm

B = 8.10 mm

C = 5.20 mm

Measurements through ProAnalyst resulted in the following values:

A = 20.68 mm

B = 8.41 mm

C = 5.25 mm

The diffraction correction coefficient results in 1.08 for object A, 1.04 for B and 1.01 for C. The use of 1.01 instead of 1.08 on the minimum diameter results in maximum 7% error.

The spatial resolution of the recorded image depends on the acquisition resolution of the high speed camera and on the size of the recorded window. As the resolution of recorded image was 800x600 pixels, the spatial resolution achieved was calculated as 0.004 cm. In Chapter 3 the smallest recorded diameter is close to 0.8 cm, while the smallest significant difference in diameter indicated is 0.15 cm. The spatial resolution (0.004 cm) represents 0.5% and 2.7%, respectively, of these values, highlighting the significance of the results presented in Chapter 3. Furthermore all average values and standard deviations are reported to the second decimal of cm. Repeatability of the diameter waveforms is also provided in Chapter

3, through reporting the standard deviation of the diameter (5 measurements taken) during the counterpulsation cycle.

2.2 Statistical analysis

Throughout experimental Chapters (3, 4, 5, 6), results are indicated as mean values ± standard deviation. T-student test two-tailed was used for the calculation of the p value. Values of $p < 0.05$ were considered statistically significant, $p > 0.05$ and < 0.1 were considered statistically low significant and > 0.1 were considered statistically non significant.

Chapter 3 Measurements of Intra-Aortic Balloon (IAB) wall movements during inflation and deflation: Effects of angulation *

3.1 Chapter outlook

It has already been exposed, in the literature review, the negative effect of placing the balloon at a semi-recumbent position. There is poor information in regard to quantitative changes in balloon diameter during counterpulsation at the horizontal and angled positions. Measurement of balloon diameter throughout its counterpulsation cycle can provide further explanation regarding its different inflation and deflation mechanism at the two positions. In this chapter balloon counterpulsation will be investigated, at a horizontal and semi-recumbent position, through the analysis of the IAB wall movements in combination with pressure changes in the fluid surrounding the balloon, with a particular focus on the deflation phase, which has been less studied in previous works.

3.2 Introduction

Although the IABP has been widely used in the clinical practice for more than 40 years and many studies have been conducted for the improvement of the device, the mechanics of balloon inflation and deflation are still not well understood. Of particular relevance is the issue of IABP decrease in performance when operating at a semi recumbent position (performed to avoid respiratory complications), which is the preferred position to avoid respiratory complications [58, 59], and to enhance atrial emptying. Specifically Lorente et al. [59] suggested that the position of the patient should never be less than 10°. Even though the position at which the patient is kept can change based on their pathology and respective hospital, a semi recumbent position is indicated for all patients undergoing IABP therapy.

In previous studies Khir et al [67] observed that the angled position might induce reduced performance of the IABP both, in terms of coronary flow and end diastolic pressure. This can be due to the angled position inducing a hydrostatic pressure difference between the tip and the base of the balloon, resulting in the tip to experience higher trans-mural pressure (pressure difference across the balloon wall) and inflate before the base, and in the base to deflate before the tip due to lower trans-mural pressure.

*published: Bruti G., Kolyva C., Pepper J.R., Khir A.W. Measurements of Intra-Aortic Balloon (IAB) wall movement during inflation and deflation: Effects of angulation. *Artif Organs*. 2015.

Previous studies aimed to investigate balloon mechanics through analysing qualitatively its wall movement during counterpulsation [63,65]. Bleifeld et al [65] used a cine-angiographic technique in hydraulic models, at horizontal and vertical positions, and animal experiments in order to obtain knowledge of the inflating and deflating behaviour of standard cylindrical and differently shaped balloons. Through this study it has been determined that the inflation and deflation pattern is pressure-dependent, by demonstrating that, if vertically, the balloon inflation starts at the tip moving towards the base and reversed for deflation, because of the higher surrounding pressure at the base of the balloon. This study also explains that the trapping phenomenon, according to which the tip and the base of the balloon inflate before the rest of the balloon at a horizontal position, disappears when a pressure difference is present between the two ends of the IAB.

Previous studies from our group [62,63,66,68] verified that the fluid volumes displaced towards tip and base of the IABP change with angle; an increase in angle corresponded to a decrease in volume displaced upstream [62,63,66,68] and an increase in volume displaced downstream [63], during inflation. Information obtained about balloon wall movement from the acquired images also enabled the quantification of the duration of inflation and deflation at different angles [62,63]. After separating the contribution of head pressure acting around the balloon from that of angle, it was demonstrated that increasing angle induces an increase in both duration of inflation and deflation [62].

In the above studies a methodical analysis of the deflation process is absent, even though this phase of the counterpulsation cycle is essential in improving the oxygen balance of the heart through decreasing end diastolic pressure, thus reducing left ventricular afterload and therefore lowering oxygen demand. A study focused on the analysis of IAB wall movements during inflation/deflation, supported by flow and pressure measurement, would add important explanations into the changes in fluid dynamics taking place at an angle and elucidate the reasons for the reduction in benefits in this setting.

Hence the overall aim of this chapter is to add to quantifying IAB diameter changes, derived from wall movements, and its effects on hemodynamic parameters during inflation and especially deflation at horizontal and angled positions. The quantification of the balloon movements, if repeated for several beats, can provide consistency to the measurement and, consequently, provide a strong scientific proof for justifying a different performance of the device when it operates at an angle. Therefore the innovative aspects of the current study that will support the required detailed examination of the physical phenomena taking place, will be the measurement of balloon wall movements throughout the counterpulsation cycle at three locations along the balloon, featuring surrounding fluid pressure distribution measurements at the same locations. The study will be focusing on the deflation phase, which has been less studied in the past and deserves a more thorough understanding. In fact, according to Cheung et al. [69] (1996), this might be the main advantage of the IAB, acting for reducing ventricular afterload.

3.3 Material and methods

3.3.1 Experimental set up

The experimental set-up is shown in Figure 3-1. A straight silicone rubber tube (AO) of 2.3cm internal diameter, 40 cm in length and 0.25 cm wall thickness was selected to replicate the aorta. Although the length of the tube was selected to resemble the average length of the aorta, the wall thickness and diameter of the tube were constant along the tube to avoid complications with the visualization technique. The compliance of the AO was measured by inserting a volume of 20 ml of water into the already filled and sealed AO, in 4 steps of 5 ml, and measuring the corresponding pressure change. It was found to be 0.084 ml/mmHg, comparable to the physiological value of 0.11 ml/mmHg measured in the thoracic aorta, reported by Westerhof et al.[70]. The AO was filled with water, and a Linear 40 cc IAB (Datascope, Fairfield, NJ, USA) with a maximum diameter of 1.6 cm and length of 27 cm was placed inside. The AO was placed on a platform, whose angle to the horizontal could be adjusted to resemble different patient postures, and connected to a reservoir. The tubes connecting the AO to the reservoir on the two sides represented the physiological resistances upstream and downstream the IABP, of 84 mmHg*min/L and 26 mmHg*min/L respectively, reported by Khir et al. [67]. These values were implemented experimentally through using tubes of diameter and length according to the relationship presented by Kolyva et al. in 2010 [116]. Physiological compliance distribution, also according to Khir et al., $8*10^{-3}$ ml/mmHg above and $21*10^{-3}$ ml/mmHg below the balloon, was resembled by placing syringes upstream and downstream the IAB. Correspondence between syringes volume and value of compliance was reported by Kolyva et al. [116] during the development of an experimental mock circulation system.

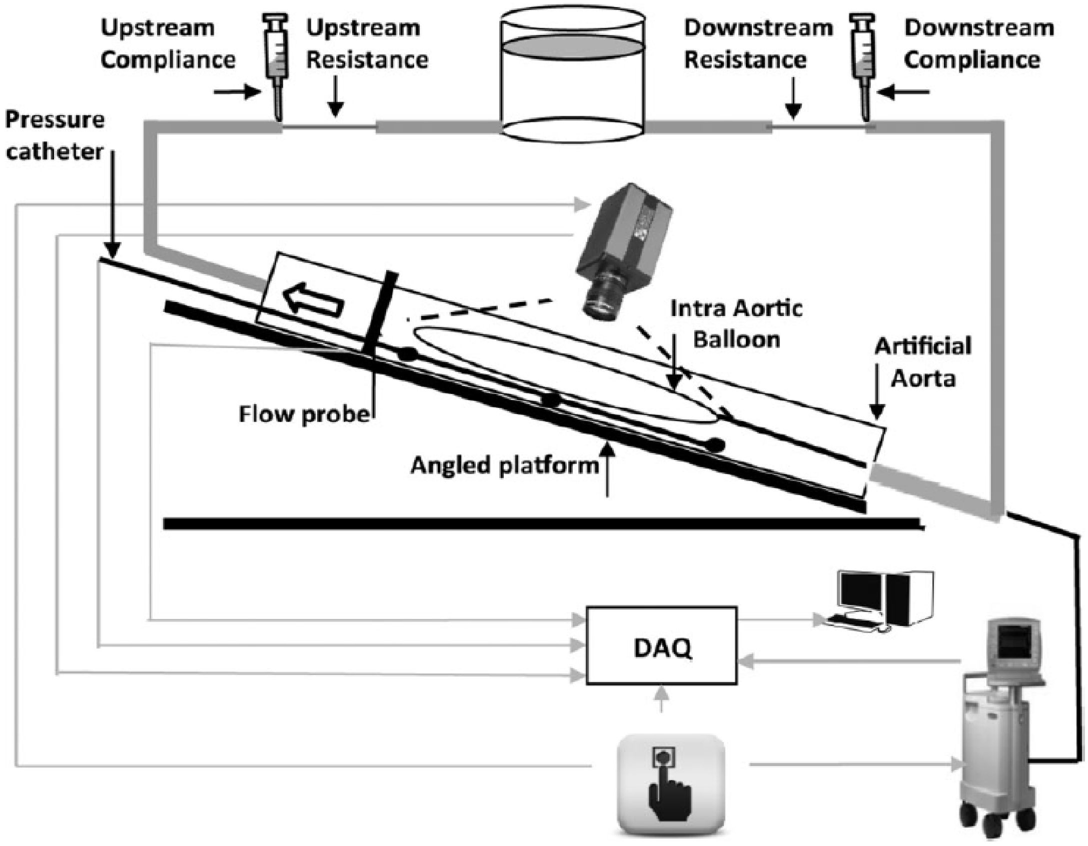

Figure 3-1*: Experimental set up. The reservoir is connected to the silicone rubber tube via two plastic tubes constituting upstream and downstream resistances. The balloon is placed in the middle of the silicone tube. A pressure transducer is placed besides the IAB, measuring pressure on its tip, centre and base, and one flow probe is secured on the upstream tube for measuring the volume displaced and sucked from upstream. Triggering of balloon pump, data acquisition and high speed camera is ensured by the button shown in the bottom of the figure.*

The reservoir provided the initial static head pressure (P_s) of 90mmHg, replicating aortic pressure at the time of the dicrotic notch (generally used as landmark for the onset of inflation). This P_s was achieved using the calculation $P_s=\rho gh$, where ρ is water density (1000 kg/m^3), g is gravitational acceleration (9.81 m/s^2) and h (1.20 m) is the lateral distance between the water level in the reservoir and the centreline of the balloon [62]. For the horizontal and angle 45° positions h was kept constant by raising the reservoir accordingly in order to maintain the same static mean pressure at the centre of the balloon.

The balloon was connected to an IABP (Datascope CS300, Datascope, Fairfield, NJ, USA), which was triggered through a wave generator replicating a heart rate (HR) of 65 bpm to simulate physiological operating conditions. A high speed camera (AOS technologies AG), used for the recording of the balloon wall movement of the longitudinal section of the IAB, at a rate of 500 Hz, was also activated by the pulse generator; in this way the starting of the IABP trigger and the filming of the balloon were synchronized, and enabled the mapping of the recorded signals. Specialized software (AOS Imaging Studio V 2.5.6.1) was used to control the camera and adjust the grey scale and luminosity.

3.3.2 Measurements

A catheter (6 Fr., Gaeltec, Scotland, UK) with 3 pressure transducers was inserted in the AO and positioned along the balloon in order to measure the pressure at 3 sites, tip-, base- and mid-point. The flow rate upstream of the balloon tip was measured through a 28 mm flow probe (28A, Transonic, Ithaca, NY, USA), snug-fitted to the AO at 5 cm away from the tip of the balloon. Un-calibrated Helium pressure and pulse generator signal were recorded to indicate landmarks of inflation and deflation, and accommodate synchronization of all recorded signals, respectively. The latter were acquired at a sampling frequency of 2000 Hz. 10 different experiments were conducted, 5 at a horizontal position and 5 at an angle of 45°, and data of 10 consecutive beats each were recorded during 1:1 counterpulsation using an analogue-digital converter and Labview software (National Instruments, Austin, TX, USA).

3.3.3 Data analysis

3.3.3.1 Filter

A Savitzky–Golay low-pass filter (windows size 51, and polynomial order 2) was used for smoothing the pressure and diameter waveforms. No filter was applied on the flow waveform, since the volume measurements from the flow waveform are not affected by white noise.

3.3.3.2 Pressure and flow data

Flow and pressure waveforms at a horizontal and at an angle of 45°, were analysed off-line using Matlab (The Mathworks, Natick, MA, USA). The inflation and deflation periods were identified, on the flow waveform, as the period between point A to point B, and point B to point C, respectively, as shown in Figure 3-2.

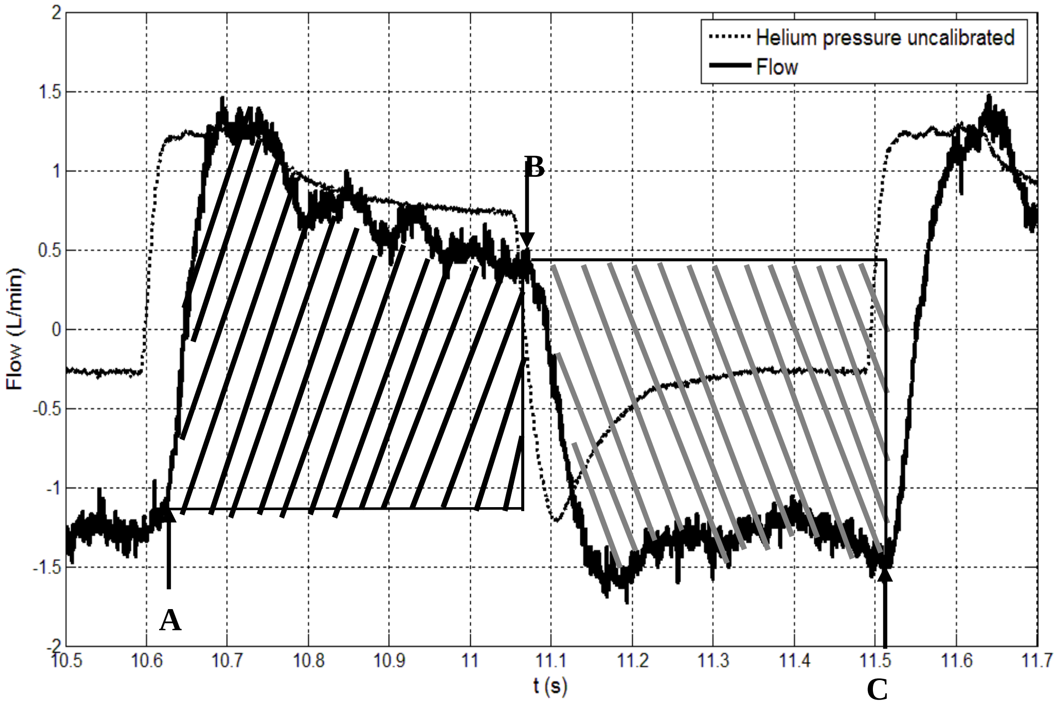

Figure 3-2: *Flow waveforms for upstream (solid black line) and IABP Helium pressure (dotted black line). The area integrated under the solid line between points A and B indicates the volume displaced away from the tip of the balloon during inflation. The area integrated above the solid line between points B and C indicates the volume sucked from the tip of the balloon during deflation. These values are divided by the nominal volume of the balloon to give VUTVi and VUTVd, respectively.*

The volumes displaced upstream beyond the tip (VU) during inflation and sucked from upstream (VS) during deflation were calculated by integrating the area below and above the flow waveform measured upstream, respectively. VU and VS were subsequently normalized as a ratio of balloon nominal volume (Vn = 40 ml), obtaining volume displaced towards upstream (VUTVi) during inflation, and volume sucked from upstream (VUTVd) during deflation. Also the pressure pulse due to inflation (PPi) and deflation (PPd) at the 3 measurement sites along the balloon was determined. PPi is calculated as the difference between the pressure value after the onset of inflation and maximum pressure, whilst PPd is calculated as the difference between the pressure value after the onset of deflation and the minimum pressure value. The pressure difference between tip pressure and base pressure has also been calculated and expressed during the cycle.

3.3.3.3 Images

Wall movement at six locations along the balloon, tip-, base- and mid-point, was tracked off-line in the ".avi" video recorded by the high speed camera, for the same beats for which flow and pressure were analysed, using ProAnalyst (Xcitex, Inc., Cambridge, MA 02141 USA). Images were analysed through a DELL laptop featuring a screen with resolution of 1024 x 768. The quality of the image hence depended on the resolution of the acquired image, smaller than the one of the screen and corresponding to 800x600. This resulted in a spatial resolution of 0.004. The diameter was then calculated at 3 pairs of locations and was followed throughout one cycle. This latest process is indicated in Figure 3-3. The duration of inflation and deflation was also calculated from the images obtained from the filming of the balloon during counterpulsation.

3.3.4 Calibration

Diameter calibration, in ProAnalyst, was made through assigning 2.8 cm to the external diameter of AO. Also, in order to eliminate the effect of light refraction through the silicone rubber tube filled up with water, a rigid object of known size was inserted in the tube and recorded by the high speed camera. Afterwards the size of the object as it appeared within the rubber tube was measured in ProAnalyst to establish the degree the over-estimation due to the refraction of the light. The correction coefficient was found to be 1.08.

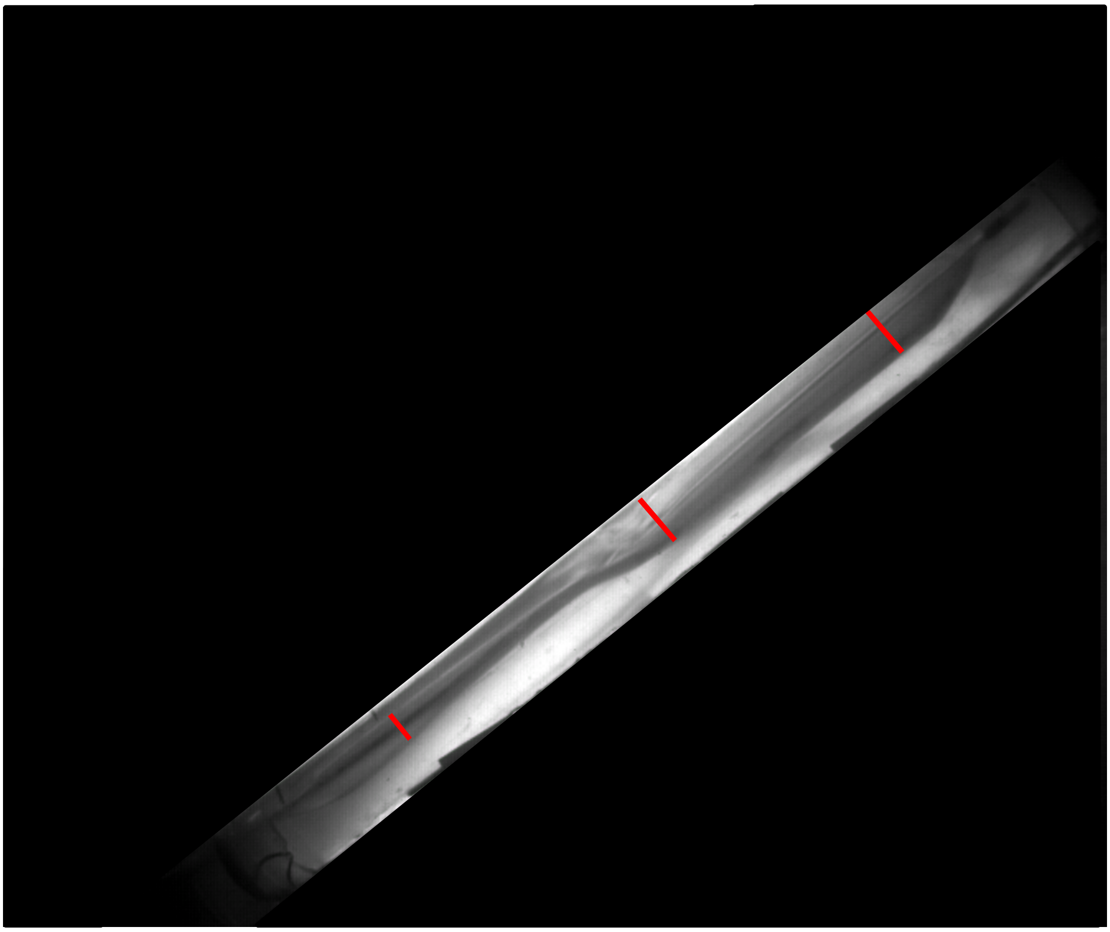

Figure 3-3: *An image of the balloon while counter-pulsating as recorded through high-speed camera at an angle of 45°: it is possible to see the tip of the balloon inflated, differently from its base. Red lines indicate where the diameter measurements were taken.*

3.3.5 Diameter measurement reproducibility

5 recordings of the IAB while counter-pulsating at each position, horizontal and angle 45°, have been considered in the calculation of the base, centre and tip diameter waveforms, to check the reproducibility of the balloon movement. The maximum coefficient of variation, expressing standard deviation over average value, throughout the cycle, position and site along the balloon was found to be 0.27 (centre of the IAB, at an angle of 45°).

3.4 Results

3.4.1 Duration of inflation and deflation

The duration of inflation, calculated as specified from the video recordings, resulted in a decrease by 15.5% when the operating position was changed from the horizontal to an angle of 45^0 (0.275 ± 0.002 vs 0.232 ± 0.009 s, $p < 0.01$). The duration of deflation was found to increase by 35% from horizontal to the angle of 45° (0.309 ± 0.015 vs 0.417 ± 0.008 s, $p < 0.01$).

3.4.2 Diameter at base, centre and tip

3.4.2.1 Base of the balloon

The measured diameter corresponding to the base of the balloon, at the horizontal position and angle of 45°, is shown in Figure 3-4 C. Standard deviation associated to the measured diameter, expressed in relation to its mean value, at each data point is shown in Figure 3-5 C. After the inflation peak at an angle of 45^0 the balloon base reaches, after the inflation peak, a local minimum diameter 0.044 s earlier, compared to the horizontal position. The diameter in the “plateau” area of inflation is 1.66 cm and 1.71 cm, at its maximum, for the horizontal and 45° angle positions, respectively. The deflation starts 0.007 s earlier at an angle of 45^0 compared to the horizontal position.

3.4.2.2 Centre of the balloon

The measured diameter at the centre of the balloon and standard deviation over mean value are shown in Figure 3-4 B and Figure 3-5 B, respectively for the horizontal and 45° angle positions. The diameter waveform follows a similar pattern for both positions. The deflation pattern between the two positions present one main difference: at 0.64 s the diameter waveform shows one peak, at an angle of 45°, which is absent at the horizontal position. The change in diameter corresponding to this peak is 0.29 cm (1.18 ± 0.22 vs 0.89 ± 0.04 cm, $p < 0.05$) and is easy to see in Figure 3-4 B. Also the minimum diameter reached by the balloon on this site is comparable: 0.67 ± 0.07 cm at a horizontal position and 0.82 ± 0.16 cm at an angle of 45°. The starting of the deflation is noticed simultaneously at an angle of 45° and at the horizontal.

3.4.2.3 Tip of the balloon

The measured diameter associated at the tip of the balloon clearly shows differences between horizontal and the angled position (Figure 3-4 A). Its standard deviation (over its mean value) is shown in Figure 3-5 A. The main differences between the two waveforms are found at the beginning of its inflation and throughout the deflation process. After the onset of inflation the diameter associated to the tip of the IAB present a first peak before increasing steeply: the maximum value of this peak is 0.92 ± 0.13 cm at a horizontal position and 1.25 ± 0.17 cm at an angle of 45°. Also, the inflation peak is reached 0.029 s before at the angled position compared to the horizontal one. At this site the IAB diameter starts decreasing after the onset of deflation simultaneously at a horizontal and angled position, but is characterized by a further increase starting at 0.93 ± 0.03 cm and 1.36 ± 0.05 cm at a horizontal position and angle of 45° respectively. This increase brings the diameter value up to 1.22 ± 0.05 cm and 1.71 ± 0.02 cm at a horizontal position and angle of 45°, respectively. Afterwards the diameter reaches its minimum value of 0.69 ± 0.05 cm at the horizontal position while at the angled position presents one further oscillation and, after a ‘plateau’, reaches its minimum value of 1.02 ± 0.12 cm. It was noticed that, at an angle of 45°, the tip of the balloon does not decrease below 1.37 ± 0.04 cm (58% of aortic diameter) before 0.91 s (0.04 s before the following cycle).

3.4.3 Pressure at base, centre and tip

The inflation pressure pulse did not change markedly along the balloon at the two different angles (Table 3-1), but decreased throughout the IAB by 9% from the horizontal to the 45^0 angle: the base and centre of the IAB are associated with the higher pressure pulse at the horizontal position, 235 mmHg, 2.13% higher than the one at the tip ($p < 0.05$); at the angled position, this pulse was 215 mmHg, 3.26% higher than the one at the tip ($p = 0.07$). Similarly, the deflation pressure pulse distribution along the balloon remained almost unchanged with angle (Table 3-1), and decreased homogeneously. At the centre the decrease was -14.2% (150 ± 3 vs 128 ± 1 mmHg, $p < 0.01$) from 0^0 to 45^0.

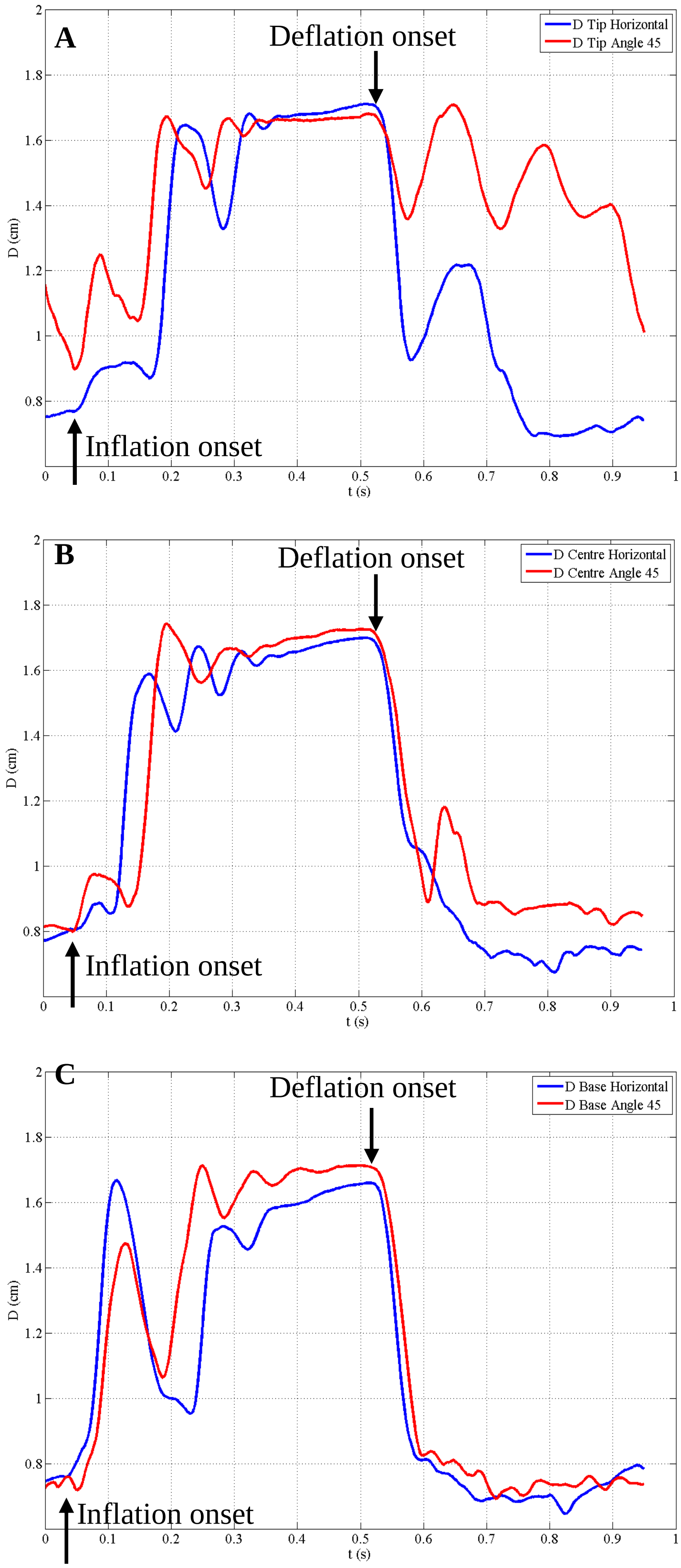

Figure 3-4: *Diameter measured in the horizontal (solid line) and the 45° (dashed line) positions at the base (A), centre (B) and tip (C) of the balloon.*

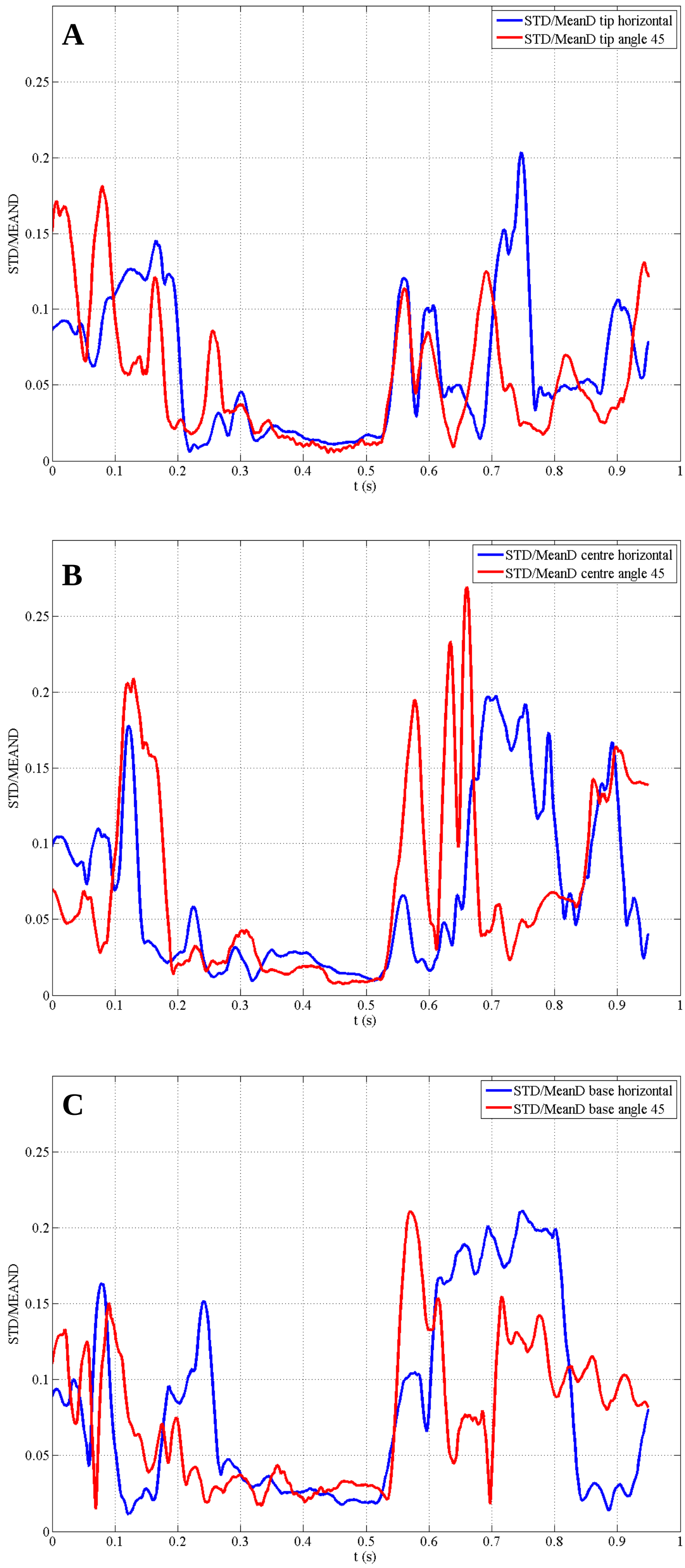

***Figure 3-5**: Ratio between standard deviation and mean value of measured diameter at the horizontal (blue line) and angle of 45° (red line) positions at balloon base (A), centre (B) and tip (C).*

Table 3-1: *Inflation and deflation pressure pulses are reported for tip, centre and base of the balloon, and for horizontal, angle 30 and angle 45 positions.*

		Horizontal (mmHg)	**Angle 45 (mmHg)**
Inflation Pressure Pulse	**Tip**	*230 ± 1*	*208 ± 4*
	Centre	*235 ± 1*	*214 ± 4*
	Base	*235 ± 1*	*215 ± 5*
Deflation Pressure Pulse	**Tip**	*147 ± 3*	*130 ± 3*
	Centre	*150 ± 3*	*128 ± 1*
	Base	*146 ± 1*	*122 ± 1*

Results in terms of pressure difference between tip and base during one cycle are shown in Figure 3-6. The main difference between horizontal (Figure 3-6 A) and the angulated (Figure 3-6 B) position was the presence of a peak after onset of deflation (indicated with an arrow) in the latter.

3.4.4 Flow

The results in terms of VUTVi and VUTVd show that with increasing angle the performance of the IABP decreases (Figure 3-7). VUTVi varied non-significantly from horizontal to the 45° angle (-3.6%, 0.41 ± 0.03 vs 0.40 ± 0.04 mmHg, $p = 0.6$). The results in terms of VUTVd, instead, showed that at an angle to the horizontal the performance of the IABP decreases. Particularly, by increasing the angle from 0 to 45° VUTVd decreased by 15% (0.33 ± 0.03 vs 0.28 ± 0.04 mmHg, $p = 0.11$).

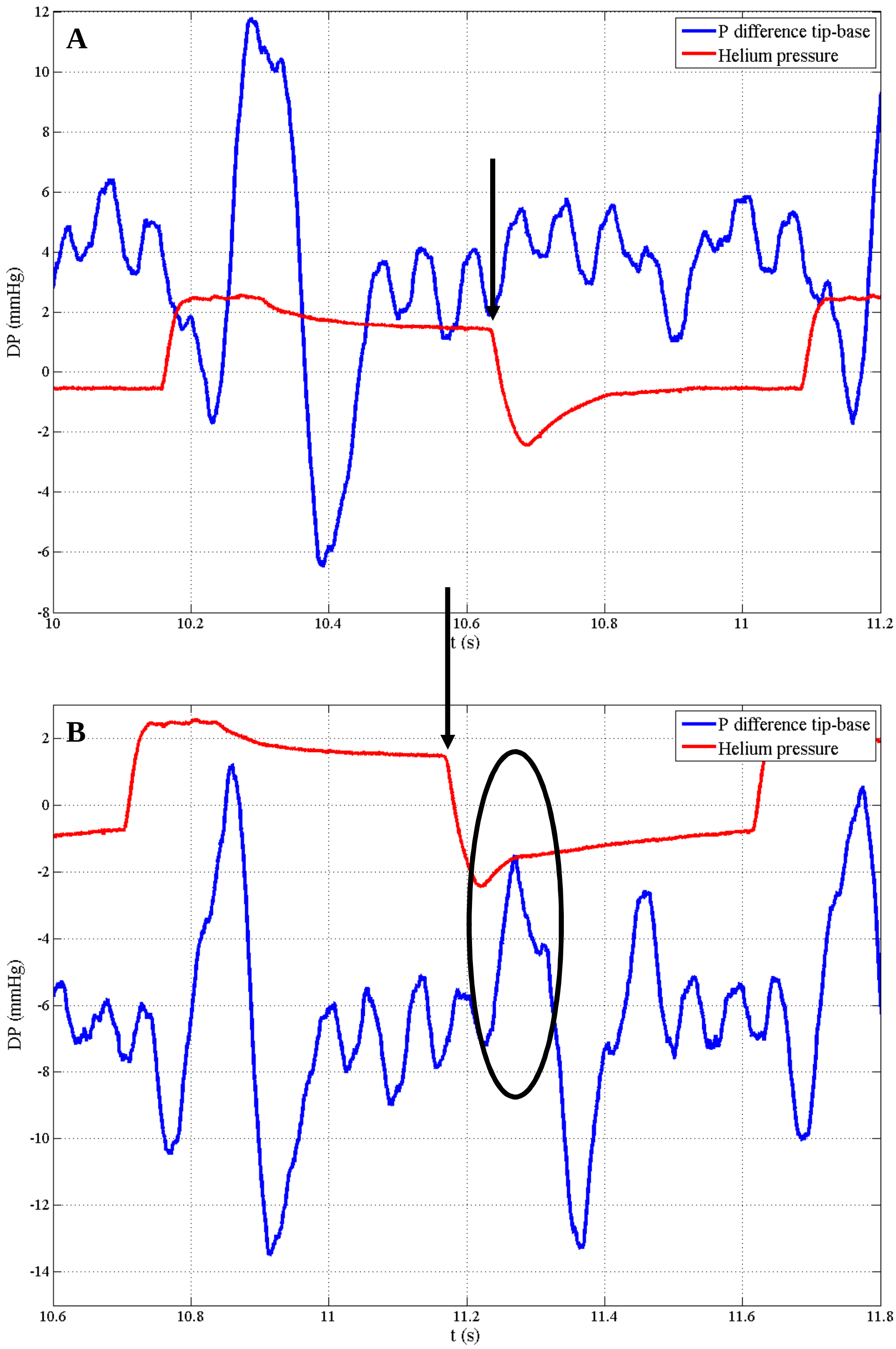

Figure 3-6*: Pressure difference between tip and base of the balloon (blue) at a horizontal (A) and at an angled position (B), plotted with the IABP un-calibrated Helium pressure (red). Arrows indicate the deflation start. A clear peak is visible immediately after deflation onset at an angled position, circled in black, and not at a horizontal position.*

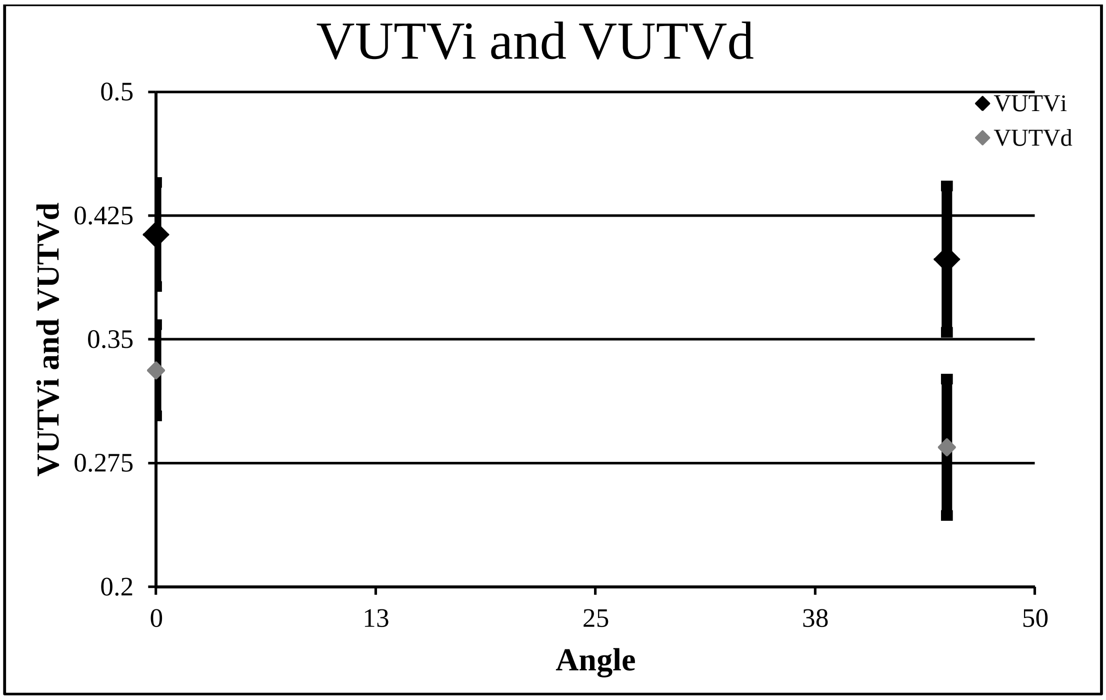

Figure 3-7*: Volume displaced upstream and sucked from upstream divided by total balloon volume (Vn).*

3.5 Discussion

The present study was conducted in a compliant tube, providing the opportunity for comparison with the findings of studies conducted in different test beds (less physiological). Measurements of balloon diameter, derived from IAB wall tracking, at the base, centre and tip during counterpulsation at horizontal and angle of 45° positions showed changes when the balloon was operating at an angle. These were accompanied by changes in surrounding fluid pressure along the balloon and in flow volume displacement. Particularly the deflation phase was markedly influenced by a change in the operating angle of the balloon: measured diameter waveforms (Figure 3-4 A, B and C) and pressure (Table 3-1) associated to the balloon showed a decrease in deflation effectiveness with increasing angle. This is expressed by a longer time for the IAB tip to deflate and a smaller deflation pressure pulse (Table 3-1) and, consequently, decreased VUTVd (Figure 3-7) with increasing angle. Also, the inflation phase was characterised by diameter and pressure contours that varied in case of angulation of the balloon. The starting of inflation is characterised by a higher peak diameter at the tip of the balloon, in case of angulation. Overall the inflation pulse is also decreased with increasing angle (Table 3-1).

Inflation and deflation phases are influenced by the external pressure acting on the balloon, since it affects the effect of trans-mural pressure across the flexible IAB wall. The trans-mural pressure is defined as the difference in pressure between the pressure in the balloon chamber and the one of the fluid surrounding the IAB. When increasing pressure of fluid surrounding the balloon, trans-mural pressure decreases and the balloon wall would tend to collapse ("bend"), disadvantaging somewhat inflation and benefiting deflation. At the same time, as described by Biglino et al.[62], the IAB cross-sectional area under these circumstances might not be circular, but ellipsoidal. Oppositely, at high trans-mural pressures inflation will be favoured and the balloon cross-section can be expected to be circular, with the balloon membrane possibly even stretching. When trans-mural pressure varies along the balloon, clearly a mixture of the above behaviours will be observed at different balloon segments.

3.5.1 Inflation

The results here presented showed that, when the balloon is placed horizontally, its diameter increases first at the base, then at the centre and finally at the tip. This finding contrasts with observations in one earlier work. Indeed Bleifild et al. [65] observed that at a horizontal position the IAB inflated first at its tip and base, almost simultaneously, and finally at its centre. The main reason could be found in the tube containing the balloon. Bleifeld et al. used a PersPex case filled up with both water and air, to recreate the mechanical characteristics of a physiological aorta [65], and placed a stiff tube accommodating the balloon inside the chamber. The authors concluded that free radial volume displacement of the balloon is prevented by the surrounding stiff tube. Consequently the initial inflation of balloon at both ends, and not in the middle, occurs because the rapid gas filling of the balloon prevents the fluid surrounding the balloon from being displaced [65] when the balloon is placed in a stiff tube. On the other hand, in this study a silicone rubber tube, with size and elasticity similar to the ones of the aorta, has been used for containing the balloon. Hence, as shown by the results at a horizontal position, the compliance of the tube could affect the balloon inflation mechanism through accommodating a part of the fluid displaced by the balloon, resulting in the inflation to start at the base and continue towards the centre and tip.

The diameter waveforms after the peak of inflation shows that at a horizontal position the tip of the IAB has a smaller diameter compared to the centre and base for the first part of inflation, till 0.185 s (Figure 3-8 A), while at an angled position the tip of the balloon (Figure 3-8 B), presents a first small inflation peak resulting in this segment of the IAB to be bigger than the rest of the balloon till 0.098 s. Hence the obstruction to upstream flow displacement imposed by the tip of the IAB during this phase can be expected to have more detrimental effects at an angled position compared to the horizontal position. This may affect negatively VUTVi, which however decreased not significantly by 3.6% ($p = 0.6$) when changing from horizontal position to an angle of 45°.

Finally the duration of inflation measured in this study did not confirm Biglino et al. [62] measurements, taken at a pressure of 90 mmHg. In their study the duration of inflation was found not to vary significantly from 0^0 to 75^0, on average 0.27 s, while in the current study this duration varied from 0.275 ± 0.002 s at a horizontal position to 0.232 ± 0.009 s at an angle of 45^0. However, Khir et al. [63] found a similar variation in the duration of inflation compared to the present study (-20% in duration of inflation from 0 to 60^0, comparable to -16% ($p < 0.05$) from 0 to 45^0 presented here), even though the duration of inflation at the horizontal position was slightly different (0.20 vs 0.275 s).

3.5.2 Deflation

This study showed that an increase in the operating angle of the balloon induces a decrease in both VUTVd (Figure 3-7) and deflation pressure pulse (Table 3-1), thus compromising fundamental hemodynamic benefits associated with balloon deflation. A reason can be found through the comparative assessment of the pressure and diameter tracings at the tip of the balloon, at a horizontal position and at an angle of 45° (Figure 3-9). After the onset of deflation, the negative slope of the diameter waveform at the tip of the balloon is smaller at an angle than at the horizontal position, with the diameter decreasing by 0.4 cm in 0.054 s at an angle and 0.83 cm in 0.07 s at a horizontal position. In addition at the tip the balloon reaches its minimum diameter 0.19 s later at an angled position compared to the horizontal one. Both effects lead to a smaller deflation pressure pulse.

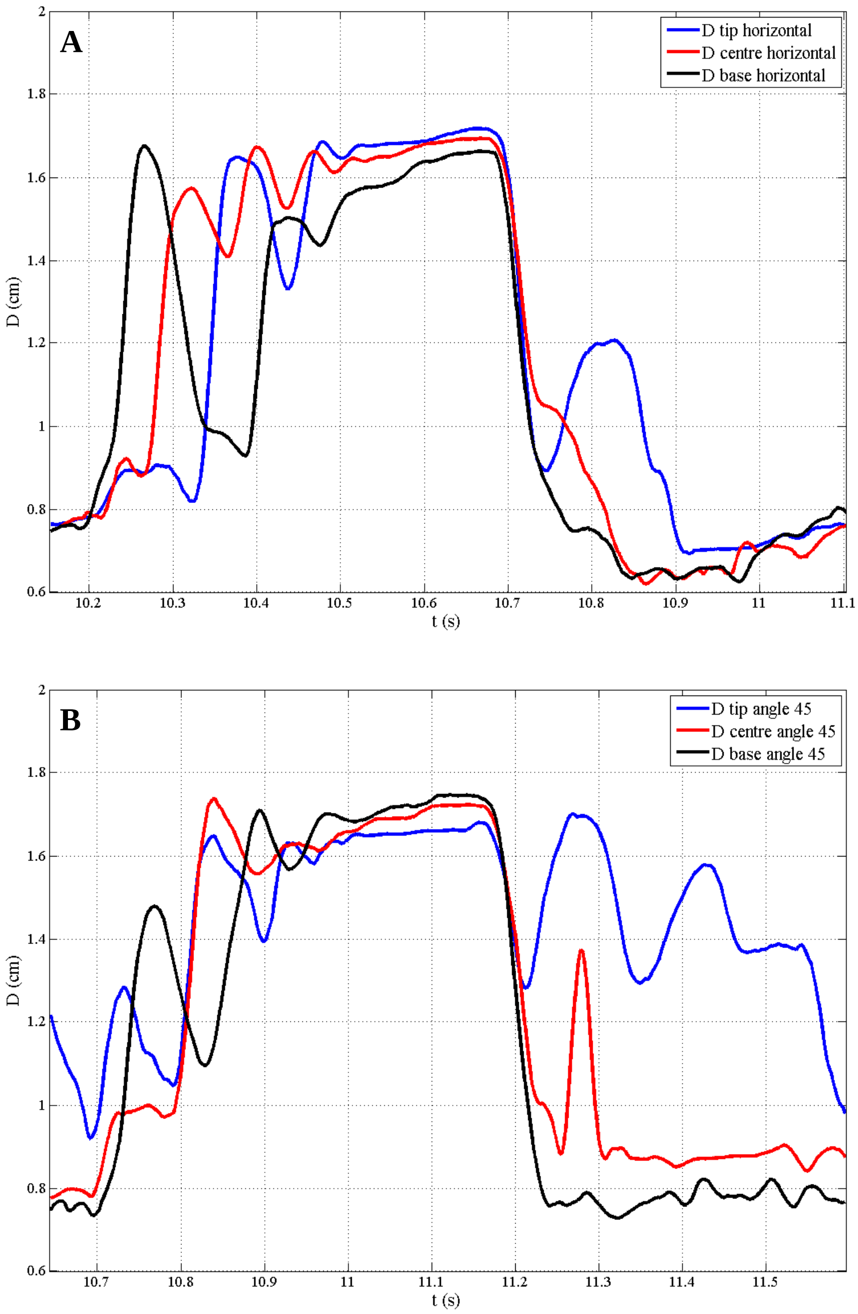

Figure 3-8: *Diameter measured in the horizontal (A) and angled (B) positions for tip (blue line), centre (thick red line) and base (black line) of the balloon. While at a horizontal position (A) the inflation peak appears first at the base followed by centre and tip, at an angle (B) inflation is less linear and shows a first smaller inflation peak at the tip of the IAB.*

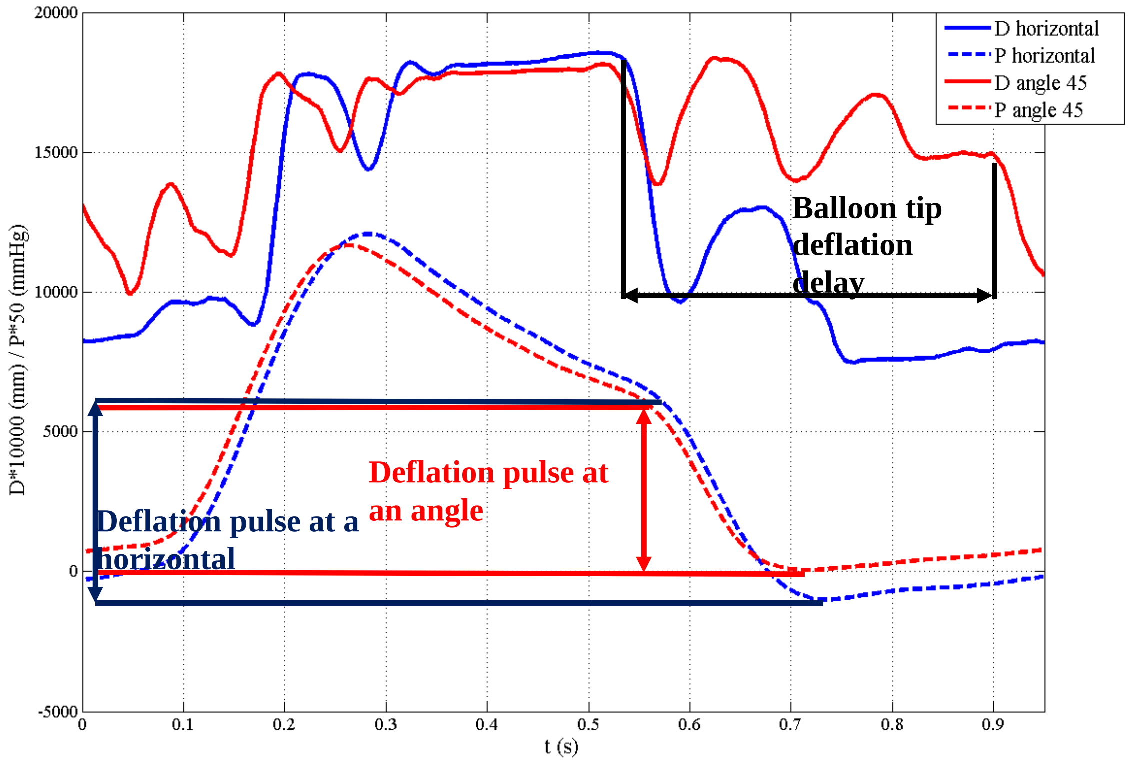

Figure 3-9*: Diameter and pressure waveforms in the tip of the balloon at a horizontal (blue) and angle of 45° (red) positions.*

The quantification of the delay in deflation starting in vitro could be useful when projected in clinical settings and particularly in patients with fast heart rate for whom systole might start before the IAB base diameter reaches its minimum. An earlier onset of deflation might counterbalance this loss/drawback by shifting earlier the time minimum pressure is achieved at an angled position and thus allowing improved reduction in afterload. It has to be taken into consideration, though, that inflation would be more productive if elongated.

Because diameter waveforms showed that the base is the first IAB segment to completely deflate at an angle, while the tip is only partially emptied (Figure 3-8 B), the Helium flow can be expected to encounter a higher resistance flowing back towards the pump and therefore the balloon will empty, especially at the tip, at a slower pace. This loss in efficiency is reflected in a 15% reduction ($p = 0.11$) in VUTVd. An additional reason for the deterioration in VUTVd and deflation pulse at an angle might be found in the increased resistance imposed on flow suction from upstream with increasing angle. As already mentioned, when the IAB is tilted it starts deflating from the base while the tip is the last to deflate **(**Figure 3-8 B**)**; this event results in the tip remaining the IAB segment with the largest diameter throughout the deflation phase and thereby imposing the largest obstruction to flow sucked from upstream [68].

To this issue it is also relevant to underline the differences between tip-base differential pressure at a horizontal position and at an angle. If the balloon is at a horizontal, no sharp change in differential pressure is noted after the onset of deflation, confirming that the deflation starts simultaneously at the tip and base of the balloon (Figure 3-6 A - C). Differently, when the balloon is tilted, a peak is observed (increasing differential pressure between tip and base) immediately after deflation starts (Figure 3-6 B), underlying the different deflation mechanics which, influenced by hydrostatic pressure difference, starts at the base and proceeds towards the tip.

The loss in performance of IAB deflation pulse is also related to the duration of deflation, which was found to increase when changing the position from horizontal to the angle of 45°, confirming what was found by Biglino et al. [62] at a pressure of 80 mmHg. In fact Biglino et al. report a duration of 0.40 s at a horizontal position and 0.47 s at an angle of 75^0 (+ 17%); such an increase was also found in the present study, even though the duration was overall shorter, from 0.309 ± 0.015 s at a horizontal position to 0.417 ± 0.008 s at an angle of 45^0 (+ 35%, $p < 0.05$). This latest result is in contrast with findings by Khir et al. [63] who reported an overall unchanged duration of deflation of 0.28 s between the horizontal position and angle of 60^0.

3.5.3 Experimental and measurements Considerations

The values of pressure presented in Table 3-1, are exceptionally higher than those observed in vivo. This could be due to a number of reasons; a) the experimental set up is simple with resistances and compliances simulated in the mock loop as lumped parameters, b) the distance travelled by the waves generated by IAB inflation and deflation is rather short, compared to that in vivo, which enhances the magnitude of reflected waves causing an increase in pressure, c) the volume of fluid used in this study is less than the volume of blood in the human body, and therefore the effect of balloon inflation and deflation will be magnified as it operates on a smaller volume. Nevertheless, replicating in vivo pressure or flow waveforms was not the focus of the current work, but rather analysing IAB wall movements at the horizontal and angled positions.

In this work, the diameter of the IAB was taken as the distance between the two walls at the frontal plan, rather than actual diameter. Also, the IAB is filled with helium and the pressure is expected to be radially uniform throughout its cross-section. Further, the camera was always placed as a right angle to the IAB long axis. Therefore, the measured distance between the two walls during inflation can be reliably used as the nominal diameter of the IAB cross section at the given location. When the IAB walls are totally collapsed at end of deflation, the measured diameter will reduce to be the thickness of the walls.

The refraction factor determined in this study takes into account the distortion effects of both the silicone tube and water together, and hence corrects for their combined effect. We note the refraction factor was determined by placing the rigid object inside the silicon tube only at a one distance away from the wall of the silicon tube, whilst the balloon walls will be moving at a varying distance from the silicon tube wall during inflation and deflation. Given the distance travelled by the balloon walls as it approaches the walls of the silicon tube is small (0.8 cm), we expect the different refractions will be inconsequential to our results.

As a further analysis on refraction coefficient, different objects size has been measured outside a tube filled with water and, through the use of high speed camera and ProAnalyst software, inside a tube characterized by the same size and properties of the one containing the IAB. This type of verification would highlight the difference in light refraction in case IAB is deflated, partially inflated or totally inflated. The diameters of the three objects were the following:

A = 19.10 mm

B = 8.10 mm

C = 5.20 mm

Measurements through ProAnalyst resulted in the following values:

A = 20.68 mm

B = 8.41 mm

C = 5.25 mm

Hence diffraction correction coefficient results in 1.08 for object A, 1.04 for B and 1.01 for C. It was calculated that the use of 1.01 instead of 1.08 on the minimum diameter results in maximum 7% error.

3.5.4 Limitations and future work

The main limitation of the study is related to the recording plane of the balloon. In this study the IAB has been filmed and analysed just on the frontal plane (side view) and consequently only information about the wall movement on that plane can be obtained. However, recording simultaneously the movement of the balloon wall from the top plane would in fact provide information about the shape of the cross-sectional area and make the analysis more complete.

The current experimental set-up did not include a physical model of the coronary circulation. This would have been useful to study the effect of angulation on coronary flow. However, given that the focus of this work is placed on studying the IAB wall patterns of inflation and deflation at the 0° and 45°, an inclusion of a coronary circulation model would not have likely changed the results or the conclusions drawn from the current work.

3.6 Conclusions

A study showing changes in diameter of the IAB during its inflation and deflation in a compliant tube is absent from the literature. The research presented here revealed some critical aspects of the mechanics of deflation of the balloon. This phase changes radically when angulating the balloon: the deflation is confirmed to be slower and deflation pulse to be smaller in case of angulation, compared to a horizontal position. In fact the diameter waveforms showed that the balloon base completely deflates first, and might provide a high resistance against the flow of Helium from the balloon towards the pump, causing the tip to stay almost completely inflated, as shown by the diameter measurements, till 0.04 s before next inflation. As a result VUTVd decreased with increasing angle. Also the mechanism of inflation changes when balloon operates at an angle: at this position the IAB tip shows to inflate before the rest of the balloon and might consequently provide a high resistance against the flow to be displaced towards coronary circulation.

The quantification of the delay for the tip of the IAB in reaching the minimum diameter at an angled position compared to the horizontal can be useful from a clinical point of view and should be considered when determining optimal deflation timing, particularly taking into consideration the impedance against the systolic flow that the tip of the balloon would provide if not completely deflated.

The results of this work, although *in vitro*, have clinical implications and suggest that from efficacy viewpoint, IABP patients are best nursed at the horizontal position. Since most patients using the IABP need to be nursed at the semi-recumbent position, it seems that modification to the balloon shape, filling patterns, inflation and deflation timing at the various angles require further investigations to achieve maximum benefit of this therapy.

Chapter 4 Effect of changes in Intra-aortic balloon shape on IAB performance **

4.1 Chapter outlook

The work described in Chapter 3 about the lack of IAB deflation effectiveness at a semi-recumbent position, and of previous works [63,66-68,71] on the detrimental effect of an angled position on coronary flow supported by IABP, suggest the need for modifications of the current balloon design, aiming at containing the drawbacks of operating the IAB when tilted. With the present work it is aimed at assessing the changes in IAB volume displacement and pressure pulse, during inflation and deflation, in case the balloon is characterized by a different shape, at horizontal and angled positions. This chapter describes a pilot study attempting to define the differences induced by a change in the balloon shape, and as such relates the different behaviour of the balloons at different positions only to the different shape.

4.2 Introduction

In the past years different studies compared balloons with different volume but same shape [72,73] in the same experimental set-up in an attempt of defining the relationship between the hemodynamic parameters and the balloon's nominal volume. Surprisingly, the authors did not report any difference between the different sized balloons.

As already reported in the Introduction Chapter of this thesis, also the question of balloon shape has previously been investigated, but our understanding of the effect of these variables on the performance of the balloon remains incompletely understood. To improve the efficacy of the balloon Anstadt et al.[47] introduced a balloon with a valve placed distally aiming at reducing retrograde flow in the abdominal aorta during deflation, in order to increase thoracic aortic flow and consequently improve systolic unloading. Further Bai et al.[46] designed and tested computationally and experimentally a multi-chamber balloon, and compared the results to one- and two-chambered balloons. The authors suggested that an optimally controlled multi-chamber balloon provided additional benefits and may potentially be applied in the counterpulsation treatment. Furthermore Meyns et al [51] tested a pre-shaped balloon that is placed in the ascending aorta of sheep with coronary stenosis,

**published: Khir AW, Bruti G. Intra-aortic balloon shape change: Effects on volume displacement during inflation and deflation. *Artif Organs*. 2013.

and compared the results to those of standard cylindrical balloon placed in the descending aorta. The pre-shaped balloon has significantly increased myocardial blood flow in ischemic regions more compared to the standard balloon, without compromising cerebral flow.

Nevertheless none of these balloons has been introduced to the market. Also the devices have not been operated at a semi-recumbent position, leaving the issue of the compromised balloon performance at an angle open. As already mentioned before operating the IAB at an angle might reduce its benefits, as reported by Khir et al. [63]. Moreover, as exhaustively reported in Chapter 3, when operating the balloon at an angle the deflation effectiveness decreases. Hence, a balloon that can displace more volume towards the ascending aorta when tilted or avoid to be affected by the operating angle would be advantageous and highly desirable.

For this reason Biglino et al. [71] conducted a work based on the comparison between two tapered balloons, which are described later in this chapter, and the standard cylindrical ones, focused on finding a pressure locus along the balloons and on the measurement of the volume displaced towards the upstream. The main finding consisted in one of the two tapered balloons showing a higher volume displaced upstream (divided by the total volume displaced by the balloon) compared to a 34 cc standard cylindrical balloon both at a horizontal position (+ 7%) and at an angle of 19 degrees (+ 14%). Although the experiments have been conducted at a non-physiological pressure (3200 Pa = 24 mmHg), two single positions have been studied and in case of angulation the pressure in the middle of the balloon was not maintained constant. Furthermore the work concentrated on analysing the performance of the balloons during inflation, and did not report differences in performance between the balloons at different angulations during deflation phase [71].

The aim of the present chapter is to further analyse the two new shaped balloons which could potentially displace higher volumes than those displaced by the traditional cylindrical balloon, during inflation and reduce the end diastolic pressure, hence ventricular afterload, more than cylindrical balloon, during deflation, at both the recumbent and semi-recumbent positions. Moreover, the balloons have been studied in different conditions of intra-lumen pressure and heart rate in order to identify the effect of these parameters on the balloon's performance.

4.3 Materials and methods

4.3.1 Balloons

Three different shaped balloons (Datascope, Fairfield, NJ, USA) were compared: a cylindrical balloon with diameter (d) of 1.8 cm and length (L) of 27 cm and two tapered balloons, one decreasing in diameter from the base to the tip (TDD) and the other increasing in diameter from the base to tip (TID). The length of each of the tapered balloons is 37cm and the maximum diameter (at the base for TDD and at the tip for TID) is 2 cm. The three balloons are shown in Figure 4-1. The nominal volume of each balloon was established by placing each balloon in a graduated beaker and inflating with a syringe, recording the volume displaced once the pressure within the balloon reached 70, 100 and 130 mmHg. The volume displaced was then obtained through subtracting from the final volume, with inflated IAB, the beginning volume, with deflated IAB. The average of the three values of volume displaced has then been calculated. The displaced volumes were 42.9cc, 37.1cc and 36.2cc for the cylindrical, TID and TDD respectively.

4.3.2 Experimental set up

The experimental set up is shown in Figure 4-2**.** A straight silicone rubber tube of 2.3 cm internal diameter, 35 cm in length and 0.26 cm of wall thickness has been chosen to replicate the aorta. The compliance of the tube is 0.084 ml/mmHg, which is comparable to that of the thoracic aorta of 0.11 ml/mmHg as measured by Westerhof et al. [70]. The tube was water filled and used to host each balloon, and it was connected to an overhead reservoir through a pair of lateral tubes that included two one-way valves to separate the volume displaced due to inflation from that due to deflation. The set up was symmetrical compared to the IAB, to provide equal resistance to each side of the balloon. The tube accommodating the balloon was placed on a platform whose angle to the horizontal was adjusted to replicate a patient's posture. Each balloon was operated by the same pump (Datascope 97xt, Datascope, Fairfield, NJ, USA), which was triggered using the ECG of a patient simulator. The reservoir provided the initial static head pressure (P_s), replicating pressure at the time of the dicrotic notch (generally used as onset of inflation) using $P_s=\rho gh$, where ρ is water density (1000 kg/m^3), g is gravitational acceleration (9.81 m/s^2) and h (varied between 0.68 m and 1.20 m) is the lateral distance between the water level in the reservoir and the centreline of the balloon to present the balloon mean pressure[62].

4.3.3 Independent and dependent parameters

The independent parameters involved in the experiment are:

- **Static head pressure. T**he P_s acting on the system consisted in 50, 70 and 90 mmHg. The change in pressure was performed by regulating the height of the reservoir.

- **Heart rate.** Three different heart rates influencing the duration of inflation and deflation associated to the balloons have been studied (60, 80, 100 bpm). The heart rate was settled and varied by using a patient simulator (System trainer 90 series, Datascope) with the ECG set at sinus rhythm.

- **Position.** Four different balloon inclinations have been tested: 0, 20, 30, 45 degrees, to replicate patient posture. These angles were chosen to compare a possible inclination in the clinical environment to the horizontal. For all angles h was kept constant by raising the reservoir accordingly to maintain the same static mean pressure at the centre of the balloon.

The parameters selected to characterize the IABs performance are the volume displaced towards the upstream (beyond the tip) by the balloon over total balloon volume (VUTVi), the volume sucked away from upstream (from the tip) by the balloon over total balloon volume (VUTVd), the balloons inflation pressure pulse (PPi) and deflation pressure pulse (PP d) in three different sites along the device

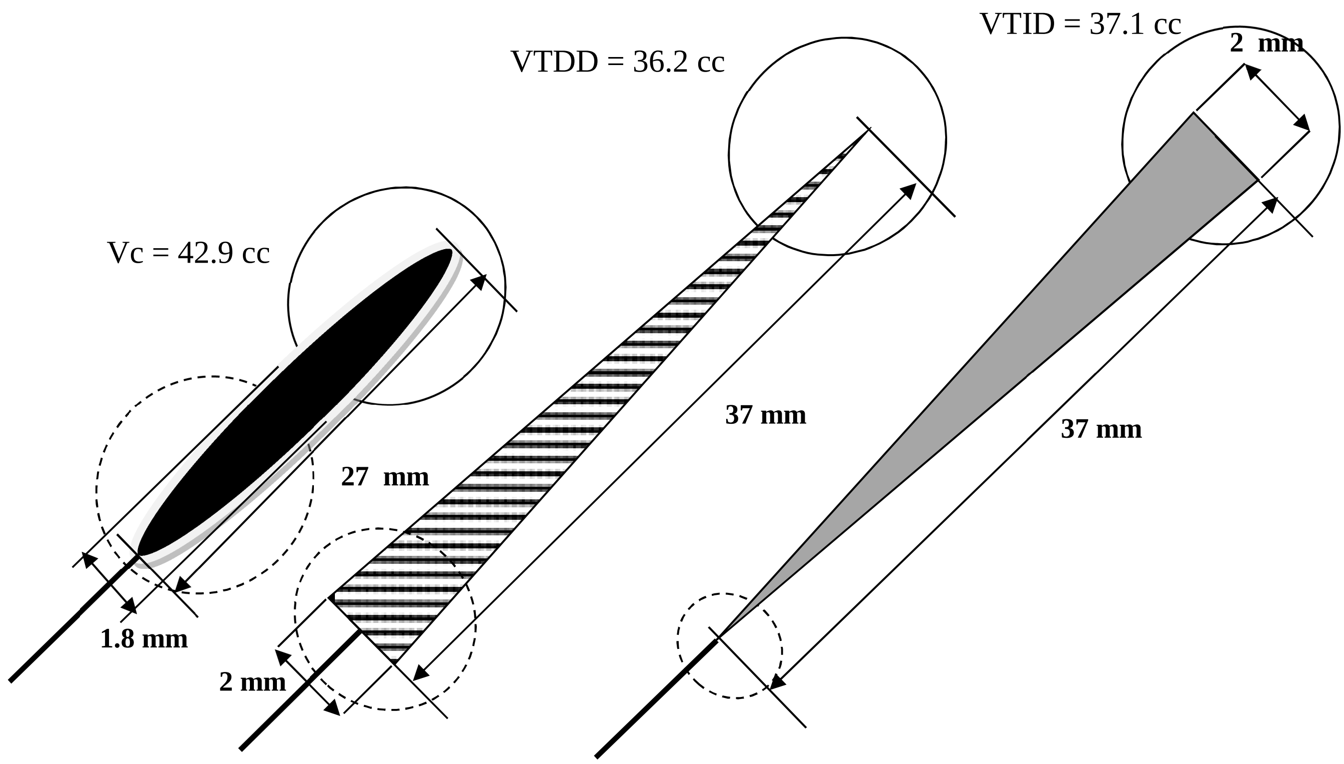

Figure 4-1*: Schematic of the tested balloons, cylindrical (left), TDD (middle) and TID (right). All dimensions are expressed in cm. The solid circle indicates the end of the balloon to inflate first and the dashed circle indicates that to deflate first.*

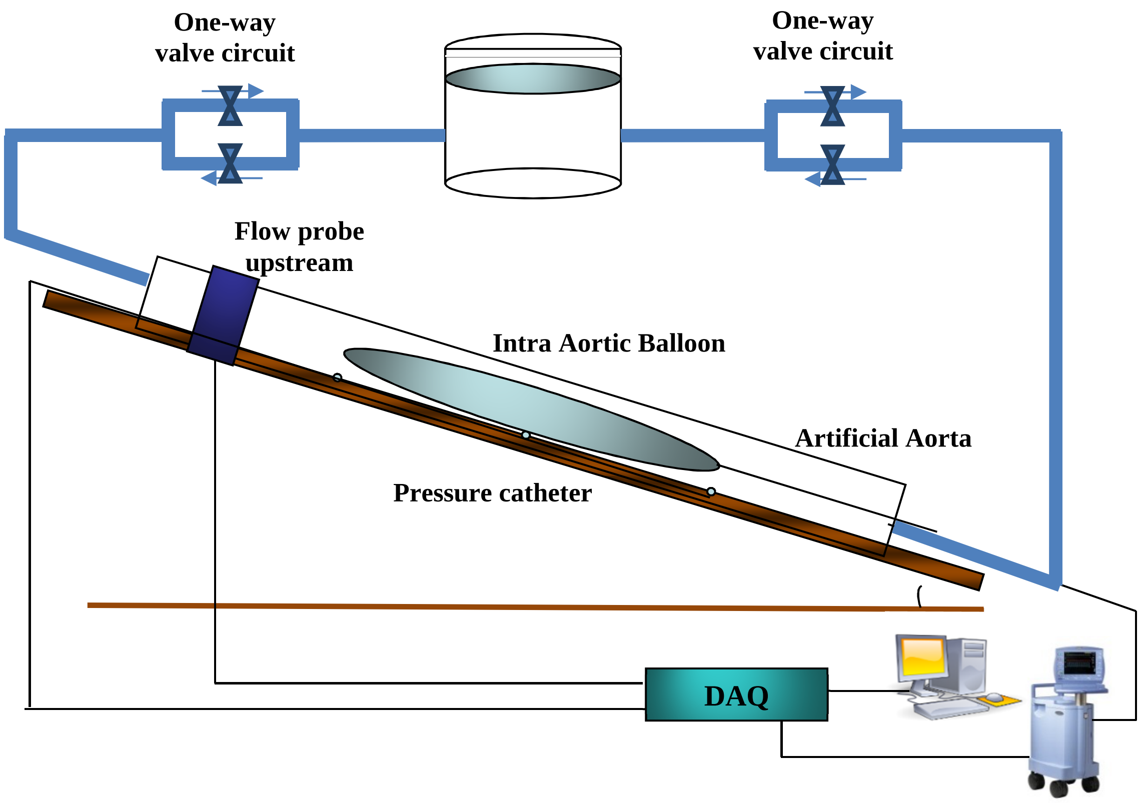

Figure 4-2: *Schematic representation of the experimental set-up in which all balloons have been tested.*

4.3.4 Measurements

Pressure at 3 sites, tip-, base- and mid-point of the balloon, and flow rate upstream the balloon were simultaneously measured at a sampling frequency of 2 KHz. One flow probe (28A, Transonic, Ethica, NY, USA) was snug-fitted to the artificial aorta at 5 cm away from the tip of the balloon. A Gaeltec multi sensor (n = 3) pressure catheter (Gaeltec, Scotland, UK) was inserted in the artificial aorta from the left side, and placed along the balloon. Also, pump pressure was recorded to indicate balloon pressure and landmarks of inflation and deflation. The data of 25 beats for each experiment were recorded using an analogue-digital converter and Labview software (National Instruments, Austin, TX, USA). Data were analysed off-line using Matlab (The Mathworks, Natick, MA, USA).

4.3.5 Data analysis

The inflation and deflation periods are defined in Figure 4-3. The volume displaced upstream beyond the tip (VU) and sucked from above the tip (VUs) were calculated by integrating the area below and above, respectively, the flow waveform measured upstream. The two integrations take into account the flow changes due to IAB inflation and deflation, hence the flow was integrated in correspondence of flow waveform changes after inflation and deflation onset, as indicated in Figure 4-3. To compare the results of all the balloons that have different nominal volumes (Vn), we normalised VU and VUs as ratios of Vn, for volume displaced upstream (VUTVi) during inflation and similarly, (VUTVd) during deflation. We determined the pulse pressure due to inflation (PPi) and deflation (PPd) at the 3 measurement sites along the balloon. PPi is calculated as the difference between the pressure value at the onset of inflation and max pressure, whilst PPd is calculated as the difference between the pressure value at the onset of deflation and the min pressure value. To ensure steady state 10 beats were analysed (9^{th}-18^{th}) for each experiment.

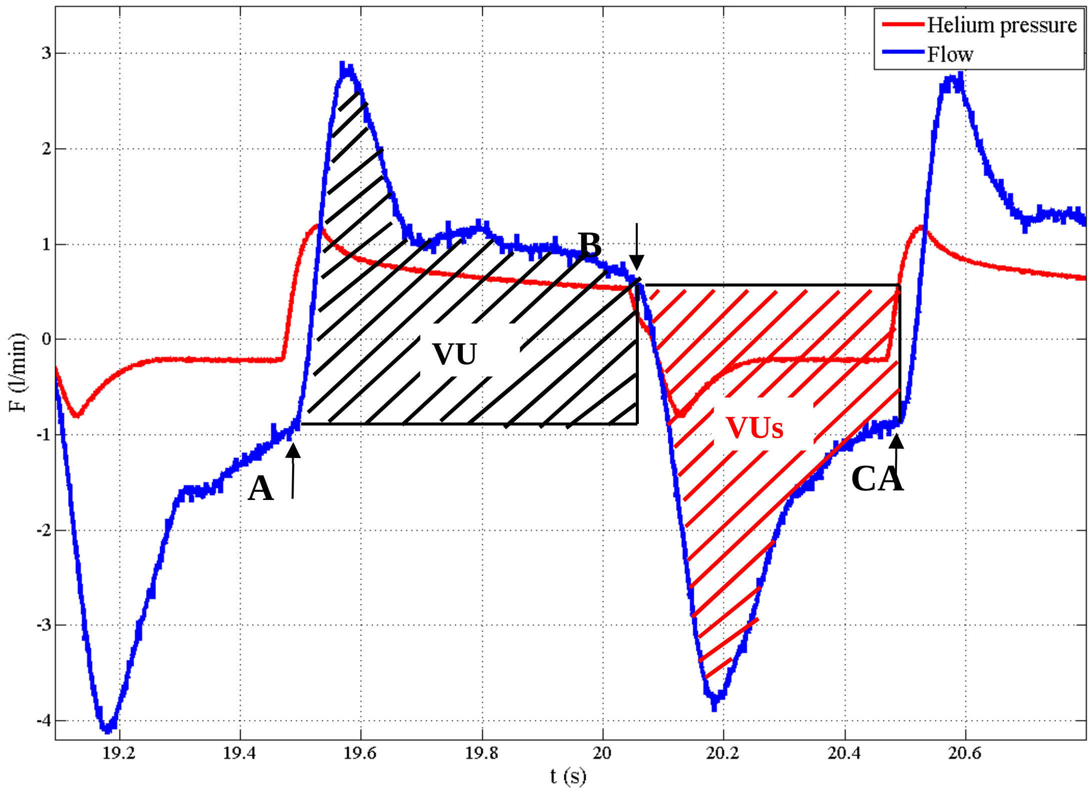

Figure 4-3*: Flow waveform on the upstream of the balloon (blue line). The arrows and points A, B and C indicate onset of inflation, onset of deflation and end of deflation respectively. The red line indicates the balloon pressure (not calibrated) as recorded from the IABP. The area integrated below the blue line between points A and B indicates the volume displaced away from the tip of the balloon during inflation VU. The area integrated above the blue line between points B and C indicates the volume sucked away from the tip of the balloon during deflation VUs. These values are divided by the nominal volume of the balloon to give VUTVi and VUTVd, respectively.*

4.4 Results

4.4.1 Volume displaced

4.4.2 Inflation

VUTVi is shown in the graph in Figure 3.4 for each balloon, from 0° to 45°, for 60 bpm and 100 bpm heart rates, 90 mmHg of P_s. This pressure is highlighted because it is the closest one to the physiological pressure acting on the balloon at the onset of inflation.

At 60 bpm VUTVi decreased with increasing the angle from 0° to 45° for the cylindrical balloon by 25% (0.48 ± 0.04 vs 0.36 ± 0.02, $p < 0.05$), and marginally changed for the TID (0.38 ± 0.02 vs 0.38 ± 0.03, $p = 0.74$) but increased for the TDD 13% (0.47 ± 0.03 vs 0.53 ± 0.02, $p < 0.05$).

At 100 bpm VUTVi did not change markedly (+2%, 0.17 ± 0.01 vs 0.18 ± 0.01, $p = 0.1$) for the cylindrical balloon, increased 23% (0.26 ± 0.02 vs 0.32 ± 0.02, $p < 0.05$) for the TID balloon and did not vary significantly (-3.5%, 0.27 ± 0.01 vs 0.26 ± 0.01, $p = 0.3$) for the TDD balloon, but in all cases it sharply decreased compared to using 60 bpm, as visible in Table 4-1.

4.4.3 Deflation

VUTVd is shown in the graph in Figure 3.5 for each balloon, as for VUTVi from the 0° and 45° positions, for 60 bpm and 100 bpm, 90 mmHg of P_s.

At 60 bpm VUTVd also decreased with increasing angle from 0° to 45° by 21% (0.39 ± 0.02 vs 0.31 ± 0.02, $p < 0.05$) for the cylindrical balloon and by 6% (0.33 ± 0.01 vs 0.31 ± 0.02, $p < 0.05$) for the TID, but slightly increased by 4.5% (0.44 ± 0.01 vs 0.46 ± 0.02, $p = 0.1$) for the TDD.

Using a heart rate of 100 bpm, VUTVd decreased by -12.5% (0.32 ± 0.01 vs 0.28 ± 0.01, $p < 0.05$) for the cylindrical balloon, did not change (0.39 ± 0.01 vs 0.4 ± 0.02, $p = 0.6$) for the TID balloon and (0.41 ± 0.02 vs 0.41 ± 0.01, $p = 0.7$) for the TDD balloon, and, similarly to VUTVi, decreased markedly, compared to using 60 bpm, for each balloon (Table 4-1).

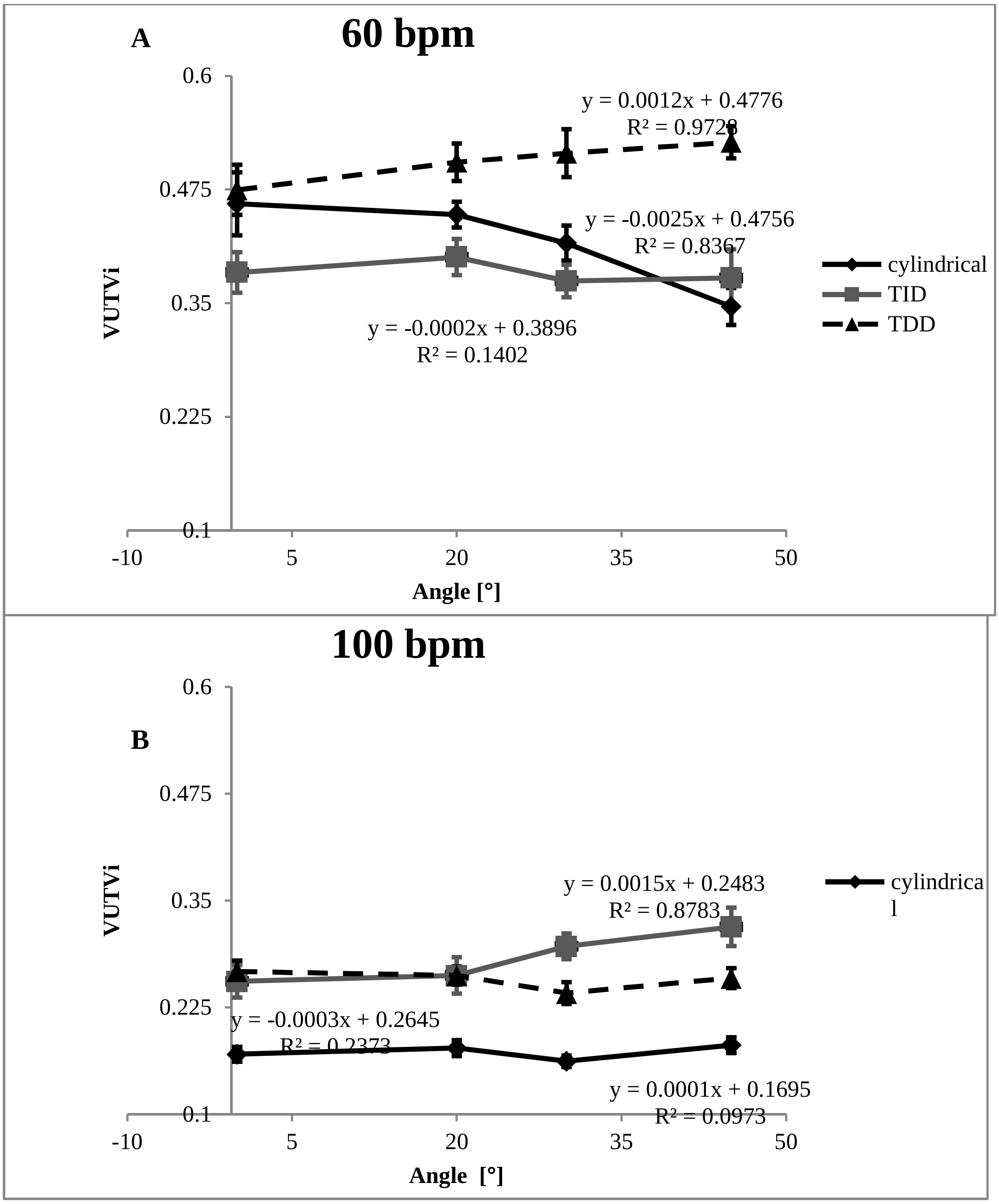

Figure 4-4*: The graphs show the change in VUTVi associated to the three balloons (dark solid line cylindrical IAB, grey solid line TID balloon and dark dashed line TDD balloon) with a change in position from 0 to 20, 30 and 45 degrees, in case of 90 mmHg of head pressure and for 60 bpm (A) and 100 bpm (B).*

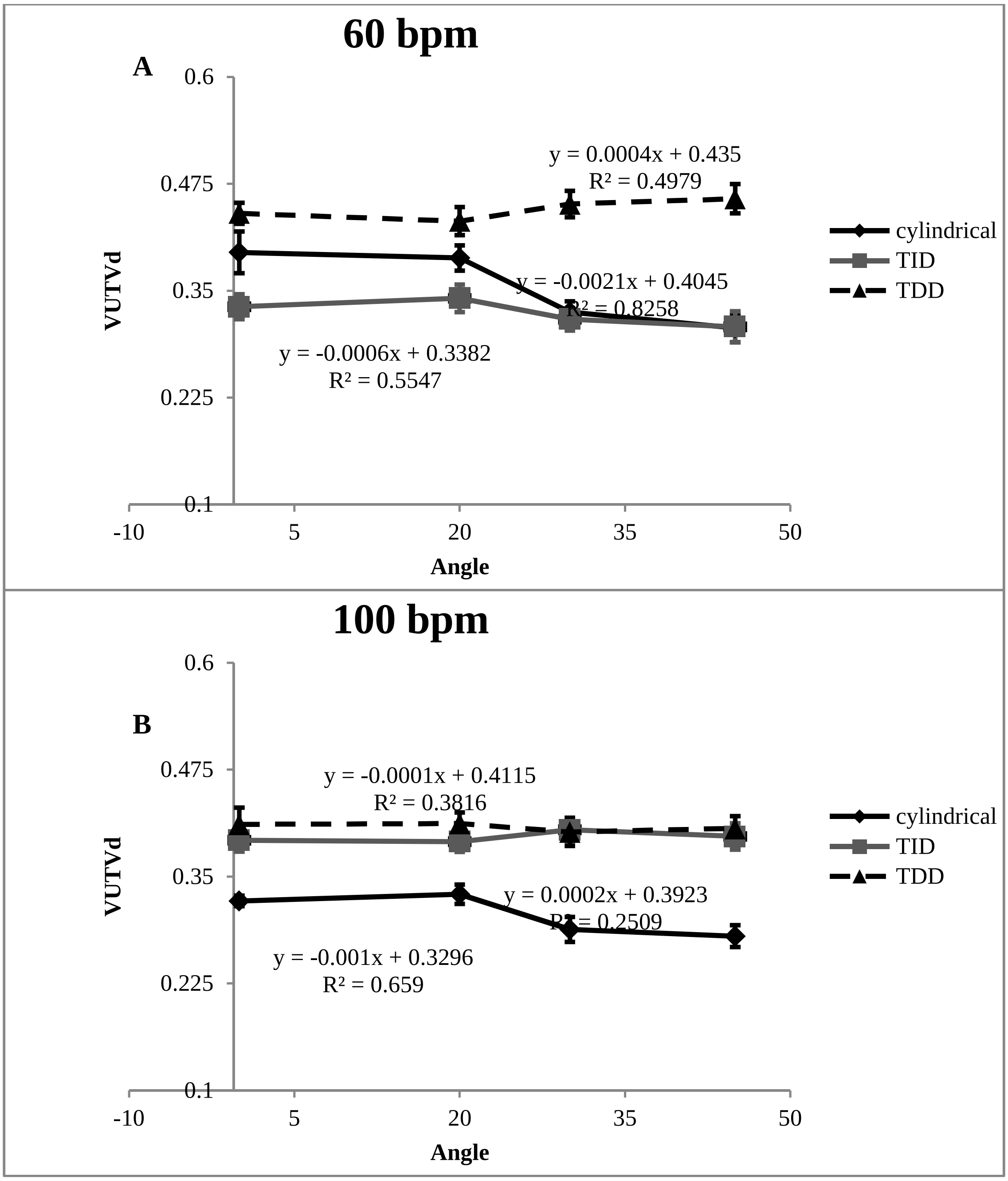

Figure 4-5*: The graphs show the change in VUTVd associated to the three balloons (dark solid line cylindrical IAB, grey solid line TID balloon and dark dashed line TDD balloon) with a change in position from 0 to 20, 30 and 45 degrees, in case of 90 mmHg of Ps and for 60 bpm (A) and 100 bpm (B).*

Table 4-1: *maximum loss in terms of VUTV between heart rate 60 bpm and heart rate 100 bpm conditions, at a pressure of 90 mmHg, during inflation on the left and deflation on the right, for each balloon.*

	Decrease in mean VUTVi (60 to 100 bpm)	**Decrease in mean VUTVd (60 to 100 bpm)**
Cylindrical balloon	-53.3%	-24.4%
TID	-45.8%	-15.3%
TDD	-53.8%	-14.8%

4.4.4 Pressure Pulse (PP)

4.4.4.1 Inflation

Consistent in all the balloons, the lowest pulse pressure due to inflation (PPi) is observed at the centre of each balloon, and the PPi at the tip is always higher than that at the base, as shown in Table 42. At the horizontal position, the difference between tip and base in PPi is 4% for the cylindrical balloon (154 ± 1.3 vs 148 ± 1.2 mmHg, $p < 0.05$), 8% for TID (136 ± 0.6 vs 126 ± 0.6 mmHg, $p < 0.05$) and 9.5% for the TDD (127 ± 0.3 vs 116 ± 0.7 mmHg, $p < 0.05$). Increasing the operating angle resulted in a decrease in the pressure difference between the tip and base of the balloons. At 45°, the difference is 2% (159 ± 0.9 vs 155 ± 0.9 mmHg, $p < 0.05$) for cylindrical balloon, 4% (158 ± 1.1 vs 152 ± 1.0 mmHg, $p < 0.05$) for TID and 4.5% (138 ± 0.9 vs 132 ± 0.8 mmHg, $p < 0.1$) for TDD.

All balloons produced a higher PPi when increasing the angle, and TID induced the highest increase. Increasing the operating angle from 0° to 45°, PPi increased by 3% (142 ± 1.1 vs 148 ± 0.8 mmHg, $p < 0.05$) for the cylindrical balloon, and 16.5% (122 ± 0.5 vs 130 ± 0.4 mmHg, $p < 0.05$) for TID and 9% (113 ± 0.7 vs 128 ± 0.8 mmHg, $p < 0.05$) for the TDD. Increasing the heart rate induced slight changes in PPi, as indicated in Figure 4-6. Differently, in case of changes in P_s, PPi shows important changes: at 60 bpm a change from 90 to 50 mmHg, PPi was found to increase +16% (142.4 ± 1.1 vs 164.7 ± 0.6 mmHg, $p < 0.05$) for cylindrical balloon, +25% (160.6 ± 0.5 vs 122.3 ± 0.5 mmHg, $p < 0.05$) for TID and +30% (113.2 ± 0.7 vs 152.7 ± 0.7 mmHg, $p < 0.05$) for TDD.

Table 4-2: *the table contains PPi measured in each site (base, centre and tip), for each balloon and for the horizontal and angle 45°.*

Inflation Pressure Pulse (mmHg)						
	Cylindrical		TID		TDD	
	0°	45°	0°	45°	0°	45°
Base	148 ± 1.2	155 ± 0.9	126 ± 0.6	152 ± 1.0	116 ± 0.7	132 ± 0.8
Centre	142 ± 1.1	148 ± 0.8	122 ± 0.5	130 ± 0.4	113 ± 0.7	128 ± 0.8
Tip	154 ± 1.3	159 ± 0.9	136 ± 0.6	158 ± 1.1	127 ± 0.3	138 ± 0.9

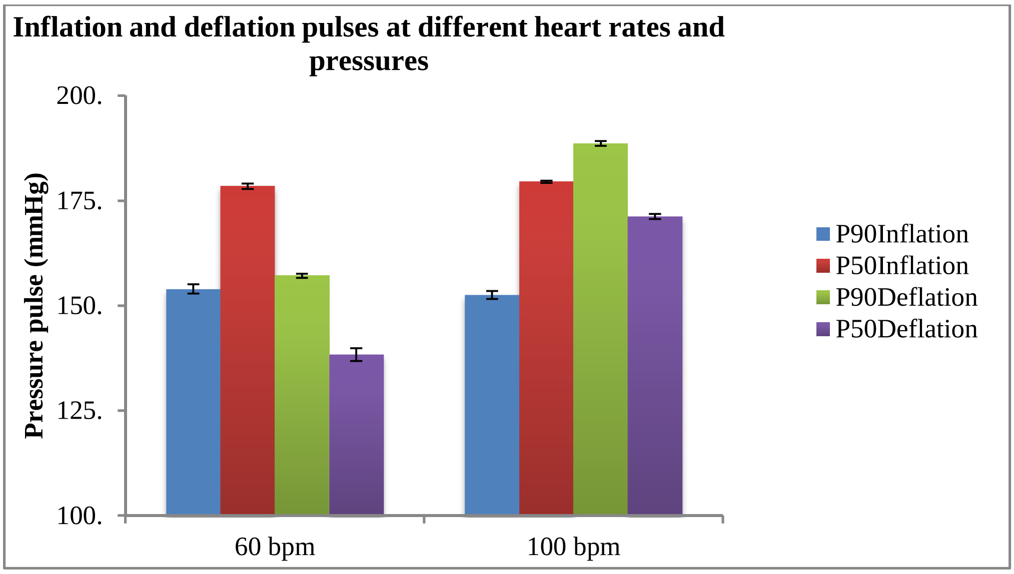

Figure 4-6: *The graph above PPi and PPd measured at the middle the cylindrical balloon in case of 90 mmHg of Ps (blue and green respectively) and 50 mmHg of Ps (red and violet, respectively) for 60 and 100 bpm of heart rate.*

4.4.4.2 Deflation

The lowest pulse pressure due to deflation (PPd) is observed at the centre of the balloon, which is consistent in all balloons, and PPd is always higher at the tip of the balloons, as shown in Table 4-3. At the horizontal position, the difference in PPd between the tip and base is 4.5% (157 ± 0.5 vs 150 ± 0.5 mmHg, $p < 0.05$) for the cylindrical balloon, 6.5% (160 ± 0.6 vs 150 ± 0.7 mmHg, $p < 0.05$) for TID and 11%

(162 ± 0.2 vs 146 ± 0.6 mmHg, $p < 0.05$) for TDD. Increasing the operating angle resulted in a reduction in the difference of PPd between the tip and base of each balloon. At 45° the difference is 3.6% (133 ± 0.6 vs 128 ± 0.6 mmHg, $p < 0.05$) for cylindrical balloon, 8% (130 ± 0.7 vs 120 ± 0.7 mmHg, $p < 0.05$) for TID and 7.8% (147 ± 0.5 vs 137 ± 0.4 mmHg, $p < 0.05$) for TDD.

Table 4-3*: the table contains PPd measured in each site (base, centre and tip), for each balloon and for the horizontal and angle 45°.*

Deflation Pressure Pulse (mmHg)						
	Cylindrical		**TID**		**TDD**	
	0°	45°	0°	45°	0°	45°
Base	150 ± 0.5	128 ± 0.6	150 ± 0.7	120 ± 0.7	146 ± 0.6	137 ± 0.4
Centre	145 ± 0.5	123 ± 0.6	132 ± 0.6	118 ± 0.7	145 ± 0.5	135 ± 0.3
Tip	157 ± 0.5	133 ± 0.6	160 ± 0.6	130 ± 0.7	162 ± 0.2	147 ± 0.5

All the balloons produced a lower PPd with increasing the angle, but TDD is associated to a lower decrease compared to the other two balloons. Increasing the operating angle from 0° to 45°, PPd decreased by 15.5% (145 ± 0.5 vs 123 ± 0.6 mmHg, $p < 0.05$) for the cylindrical balloon, by 18.5% (132 ± 0.6 vs 118 ± 0.7 mmHg, $p < 0.05$) for the TID and by 8.5% (145 ± 0.5 vs 135 ± 0.3 mmHg, $p < 0.05$) for the TDD (Table 43). Increasing the heart rate resulted in an increase in PPd (Figure 3.6): at a horizontal position + 20.4% (145.3 ± 0.5 vs 174.4 ± 0.6 mmHg, $p < 0.05$) for cylindrical balloon, 17.8% (131.8 ± 0.6 vs 155.3 ± 0.3 mmHg, $p < 0.05$) for TID and 6% (145.1± 0.5 vs 153.7 ± 0.5 mmHg, $p < 0.05$) for TDD. As found for inflation, a change in P_s provoked important changes also in PPd: at 60 bpm a change from 90 to 50 mmHg, PPd decreased -12.4% (145.3 ± 0.5 vs 127.3 ± 1.5 mmHg, $p < 0.05$) for cylindrical balloon, -15.9% (131.8 ± 0.6 vs 110.9 ± 2.5 mmHg, $p < 0.05$) for TID and -20.8% (145.1 ± 0.5 vs 114.9 ± 1 mmHg, $p < 0.05$) for TDD.

4.5 Discussion

Most patients assisted with IABP in the intensive care unit (ICU) are usually nursed in the semi recumbent position, resting at an angle of 30^{o} or 45^{o} [74, 75]. However, it was reported that operating the IABP at an angle to the horizontal changes the modus-operandi of inflation and deflation [63] and could result in reducing the IABP clinical efficacy as previously discussed [65]. For this reason two differently shaped balloons have been developed and their performances have been compared with the cylindrical balloon. The experimental set-up has been developed to provide symmetrical impedance to the balloon and, consequently, focus on the effect of the modified shape of the device on flow and pressure in the system when the balloon is placed at a horizontal position and at semi-recumbent positions.

4.5.1 Volumes

4.5.1.1 Inflation

One of the main therapeutic benefits of balloon inflation is to increase coronary flow, which depends on the volume displaced towards the tip of the balloon. Operating the balloon at an angle to the horizontal, inflation begins at the tip and proceeds to the base due to the hydrostatic pressure difference between the two ends of the balloon[9]. Biglino et al.[62] reported a loss of 30% in VUTVi when increasing the angle from 0^{o} to 45^{o}, for a cylindrical balloon tested at 45 mmHg. Our results are in agreement with these finding as shown in Figure 4-4 A; VUTVi of the cylindrical balloon is reduced by 25% when operated at 45^{o}. A possible explanation to the loss in VUTVi of the cylindrical balloon with increasing angle is that, increasing the balloon diameter at the tip, hence increasing the hydraulic resistance in this portion of the balloon, consequently reduces the flow volume displaced by the rest of the balloon.

The loss resulting from the same change at a heart rate of 100 bpm is absent, though (Figure 4-4 B). An explanation for this difference can be found in the change in duration of the balloon inflation: the shorter duration of inflation at a higher heart rate might induce the balloon to inflate only partially. The loss in VUTVi with increasing angle is due to the smaller volume displaced by the portion of the balloon which is inflating after the tip. If the balloon is only partially inflated the volume displaced upstream would depend mostly on the size of the first inflated segment of the balloon, which might not be strongly affected by the position, compared to the rest of the balloon.

The two tapered balloons showed a different behaviour with increasing angle, compared to the cylindrical balloon. Neither TID nor TDD resulted in a significant reduction of VUTVi when changing from 0^o to 45^o. The TID hardly lost its inflation performance; VUTVi decreased only by 1% and even increased by 13% for the TDD. Comparing the performance of the TDD balloon with the previous work by Biglino et al. [71], this balloon displaces +2% VUTVi compared to the cylindrical balloon at a horizontal position, against +7% measured by Biglino et al., and +13% at an angle of 20 degrees, close to +14% measured by Biglino et al.. Nevertheless it should be noted that in Biglino's study solely the first, isolated beat has been taken into account, while in the present study the balloons have been inflated and deflated for 25 beats, and ten beats (from 9^{th} to 18^{th}) have been taken into account. The results indicate that tapered balloons displace more relative volume towards the tip during inflation, compared to the traditional cylindrical balloon, at any operating angle. Possible explanations to these results follow.

TDD: the first part to inflate at an angled position (the tip, Figure 4-1), provides a smaller resistance to the flow being displaced by the rest of the balloon towards the tip (towards the coronary circulation in the clinical setting), compared to the standard cylindrical balloon. The resistance to flow towards the tip of the balloon during inflation can be derived from the momentum balance relating tangential force τrz, along the longitudinal direction, to flow pressure ΔP [76]:

$$\frac{d(rn*\tau rz)}{dr} = \frac{\Delta P}{Sn} * rn \qquad \text{(Eq. 4.1)}$$

where each balloon was divided into n = 10 sections, Sn and rn are the length and the radius of the **n** balloon's cylindrical section of which the resistance against the flow is measured. The integration gives:

$$\tau rz = \frac{\Delta P}{2Sn} * rn + \frac{C1}{rn} \qquad \text{(Eq. 4.2)}$$

where C1 is the constant of integration.

By using Newton's law of viscosity:

$$\tau rz = -\mu \frac{dvz}{dr} \quad \text{(Eq. 4.3)}$$

where vz is the velocity in longitudinal direction and **μ**= 0.001 Pa*s is the viscosity of water, and by applying the boundary conditions of no slip velocity on the balloon and aortic walls, it is possible to deduce the average velocity <vz> of flow in an annulus:

$$< vz >= \frac{\Delta P}{8\mu Sn} * Rn^2 * \left[\frac{1-\left(\frac{rn}{Rn}\right)^4}{1-\left(\frac{rn}{Rn}\right)^2} - \frac{1-\left(\frac{rn}{Rn}\right)^2}{\ln\left(\frac{Rn}{rn}\right)}\right] \quad \text{(Eq. 4.4)}$$

From 3.4 it will be possible to obtain the volume flow V through the annulus as following:

$$V = \frac{\Delta P}{8\mu Sn} * \pi(Rn)^4 * \left[1 - \left(\frac{rn}{Rn}\right)^4 - \frac{\left[1-\left(\frac{rn}{Rn}\right)^2\right]^2}{ln\left(\frac{Rn}{rn}\right)}\right] \quad \text{(Eq. 4.5)}$$

And consequently calculate

$$Rs = \Sigma_{n=1}^{10} \frac{8\mu Sn}{\pi(Rn)^4 \left\{1-\left(\frac{rn}{Rn}\right)^4 - \frac{\left[1-\left(\frac{rn}{Rn}\right)^2\right]^2}{ln\left(\frac{Rn}{rn}\right)}\right\}} \quad \text{(Eq. 4.6)}$$

where Rs, which is the total resistance of the 10 balloon cross sections, is 0.0088 and 0.1411 mmHg*min/l for the TDD and cylindrical balloons, respectively. These results offer a rationale as to the avoided loss in VUTVi when the TDD balloon is tilted.

TID: the tip of the balloon, which inflates first, provides the highest volume along the balloon **(**Figure 4-1**).** The base of the balloon, however, provides a smaller volume and is expected to displace a smaller amount of fluid towards the tip at any angle; hence the total loss in VUTVi is smaller than that of the standard cylindrical balloon.

The results of this study also showed that VUTVi decreases with increasing heart rate for all balloons. This trend is the consequence of the shorter time available for balloon inflation with increasing heart rate which, for instance in case of 100 bpm, is not ensuring the total inflation of the balloon, preventing a portion of the balloon volume to be displaced.

4.5.1.2 Deflation

The IABP deflation mechanism has not been adequately studied previously, particularly regarding the volume sucked away from upstream, which leads to reducing end diastolic pressure; LV afterload. Reduction of EDP is the direct consequence of balloon deflation and widely used as one of the IABP therapeutic benefits.

The cylindrical balloon lost deflation performance with increasing angle from 0^o to 45^o and VUTVd decreased by 21%. A possible explanation to this effect is that when the balloon is operated at an angled position, deflation begins at the base and proceeds towards the tip as previously confirmed by Khir et al. using high speed camera filming [63]. This mechanism leads to a bigger resistance at the tip than at the base, reducing the flow volume passing from upstream (the ascending aorta in the clinical setting) towards the base, and consequently a smaller VUTVd at an angle compared to the horizontal position.

The two tapered balloons showed a better performance compared to the cylindrical balloon during deflation as shown in Figure 4-5. VUTVd of the TDD and TID balloons changed insignificantly between 0^o and 45^o: +4.5% and -6%, respectively and a possible explanation for this follows:

TDD: During deflation the base of the balloon deflates first, and the tip provides a smaller resistance against the flow sucked by the rest of the balloon compared to the traditional cylindrical balloon; resistance values are 0.0088 and 0.1411 mmHg*min/l respectively, calculated using Eq. 4.1.

TID: The part of the balloon that deflates first is the base, which represents a small percentage of the total balloon volume. The portion of the balloon which deflates subsequently corresponds to most of the balloon's nominal volume. However it provides a greater resistance against the flow sucked from the tip of the balloon towards the base. Therefore, deflating the TID induces a lower volume sucked from the side of the tip because of the higher resistance associated to the tip of the balloon, calculated using Eq. 4.1 is 0.4545 mmHg*min/l.

All three balloons are however associated with a loss in VUTVd with increasing heart rate. However this decrease is noticeably smaller compared to the decrease in VUTVi, with increasing heart rate, as highlighted in **Table 41**. This marked difference can be explained in the different changes in values of PPi and PPd associated to an increase in heart rate: PPi is not influenced by the heart rate as much as PPd. For the cylindrical balloon, the maximum variation in PPi and PPd due to the increased heart rate consists in 1.7% and 24%, respectively. In case of deflation the negative influence of the higher heart rate on the VUTVd (already described for the VUTVi) is counterbalanced by the positive influence on PPd. As a result VUTVd is associated to a smaller decrease, with higher heart rate, compared to VUTVi.

4.5.2 Pressure pulse

4.5.2.1 Inflation

The distribution of PPi along the balloon changes according to the shape of the balloon: the cylindrical one is the balloon associated with the PPi the most homogenous along the balloon itself (4% of difference between the base and the tip), while the TDD is associated instead with the highest gap in pressure pulse (9.5%). The PPi measured along each balloon changes with increasing angle, and we noted that the difference in PPi between the tip and the base becomes smaller with increasing angle while the mean pressure is maintained constant (Table **4-2**). This indicates that the balloon inflation mechanism changes when the balloon is operated at an angle independently from the mean pressure. In all cases an increase in angle resulted in an increase in PPi, with the TID balloon creating the highest increase in PPi, on base and tip, with increasing angle.

Changes in heart rate produced different results according to different P_s. An increase in the heart rate at high P_s resulted in a lower PPi along the balloon, while at a lower P_s results in a slightly higher PPi (Figure 4-6). This is not surprising if it is considered that at a higher P_s it takes longer for the pressure within the balloon to reach the one in the fluid. If the duration of inflation decreases, then also the PPi produced by the balloon is affected. At a lower pressure, instead, P_s can be overtaken in shorter time and a higher heart rate would not affect negatively or positively affect PPi. The results about changes in PPi with different P_s agree with the ones from Biglino et al. [62] investigation: PPi is always reduced with increasing P_s.

4.5.2.2 Deflation

The cylindrical balloon is associated with the most homogenous PPd along the balloon itself (4.5% of difference between the base and the tip), while the TDD is associated instead with the highest difference between the two ends of the balloon in pressure pulse (11%). The difference in PPd between the tip and the base of each balloon became smaller with increasing the operating angle, while the mean pressure is maintained constant (Table 4-3). An increase in angle resulted in a decrease in PPd, also in agreement with earlier findings by Biglino et al.[62]. This result underlines the loss in balloon efficiency, with increasing angle, because of the change in deflation mechanics; at an angle to the horizontal the base of the balloon deflates first and collapses under the liquid pressure, which may restrict the flow of helium leaving the balloon towards the pump and compromising the speed of the deflation. However, PPd of the TDD balloon was the lowest affected with increasing angle. This is probably because the base of TDD is associated to the highest volume, may not collapse completely and therefore not restrict the flow of helium leaving the balloon towards the pump. PPd increased with increasing heart rate, from 60 bpm to 100 bpm, at both high and low P_s. This happens because the emptying of the balloon at a higher heart rate is faster, and this produces a higher deflation pulse.

Finally the changes in PPd induced by different P_s follow Biglino et al. [62] findings: in both studies a decrease in P_s, of 40 mmHg in the present study and 70 mmHg in Biglino's, resulted in a decrease in PPd for the cylindrical balloon, of 12.4% in the present study and 54% in Biglino's. The outcome was a decrease in VUTVd, which can be considered as a reduced balloon's efficiency, in agreement with the study conducted by Biglino et al. [62], but contrasting the results of other previous studies [77,78].

4.5.3 Limitations

The tapered balloons used in this work are larger than the physiological space available in an average aorta, which means that these balloons may not be used clinically. However, the in vitro results presented in this work indicate that the cylindrical balloon shape is not optimal. The results also present the possibility of a potential clinical therapeutic enhancement, in terms of volume displaced towards and away from the coronary arteries, should the tapered balloons be redesigned to observe the physiological space. The experimental set-up did not include an artificial heart to simulate the counterpulsation action of the physiological system. Also the experimental set-up did not include a mock aorta, but a straight rubber tube without branches, even though characterized by the same internal diameter as the aorta.

Given the aim of this study to examine the hemodynamic effects of different shaped balloons, we do not expect this to affect the trend of the results significantly. All of the balloons were tested in the same conditions, so the resulting differences can be ascribed only to the change of shape. Moreover subsequently, as described in Chapter 1, new tapered balloons, characterized by a size compatible with the physiological space, will be introduced and tested in conjunction with the use of an LVAD producing an aortic pressure waveform.

4.6 Conclusions

VUTVi and VUTVd are both reduced when a standard shaped cylindrical balloon is operated at an angle to the horizontal with a heart rate of 60 bpm and a pressure of 90 mmHg, indicating a reduction of the potential therapeutic benefit of increasing coronary flow and reducing LV afterload.

The TDD provided the greatest VUTVi and also produced the largest PPd, indicating better potential coronary perfusion and afterload reduction. Although the TID provided less VUTVi and VUTVd at smaller angles compared to the cylindrical and TDD, this balloon was not markedly affected by the change of angle. All balloons are associated with decreased VUTVi and VUTVd with increasing heart rate at a pressure of 90 mmHg, but the deflation phase was not as compromised as the inflation one. While PPi has shown to be markedly influenced mostly by the pressure acting on the system, PPd increased in case of higher heart rate and P_s, and decreased with increasing angle.

Further investigations are required to optimise the shape of the cylindrical balloon to obtain the full benefit of the IABP therapy for increasing coronary perfusion and reduction of afterload.

Chapter 5 Experimental study on novel shaped balloons for improved performance on a physiological test-bed

5.1 Chapter outlook

The changes in intra-aortic balloon performance related to different shapes have been analysed when the device is placed in a hydraulic system (Chapter 4). This system was characterized by a static pressure which varied exclusively due to the pumping activity of the balloon.

In order to specifically address and confirm the benefits associated to a different shape of the balloon, novel shapes of the IAB which derive from the ones already presented and studied, have been tested in a more physiological bed, presenting a dynamic pressure similar to the physiological one. Nevertheless, the newly developed shapes have been designed to fit the physiological space.

The aim of this experimental study is to assess the changes in pressure waveform and flow displacement associated with changes in shape of the IAB in a mock circulation which is characterized by a physiological pressure waveform. This could confirm whether the TID and TDD balloons, already tested and discussed in Chapter 4, can show evidence of improved performance compared to the standard balloon in terms of increased diastolic flow towards the coronaries and decreased end diastolic pressure, enabling to highlight their clinical benefits.

5.2 Introduction

The study described in Chapter 4 showed important changes in Intra-Aortic Balloon performances, at different angulations from the horizontal position, associated to a different shape. However, the balloons could not fit the physiological space because of the excessive length. They have been tested in a simple set-up and their performance might radically change when pressure and flow waveforms are set comparably to the physiological ones.

Biglino et al. previously tested two standard cylindrical balloons (25 cc and 40 cc in volume) in a mock aorta connected to a left ventricular simulator device [71]. The balloons were tested at different angles, from horizontal to an angle of 65°, and at three different assistance frequencies (1:1, 1:2 and 1:3). The results of that study showed a detrimental effect of the angle on balloon efficacy in terms of both, diastolic pressure augmentation and end-diastolic aortic pressure reduction.

However, the flow displaced towards coronary circulation was not particularly affected by a change in angulation. Moreover, the authors noted that the assistance frequency has an important effect on both, pressure and flow, as the frequency 1:1 induced more benefits compared to 1:2 and 1:3.

Although many differently shaped balloons [46,47,51] have been presented and discussed in previous works, most of them have not undergone an experimental testing in a set-up which resembles balloon counterpulsation in a physiological manner. This is crucial to access a possible benefit of the device by analysing changes in physiological parameters and to ensure the minimisation of the device disadvantages. In addition it would be possible to draw conclusions from the study which would be meaningful from a clinical perspective.

The present work aims at comparing the efficacy of one cylindrical and six novel balloons and at investigating their changes in performance in relation to changes in position and changes in IAB assisting frequency. All the balloons have been designed to fit the physiological space in the descending aorta and tested in a physiological set-up while counter-pulsating with a left ventricular simulator. Their efficacy is evaluated based on the increased diastolic pressure and flow towards the upstream, for the inflation, and decreased end diastolic pressure, for the deflation. In addition, the clinical benefit of the newly designed IABs will be highlighted in the PV loop.

5.3 Materials and methods

5.3.1 Balloons

Seven balloons (Teleflex, Boston, Massachusets, USA) were tested and compared: a standard cylindrical balloon with diameter (d) of 1.5 cm and length (L) of 22.4 cm; six differently shaped balloons, three with a tapered portion decreasing in diameter from the base to the tip (TDD) and the other three with a portion increasing in diameter from the base to tip (TID). Each of the three TDD balloons was characterized by a different proportion of cylindrical part and tapered part, approximately as following:

- **a.** TDD 1/3 presented one third cylindrical and two third tapered part,
- **b.** TDD 1/2 with half cylindrical and half tapered portion,
- **c.** TDD 2/3 presented two third cylindrical and one third tapered part.

The three TID balloons are the opposite of TDDs, with same proportions of cylindrical and tapered parts but with tapered part on the base of the IAB:

- **d.** TID 1/3 presented one third cylindrical and two third tapered part,
- **e.** TID 1/2 with half cylindrical and half tapered portion,
- **f.** TID 2/3 presented two third cylindrical and one third tapered part.

The length of the differently shaped balloons varied from 22.5 to 24 cm and the maximum diameter (at the base for TDDs and at the tip for TIDs) varied from 1.6 to 1.81 cm. The seven balloons are shown in Figure 5-1, together with the measurements of cylindrical and tapered portions of the IAB. The nominal volume of each balloon was established by placing it in a graduated beaker and inflating with a syringe, recording the volume displaced once the pressure within the balloon reached 70, 90, 110 and 130 mmHg. The volume displaced was then obtained through subtracting from the final volume, with inflated IAB, the beginning volume, with deflated IAB. The average of the four values of volume has then been calculated. All the values are indicated in Table 51. As reported, the maximum standard deviation of the obtained volumes at the four tested pressures, expressed as a percentage of the volume average value, is always smaller than 3%. The averaged displaced volumes were 33.83 cc, 34.2 cc, 34 cc, 33.73 cc, 34.15 cc, 33.95 cc and 30.83 cc for TDD 1/3, TDD 1/2, TDD 2/3, TID 1/3, TID 1/2, TID 2/3 and standard balloon.

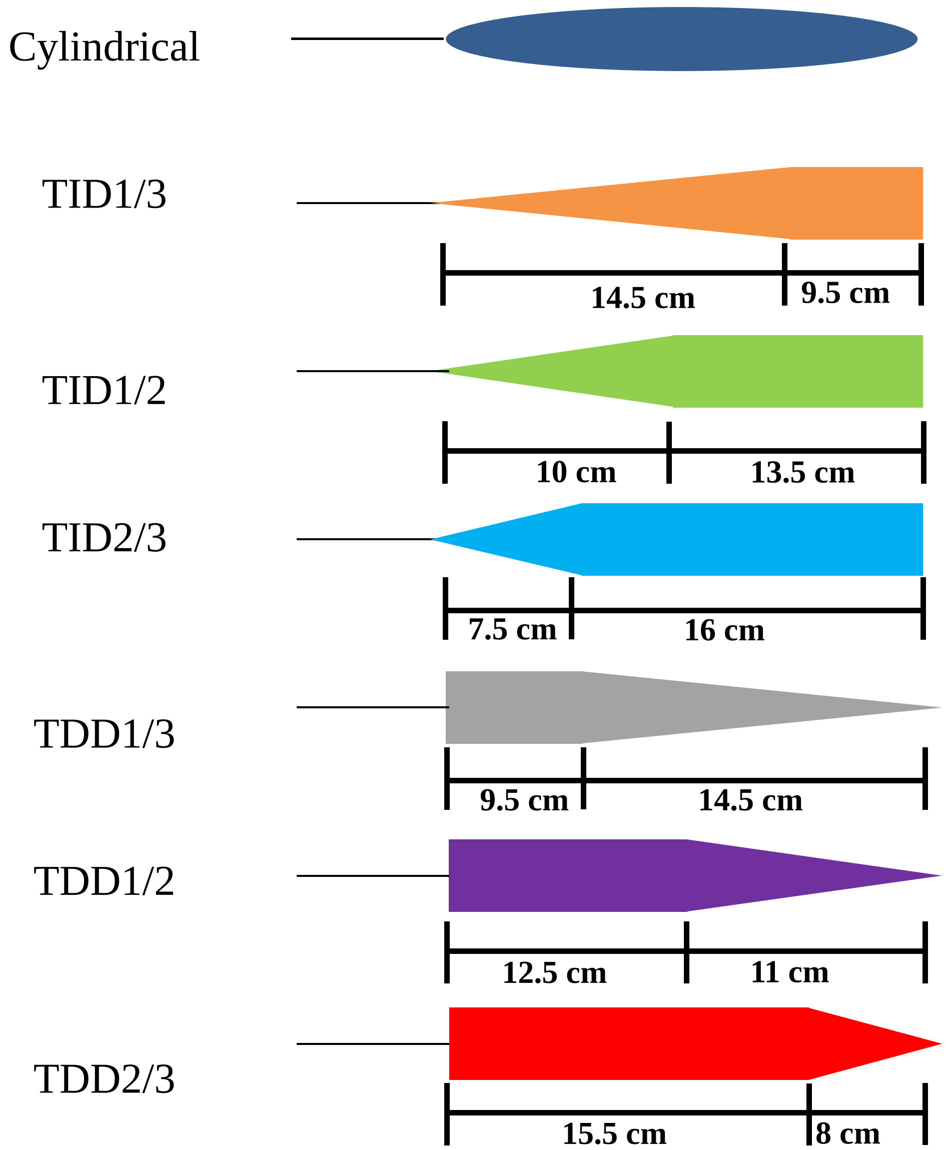

***Figure 5-1**: Representations of the tested balloons, cylindrical on the top, three TIDs and three TDDs. All dimensions are expressed in cm.*

Table 5-1: *Volume displaced by each balloon is indicated at four different pressures, together with its standard deviation expressed as percentage of mean value.*

	Intra-balloon pressure (mmHg)	**Volume displaced (cc)**	**Average Volume displaced (cc)**	**Standard deviation (% of mean value)**
Cylindrical	70	30	30.83	2.4
	90	30.5		
	110	31.1		
	130	31.7		
TID 2/3	70	33	33.95	2.4
	90	33.6		
	110	34.3		
	130	34.9		
TID 1/2	70	33.1	34.15	2.8
	90	33.7		
	110	34.5		
	130	35.3		
TID 1/3	70	32.9	33.73	2.2
	90	33.4		
	110	34		
	130	34.6		
TDD 2/3	70	33.1	34	2.4
	90	33.6		
	110	34.3		

	130	35		
TDD 1/2	70	33.2	34.2	2.6
	90	33.8		
	110	34.5		
	130	35.3		
TDD 1/3	70	33	33.83	2.2
	90	33.5		
	110	34.1		
	130	34.7		

5.3.2 Experimental set up

The experimental set up is shown in Figure 5-2**.** A straight silicone rubber tube of 2.1 cm internal diameter, 37.5 cm in length and 0.18 cm of wall thickness was chosen to replicate the aorta. The compliance of the tube was 0.075 ml/mmHg, which is relatively close to that of the thoracic aorta of 0.11 ml/mmHg as measured by Westerhof et al [70]. Note that, differently from the set-up described in the previous chapter, the mock aorta was chosen to have a smaller diameter in relation to the balloons nominal volumes, which vary between 30 and 35 cc in the current experiment and varied between 36 and 41 in the previous one.

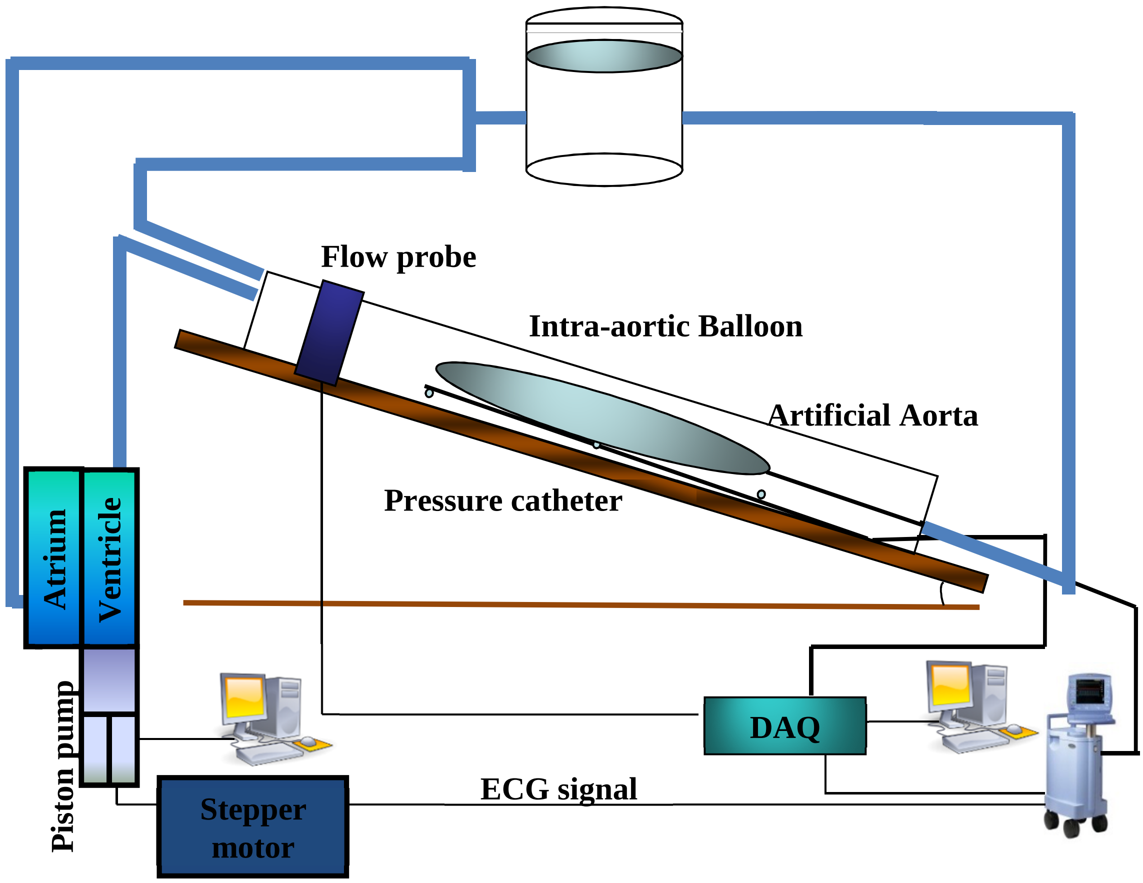

Figure 5-2: *Schematic representation of the experimental set up in which all balloons have been tested. The ECG signal generated by the IABP triggers the stepper motor which, through the piston pump and the atrium-ventricle system (BVS 5000 blood pump, Abiomed, 22 Cherry Hill Drive Danvers, Massachussetts 01923 USA), creates a physiological aortic pressure waveform in the system where the balloon is placed and counter-pulsates.*

The tube was water filled and used to host each balloon, and it was connected to an overhead reservoir used for venous return through a pair of lateral tubes that included an impedance identical for both paths and equal to 84 mmHg*min/L. This value has been used in order to resemble physiological upstream resistance, as reported by Khir et al [67]. The set up was symmetrical to provide equal impedance to each side of the balloon. The compliance characterizing the system was also symmetrically distributed in the system and equal to $4.5*10^{-2}$ ml/mmHg on each side.

The impedance on the two sides was chosen identical to dissect the effect of impedances on flow and pressure distribution from the one of the different shape. The tube accommodating the balloon was placed on a platform whose angle to the horizontal was adjusted to replicate patient's posture. The upstream side of the set-up (above the balloon tip) was connected to a left ventricular simulator, which was interfaced with a stepper motor driver set up to produce a stroke volume of 26 cc, with a duration of systole and diastole of 0.3 and 0.7 s respectively. The resulting pressure waveform is shown in Figure 5-3.

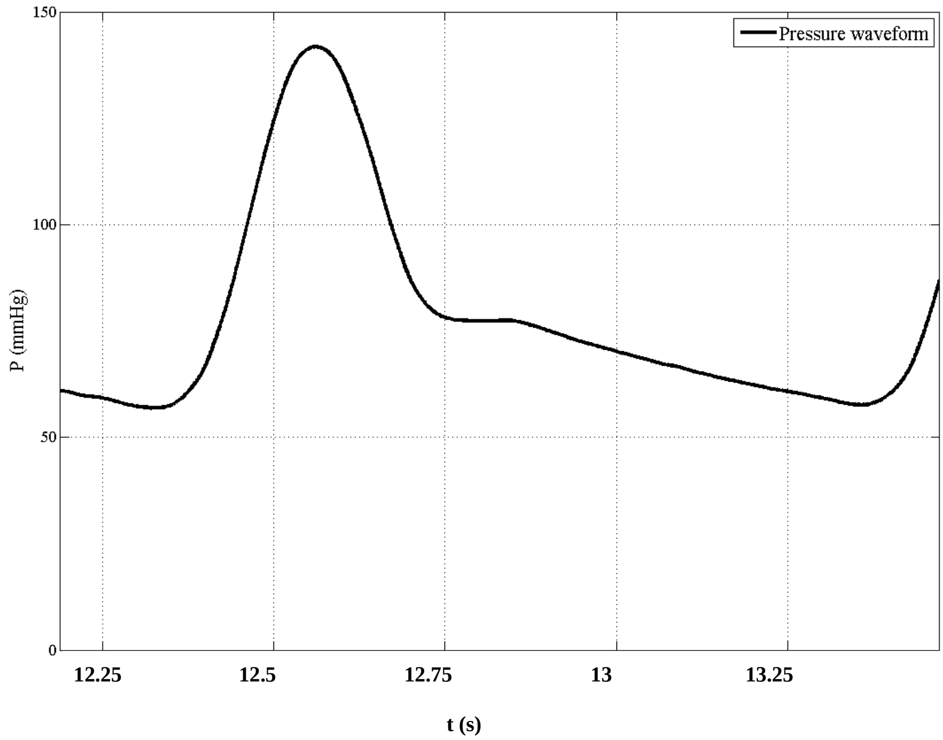

Figure 5-3*: Pressure waveform measured at the centre of the balloon while not counter-pulsating, obtained through the activity of the left ventricular simulator.*

The balloon was operated at four different positions: 0°, 20°, 30°, 45°. At each platform position the overload reservoir connected to the circuit was raised in order to maintain a constant hydrostatic pressure in the middle of the balloon ρgh (where ρ is water density (1000 kg/m^3), g is gravitational acceleration (9.81 m/s^2) and h is the lateral distance between the water level in the reservoir and the centre-line of the balloon). The left ventricular simulator was also lifted as much as the reservoir in order for the venous return to provide a constant pressure on the atrial chamber of the device. This process would result in the pressure waveform systolic peak and end diastolic pressure to be almost unvaried at the middle of the balloon, with a maximum difference of 7% in systolic peak throughout positions.

Each balloon was operated by the same pump (Teleflex, Boston, Massachusets, USA), which was triggered using the ECG signal provided by the stepper motor driving the flow. Since the pressure applied by this pump onto the balloon varies according to the catheter used for connecting the IAB to the machine, a different catheter was used, according to the nominal volume of the balloon, for the cylindrical and for all other balloons: a 30 cc catheter was used for the standard balloon and a 35 cc one was used for the differently shaped balloons.

The mode of the pump was set to 'OPERATOR' on the console, and 'PEAK' (QRS peak of ECG) was selected as a trigger, in order to ensure the same onset of inflation and deflation for each balloon and each position. This mode was selected in to maintain an unvaried duration of inflation/deflation: when selecting 'AUTOMATIC' the un-calibrated Helium pressure signal revealed a longer duration of inflation in case the set-up was angulated, while 'OPERATOR' mode on 'PEAK' signal resulted in the duration of inflation/deflation to be constant throughout angulations, as shown in Figure 5-4. The performance of the balloon at horizontal and angled position would then exclusively depend on the IAB shape.

For all balloons and all angulations the IAB was tested with two assistance frequencies (AF), 1:1 and 1:4. AF 1:1 was studied with the target of assessing the performance of the balloons in clinical settings. AF 1:4 was studied for analysing the hemodynamic changes associated with the use of the device, separating the effects of each balloon beat on the fluid-dynamics of the system. The parameters controlling the stepper motor driver have not been changed throughout the experiments, ensuring a correct comparison among all balloons and all positions.

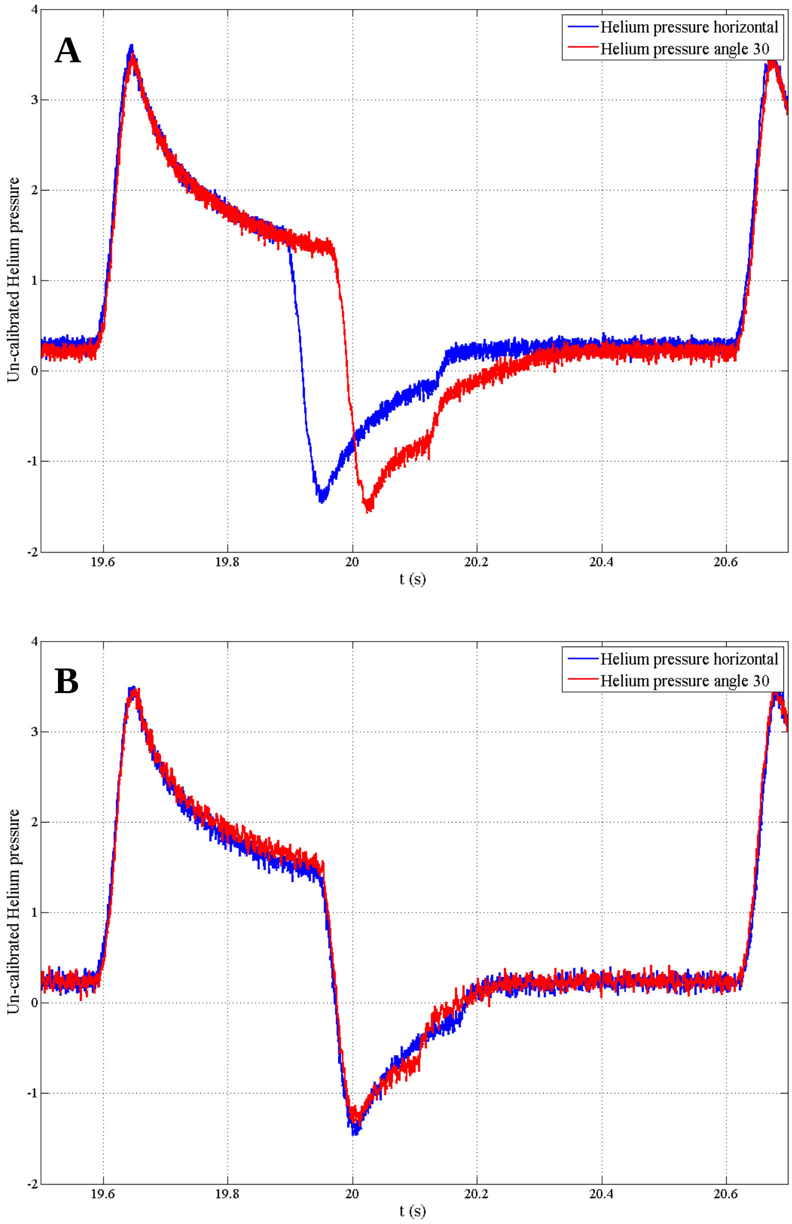

Figure 5-4*: Un-calibrated Helium pressure signal in case of horizontal (blue line) and angle of 30° (red line) when 'AUTOMATIC' (A) or 'OPERATOR' mode with 'PEAK' signal triggering (B) are selected. The first case shows a net difference in duration of inflation, while the second one presents both signals almost identical.*

5.3.3 Measurements

Pressure was measured in 5 positions: 3 sites along the balloon, base, middle and tip, and 2 sites away from the balloon, 10 cm from each side. In the two latter sites, flow was also measured simultaneously. Measurements were recorded at a frequency of 2 kHz. A Gaeltec multi sensor (n = 3) pressure catheter (Gaeltec, Scotland, UK) was inserted in the artificial aorta from the same side of the balloon, and placed along it. Pressure measurements away from the balloon were obtained through two different pressure catheters (Millar, Houston, Texas) inserted from the opposite side of the balloon catheter. Flow measurements was performed by snug-fitting two flow probes (28A, Transonic, Ethica, NY, USA) to the tube accommodating the balloon, at the same positions of the Millar pressure transducers. Helium un-calibrated pressure was also recorded to indicate balloon inflation/deflation pattern. Data of 100 beats for each experiment were recorded using an analogue-digital converter and Labview software (National Instruments, Austin, TX, USA). Data were analyzed off-line using Matlab (The Mathworks, Natick, MA, USA).

5.3.4 Data analysis

Inflation and deflation were distinguished as the periods between point A to point B, and point B to point C, respectively, as shown in Figure 5-5. The volume displaced upstream beyond the tip (VU) was calculated by integrating the area above the flow waveform measured during inflation period. As already explained in the previous Chapter (4), the two integrations take into account the flow changes due to IAB inflation and deflation, and it was chosen to integrate the flow in correspondence of flow waveform changes after inflation and deflation onset (Figure 5-5). Volume sucked from upstream (VUs) was also obtained by integrating the area below the flow waveform measured upstream during the deflation period. In order to compare the results of all the balloons that have different nominal volumes (Vn), VU and VUs were normalized as ratio of Vn, obtaining, respectively, volume displaced upstream during inflation (VUTVi) and during deflation (VUTVd).

The performance of balloon counterpulsation was related to the increased diastolic pressure (PPi) during inflation, established as the difference between maximum diastolic pressure and pressure at the onset of balloon inflation, and to the end diastolic pressure (EDP) during deflation, established as the minimum pressure before systolic pressure rise. PPi and EDP were calculated at the 3 measurement sites along the balloon. The beats analysed are from the 6^{th} assisted to the 20^{th} assisted for each experiment, to ensure the system was operating on steady-state and to obtain a good statistical analysis in terms of mean value and standard deviation.

For comparing the variability of VUTVi between different AF and of VUTVi and VUTVd it will be used the coefficient of variation CV, defined as:

$$CV = \frac{\sigma}{\varepsilon} \qquad \textbf{(Eq. 5.1)}$$

where σ is the standard deviation of the values and ε is their mean value.

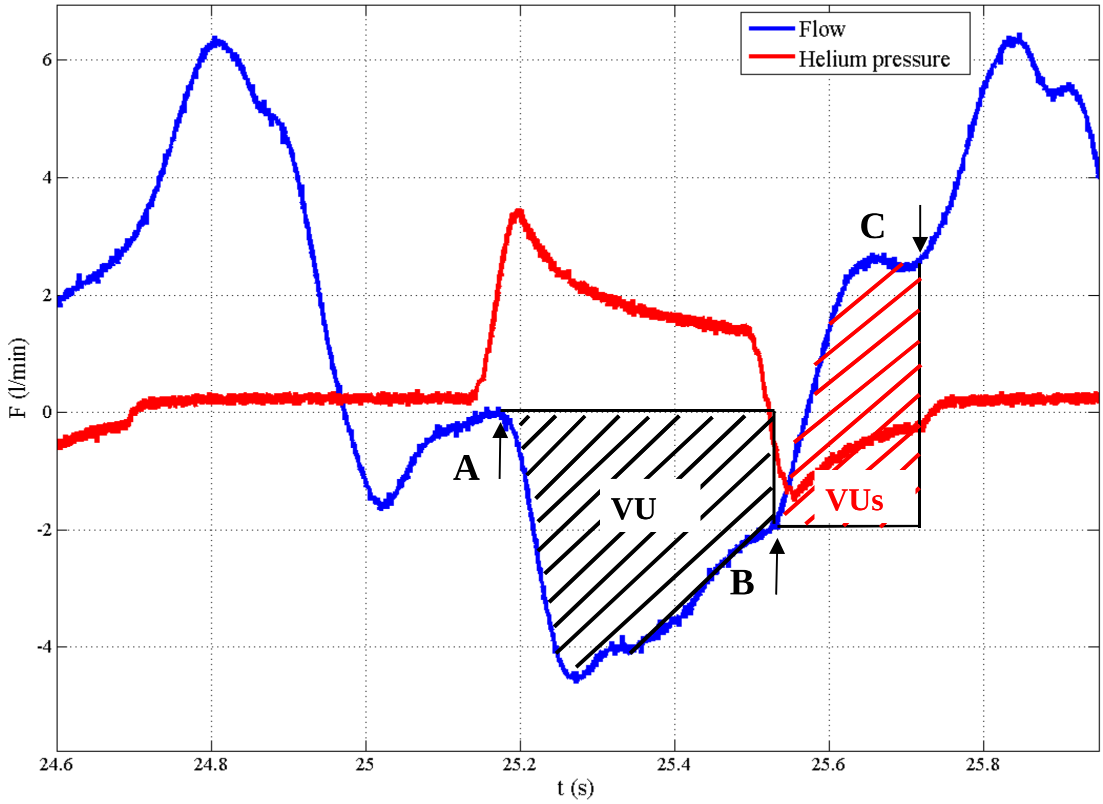

***Figure 5-5**: Flow waveform on the upstream of the balloon (blue line). The arrows and points A, B and C indicate onset of inflation, onset of deflation and end of deflation, respectively. The red line indicates the balloon pressure (not calibrated) as recorded from the IABP. The area integrated below the blue line between points A and B indicates the volume displaced away from the tip of the balloon during inflation (VU). The area integrated above the blue line between points B and C indicates the volume sucked away from the tip of the balloon during deflation (VUs). These values are divided by the nominal volume of the balloon to give VUTVi and VUTVd, respectively.*

5.4 Results

5.4.1 Inflation

5.4.1.1 Volume displaced upstream

5.4.1.1.1 Changes with angle

Figure 5-6 shows VUTVi for the best balloons and standard cylindrical one, and for both AF. TDD 1/2, TID 2/3, TID 1/3 and TID 1/2 are the balloons whose VUTVi is not negatively affected by angulation, for both 1:1 and 1:4 assistance frequencies. Considering a change from horizontal to 45° position, the reported shaped balloons are associated to a mean VUTVi higher by 9% (0.39 ± 0.19 vs 0.43 ± 0.12, $p = 0.6$) in the worst case (TID 1/2) for AF 1:1 and mean VUTVi higher by 4% (0.39 ± 0.10 vs 0.41 ± 0.15, $p = 0.7$) for AF 1:4. Differently, the standard balloon studied is associated to a decrease of 23% (0.44 ± 0.12 vs 0.34 ± 0.11, $p < 0.05$) for AF 1:1 and 15% (0.42 ± 0.11 vs 0.36 ± 0.07, $p = 0.07$) for AF 1:4. If the VUTVi standard deviation obtained from the analysis of each experiment is expressed as a percentage of VUTVi mean value, through the parameter CV, an estimation of the reliability of the results is obtained. This value varies according to position and balloon, and its average is 27%.

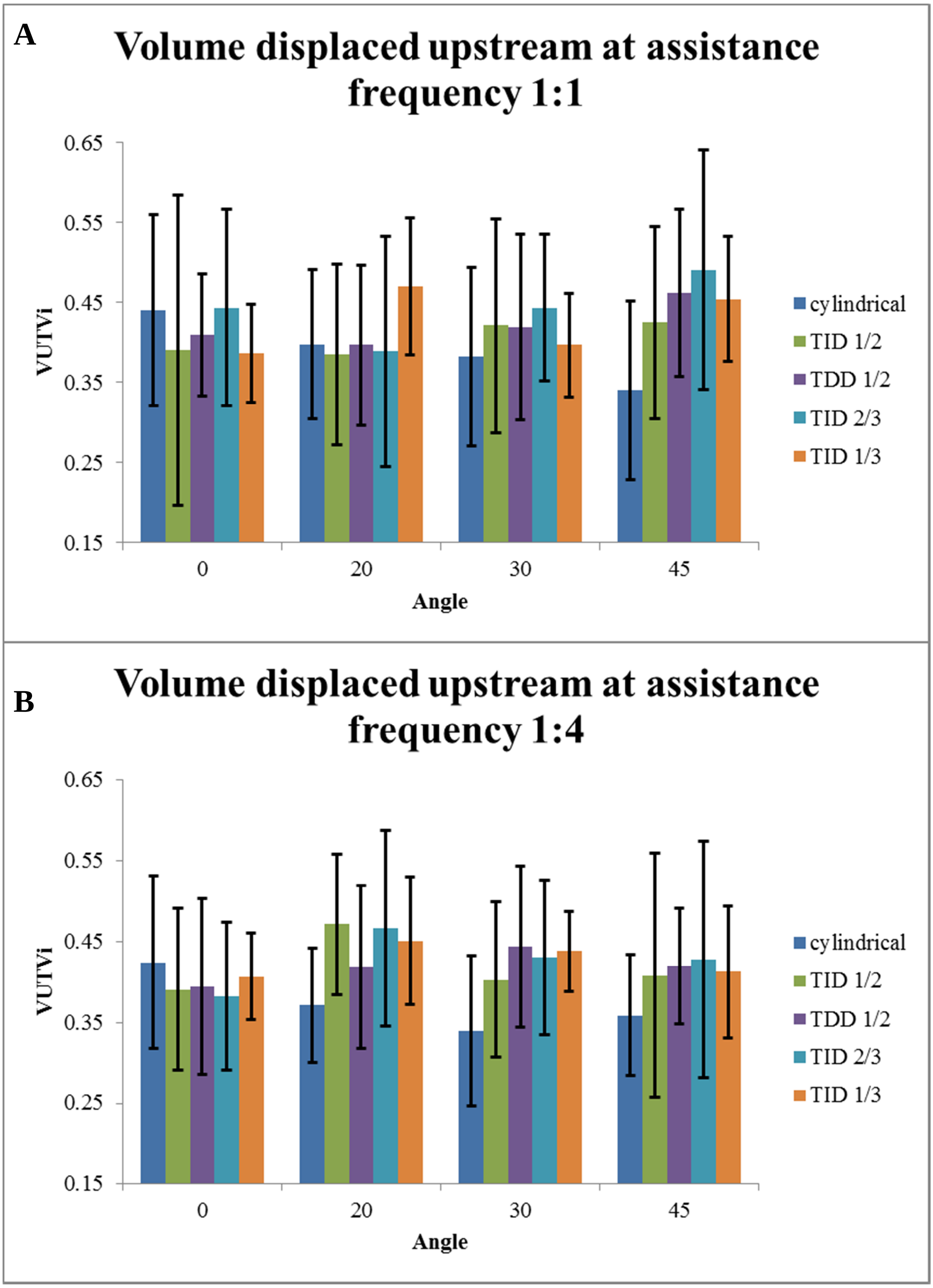

Figure 5-6*: VUTVi is indicated for the 4 best performant balloons and for the cylindrical one, for all positions and for 1:1 (5 A) and 1:4 (5 B) assistance frequencies. With the aim of comparing the four best balloons with cylindrical one and in order to avoid confusion TDD 1/3 and TDD 2/3 are not represented.*

5.4.1.1.2 Changes with assisting frequency

Figure 5-7 shows the changes in the cylindrical balloon VUTVi with increasing angle for both 1:1 and 1:4 AF. All positions are associated to a value of VUTVi with smaller standard deviation in case of AF 1:4 rather than 1:1. The experiments revealed a strong similarity in VUTVi, between assistance frequencies of 1:1 and 1:4, for the cylindrical balloon. As seen in the graph in Figure 5-7, for this IAB, the maximum difference in AF is 11.2 % (0.38 ± 0.11 vs 0.34 ± 0.09, p = 0.27), in case of 30° position. However, throughout the analysis of VUTVi values (all experiments and balloons), CV was found to be smaller when the applied assistance frequency was 1:4 rather than 1:1, as shown in Figure 5-8.

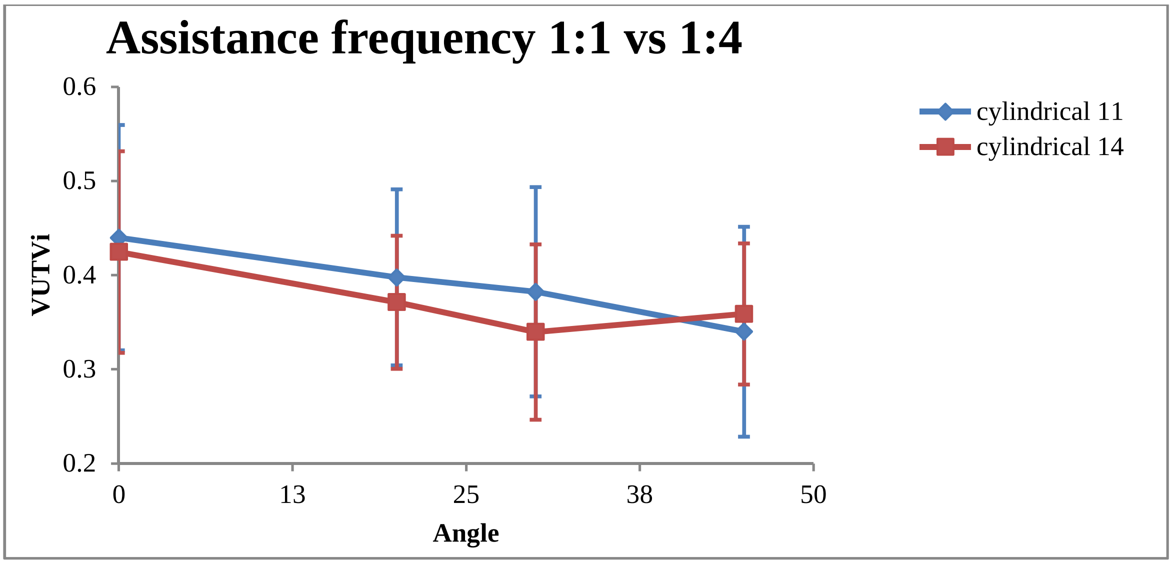

Figure 5-7*: The graph shows the comparison between VUTVi induced by cylindrical standard balloon at all studied positions and AF 1:1 and 1:4, underlying the differences between the two configurations. The maximum difference, of 12% (p = 0.56), occurs at 30°.*

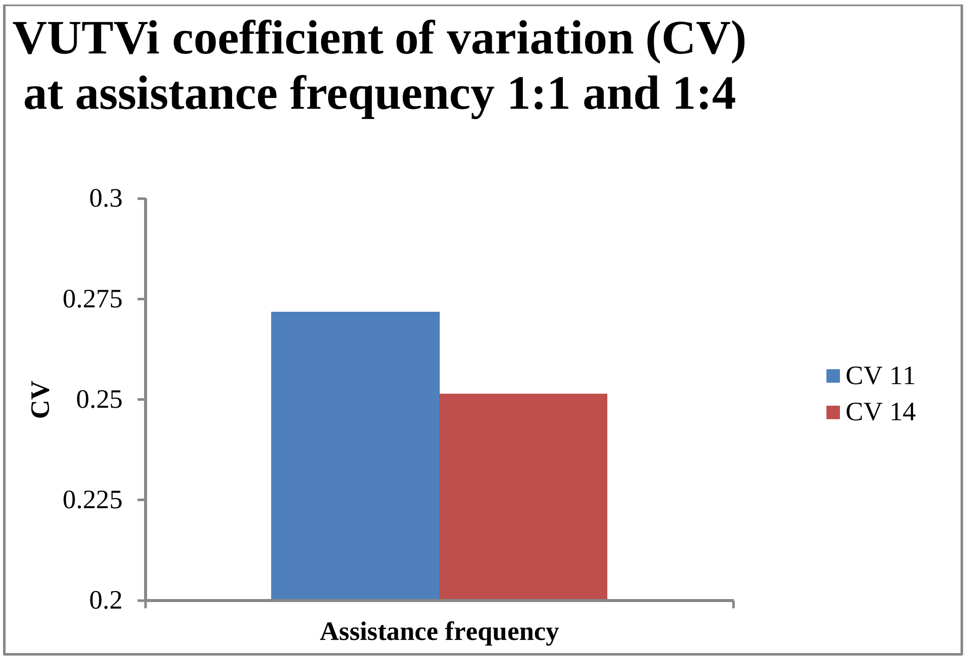

Figure 5-8*: Coefficient of variation (CV) characterizing the measurements of VUTVi, throughout balloons and positions, is indicated for 1:1 and 1:4 assistance frequencies.*

5.4.1.2 Augmentation in diastolic pressure

All balloons at an angle have a distribution of inflation pressure pulse which is different from the one at horizontal position (excluding TID 2/3, which is associated to a similar distribution at horizontal and angled positions). Whilst at a horizontal position the pulse was higher at the tip of the balloon compared to the base, at angled positions this difference became much smaller or negative (base of the balloon is associated to a higher pulse). Particularly, in case of standard cylindrical balloon, at the tip of the IAB the inflation pulse decreased by 9% (85.96 ± 0.24 vs 78.16 ± 0.47 mmHg, $p < 0.01$) while at its base the inflation pulse did not vary significantly (-0.32%, 82.86 ± 0.22 vs 83.13 ± 0.48 mmHg, with $p = 0.7$).

This difference in pulse between the balloon tip and base was confirmed by the results of inflation pulse above the tip (upstream) and below the base (downstream) of the cylindrical standard balloon, markedly changing from horizontal to an angled position. According to **Table 52** pulse upstream decreases by 6.7% (90.80 ± 0.50 vs 84.70 ± 0.90 mmHg, $p < 0.01$) for a change in position from 0° to 45°, while pulse downstream increases by 6.7% (84.40 ± 1.60 vs 90.10 ± 0.70 mmHg, $p < 0.01$).

Table 5-2: *Inflation pressure pulse measured upstream and downstream for the standard balloon at a horizontal position and at an angle of 45°.*

	Inflation pulse upstream	**Inflation pulse downstream**
Horizontal	90.8 ± 0.5	84.4 ± 1.6
Angle 45	84.7 ± 0.9	90.1 ± 0.7

All balloons pulses at a horizontal position were in a range between 95 to 101 mmHg at their tip, apart from the standard cylindrical one which was associated to a maximum of 86 mmHg in its tip part. TID 1/2 balloon is associated to the highest pulse at a horizontal position, while TID 2/3 was found to perform best at an angle of 45°. No significant changes to any of the balloons inflation pulse was induced by a change in AF from 1:1 to 1:4.

5.4.2 Deflation

5.4.2.1 Volume sucked from upstream

5.4.2.1.1 Changes with angle

Changing the angle from horizontal to angle 45° resulted, for the cylindrical balloon, in a decrease of VUTVd by 34% for AF 1:1 (0.39 ± 0.04 vs 0.26 ± 0.04, $p < 0.01$) and 37% for AF 1:4(0.41 ± 0.04 vs 0.26 ± 0.01, $p < 0.01$). TDD 1/3 is the balloon inducing the highest VUTVd for all angled positions at AF 1:1, and also associated to an almost unchanged VUTVd between horizontal and angle 45° position (0.36 ± 0.03 vs 0.37 ± 0.10, $p = 0.7$). At an AF of 1:4, instead, TDD 2/3 is the one inducing the highest VUTVd across all angled positions, and is characterized by an approximately unchanged VUTVd between horizontal and angle 45° position (+1%, 0.33 ± 0.02 vs 0.34 ± 0.05, with $p = 0.8$).

Hence, excluding horizontal position, a clear difference emerges between the balloon’s series of TDD and TID and standard balloons. Figure 5-9 A shows that all TDD balloons are associated with a higher VUTVd at any angle, compared to the standard balloon. In Figure 5-9 B, instead, it emerges that TID balloons induced a lower VUTVd compared to the cylindrical balloon.

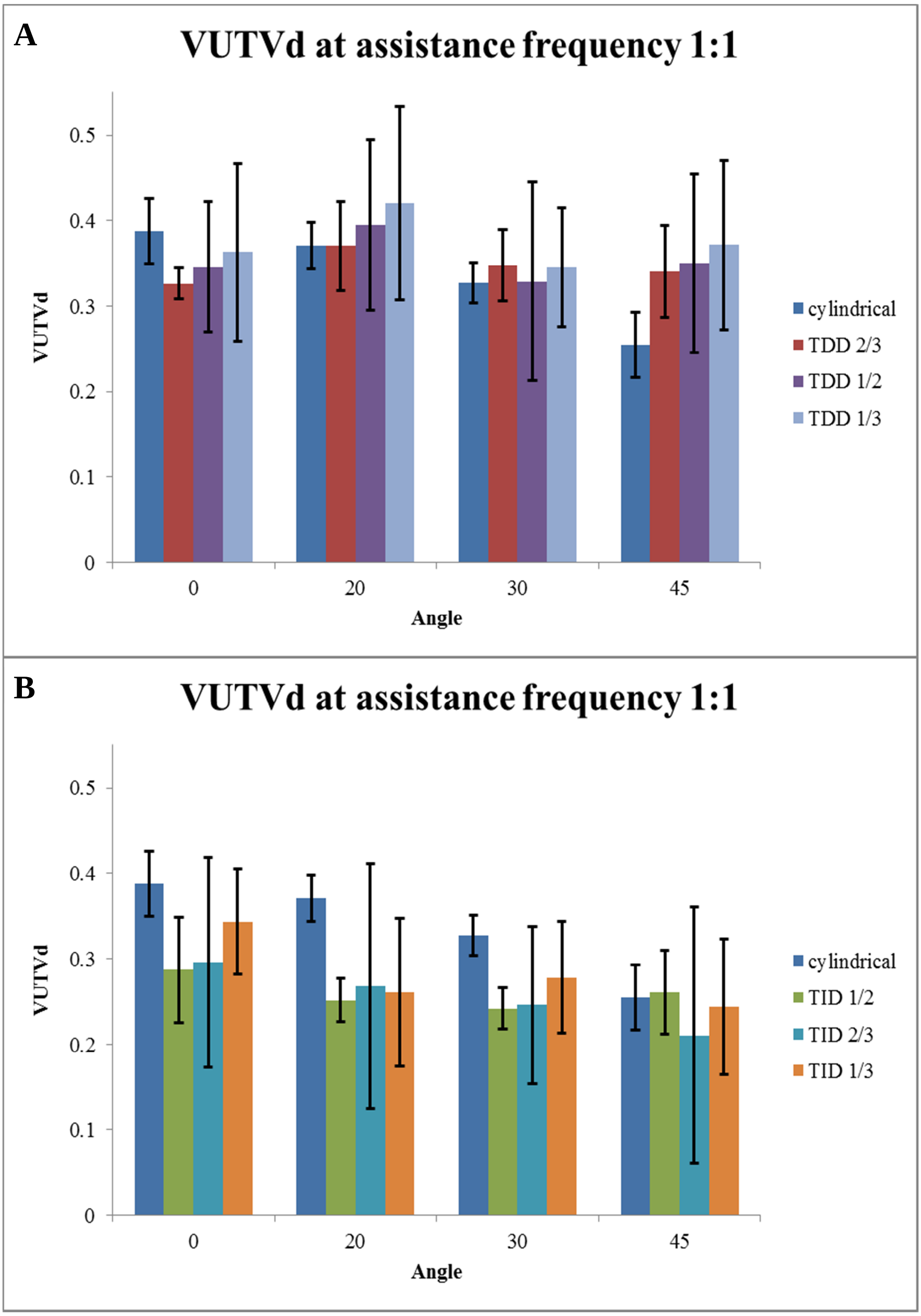

Figure 5-9*: VUTVd for 1:1 assistance frequency is indicated showing the differences between standard cylindrical balloon and TDD balloons (9 A) and between standard cylindrical balloon and TID balloons (9 B) for all positions.*

The performance of the cylindrical balloon hence locates in the middle between the two series of balloons, generally better than TIDs but worse than TDDs. It was shown that an increasing of angulation decreases VUTVd of all TID balloons. Particularly TID 2/3 balloon is associated to the lowest VUTVd at all positions for AF 1:4 and one of the lower at AF 1:1. Deflation VUTVd standard deviation of each experiment is expressed as a percentage of VUTVd mean value, obtaining the value of CV. In this case the value averaged throughout experiments is around 11%, showing the reliability of the measurements.

5.4.2.1.2 Changes with assisting frequency

The increase induced by TDD balloons is effective at both 1:1 and 1:4 assistance frequencies. In fact VUTVd values, differently from VUTVi, did not change markedly for each balloon by changing the AF from 1:1 to 1:4. The CV associated to the VUTVd throughout the positions and balloons corresponds to less than half of the one associated to the VUTVi, as shown in Figure 5-10.

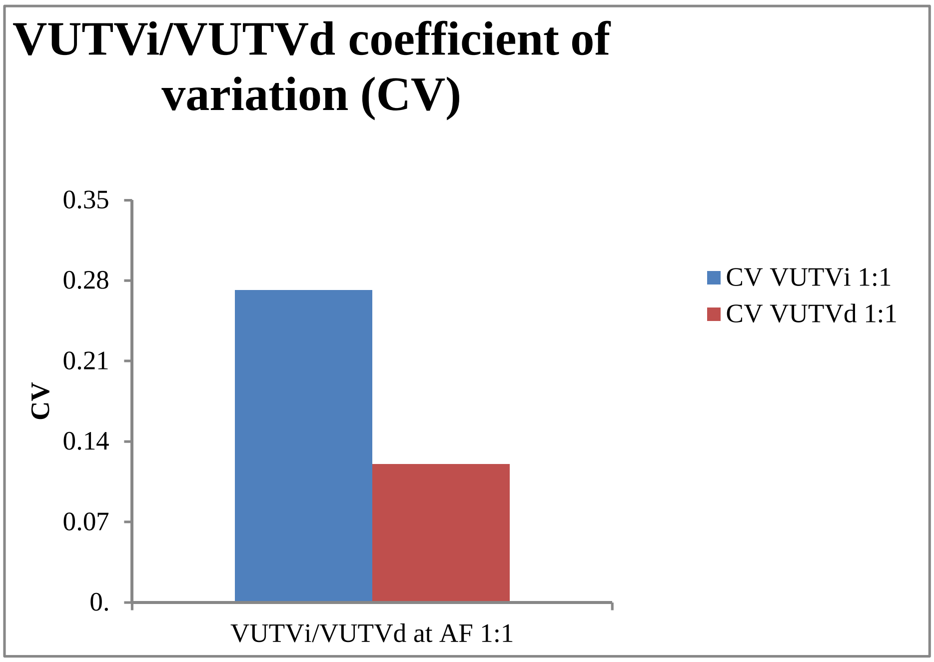

***Figure 5-10**: Coefficient of variation of VUTVi and VUTVd measurements throughout balloons and positions, at an assistance frequency of 1:1, is indicated and compared, showing a radical difference between the two measurements.*

5.4.2.2 Decrease in end diastolic pressure

EDP increased with increasing angle for all IABs. This is shown in Figure 5-11, representing the EDP at the centre of the balloons for AF 1:1 and 1:4. It has been chosen to show the pressure associated to the mid-point of the IAB because it is the only point on which the overload pressure was maintained constant throughout positions. EDP along the balloon also changed with increasing angle (Figure 5-12). In fact changing the position of the cylindrical balloon from horizontal to an angle of 45° resulted in an increase of 29 mmHg (-12.2 ± 0.2 vs 17.0 ± 0.9 mmHg, $p < 0.01$, $r^2 = 0.88$) in EDP and of 40 mmHg (-8.6 ± 0.3 vs 31.7 ± 1.1 mmHg, $p < 0.01$, $r^2 = 0.99$) at the base. In the middle portion of the IAB, a change in angulation from 0° to 45° resulted in an increase in EDP of 34 mmHg (-12.2 ± 0.2 vs 22.2 ± 0.9 mmHg, $p < 0.01$, $r^2 = 0.93$) for the cylindrical IAB, of 10 mmHg (-18.6 ± 0.2 vs -8.6 ± 1.3 mmHg, $p < 0.01$, $r^2 = 0.88$) for the TDD 1/3 balloon, also associated to the lowest EDP throughout positions and assistance frequencies, and of 27.4 mmHg (-7.8 ± 0.5 vs 35.2 ± 3.1 mmHg, $p < 0.01$, $r^2 = 0.96$) for the TID 2/3 balloon, which is the least performant and resulted in the highest EDP in most of the positions and assistance frequencies.

All TDD balloons are associated to a lower EDP at a horizontal position and, generally, to a lower loss in deflation pulse (more contained rise in EDP) with increasing angle. The results of the cylindrical balloon fall between TDD and TID series. The deflation pulse associated to the balloons for all angles was generally similar for assistance frequency 1:1 and 1:4. The only exception is the TID 1/2 balloon at an angle of 30°, where EDP is 30 mmHg higher at an AF 1:1 compared to 1:4.

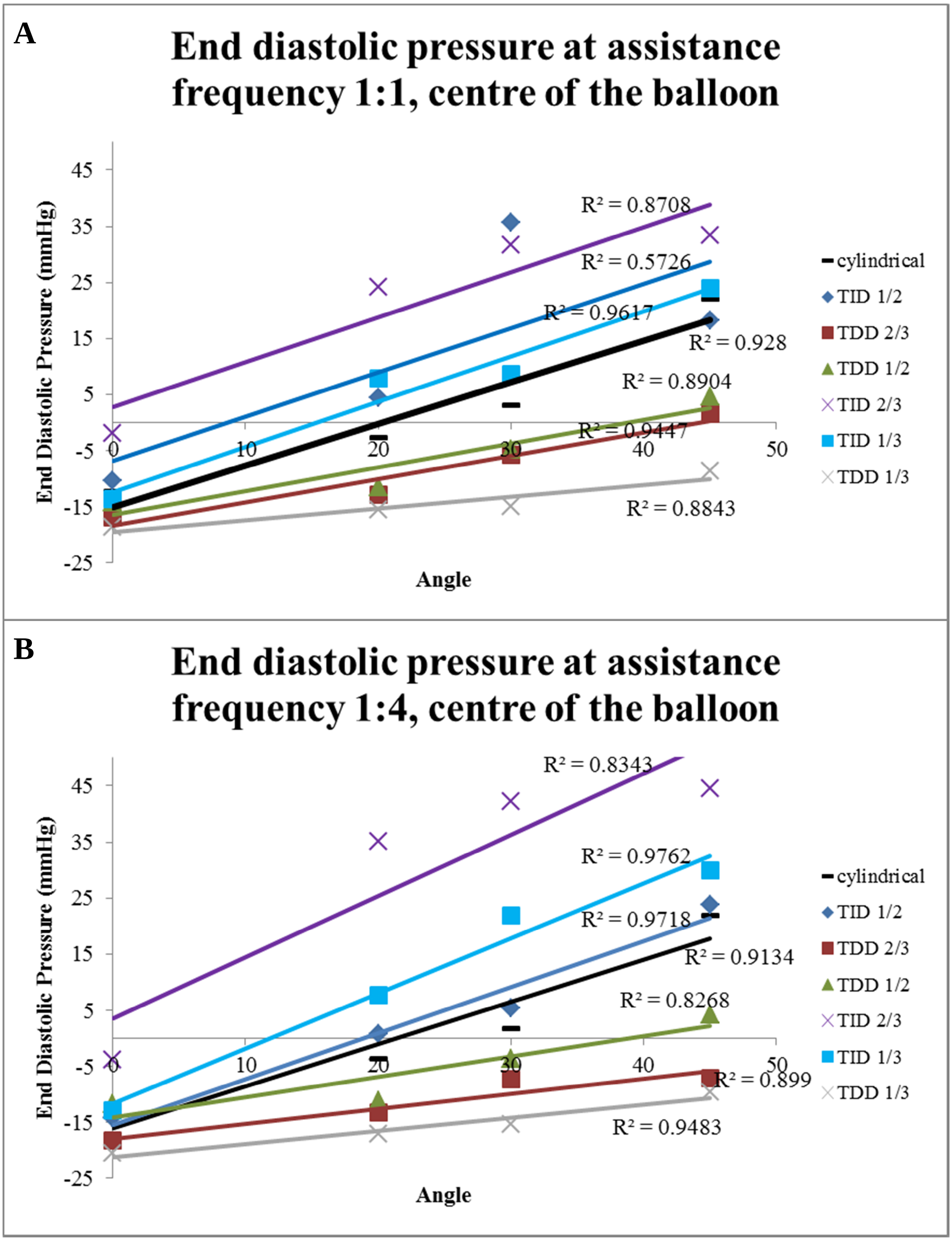

Figure 5-11*: The above graphs present the trend lines of EDP at the centre of the balloon for all IABs, throughout the positions from 0° to 45°, and for the two AF 1:1 (12 A) and 1:4 (12 B). The differences between the balloons increase if the device is tilted, but some of the IABs perform already better at a horizontal position.*

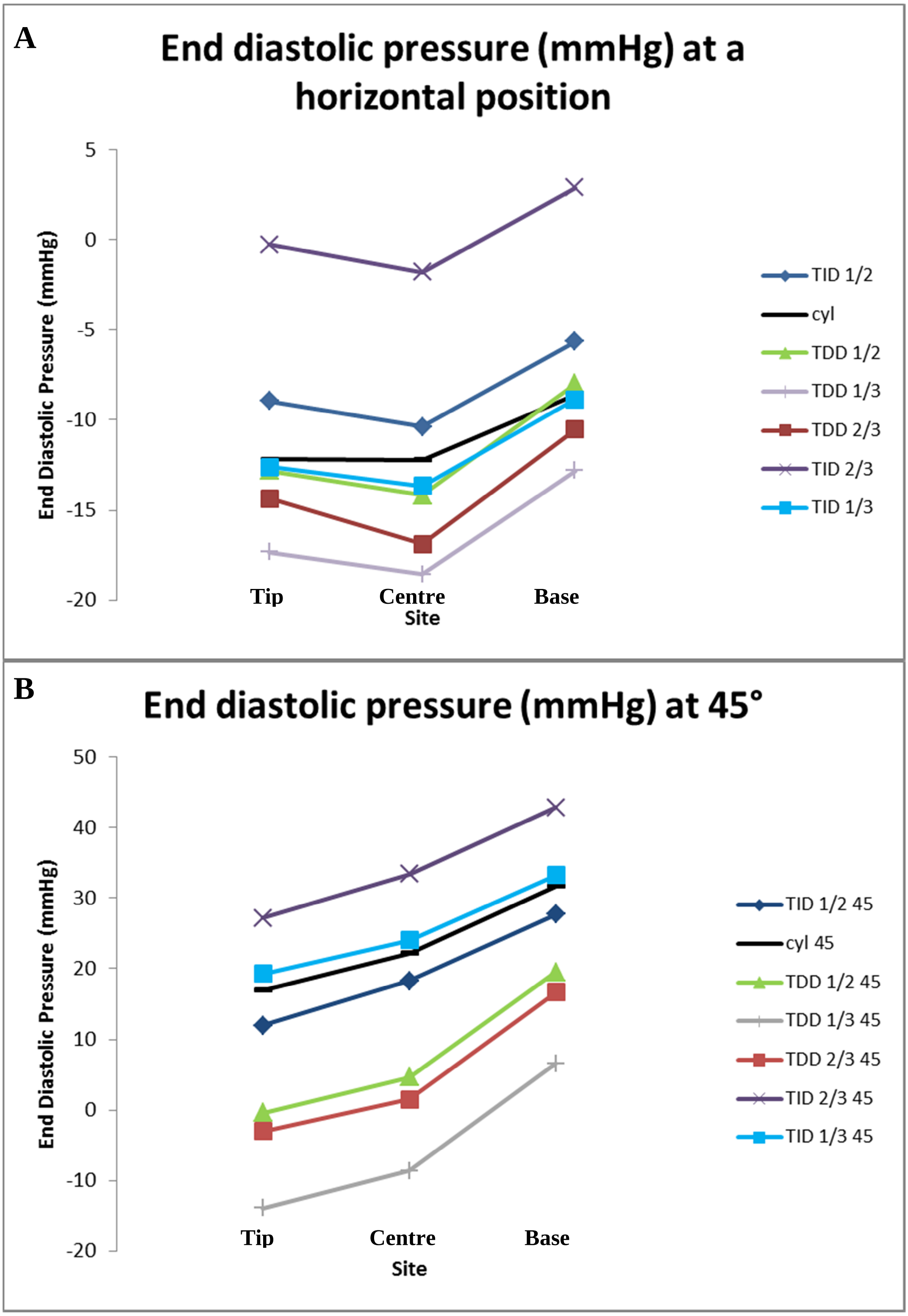

Figure 5-12: *The value of EDP is here indicated for all balloons at three different sites, tip, centre and base, for AF 1:1 and at a horizontal (A) and angle 45° (B) positions. Note that the scale of the y axis is different between the two figures, in order to underline the differences among the balloons at each position.*

5.5 Discussion

The main aim of this work was to establish whether a change in IAB shape, with a different volume distribution throughout it, would result in the favourable effect of maintaining benefits of increased coronary flow and decreased end diastolic pressure at different inclinations to the horizontal position in a physiological system. As already described in detail in the introduction chapter, the two main benefits of IABP are related to inflation, in terms of volume displaced towards the coronary circulation, and to deflation, in terms of decreasing end diastolic pressure and hence lowering ventricular afterload. These two parameters are analysed by comparing the results of different balloons in terms of VUTVi, inflation pressure pulse, EDP and VUTVd. Moreover, the whole analysis was performed at different angulations to the horizontal, with the target of resembling the position of patients nursed at a semi-recumbent position in the clinical environment. Whilst standard cylindrical balloon showed a decrease in all parameters with increasing angle, TID balloons resulted in an overall unchanged VUTVi at an angle to the horizontal, and TDD balloons, particularly TDD 1/3, induced a higher reduction in EDP at all positions.

5.5.1 Effect of a different shape on pressure waveform

The different hemodynamic induced by the use of a different shape is also evident if the difference between the pressure at the tip and the one at the base of the balloon is calculated throughout the cycle. Figure 5-13 shows this pressure difference for the standard, TID 1/3 and TDD 1/3 balloons during one cycle, together with the un-calibrated balloon Helium pressure.

At a horizontal position (solid colored lines) an important difference between the balloons is noticed during inflation: TID 1/3 is characterized by smaller oscillations compared to the two other balloons. This translates to a more simultaneous inflation of the TID 1/3 IAB.

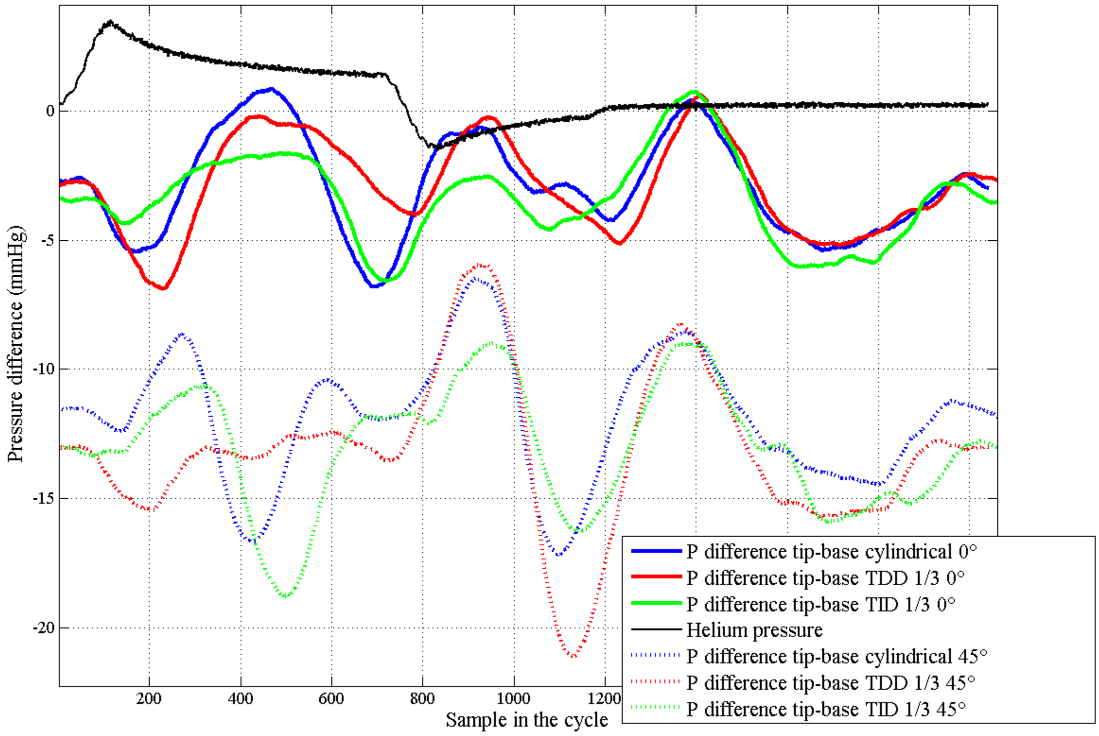

Figure 5-13*: Pressure difference between balloon tip and base is shown for standard cylindrical (blue line), TID 1/3 (green line) and TDD 1/3 (red line) balloons, for horizontal (solid line) and angle 45° (dashed line) positions, together with Helium un-calibrated pressure (black line).*

At an angle of 45° (dashed colored lines) the waveform of the pressure difference between the tip and the base changes for all IABs: specifically the increase in pressure difference between tip and base of the standard IAB starts earlier (tip inflates earlier compared to horizontal position) and fluctuations during inflation phase are smoother compared to the ones found at the horizontal position.

During the deflation phase the biggest variation in pressure difference tip-base was found on the TDD 1/3 IAB which at an angle of 45° is associated to a significantly higher increase in pressure difference immediately after deflation onset, compared to the cylindrical and TID 1/3 IAB. This is related to the higher volume characterizing the balloon base, which is the first part to deflate in case of angle and consequently induces a steep pressure drop resulting in an increase of the pressure difference between balloon tip and base.

5.5.2 Benefits induced by novel IABs

5.5.2.1 Inflation

5.5.2.1.1 Volume

The most important parameter to consider during balloon inflation is VUTVi. The standard cylindrical balloon produced the worst results for all angled positions in case of AF 1:4 and to one of the worse in case of AF 1:1. Moreover the cylindrical balloon showed a marked decrease in VUTVi with increasing the angle from 0 to 45°. The loss in VUTVi measured in the described experimental set-up is similar to that observed earlier by Khir and Bruti using different shaped balloons, 23% and 25% in the current and previous work [68], respectively. A further similarity is noticed by comparing the results of VUTVi associated to the TDD 1/2 balloon with the ones of the TDD studied in the previous work: its value increased by 13% in the two works by changing position from horizontal to an angle of 45°. TID balloons VUTVi did not change markedly in the current or in the previous experiment. The main difference with the previous work was found in the results of the rest of TDD balloons, and especially the TDD 1/3, which is the closest to the already studied TDD shaped balloon.

25 cc and 40 cc standard cylindrical balloons have been studied by Biglino et al. [71] in a mock circulation with a physiological set-up that included a ventricular simulator: in that study the IABs did not result in a markedly decreased volume displaced upstream corresponding to an increase in angulation. However, it should be underlined that the configuration of the set-up was changed for each position in a different manner compared to the study described in this chapter. Biglino et al [71] lifted the ventricular simulator and the venous return reservoir according to the height of the tip of the aorta rather than the mid-point of the balloon. The fluid-dynamics in case of angulation is then expected to be different between the two situations.

To grasp the mechanism associated with a different performance between the standard balloon and differently shaped balloons one should recall what was previously hypothesized [63,67] and later confirmed [66,68,71],[62]: at an angle to the horizontal the IAB starts inflating from the tip and this might result in an impedance against the flow displaced towards upstream, hence decreasing with increasing angle, as demonstrated. Differently though, all TID balloons targeted one of the aims of the study, regarding the volume displaced towards the coronary circulation: none of them resulted in a decrease in VUTVi with changing angle from horizontal to angle 45° position. The angulation would induce the tip of the balloon to inflate first, but in case of the TID balloon a higher percentage of volume corresponds to this part of the balloon, compared to the cylindrical balloon. Hence the rest of the IAB, which inflates afterwards, does not contribute markedly to the total volume displaced upstream.

5.5.2.1.2 Pressure

The inflation pressure pulse along the balloon is influenced by changing the position. Since this happens for all balloons with the exception of TID 2/3, the reason can be found in the difference in compliance along the tube in case of angulation. If the system is tilted the bottom area of the tube, around the base of the balloon, would fall into a higher pressure, hence smaller compliance, compared to the tube's top area. This difference in compliance could affect the inflation pulse characterizing different sites along the balloon. For verifying the validity of this hypothesis two experiments have been conducted on a 40 cc standard cylindrical balloon, activated in a glass tube and in a silicone rubber tube, at four different head pressures: 15, 38, 75, 135 mmHg. The pump settings were the same for both experiments. Testing the balloon in a glass tube allowed for monitoring the variation in inflation pulse with increasing pressure in the absence of compliance, while when the balloon is tested in a silicone rubber tube the change in inflation pulse with increasing pressure would be related to both variation of the compliance (which decreases with increasing pressure) and increase in static pressure. As shown in the graph in Figure 5-14 when the balloon counter-pulsates in a glass tube the inflation pulse decreases with increasing head pressure by a higher slope compared to when IAB counter-pulsates in a compliant tube, if just the first beat of the IAB is taken into account (slope value is -0.44 and -0.32 in the glass tube and compliant tube, respectively). This finding confirmed that a pressure difference, translating to a compliance difference, along the tube could have affected the balloon inflation pulse distribution according to what has been observed.

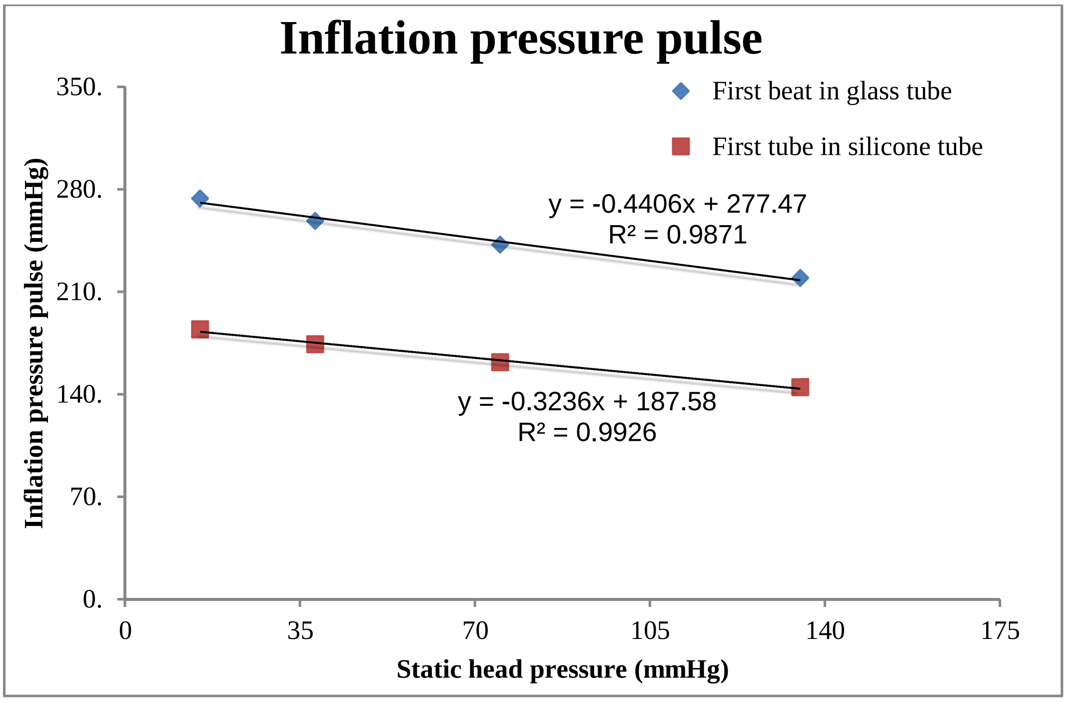

Figure 5-14*: Inflation pressure pulse at first beat, associated to cylindrical standard balloon tested on a glass tube (blue) and on a compliant silicone rubber tube (red). The graph underlines the influence of a variable compliance on the pressure pulse associated to the counterpulsation of the IAB.*

However the overall inflation pulse was found to be notably smaller for the cylindrical balloon compared to the rest of the balloons tested, with a minimum difference of 10% ($p < 0.01$) compared to TDD 1/2 and maximum difference 17% ($p < 0.01$) compared to TID 2/3. This effect is probably related to the different nominal volume characterizing each balloon. As the nominal volume is higher for all shaped balloons compared to the cylindrical one, the overall amount of volume displaced, and consequently the inflation pulse, is higher in case of shaped balloons. However Figure 5-15 shows that while the cylindrical balloon inflation pressure pulse decreases with increasing angle at the IAB tip and centre, the TID balloons inflation pulse is less or even positively affected by an increase in angle. This confirms that a change in shape of the balloon could result in a different behaviour at different angulations in a physiological environment. Total pressure is not taken into consideration due to the difference in balloon size.

A change in the assisting frequency of the IAB influenced the VUTVi of each balloon studied. Nonetheless their inflation pressure pulse was not affected. The balloons which showed an increased volume displaced upstream at an AF of 1:1 also manifested an improved performance compared to cylindrical standard balloon at an AF 1:4.

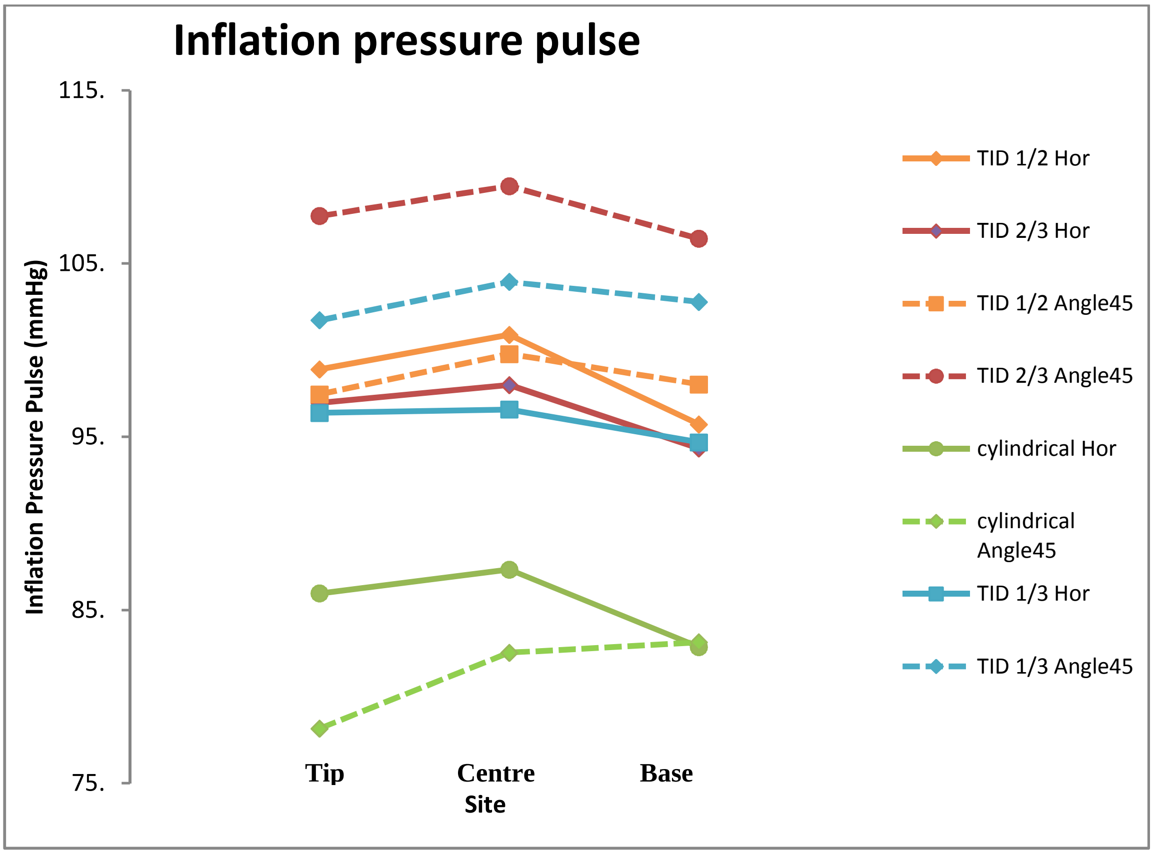

Figure 5-15: *The graph shows the inflation pressure pulse for cylindrical balloon and TID balloons at three different sites, tip, centre and base, for AF 1:1, at a horizontal and angle 45° positions. The results indicate the variation in inflation pulse with increasing angle associated to the standard balloon and to the ones which are performing better, bringing evidence of an improved performance in case of different shaped balloons.*

5.5.2.2 Deflation

5.5.2.2.1 Volume

VUTVd changes throughout balloons at different positions showed an evident influence of the shape on the deflation mechanism of the balloon. All TDD balloons performed better than the standard cylindrical one when at an angle, with TDD 2/3 resulting in a 33% increased VUTVd, compared to the standard IAB, at

45°. As expected TID balloons induced a smaller VUTVd compared to TDD and standard cylindrical balloon at any angulation.

5.5.2.2.2 Pressure

The benefits of the deflation phase of the balloon is reducing ventricular afterload by reducing aortic EDP. The fluid pressure immediately before onset of systole is referred to as end diastolic pressure (EDP). The drop in EDP is nevertheless related to the volume sucked from upstream by the balloon during its deflation (VUTVd). EDP also follows the trend of VUTVd changes with angles for all balloons: the standard balloon is located in the middle between TDD and TID series, and specifically TDD 1/3 is the least affected by angle among all balloons (10 mmHg loss changing from horizontal to angle 45 position). Moreover this balloon shows the lowest EDP in case of horizontal position. EDP at a horizontal and at an angle of 45° is shown in Figure 5-16, for the standard balloon and the TDD series, and underlines the differences between these balloons at both positions.

The decrease in deflation efficacy shown by the standard balloon has already been discussed in previous works, especially the one presented in Chapter 3. In the current study an increase in EDP of 34 mmHg was measured at the centre of the balloon for an increase in angle from 0° to 45°, whereas in the experiment described in Chapter 3 a decrease in deflation pressure pulse by 22 mmHg in the same site and for the same change in angulation was recorded. Similarly, the first comparison between the differently shaped balloons [68] showed that the cylindrical standard balloon induced a decrease of 22 mmHg in deflation pulse for an increase in angle from 0 to 45°. TDD 1/3 and TID 1/3 balloons are used for comparison with the TDD and TID balloons tested in the experiment exploited by Khir and Bruti [68]: while the first ones resulted in an increase in EDP of 10 and 38 mmHg, respectively, for a change in angulation from horizontal to angle 45° position, the latter ones brought a decrease in deflation pulse of 10 and 14 mmHg.

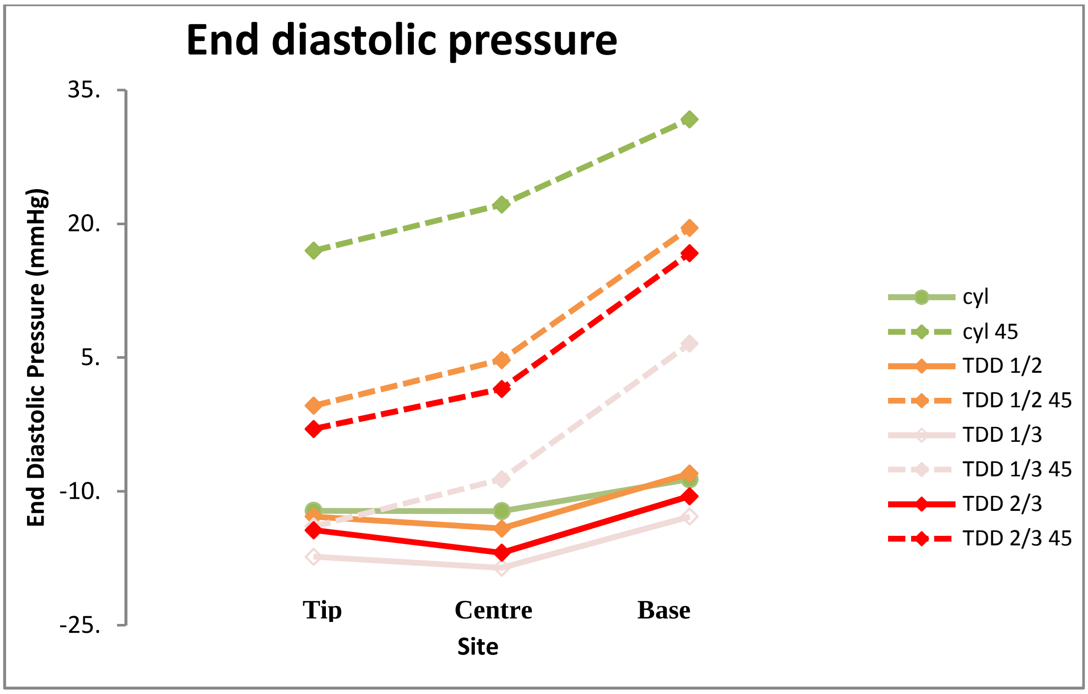

Figure 5-16*: EDP for the cylindrical balloon and TDD balloons at three different sites, tip, centre and base, for AF 1:1, at a horizontal and angle 45° positions. The variation in EDP with increasing angle associated to the standard balloon is different compared to the TDD balloons, which proved to perform better in case of angulation.*

According to the findings both in the literature [68] and from the analysis of the current data, obtained in a more physiological test-bed, it can be stated that the balloon's shape influences the EDP value for horizontal and angled positions. The cylindrical balloon's performance is compromised because of the already explained phenomena of 1) obstruction of the balloon tip towards the flow sucked from upstream and 2) obstruction of the balloon base towards the flow of Helium from the balloon tip towards the pump; the TDD balloons resulted in a lower EDP which was also less affected by a change in the angulation. In fact, the shape of this balloon is such to contain a bigger proportion of its nominal volume in the base, so that, even though this is the first part to deflate throughout the balloon in case of angle, the flow sucked from upstream would not be obstructed by the upstream impedance and the flow of Helium would not be reduced, differently from other shaped balloons. The confirmation of the phenomena on an experimental set-up including a ventricular simulator and characterized by a physiological pressure waveform suggests a concrete benefit following from the clinical use of this type of balloon, which should be verified through further ‘in vivo’ tests.

It should be noted that, even though the two TDD and TID balloons have also been studied by Biglino [71], neither EDP nor deflation pressure pulse have been investigated and the work was not focused on this aspect of the balloon counterpulsation activity. Hence this work, together with the one described in Chapters 3 and 4, fills an important gap constituted by the poverty of information about the IAB deflation phase and thus suggests a solution to the decreased balloon performance.

A decrease in EDP is associated to a decremented left ventricular afterload. This is related to the point **EDP** in the PV loop represented in Figure 1-17, Introduction Chapter, and here shown in Figure 5-17. This is, as indicated before (Chapter 1), the most prominent and immediate effect of the use of an IABP in a patient affected by ischemia. Through a reduction in EDP the end systolic point moves towards the left side of the pressure-volume diagram (point c in Figure 5-17). In addition to an increased stroke volume, the effect of IABP is also a reduced left ventricular stroke work (and reduced left ventricular end-diastolic pressure and volume). In addition the decrease in stroke volume depends on the contractility state of the ventricular muscle, represented by the dashed line with slope end-systolic elastance (Ees), in Figure 1-14. A lower slope of this curve (patients with lower contractile state) is associated to a larger increase in stroke volume due to IABP therapy. A PV loop related to the current experiment could not be traced because of the mechanical nature of the pump: in the present experiment the left ventricular function is simulated by a piston pump which is mechanically controlled and does not change in volume in case of a deflation generated by the balloon.

The results related to IAB deflation, here presented and discussed, are not relevantly affected by a change in the assistance frequency of the balloon from 1:1 to 1:4. This implies that using the balloon at an AF of 1:1 would induce a much higher benefit to the patient compared to AF 1:4, since the IAB is assisting the heart for each cardiac cycle without decreasing its efficacy.

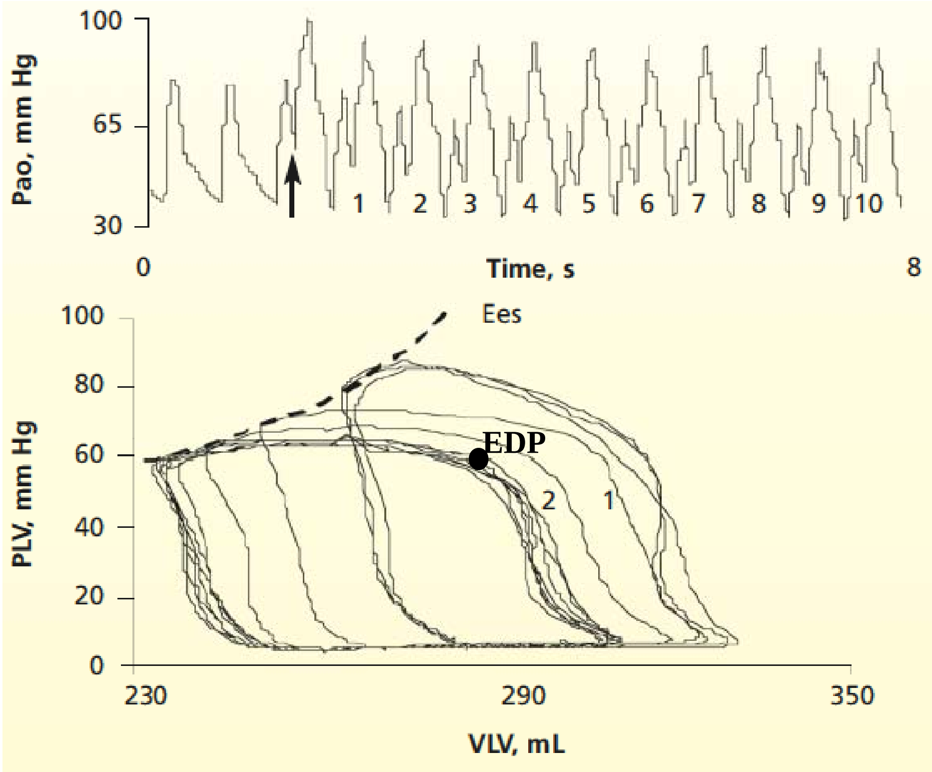

Figure 5-17: *PV loop and arterial pressure (Pao) show the immediate and beneficial effect of a properly used intra-aortic balloon counterpulsation on left ventricular function. The effect of the intra-aortic balloon pump is seen on the first beat of counterpulsation (1) and has reached its full effect within 4 beats. The shift of the pressure-volume loop down and to the left indicates a reduction in left ventricular work, whereas a widening of the pressure-volume loop indicates an increase in stroke volume. (Schreuder et al. [121]). The point EDP represents the end diastolic pressure, reduced in case IABP is counterpulsating.*

5.5.3 Final considerations

For organizing the main findings of the study, the best and worst balloons for the two assisting frequencies and for horizontal and 45° positions are reported in Table 53. It emerges that none of the tested balloons emerged for a better performance on both, inflation and deflation. Hence the two phases will be considered separately. TDD 1/3 balloon showed a net advantage in terms of deflation pulse: for all positions this balloon is associated to the lowest EDP for any angle. This is related to the higher concentration of balloon volume on its base, which was demonstrated (Chapter 3, [63]) to be the first part to deflate in case of IAB operating at an angle. On the other hand not all TDD balloons succeeded in maintaining a constant VUTVi with increasing angle and showed to be influenced by the semi-recumbent position.

TDD 1/2 instead induced a higher VUTVi for 20, 30, 45°, compared to cylindrical balloon, for both 1:1 and 1:4 assisting frequencies (the increase in VUTVi associated to TDD 1/2 compared to cylindrical balloon is 9.7% ($p = 0.4$) and 35% ($p = 0.008 < 0.05$) for angle 30 and angle 45 respectively, at assisting frequency 1:1, and 13% ($p = 0.16$), 31% ($p < 0.05$) and 17% ($p < 0.05$) for angle 20, 30 and 45 respectively, at assisting frequency 1:4), and lower EDP for all positions from horizontal to angle 45, with a minor rise in EDP, compared to the cylindrical and TID balloons.

All TID balloons deflation effectiveness is markedly affected by an inclination of the system, which, for a change in position from 0° to 45°, results in a decreased deflation pulse and an increase in EDP by at least 29 mmHg (TID 1/2). TDDs are associated with a maximum 19 mmHg increase in EDP. However, among all TID balloons, TID 2/3 was the most advantageous during inflation because it displaced a VUTVi comparable to the cylindrical balloon at a horizontal and higher for 20, 30, 45° positions. Also in this case the TID benefit is not surprising if it is considered that a bigger portion of the balloon volume locates on its tip, and, although this is the first part to inflate at an angle and might provide a higher impedance against the flow displaced upstream, there would not be a critical difference in volume displaced upstream between horizontal and angled positions.

Table 5-3: For each parameter relevant for the study, the balloon inducing the highest value and the one inducing the lowest value are indicated, at AF 1:1 and 1:4 and at a horizontal and 45° position. In some cases at a horizontal position the standard cylindrical balloon is the best one, but the majority of situations are characterized by a better performance of one of the differently shaped balloons.

			HIGHEST	**LOWEST**
VUTVi	AF 1:1	0°	Cylindrical + TID 2/3	TDD 2/3 + TDD 1/3
		45°	TID 2/3	TDD 2/3 + TDD 1/3
	AF 1:4	0°	Cylindrical + TID 1/3	TID 2/3
		45°	TID 2/3	Cylindrical + TDD 1/3
VUTVd	AF 1:1	0°	Cylindrical	TID 1/2
		45°	TDD 1/3	TID 1/3
	AF 1:4	0°	Cylindrical	TID 1/3
		45°	TDD 2/3	TID 1/3
Inflation Pulse	AF 1:1	0°	TID 1/2	Cylindrical
		45°	TID 2/3	Cylindrical
	AF 1:4	0°	TID 1/2	Cylindrical
		45°	TID 2/3	Cylindrical
EDP	AF 1:1	0°	TDD 1/3	TID 2/3
		45°	TDD 1/3	TID 2/3
	AF 1:4	0°	TDD 1/3	TID 2/3
		45°	TDD 1/3	TID 2/3

The analysis of inflation pressure pulse value at different positions to the horizontal strengthened the hypothesis of an advantageous effect induced by changing the shape of the cylindrical balloon into TID 2/3. This balloon resulted in an inflation pulse increased throughout the IAB for an increase in angulation, which could be related to the performance of the balloon in terms of VUTVi at different angles to the horizontal. Even though all TIDs showed a decrease in EDP with increasing angle bigger than the cylindrical balloon, TID 1/2 was generally performing similarly to the standard IAB, while still resulting in improved inflation efficiency at semi-recumbent positions.

5.5.4 Future works

The experimental set-up used in the current work aimed at testing different shaped balloons at the horizontal position and different angles to resemble patients being nursed at the hospital. Even though a left ventricular simulator was used, and the balloon was counter-pulsating with a physiological pressure waveform, the test-bed used was not comparable to a physiological arterial tree. The results obtained highlighted the differences in hemodynamic benefits associated to different shapes of the IAB, but before being ascribed to the physiological condition they should be confirmed through testing the balloons in a physiological aorta with arterial tree and through ‘in vivo’ experimental analysis.

Further development of the shape of the balloon could be also studied, once the evidence of an improved performance of the IAB is confirmed by further experiments. The tapering of the balloon could provide a basic rationale for a modification of the shape of the device and, according to the latest results, a combination of the two TDD and TID balloons could result in the balloon increasing its performance on both inflation and deflation phases.

5.6 Conclusions

Experimental tests conducted on cylindrical and differently shaped balloons counter-pulsating with a left ventricular simulator showed improved benefits of the IAB which can be imputed exclusively to the different shape of the device. TDD balloons showed an improvement compared to the standard cylindrical balloon during deflation, inducing a lower EDP at all angulations to the horizontal, while TID balloons were associated to an improvement in inflation activity in case the device is tilted. A good compromise consists in the use of the TDD and TID 1/2 balloons, even though the delivered benefit of each of the balloon would be clearer during deflation, for the first one, and inflation, for the latter one. If the improvement of each IAB will be confirmed, the use of the amended design balloon could be indicated according to the specific patient condition: for a patient affected by ischemic heart would be recommendable the use of TDD 1/2 balloon, since little advantage would be associated to a backward flow towards the restricted coronary arteries; on the other hand the left ventricle of a patient affected by myocardial infarction would benefit from the use of TID 1/2 balloon, which could support an increased flow in the coronary arteries.

Even though it was not possible to accurately graphically represent the changes in PV loop diagram as the left ventricle was simulated by a mechanically controlled piston pump, important clinical conclusions can be drawn when reporting the decrease in EDP obtained through the use of the TDD IABs on the PV loop diagram. It was in fact shown that the reduction of EDP would be followed 'in vivo' by the end systolic pressure point moving towards the left side of the diagram, and resulting in a smaller ventricular volume at the end of systole, an increased stroke volume and a reduced left ventricular end diastolic pressure and volume. This clinical advantage is crucial and it was indicated as the main immediate benefit related by IABP therapy by other researches (Schreuder al. [121], Barnea et al. [36, 96] and Cheung et al. [69]), as improvements due to increased coronary circulation would be effective at a second stage after the use of IABP therapy.

The findings here presented can enable the use of these devices for animal testing to assess whether their advantages are confirmed in a physiological system close to the human one. In case these results are confirmed after the testing of the seven balloons in a mock aorta connected to a left ventricular simulator, the two differently shaped balloons will be studied together with the standard cylindrical one in an in vivo set-up, to confirm the evidence of improved benefit in a complicated physiological condition characterized by a sophisticated regulatory system. However the improved deflation performance associated to TDD balloons and the inflation performance characterizing the TID balloons are in line with previous findings on a different and simpler experimental set-up.

Chapter 6 Influence of pump setting modes and ECG on IAB inflation and deflation timings in an experimental set-up

6.1 Chapter outlook

The work described in this chapter aims at investigating and comparing the effects of different settings (automatic and semi-automatic) and triggers (ECG, Aortic pressure and FOS sensor pressure), selected in two different IABP commercial machines (Teleflex AutoCat 2 WAVE and Datascope CS300), on the pressure waveform generated in an experimental set-up. For each configuration, changes in pressure, specifically on inflation and deflation pattern will be reported. The corresponding potential benefits and drawbacks will also be discussed. Furthermore, the ratio between the number of missed beats and the total number of beats will be presented for each ECG, revealing the effectiveness of each pump and setting on different types of ECGs. This Chapter eventually addresses specific uses of each pump for patients with different types of pathological conditions.

6.2 Introduction

The market of IABP is predominantly shared by two manufacturers, Datascope (currently Maquet) and Arrow international (currently Teleflex). The equipment produced by these companies for IABP therapy can be grouped under two categories: balloons and pumps. The effectiveness of IABP therapy relies on the performance of the pumps and balloons.

It is essential that inflation and deflation timings, including time of onset and duration, are calculated to maximize the hemodynamic benefits of IABP therapy, as also highlighted by previous works in the literature [79]. The most commonly used timing to guide IABP counterpulsation consists of conventional and real-time (R-wave deflation) [80]. While the former one sets the deflation starting before the next systolic ejection, the latter one alters deflation onset to correspond to systolic ejection. In fact, previous studies [81] found that real-time deflation, although extending the length of isovolumetric contraction and increasing myocardial oxygen demand, increased length of ejection and stroke volume compared to conventional timing. However, both methods are accepted and the choice of the method must be made according to the purpose of IABP therapy for the specific patient and following an assessment of hemodynamic effects of the selected timing method.

Further, most patients requiring IABP therapy usually have higher heart rates or arrhythmias and unusual ECG, which is one of the main triggering signals that the pump uses to activate inflation and deflation. A higher heart rate (HR) and an irregular ECG provide a further challenge for a successful therapy as the pump may miss some of the beats and hence the therapeutic effect would be reduced. To meet this challenge, every manufacturer operates the pump with the proprietary algorithmic software which is developed for detecting and assisting all beats. In fact, after first measurement tests on the reliability of fibre-optic sensors (FOS) [82], and following the implementation of algorithms for the detection of the dicrotic notch based on measurements with this technique [83-86], this method of pressure tracking was indicated as a potential solution for timing errors [87,88] occurring in case of high/irregular HR or ECG.

Bakker et al. [83] tested the latest developed pump by Teleflex (AutoCAT 2 WAVE) to investigate inflation and deflation timing errors when using the autopilot setting of the machine, to have an insight of the influence of poor quality ECG or arrhythmia on the hemodynamic outcomes shown on ECG strips related to the use of IABP in 60 patients. Out of all analysed strips 16% showed incorrect timing, in which 54% of the time errors were consistent since more than 50% of beats showed incorrect timing. 69% and 37% of strips showing incorrect timing also showed arrhythmia and poor quality ECG, respectively. However, automating the operation of the IABP has become a prevalent task targeting the benefit of reducing the operator error and minimising human intervention. For instance, a manually set up IABP for ECG trigger, may require a different set up for triggering, possibly the pressure signal, if the patient undergoes a period with irregular or loss of the ECG signal.

IABP inflation and deflation timings appropriateness and its ability to detect cardiac beats can vary and is challenged with unusual ECG, higher heart rates or arrhythmias. Hence, the comparison between two of the most widely used pumps in the market can address the effect of different ECGs, settings with operating algorithms and manufacturers on fluid-dynamics changes as well as add to the current knowledge of IABP therapy appropriateness. The aim of the study in this chapter is to provide a detailed performance comparison between two of the most widely clinically used pumps, tested under different settings and with different balloons, in an *in vitro* set-up that resembles the physiological settings.

6.3 Materials and Methods

6.3.1 Experimental set up

The experimental set up used for the comparison is described in Figure 5/1, and consists of the following elements:

A. Mock aorta accommodating the balloon; a flexible tube of 2.6 cm internal diameter, 0.2 cm wall thickness and 40 cm length
B. Air compressor (Jun-Air, Bromgrove, UK) providing pressure to the system
C. Control box, controlling valves opening and closing based on ECG signal
D. Datascope (CS300) and Teleflex pump (AutoCat 2 WAVE)
E. PC for ECG signal to the pump/control box and for data acquisition
F. Data acquisition system using data acquisition card (National Instruments, Austin, TX, USA) and data acquisition software (Labview, National Instruments, Austin, TX, USA)
G. Pressure transducer (SPC 760, Millar, Houston, Texas)
H. Balloons: Datascope Linear and Sensation, Teleflex LWS

The Teleflex pump was tested on ‘Automatic’ mode of operation, while the Datascope pump was tested on ‘Automatic’ and ‘Semi-Automatic’ modes of operation. This was done because the ‘Semi-Automatic’ mode, although still limiting operator intervention, selects different algorithms for inflation and deflation onset compared to ‘Automatic’ mode.

Each of the two pumps was provided with 15 recordings of ECG from the AHA heart failure data set identified by the following numbers: 1001, 1002, 1005, 2006, 3003, 3004, 4002, 4006, 5002, 6003, 6009, 7004, 7006, 7007, 8010. These are indicated in the figures, results and discussion with numbers from 1 to 15.

Datascope Linear and Teleflex LWS balloons were tested with the pump of the own and the other manufacturer.

Furthermore several triggering signals were connected to each pump: ECG, providing QRS waveform, Aortic Pressure (AP) transducer, providing pressure measured through water filled catheter, and Fibre optic sensor (FOS), also performing pressure measurements. The total number of configurations, combining pump, balloon and mode of triggering, is 9, and they are listed in Table 5.1. Totally 135 experiments were carried and registered: 15 ECGs for 9 configurations.

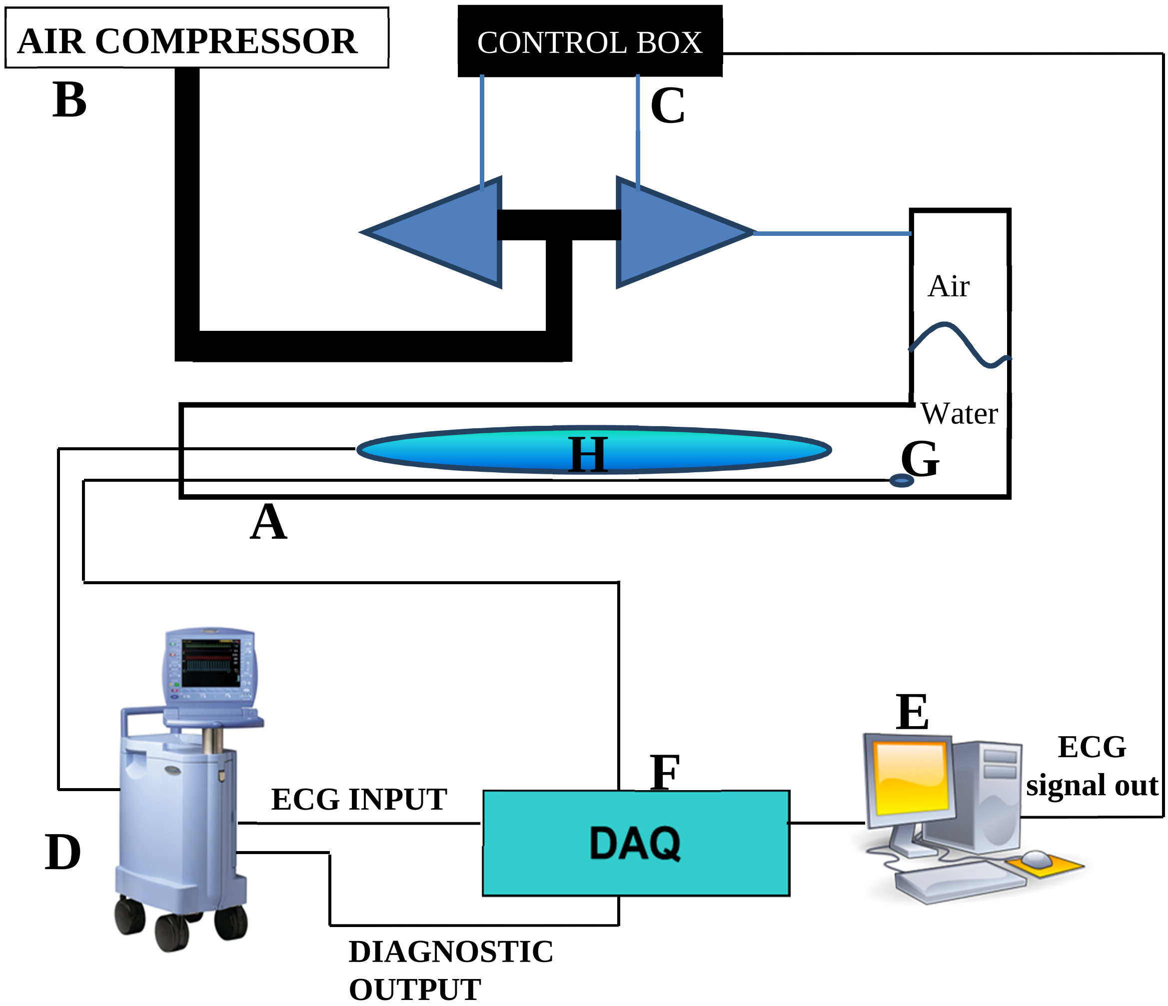

***Figure 6-1**: A schematic picture of the in vitro experimental set-up. The air-compressor provides pressure to the system which is controlled by the control box and valves, resulting in physiological pressure waveform on the mock aorta. The ECG input on the system directs both, control box and IABP resulting in counterpulsation mechanism according to ECG, pump mode and triggering signal.*

Table 6-1*: List of all configurations tested, combinations of pump, balloon, triggering signal and pump mode. 15 ECGs have been run through all listed configurations, resulting in 135 experiments.*

	Pump	**Balloon**	**Trigger**	**Signals Selection/ Connection**	**Mode**
1) ptbtFOS	Teleflex	LWS	AP FOS	ECG AP FOS	Automatic
2) pdbdFOS	Datascope	Sensation	AP FOS	ECG AP FOS	Automatic
3) ptbtAUTO	Teleflex	LWS	ECG or AP Transducer	ECG AP Transducer	Automatic
4) pdbdAUTO	Datascope	Linear	ECG or AP Transducer	ECG AP Transducer	Automatic
5) pdbdSEMIECG	Datascope	Linear	ECG	ECG AP Transducer	Semi-Automatic

6) pdbtSEMITRA	Datascope	Linear	AP Transducer	ECG AP Transducer	Semi-Automatic
7) pdbtAUTO	Datascope	LWS	ECG or AP Transducer	ECG AP Transducer	Automatic
8) ptbdAUTO	Teleflex	Linear	ECG or AP Transducer	ECG AP Transducer	Automatic
9) ptbtECG	Teleflex	LWS	ECG	ECG	Automatic

6.3.2 Measurement

Pressure, ECG signal and un-calibrated Helium pressure were measured at a frequency of 2 KHz. The pressure transducer (SPC 760, Millar, Houston, Texas) was inserted in the mock aorta from the left side, as indicated in Figure 6-1, and placed beyond the tip of balloon. Each tested ECG lasted for approximately 90-120 seconds, recorded using an analogue-digital converter and Labview software (National Instruments, Austin, TX, USA), and the analyzed beats for each ECG started from the 30th beat, to ensure the system to be on steady state. Data analysis was performed using Matlab (The Mathworks, Natick, MA, USA).

6.3.3 Data analysis

The system described resulted in the generation of a pressure waveform, shown in Figure 6-2, resembling physiological pressure with balloon counterpulsation. Five indexes, also indicated in Figure 6-2, have been derived from the waveforms and used to compare the timing performance of each configuration:

a) Time between R-wave (peak of QRS) to onset of inflation - **RpIs**

b) Time between onset of inflation to onset of deflation (inflation duration) - **DoI**

c) Ratio of missed beats over total number of beats – **Ratio**

d) Time between R-wave (peak of QRS) to peak systolic pressure - **RpSp**

e) Time between onset of inflation to end of deflation – **IsDe**

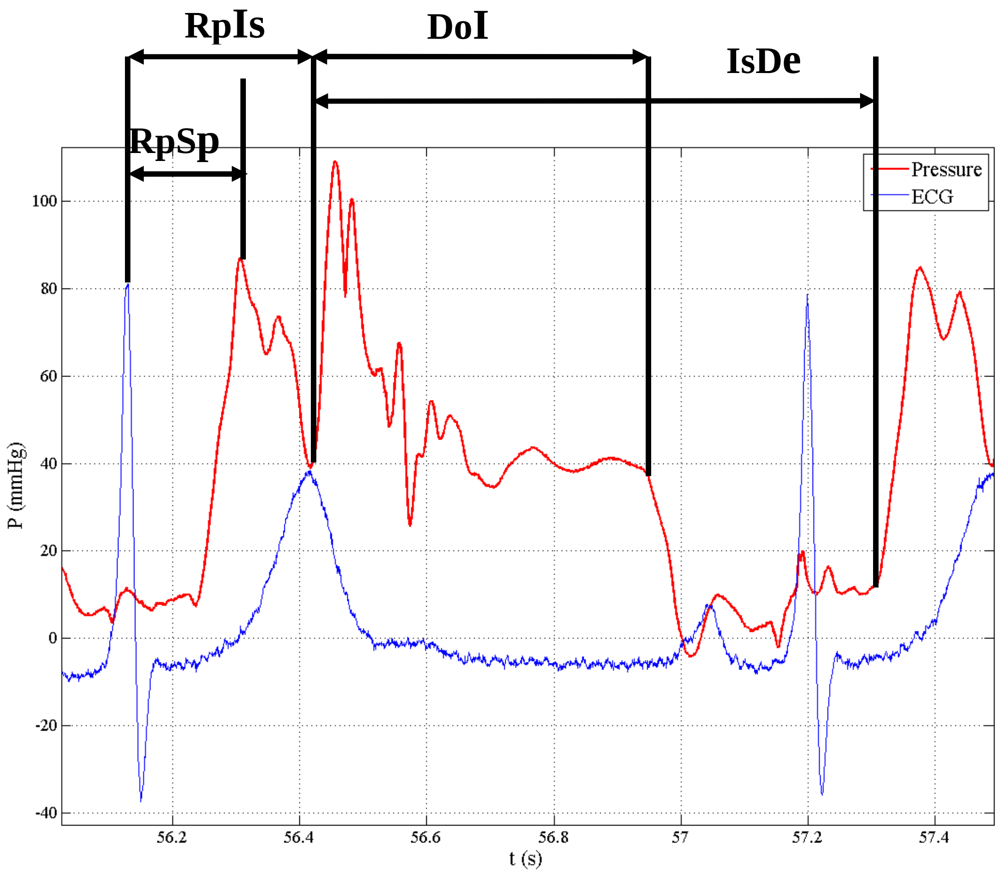

Figure 6-2*: Above shown pressure waveform (red) and ECG signal (blue) corresponding to one of the analyzed ECGs. The four indexes derived from the pressure waveform are indicated: RpSp, RpIs, DoI, IsDe. The presence of counterpulsation on the pressure waveform reveals the triggering of the beat by the IABP, giving an estimation of the index Ratio.*

6.4 Results

All results are categorized under each index used for the evaluation of the 9 configurations:

1. Time between R peak to onset of inflation - RpIs
2. Time between onset of inflation to onset of deflation (inflation duration) - DoI
3. Ratio of missed beats compared to total number of beats – Ratio
4. R-peak to systolic peak - RpSp
5. Inflation starting – Deflation ending - IsDe

6.4.1 Time between R peak to onset of inflation - RpIs

The value of this index for each ECG and configuration is shown in Figure 6-3. Figure 6-4 instead shows, for each configuration, RpIs average and standard deviation throughout ECGs. The Teleflex pump on automatic mode and the FOS trigger is the configuration that produced the shortest RpIs in 14 out of 15 ECGs (except the ECG 13), showing a rapid pump response after peak systolic pressure. Averaged for the 15 ECGs RpIs was 0.2771 ± 0.0308 s. The difference, averaged for all ECGs, between this configuration and the one giving the second best result is of 15% (0.277 ± 0.0308 vs. 0.3190 ± 0.0466 s, $P < 0.01$).

Comparing the Teleflex pump with the Datascope pump when the same mode and trigger are selected (automatic mode and FOS trigger) shows that the first one produces a smaller standard deviation of this index in 9 ECGs out of 15, comparable in 4 and higher in only 2. The Datascope pump on automatic mode and Teleflex LWS or Linear balloon produced the longest RpIs on all ECGs, with an average value of 0.3875 ± 0.0425 s and 0.4083 ± 0.0575 s, respectively. These two configurations are comparable to those of the Teleflex pump on automatic mode and LWS or Linear balloon just in case of ECG 13. Inverting the balloon with the Teleflex pump did not induce particular changes in RpIs in any of the ECGs ($p > 0.11$).

ECG 13 is the most irregular ECG and the only case where the Teleflex pump on automatic using FOS triggering did not produce the shortest RpIs. In case of ECG 13, the Teleflex pump on automatic mode and Datascope on semi-automatic mode, both with ECG as a trigger, are the configurations associated with the shortest

RpIs and smallest standard deviation, of 0.2997 ± 0.0232 s and 0.2797 ± 0.0326 s, respectively. Even though ECG 4, 6, 10 and 11 are also slightly irregular, in these cases the Teleflex pump on automatic mode and FOS as trigger is the fastest to inflate the balloon after the systolic peak.

The different mode settings on the Datascope pump had a big influence on RpIs. Automatic mode guiding the pump's triggering resulted in longer RpIs compared to when semi-automatic mode is selected, for both, ECG and pressure transducer triggering (0.4083 in average for automatic mode, 0.3330 and 0.3380 for semi-automatic mode with ECG and transducer trigger respectively, shorter with a $p < 0.01$). At semi-automatic mode, changing the trigger from ECG to pressure transducer did not affect the RpIs index in most of ECGs ($p > 0.1$).

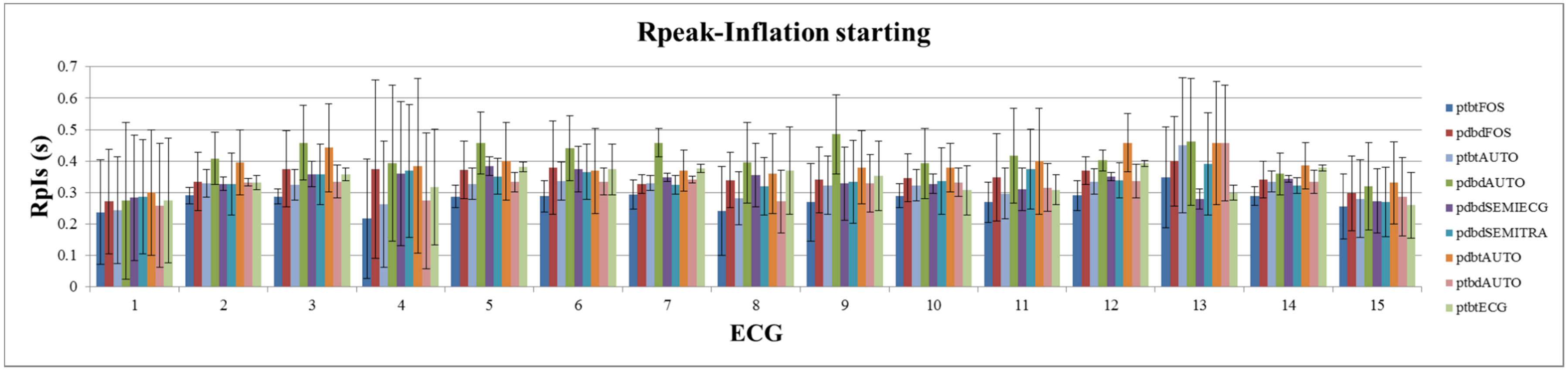

***Figure 6-3**: between R-wave (peak of QRS) to onset of inflation. Error bars indicate the standard deviation and all values are expressed in seconds.*

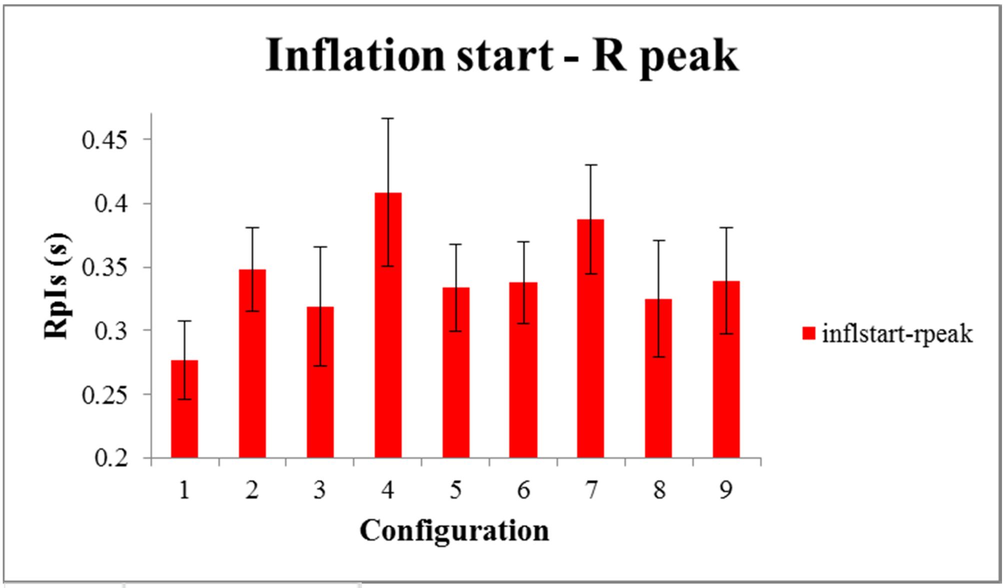

1	ptbtFOS
2	pdbdFOS
3	ptbtAUTO
4	pdbdAUTO
5	pdbdSEMIECG
6	pdbdSEMITRA
7	pdbtAUTO
8	ptbdAUTO
9	ptbtECG

Figure 6-4*: Mean values of RpIs for each of the 9 configurations tested. Configuration 1, ptbtFOS, provided the shortest value of RpIs.*

6.4.2 Time between onset of inflation to onset of deflation (inflation duration) - DoI

The values of this index for each ECG and configuration are shown in Figure 6-5, while its average and standard deviation throughout ECGs is indicated in Figure 6-6, for each configuration. The Datascope pump on semi-automatic mode with trigger on ECG or pressure transducer, and the Teleflex pump on automatic mode with ECG as a trigger induced the longest DoI in most of ECGs. Particularly the Datascope pump on semi-automatic mode with ECG trigger generates the longest DoI in 11 out of 15 ECGs, including the most irregular ECGs. The Teleflex pump on automatic mode with ECG as trigger generates the longest DoI in just 3 out of 15 ECGs (11, 13, 15).

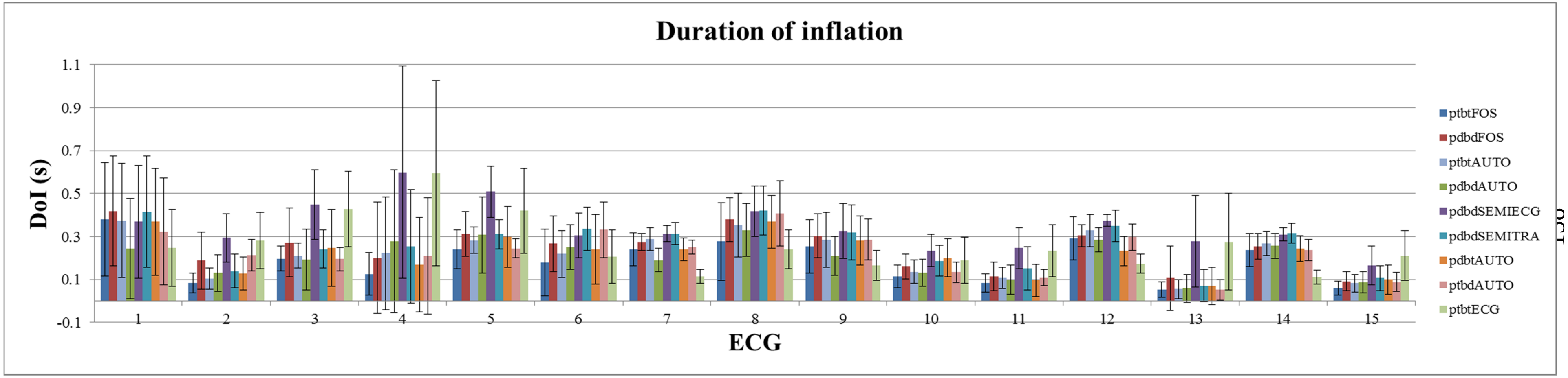

Figure 6-5*: Duration of inflation (DoI) values for each configuration and each ECG, average and standard deviation. The value is expressed in seconds. The high standard deviations in ECG 4 and 13 are due to the heart beat frequency, highly variable in the two cases.*

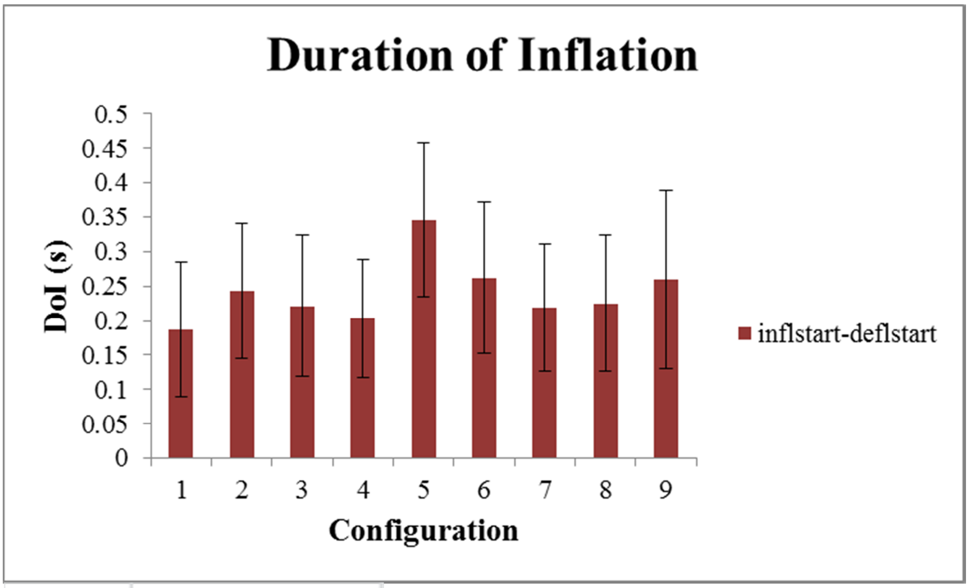

1	**ptbtFOS**
2	**pdbdFOS**
3	**ptbtAUTO**
4	**pdbdAUTO**
5	**pdbdSEMIECG**
6	**pdbdSEMITRA**
7	**pdbtAUTO**
8	**ptbdAUTO**
9	**ptbtECG**

Figure 6-6*: Mean values of DoI for each of the 9 configurations used. As shown configuration 5, pdbdSEMIECG, provides the longest value of RpIs.*

Both, the Datascope and Teleflex pumps worked with the pressure transducer as a trigger when the automatic mode is selected and both pressure and ECG signals are available. When the Teleflex pump is working with only the ECG signal available the trigger mode automatically selected is either “PATTERN” or “AFIB” (atrial fibrillation). DoI associated to ECGs triggered with PATTERN mode is different from those triggered with AFIB mode.

It can be noted that, apart from ECGs 1 and 4, all ECGs have perfect agreement between DoI and PATTERN or AFIB triggering. In case of PATTERN triggering DoI is one of the shortest among all configurations, while in case of triggering with AFIB DoI is one of the longest, and specifically in ECG 4, 13 and 15 the longest throughout all configurations.

In case of irregular ECG 13 AFIB is selected automatically immediately with the Teleflex pump. Using the ECG as a trigger in this case generates the longest DoI throughout all configurations, which applies also to the Datascope pump on semi-automatic mode (0.27 ± 0.22 s in both cases, 62% longer than the highest of the remaining cases, with $p < 0.05$).

In addition, averaging DoI just among ECGs triggered by Teleflex pump with AFIB and comparing the results to those of Datascope pump in semi-automatic mode with ECG as trigger (the configuration corresponding to the longest averaged DoI throughout all configurations) the difference becomes almost negligible as seen in Figure 6-7. If all ECGs are considered the averaged difference between the two configurations inducing longer DoI, the Datascope on semi-automatic mode and Teleflex on automatic mode with only ECG signal available, is 25% with $p < 0.1$. However if only ECGs triggered with AFIB by Teleflex pump are considered the difference decreases to 10%, with $p > 0.1$.

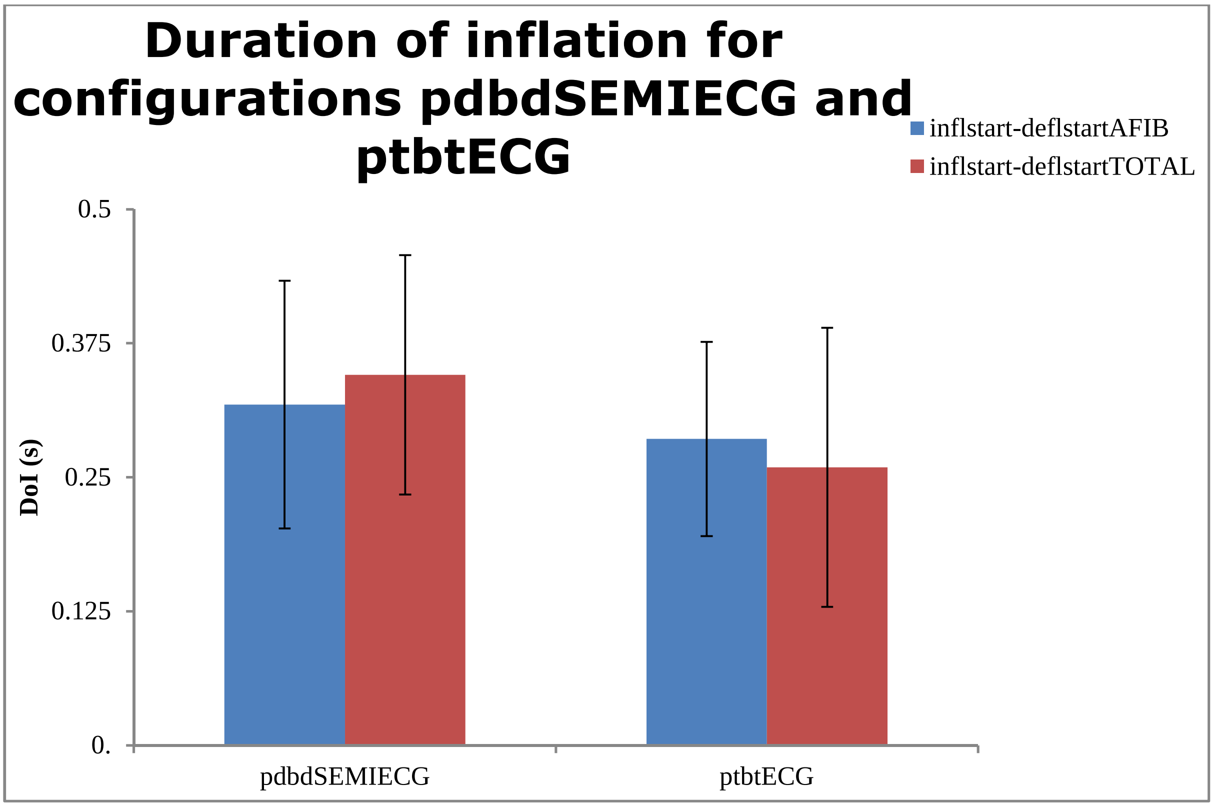

Figure 6-7: *Average index DoI for the configurations pdbdSEMIECG and ptbtECG in two cases: 1) blue bars, ECGs considered (1, 2, 3, 5, 10, 11, 13, 15) are just those in which ptbtECG uses AFIB as a trigger for onset of deflation; 2) red bars, all 15 ECGs are taken into consideration.*

In the case of highly irregular ECGs (4 and 13) the difference in DoI between the Datascope and Teleflex pumps working with ECG as trigger and the rest of configurations is very high: the other configurations calculate the duration of inflation mostly based on the previous beats, and if the ECG is irregular the time between one beat and the following one is highly variable, which results in the pump to produce an inaccurate duration of inflation. The high variability of the irregular ECGs is associated to the standard deviation. Indeed in case of ECGs 4 and 13 the standard deviation associated with DoI for all analyzed beats splits the configurations into two groups: Datascope and Teleflex working with ECG as a trigger induced minimum 23.2% and 30% higher deviation, on ECG 4 and 13 respectively, compared to the other configurations.

6.4.3 Ratio of missed beats compared to total number of beats – Ratio

The desirable value of this index is closest to zero. This ratio is highly indicative of the efficiency of the pump, and it varied greatly between different configurations in case of irregular ECGs. Values of this index for each configuration and ECG are shown in Figure 6-8, while averaged values of Ratio throughout ECGs, for each configuration, are shown in Figure 6-9.

The Datascope pump working on automatic mode gives the highest ratios (undesirable) in most of ECGs, regardless of the Linear or LWS balloon used. In case of automatic mode, the pressure transducer signal was generally selected automatically as the triggering signal. The average missed beats ratio is 10% of all beats throughout all ECGs. Operating the Datascope pump on the semi-automatic mode and ECG as a trigger resulted in an increase in the efficiency of the pump (reduction in the ratio): missed beats have become 2.7% of the beats in the most irregular ECGs (ECG 13). This Datascope mode performed much better, achieving positive response to 100% of the beats in the remaining 14 ECGs. The Teleflex pump on automatic mode and ECG as a trigger also achieved 100%, triggering all analyzed beats in all 15 ECGs.

Calculating the Ratio index in the highly irregular ECG 13 has a particular importance. The difference in performance between the configurations increases steeply, underlying the beneficial effects of selecting automatic mode with ECG triggering on the Teleflex pump and semi-automatic mode with ECG triggering on the Datascope pump. However the analysis of the Ratio in ECG 4 (irregular with a lower degree compared to 13) showed that the performance of the Teleflex pump on an automatic mode and FOS as a trigger is very similar to the Datascope pump on semi-automatic mode and ECG as a trigger.

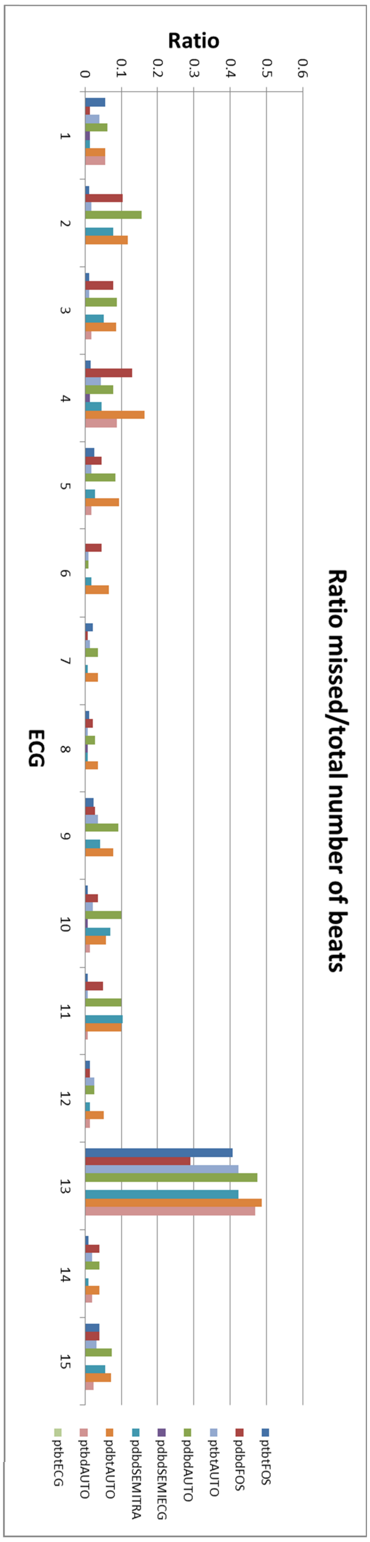

Figure 6-8: *Ratio of missed beats to total number of analyzed beats for each configuration and each ECG.*

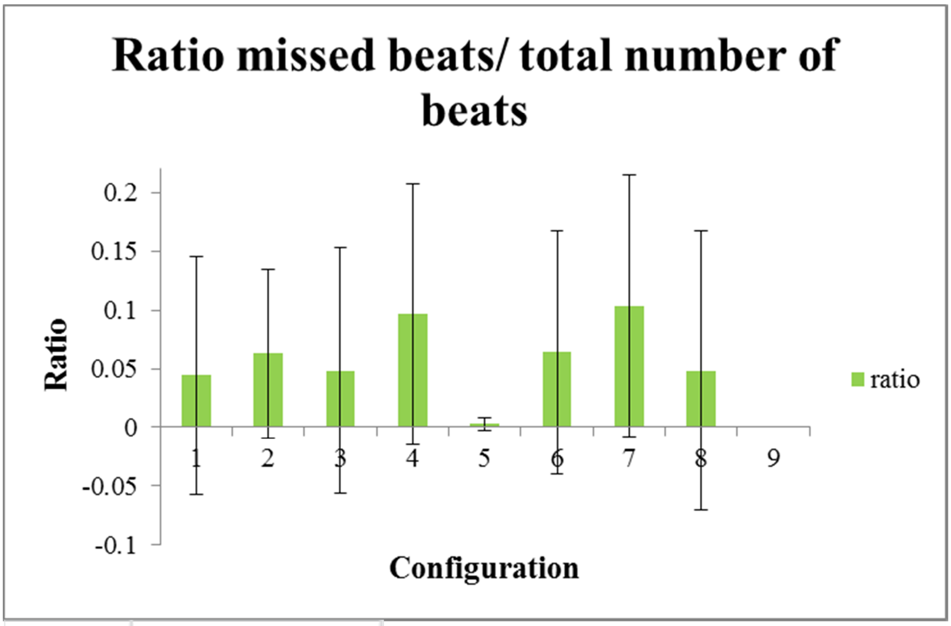

1	**ptbtFOS**
2	**pdbdFOS**
3	**ptbtAUTO**
4	**pdbdAUTO**
5	**pdbdSEMIECG**
6	**pdbdSEMITRA**
7	**pdbtAUTO**
8	**ptbdAUTO**
9	**ptbtECG**

Figure 6-9*: Mean values of Ratio for each of the 9 configurations used. As shown configuration 9, ptbtECG, provides the shortest value of RpIs.*

On the other hand, comparing different pressure triggers (FOS and transducer) and balloons (LWS and Linear) on the Teleflex pump on automatic mode it is possible to notice an almost unchanged Ratio. However, comparing different pressure triggers and balloons on the Datascope pump on automatic mode produced higher Ratios which were also higher (more missed beats) than those of the Teleflex pump, in all cases.

6.4.4 R-peak to systolic peak - RpSp

The RpSp index averaged throughout ECGs (Figure 6-10), changed maximum 0.0075 s (with $p = 0.46 > 0.1$) from one configuration to the other, showing that a change in configuration would not significantly affect the timing of the systolic pressure rise. It should be noted that the experiment has been conducted on a left ventricle simulator, which might affect the influence of the IAB on the pressure waveform compared to a physiological environment.

The analysis of all ECGs pointed out that RpSp index changes smaller in the ECG 2, 4, and 8, which are associated to the lowest heart rate (HR). In case of higher HR, the use of IABP might influence the time of peak systole because of the higher end diastolic pressure (EDP), independently from the selected mode. Following this logic, in case of lower HR EDP will instead be lower because a longer time is available between end of deflation and systolic rise.

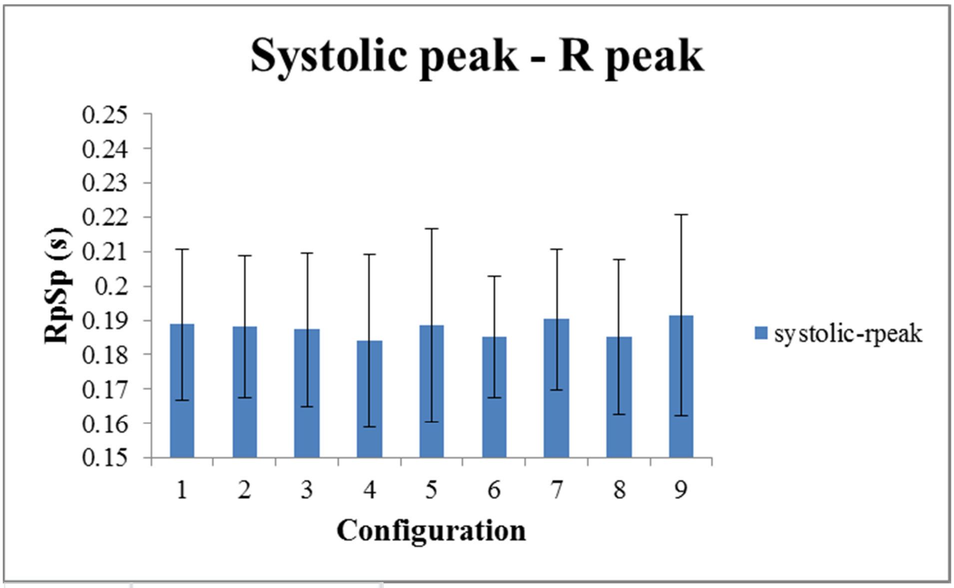

1	**ptbtFOS**
2	**pdbdFOS**
3	**ptbtAUTO**
4	**pdbdAUTO**
5	**pdbdSEMIECG**
6	**pdbdSEMITRA**
7	**pdbtAUTO**
8	**ptbdAUTO**
9	**ptbtECG**

Figure 6-10*: Mean values of RpSp for each of the 9 configurations used. As shown configuration 4, pdbdAUTO, provides the shortest value of RpIs.*

6.4.5 Inflation starting – Deflation ending - IsDe

This index depends on both RpSp and RpIs. The variability of the index RpSp for different configurations is 4% on average, hence the differences in IsDe depend mostly on the different timing of RpIs; the shorter RpIs, the longer IsDe. The analysis of the timing of the IsDe index confirms the above statement. The Teleflex pump on automatic mode and FOS as a trigger is associated with the shortest RpIs throughout configurations on 14 ECGs out of 15, and in these same ECGs it also results in the longest IsDe. As already observed for RpIs, ECG 13 resulted in a different trend from all other configurations: in this irregular ECG Datascope and Teleflex pumps, working on semi-automatic and automatic mode, respectively, and with ECG as a trigger, are associated to the longest IsDe.

The dependence of IsDe on RpIs index is also clear from the graphs in the following page, Figure 6-11, showing the values of the two indexes for all configurations and ECGs, and at Figure 6-12, reporting IsDe average values with standard deviation throughout ECGs for each configuration. As shown configuration 1, ptbtFOS, provides the longest value of IsDe.

6.5 Discussion

The need to elaborate automatic algorithms for the correct onset of balloon inflation and deflation according to the particular situation of each patient is well acknowledged from previous works. In fact, studies from Kantrowitz [90] and Schreuder [84], investigating the accuracy of inflation and deflation timing, demonstrated that in case of arrhythmia, fully automatic timing could be more precise. Schreuder also found that fully automatic timing was related to [91] 1 ms time accuracy from dicrotic notch together with 99.4% assisted arrhythmic beats.

In the present study, the main target was to quantify the difference in results produced by two IABPs in an in vitro setting that simulates the physiological environment, and also to identify the different results generated by each pump when operated under different settings. The tests used 15 different ECGs, taken from the AHA heart failure dataset.

Previous studies already tested one of the machines, the Teleflex AutoCat, with the aim of investigating error inaccuracies on 60 patients, evaluating the automatic mode of the pump [83]. However, the investigation was focused exclusively on timing errors, rated as early or late inflation and early or late deflation. In the current study instead, performance of the pumps was rated, and 5 different indexes have been proposed and measured for approximately 100 beats in each ECG.

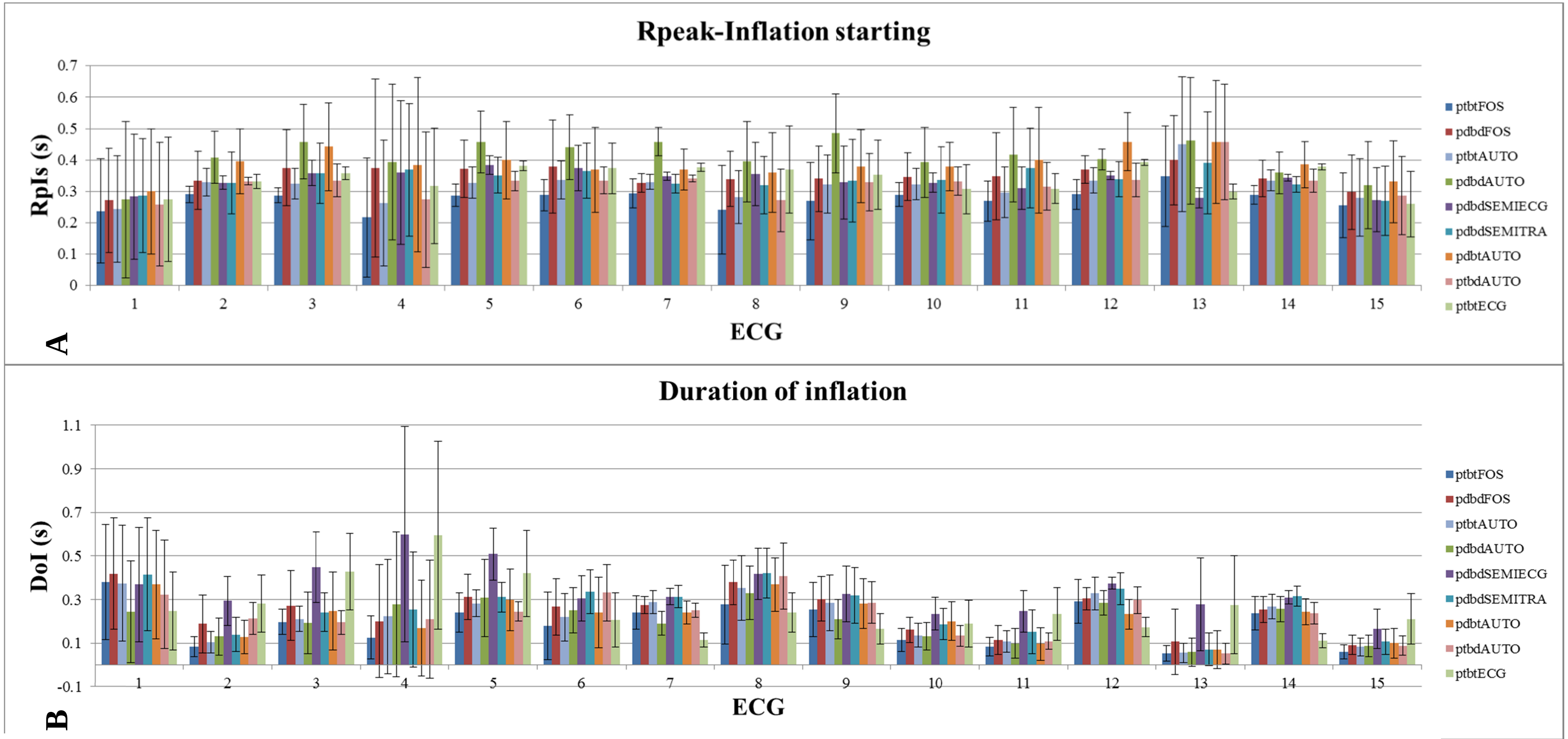

Figure 6-11*: (A) RpIs, already reported in figure 6-3; (B) Duration of inflation (DoI), generally inversely correlated to the index RpIs (the shorter RpIs, the longer IsDe). This is because a delay in the pump responding to the systolic peak also causes the overall duration of assistance to the heart to decrease.*

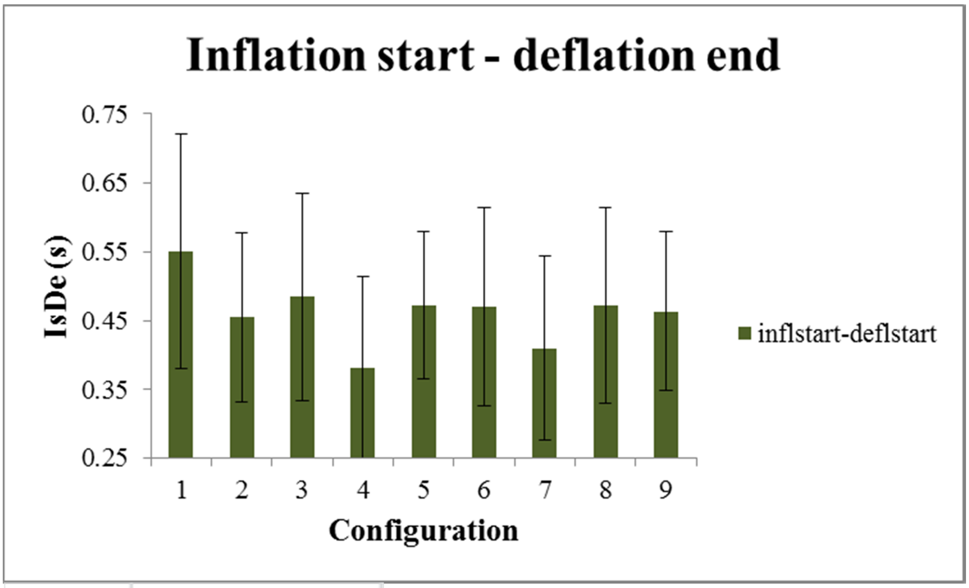

1	**ptbtFOS**
2	**pdbdFOS**
3	**ptbtAUTO**
4	**pdbdAUTO**
5	**pdbdSEMIECG**
6	**pdbdSEMITRA**
7	**pdbtAUTO**
8	**ptbdAUTO**
9	**ptbtECG**

Figure 6-12: *Mean values of IsDe for each of the 9 configurations.*

Particularly, 3 of these indexes, RpIs, DoI and Ratio, are relevant for classifying the effectiveness and efficiency of each pump. Different pump configurations (the combination of pump/balloon/trigger signal/mode of operation) performed best in certain indices, and the following is the ranking of pumps at each index:

1) **RpIs**: Teleflex pump with FOS as a trigger generally produced the smallest values of the RpIs index;
2) **DoI**: Datascope pump, when used on a semi-automatic mode and ECG as a trigger, generally produced the highest values of DoI;
3) **Ratio**: Teleflex pump with ECG trigger or Datascope pump on semi-automatic mode and ECG as a trigger induced the smallest Ratio throughout all of the configurations;
4) **RpSp**: Datascope pump on automatic mode is associated to an average shorter RpSp compared to the other configurations;
5) **IsDe**: Teleflex pump with FOS as a trigger is the configuration which

induced the longest IsDe, as a consequence of the shorter RpIs, compared to all other configurations.

6.5.1 RpIs

The importance of this index relies on the fact that it expresses the pump speed in responding to inflating the balloon after systolic peak. Although the lack of information regarding the effect of a late inflation, previous studies [92-94] have indicated a possible reduction in augmentation time and coronary perfusion pressure related to late inflation. The use of the FOS trigger on Teleflex pump induced the shortest RpIs. Using ECG trigger did not produce as good results.

The performance is different when FOS technology is used in the Datascope pump, obtaining a longer RpIs in all ECGs and hence longer time to respond before inflation onset. As the same triggering technique is used, it is believed that the difference in performance between the pumps in RpIs is related to the algorithm used by each pump to commence balloon inflation.

The variability of the RpIs index is also indicative of the pump effectiveness, since ideally RpIs should not change throughout the ECG regardless of its irregularity. A variability test showed that some configurations were more consistent than others. When FOS triggering is used, Teleflex pump performed better than Datascope in terms of variability for 9 ECGs: 2, 3, 4, 5, 6, 10, 11, 14, 15.

In case of highly irregular heartbeats (ECG 13), the best choice for ensuring optimized onset of balloon inflation is Datascope pump on semi-automatic mode or Teleflex pump on automatic mode, with ECG as a trigger; these two configurations produced the lowest mean value of RpIs and the smallest RpIs variability throughout all configurations. This result is caused by the high variability and frequency characterizing ECG 13. The pressure waveform resulting from this ECG is radically different from the physiological one. However, when Datascope and Teleflex pumps use ECG as trigger for onset of inflation and deflation, balloon inflation occurs with higher precision and reliability compared to the other configurations.

When the Datascope pump was tested on automatic mode the RpIs index was much higher than on semi-automatic mode, even if the pressure transducer was selected as a trigger in both cases. This suggests that the algorithm used by this pump is different between the two modes, and semi-automatic mode is superior. The relevance of this finding indicates that although automatic mode maybe preferred in clinical practice to avoid operator-dependent mis-judgement, the semi-automatic mode would lead to an improvement of the reaction of the pump in inflating the balloon.

6.5.2 DoI

The outcome of the analysis of this index is that the Datascope pump on a semi-automatic mode seems to provide a longer inflation support. The reason of Datascope pump elongating DoI compared to the Teleflex pump on automatic mode and ECG as trigger is that the first pump, in this configuration and semi-automatic mode, always associates the onset of balloon deflation to R peak, while the Teleflex pump normally (PATTERN trigger) calculates the DoI based on previous beats, and uses R peak as the onset of deflation only in case of irregular beats (AFIB trigger). When the Teleflex pump recognizes the irregularity of the ECG, the trigger changes from PATTERN to AFIB, and consequently DoI increases.

The Datascope pump always provides a longer DoI than that provided by the Teleflex pump, because the triggering is continuously in the AFIB mode which systematically deflates the balloon at the R peak. The Teleflex pump produces on average a shorter DoI if all ECGs and heartbeats are taken into consideration. This pump employs an algorithm software program, when arrhythmia is first detected, to assess if time is sufficient for the balloon to deflate at least 70% before following systole, and if it is not the case it will select AFIB triggering. Hence the pump works initially in PATTERN mode even with irregular beats, as the program appears to take into consideration 60 beats to determine if conditions for adequate deflation exist, before switching to AFIB mode. Contrarily, Datascope pump appears to always activatethe onset of deflation at the R peak without a verification of the possible extent of balloon deflation.

The initial 30 analyzed heartbeats, even in case of irregular ECG, might be triggered in PATTERN mode when Teleflex is working in ECG as a trigger instead of AFIB mode. However, it is noted in Figure 6-7 that, taking into consideration only the ECGs assisted by the Teleflex pump on AFIB mode, the difference between Teleflex and Datascope pump with ECG as trigger decreases consistently.

Unlike the Ratio and RpIs, the DoI index value should be interpreted carefully and not be considered as an indication of full pump efficacy simply in case of high values. The beneficial effect of a long DoI associated to the AFIB mode of the pump is indeed questionable because in some cases ventricular systole might be compromised by a late deflation, provoking an increased workload, as already expressed earlier by Hanlon-Pena et al. [80]. In any case, for an irregular ECG, this mode is favourable because of safety reasons: the balloon would deflate if an unexpected beat appears on the ECG. The trigger selection consists in a compromise by the Teleflex pump to ensure balloon deflation in case of irregular ECG and simultaneously to have the potential of achieving optimal DoI.

One of the parameters which reveals the consistency of the Datascope and Teleflex pumps working on ECG as a trigger is the DoI standard deviation. Considering the two most irregular ECGs (4 and 13), it is clear thatall the configurations are divided into two groups: Teleflex and Datascope working with ECG as a trigger and all the rest of configurations. In these two cases the value of DoI with its standard deviation shows that:

1. The Teleflex and Datascope pumps produce an exactly identical value of DoI, which confirms that when Teleflex works in AFIB mode (irregular heartbeats) it generates the same DoI as Datascope does
2. The two pumps have a much better performance when triggered by ECG than all others. DoI standard deviation gives an estimate of the reliability of the pumps working on this mode: the values of standard deviation are much higher in case Datascope and Teleflex pumps trigger with ECG signal, revealing the irregularity of the heartbeats, which need to be assisted for different times in each beat, hence different lengths of DoI. If the standard deviation of duration of inflation is high, it means that the pump assists each heartbeat for different time. This is in line with the irregularity of the ECG as each heartbeat would have a different duration compared to others. In these two cases (4 and 13 in figure 6-5), the standard deviation reaches negative values further confirming the high irregularity of the heart beats duration.

6.5.3 Ratio

The Ratio index, representing the number of missed beats over the total number of heart beats, indicates the efficiency of the pump and it is the index that can be directly used to rate the performance of an IABP. A small percentage of missed beats may be critical for the recovery of the heart.

Mean values of the ratio across all 15 ECGs are shown in the previous section, Figure 6-8. The Teleflex pump with ECG as a trigger comes first and in second place the Datascope pump in semi-automatic mode and ECG as a trigger. Then follows the Teleflex pump with FOS or AP as a trigger, with similar values, and the Datascope pump on automatic mode with FOS as a trigger or semi-automatic mode with AP as a trigger, with slightly higher ratios. Finally the Datascope pump on automatic mode without FOS signal is associated to the highest ratio among all configurations.

Changing the mode from automatic to semi-automatic in the Datascope pump results in an increase of the pump's efficiency in both cases AP or ECG signals are used as a trigger. The semi-automatic mode on the Datascope pump not only allows to choose the trigger signal and other minor settings, but it also appears to change the algorithm used for choosing the onset of balloon inflation and deflation compared to automatic settings. This information is crucial since in the clinical practice the pump is generally used in automatic mode and there is a lack in awareness of the changes induced by selecting one mode rather than the other.

Since clinically the balloon is used in case of a failing heart, it is expected to deal with patients showing an irregular ECG, to which the IABP has to adapt to be effective. The analyzed ECGs include some highly irregular ones, with the most interesting ECGs to consider consisting in ECG 4 and 13, both of which are highly irregular but with irregularities of a different nature and degree. ECG 4 shows, each 4/5 regular beats, an irregular one with a higher amplitude and shorter systolic peak to peak time difference. ECG 13 shows instead trains of 3 to 4 QRS waves with high HR (around 120 bpm) followed by a period of about 1-2 seconds characterized by the absence of any heartbeat. The Teleflex pump with FOS as a trigger results in a better Ratio in ECG 4 compared to Datascope with FOS as a trigger, with values close to the ones obtained with ECG as a trigger, approximately 1.5 %. In case of ECG 13, however, the two configurations have similar Ratio with each other, of almost 50%, significantly larger from the one obtained if the pumps are working with ECG as a trigger. This latest ECG is highly irregular, and this kind of irregularity negates the differences between these two configurations (Teleflex and Datascope with FOS as trigger), because of repeated irregular heartbeats at a very high frequency, showing the disadvantages associated to the algorithm using as a reference the pressure signal. On the other hand, ECG 4 consists of a small percentage of irregular heartbeats, and characterized by a lower frequency compared to ECG 13, in which case the pressure algorithm implemented in the Teleflex machine shows a better performance, in terms of triggered beats over total number of beats, compared to the algorithm used by the Datascope pump.

In Figure 6-13 is indicated, for both Teleflex and Datascope pumps working with FOS, the average and standard deviation of the value of Ratio throughout the regular ECGs (10 out of 15), while in Figure 6-14 for the irregular ECGs 4 and 13. The Teleflex FOS Ratio is statistically non significantly lower than the Datascope FOS ratio in case of regular ECGs and all arrhythmic ECGs ($p > 0.1$), but it is statistically significantly lower ($p < 0.05$) in all cases of arrhythmic ECGs, excluding ECG 13 (the most irregular), reinforcing the hypothesis that an irregularity such as the one presented in ECG 13 decreases the differences between the two pumps.

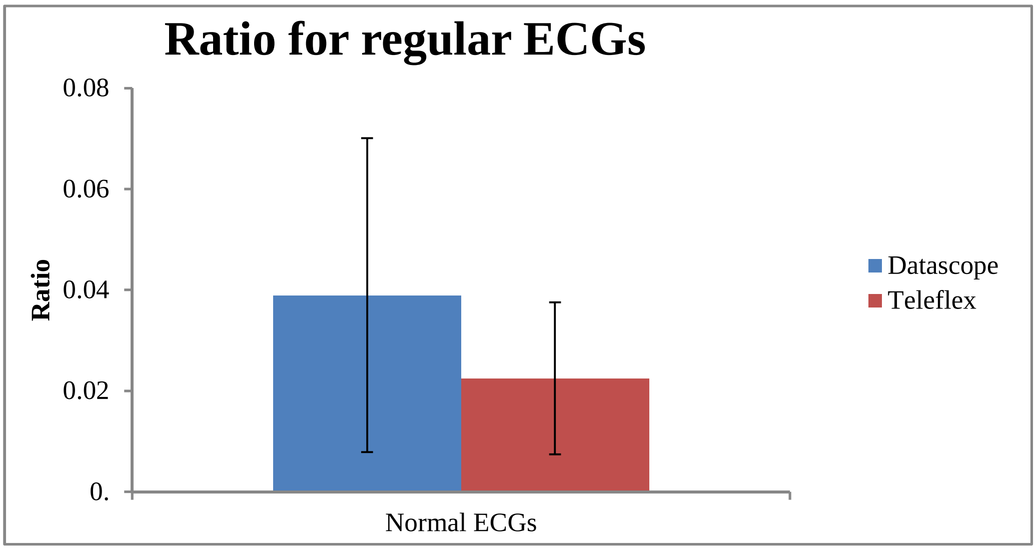

Figure 6-13*: Ratio of missed beats over total number of analyzed beats (Ratio) values, for Teleflex and Datascope pumps working with FOS as a trigger, averaged throughout the regular ECGs (1, 2, 3, 5, 7, 8, 9, 12, 14, 15), indicated as mean values and standard deviation.*

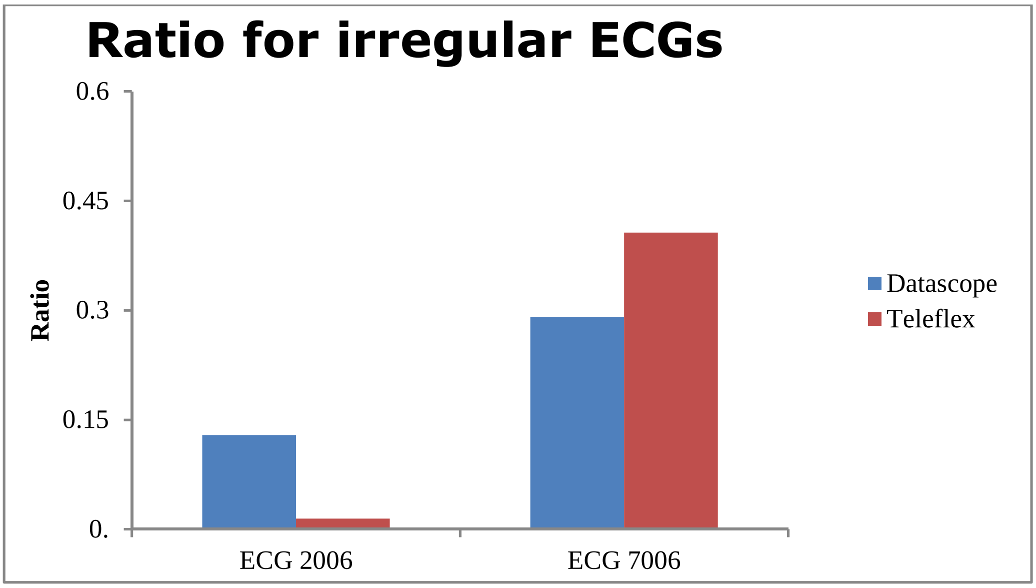

Figure 6-14: *Ratio of missed beats over total number of analyzed beats (Ratio) values, for Teleflex and Datascope pumps working with FOS as a trigger, for ECGs 4 and 13.*

6.5.4 Final considerations

No singular optimal configuration for all indexes is emerging after the analysis of the results obtained from the test of different pumps, pump modes and triggers on the 15 ECGs. Different configurations produce better results with different indices but no configuration is superior overall.

It should be considered that the comparison between the Teleflex and Datascope pump working on automatic mode and with both ECG and pressure transducer signals connected may not be straightforward. This is because in some cases, even for the same ECG, each pump selects a different trigger. Both Datascope and Teleflex pumps on the automatic mode selected the pressure transducer as a trigger for most ECGs, probably due to the characteristics of the ECG signal. It should also be noted that most of ECGs belong to patients with heart failure or pathological ventricle, and the shape of QRS wave is radically different from those of healthy patients. In these cases the pumps are supposed to switch to pressure transducer signal, if available, and the algorithms used for selecting inflation and deflation onsets are different from the ones used in case of triggering through ECG signal.

Five of the ECGs (1, 11, 12, 14 and 15) have been triggered with the pressure transducer signal by both pumps in automatic configuration, regardless of the balloon used. To avoid the possible interference of any other variables just these ECGs should be considered. Using the Teleflex pump produced a shorter RpIs (for either Linear or LWS balloons are used) and smaller Ratio (bigger number of beats detected) compared to the Datascope pump. Hence in these 5 ECG cases the Teleflex pump showed a faster response to the pressure stimulus and a higher efficiency in detecting the beats.

For evaluating the advantages of a pump on a certain mode compared to another it is important to point out the relevance of the different indices and the performance of the pumps for each of them. RpIs indicates the speed of the pump in activating the balloon inflation after the peak systolic pressure (when the pressure is being used as a triggering signal) or immediately after the QRS (when ECG is used as the triggering signal).

The pressure waveform measured by the balloon at its tip varies for different persons according to different physiological properties (ventricular contraction, aortic wall and arterial elasticity). These variations are neglected in case the balloon is inflated with ECG as a trigger, exclusively depending on QRS waves. The other way, if the pressure transducer or FOS is used as a trigger, the reference is the variation in pressure and this would ensure the efficacy of the pump in selecting the onset of balloon inflation. For the analyzed ECGs the pump with the best performance, for this index, was the Teleflex pump with FOS as a trigger. This pump on this mode performs better than when using a standard pressure transducer as a trigger: the improvement in the pressure signal introduced by the FOS resulted in an earlier inflation of the balloon, compared to the case in which a simple pressure transducer is used. In case the FOS technology is used by the Datascope pump, RpIs is longer compared to the one of the Teleflex pump triggering with the FOS or pressure transducer, and the value is generally similar to the one obtained when using Datascope pump on semi-automatic mode and pressure transducer as a trigger, hence not enhancing the advantage of the use of FOS compared to simple pressure transducer triggering.

DoI does not provide clear information about the beneficial effect induced by a pump or by a mode: if the value is high, it indicates a longer inflation, a probably higher mean diastolic pressure, but also a risk of higher EDP, while if the value is low, it indicates a possible lower EDP but shorter inflation and smaller mean diastolic pressure. Kern et al. [95] analyzed different deflation timings and suggested that end-diastolic pressure, assisted systole and mean arterial pressure should be the parameters determining the optimal deflation point for conventional timing. Specifically Schreuder et al. [81] quantified stroke volume and left ventricular stroke work changes corresponding to deflation onset established through R-peak (late deflation) and found that, although aortic valve opening was slightly delayed and myocardial oxygen demand increased, stroke volume increased by 14% and left ventricular stroke work by 6%.

It is then difficult to establish whether a long DoI would be completely beneficial or detrimental, since it should be considered that it is associated to an increase in mean arterial pressure [80] while not totally beneficial effects are associated to the deflation phase. Datascope pump on semi-automatic mode and ECG as trigger induced for most of ECGs the longest DoI, but it uses an algorithm which is not distinguishing between regular and irregular heartbeats, maintaining the same trigger mode for all ECGs. Teleflex pump with ECG as a trigger, instead, automatically selects a trigger mode according to the regularity of the ECG, targeting ensured balloon deflation in case of irregular heartbeats, and minimized EDP when the ECG is regular.

Ratio provides an estimation of efficiency of the pump in detecting all the heartbeats. It is important to consider the risks associated to a pump or a mode which is missing a certain percentage of beats. When the Datascope pump was used in semi-automatic and Teleflex pump in automatic mode, with ECG as a trigger, the number of missed beats was the smallest. These two configurations had a consistent better performance especially in case of a highly irregular heartbeat, as for ECG 13. When the Teleflex pump was used with the pressure transducer or FOS as a trigger, the number of missed beats was normally smaller than the one associated to the Datascope pump in same settings, but still critically high in case of irregular ECG.

The benefit associated with the use of a configuration compared to others has to be evaluated according to the condition of the patient. As already mentioned before, there are several levels of irregularities characterizing the patient ECG and hemodynamics. Dealing with a regular ECG or slightly irregular, such as most of ECGs analyzed in this study, the configuration which provided better indices in this study is the Teleflex pump on automatic mode and FOS as a trigger: optimal RpIs and good efficiency in terms of detected beats (Ratio). In case of highly irregular heartbeats, which is a typical condition for patient treated with IABP therapy, the most advantageous and safe configuration is the Teleflex pump on automatic mode and ECG as a trigger. This configuration allows obtaining a perfect triggering of all beats (100% of analyzed beats, throughout all ECGs), a safe deflation of the balloon and an adaptable duration of inflation. In case of irregular portions of the ECGs this configuration guarantees balloon deflation before the starting of systole. The difference in performance between the automatic and semi-automatic modes of the Datascope pump is a clear and important observation of this work. For all indices and all ECGs this pump performed better when used in a semi-automatic mode.

6.6 Conclusions

The study showed important differences between the setting modes of the pumps and trigger signal used, underlying that the setting should be considered according to the patient specific condition and on the quality of the ECG. Table 6-2 indicates a summary of the main findings on the different configuration's performance.

It was found that in case of a regular or slightly irregular ECG the use of Teleflex pump on automatic mode using fibre optic sensor (FOS) technology is suggested since it combines a fast response of the pump to systolic peak and a small value of Ratio (high effectiveness). When the ECG was characterized by high irregularity, Teleflex pump on automatic mode and ECG triggering was the one associated to the best value of Ratio index (100% of analyzed beats were triggered), a crucial index in terms of clinical significance, and to a safe deflation of the IAB. Nevertheless. the Teleflex pump showed to discriminate regular and irregular heartbeats and selected different triggering modes for deflation onset even though the same signal was provided (ECG).

Table 6-2: *List of configurations tested with the best (green) and the worst (red) performance for the three main analysed indeces. From this summary it is discernible that FOS technology in the Teleflex pump is associated to a faster response of the pump, and that semi-automatic mode on the Datascope pump performs better than the automatic one.*

	RpIs	DoI	Ratio
ptbtFOS			
pdbdFOS			
ptbtAUTO			
pdbdAUTO			
pdbdSEMIECG			
pdbdSEMITRA			
pdbtAUTO			
ptbdAUTO			
ptbtECG			

Moreover the analysis showed that the Datascope pump performs better in case semi-automatic setting is selected instead of the automatic one, since it induced a lower value of Ratio index (0 is best). Finally, the operator should establish which setting is best to be applied to exploit the benefits of the device on a specific patient, according to findings presented in this and in previous studies [80,81,83,95].

Chapter 7 Multi-dimensional computational model for simulating balloon inflation and deflation in a physiological system***

7.1 Chapter outlook

This chapter aims at discussing the development of a multi-dimensional computational model allowing an insight to the hemodynamic changes induced by the use of an IAB in the human body. The model also aims at giving an insight on the 3-D fluid-dynamics in the area surrounding the balloon during its inflation and deflation, to assess the effect of balloon counterpulsation on the main branches of the systemic circulation and, specifically, on the aortic root and ascending aorta. The developed model will be of importance when considering any change in IAB shape or inflation/deflation dynamics, providing an insight into the potential benefit of the changes on the systemic circulation and, specifically, on the aortic root.

7.2 Introduction

The purposes of using the IABP are the increase in coronary flow and the reduction in left ventricular afterload, associated to its counterpulsation. However the evidence of these two benefits is still subject of debate and little is known about the distribution of flow and pressure on the surrounding of the IAB.

Many 0-D models of the arterial system have been developed, also for simulating the effect on the cardiovascular system of human exercise [96], cardiac mechanical devices [97] and other pathophysiological situations [98] [99], which are described in the literature.

An important study by Stergiopulos et al. summarized in two scientific publications [100],[101] aimed at computationally simulating arterial flow in the human arterial system, with particular attention to the development of peripheral pressure and flow pulses. Fifty five vessels were modelled through electrical circuits based on their geometrical and mechanical properties. Normal and aortic stenosis conditions were modelled and the system demonstrated the ability to reproduce pressure and flow distribution in the arterial system in both situations, reasonably matching 'in vivo' data.

A computational study conducted by Abdolrazaghi [102] introduced a 0-D model including an IAB. All compartments of the 0-D model, representing the circulation in the human body, are electrical circuits constituted by one conductance,

***ESAO oral presentation: 3-D Computational model of intra-aortic balloon pump (IABP) coupled with a 0-D model of the arterial tree by Bruti, G. and Khir, A.W. [ESAO 2013] one resistance and one inductance, resembling the mechanical properties of the vessels (their analogies will be better explained in the method section of this chapter). The IAB is also represented through electrical components: one varying conducta-nce, two varying resistances and two varying inductances, resembling the inflation and deflation of the balloon. Although the model could well reproduce hemodynamics during normal and myocardial infarction conditions, the changes induced by the use of IAB reproduced only partially pressure and flow changes measured ‘in vivo’. Moreover 3-D distribution of flow and pressure on the surroundings of the balloon was not represented.

One of the first studies investigating 3-D blood flow associated with IAB inflation and deflation activity was published in 1991 by Natan et al.[64]. The study used dimensionless Navier-Stokes equations, a technique previously used by the same group [103], for representing 3-D distribution of flow and pressure due to the IAB counterpulsation and describes the effect of different balloon size on the pressure and flow waveforms within the thoracic aorta. The disadvantage of the work consists in the absence of information about the effect of balloon activity on the branches of the systemic circulation and, particularly, on the aortic root, since just the thoracic aorta was modelled. While data about pressure and flow in this region are crucial to understand the balloon effectiveness, the mechanical properties of the vessels in all main branches of the arterial bed can have a big influence on the distribution of flow and pressure in the IAB surrounding.

Ferrari et al. [104] developed a hybrid model based on a computational 0-D model of the circulatory bed interfacing with an experimental model of aorta accommodating an IAB. The study resulted in the reproduction of the hemodynamic effects of the IAB activity, asserting that the model represented the re-balancing effect of the use of the balloon in myocardium infarction condition. Nevertheless the publication does not provide information on the 3-D distribution of flow and pressure around the balloon. Moreover, to analyse the effect on hemodynamic parameters induced by different balloon shapes or materials, a prototype has to be specifically produced and tested.

The aim of the work described in this chapter was to develop a computational model that can describe the 3-D pressure and flow distribution, in the aorta, and in each main vessel of the systemic circulation, and which could potentially enable the modification of IAB geometry to optimise its benefits. For this purpose a model has been developed based on the coupling of a 0-D computational model of the systemic circulation with a 3-D computational model of IAB within the thoracic aorta.

7.3 Multi-dimensional model for IAB counterpulsation

The main purpose of this study is to investigate the effectiveness of the IAB. It is hence essential to have information about the amended pressure in the aortic root, which is one of the main parameters regulating the increase in diastolic coronary flow, and early systolic left ventricular afterload. It is also important to model the mechanical characteristics of each main compartment on the arterial system to resemble the effect of these parameters on the flow and pressure distribution on both sides of the balloon during its counterpulsation.

One-dimensional models can treat the matter of propagation of pressure and flow waves in the vessel network, possibly addressing valuable information regarding cardiac function, elastic properties of the vessels, and patho-physiological conditions of important organs. A 0-D model resembling the systemic circulation through a number of main compartments, in which information about pressure and flow waveforms will be available, takes into account the effect of the vasculature mechanical properties and gives information about pressure and flow distribution without high computational requirements. In the current case the target is to have an initial evaluation of the effect of the IAB counterpulsation on the failing heart. Hence a multiple-compartment model for the systemic vasculature is the best compromise between computational time and accuracy to provide physiological impedance at boundary conditions on the 3-D modelled thoracic aorta.

Nevertheless, the thoracic aorta accommodating an IAB should be modelled three-dimensionally because of two main reasons:

- The counterpulsation of the IAB generates blood flow with three dimensional characteristics, because of the expansion of the balloon wall during inflation and the collapse of balloon wall during deflation. The velocity and pressure changes in the region between the balloon and arterial wall are clearly a 3-D phenomena. Since the detailed 3-D flow in the region will influence the hemodynamic parameters in the aortic root, a 3-D simulation is necessary to produce more accurate results;

- 3-D fields of velocity and pressure, at any point, will be available, to aid the design of a balloon characterized by a different shape or material.

7.4 Methodology

A 0-D computational model of the systemic circulation based on a Windkessel model was coupled with a 3-D computational model of an IAB placed inside the thoracic aorta. The 0-D model was used for imposing boundary conditions on the 3-D model. In fact flow data extracted from the solution of the mass and momentum equations in the 3-D domain were used as input condition for the 0-D model, where pressure and flow were calculated in the lumped circuits characterizing it, through the solution of ordinary differential equations (ODEs). In the following paragraphs the 3-D computational model will be first described in detail, and then the boundary conditions depending on the 0-D compartmental model with related coupling criteria between the two will be presented.

7.4.1 3-D domain

7.4.1.1 IAB counterpulsation geometrical model

The 3-D model was developed in Ansys ICEM CFD 14.0 (Cecil Township, Pennsylvania, USA). The model developed consists of a cylindrical tube, resembling the thoracic aorta, of 2.2 cm in diameter D, accommodating a model of the IAB based on experimental high-speed camera recordings. The balloon was divided into 7 parts: base, centre, tip and the links between these parts and with the two ends of the balloon. See Figure 7-1 for clarifications.

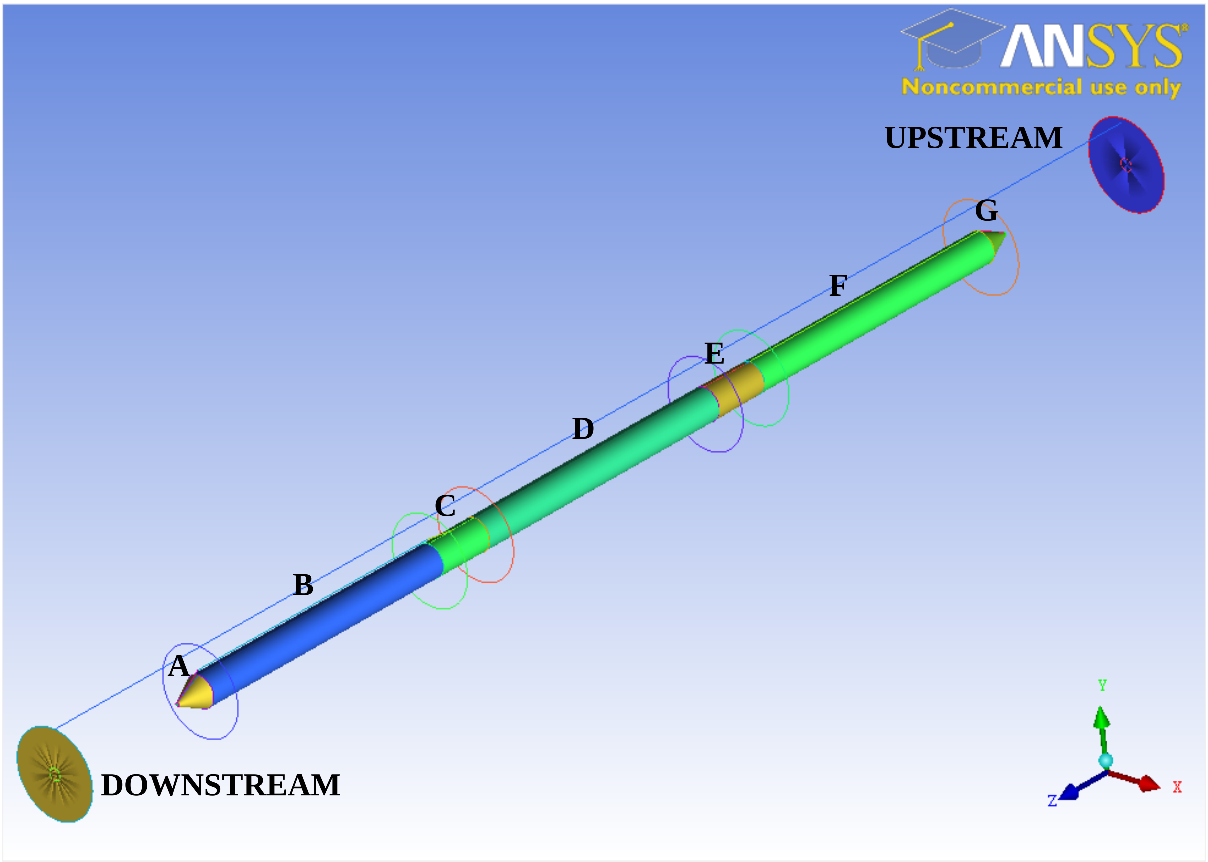

Figure 7-1*: 3-D model of the IAB with dimensions imported from high speed camera recordings. The balloon has been divided into 7 parts (A, B, C, D, E, F, G), in which the three longest portions (B, D, F) are moving according to high-speed camera movements and the remaining ones (A, C, E, G) are moving according to a linear interpolation between the two connecting parts.*

The axisymmetric radial movements associated to the balloon tip, base and centre (B, D, F) are established according to the tracking of the balloon tip, base and centre wall movements from high speed camera videos of the balloon counter-pulsating inside a silicone rubber tube (a representative image is shown in Figure 7-2). Although during IAB counterpulsation, especially in the beginning of inflation and end of deflation, the balloon cross-section is not completely representative of a circle diameter, the computational model was assumed to be constituted by a series of cylinders with diameter established from the value of wall-to-wall distance. The movements associated to the connecting volumes indicated by A, C, E, G in Figure 7-1 correspond to a linear interpolation function between the movements at the opposite ends of the volume. The function is described in equation 7.1, taking as an example the linking volume between IAB base and centre:

$$M(z,t) = \frac{M_b(\mathrm{t}) - M_c(\mathrm{t})}{z_b - z_c} \times \mathrm{z} + M_c(\mathrm{t}) - \frac{z_c}{z_b - z_c} \times (M_b(\mathrm{t}) - M_c(\mathrm{t})) \qquad \textbf{(Eq.7.1)}$$

Where M(z,t) indicates the radial movement of the IAB membrane along axis z and during time t, 'M_b(t)' and 'M_c(t)' describe the motion of IAB base and centre, respectively, during time t, 'z_b' and 'z_c' are the axial coordinate of the location where motion is defined in the base and in the centre, respectively, and 'z' is the axial coordinate where the motion of the IAB is defined.

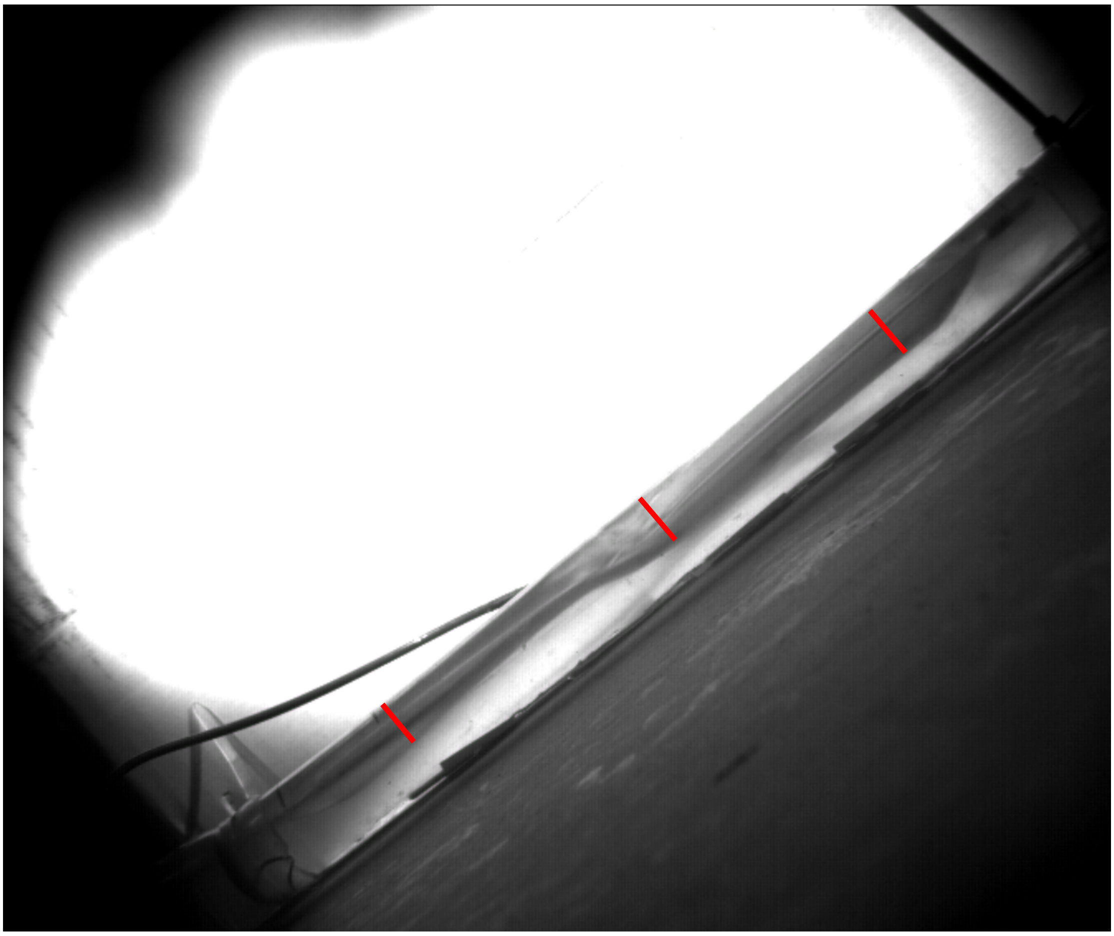

Figure 7-2*: Image of IAB inflation, recorded through high speed camera, while processed for obtaining measurements of balloon diameter, at its base, centre and tip (red lines), throughout the cycle.*

Figure 7-3 shows a recording of IAB wall-to-wall distance, which guides the motion in the 3-D domain for the base (B), centre (D) and tip (F) volumes, during balloon counterpulsation cycle. At a second stage the IAB wall movements were imposed according to the tracking of IAB wall following high speed camera recordings during balloon inflation and deflation at an angle of 45°.

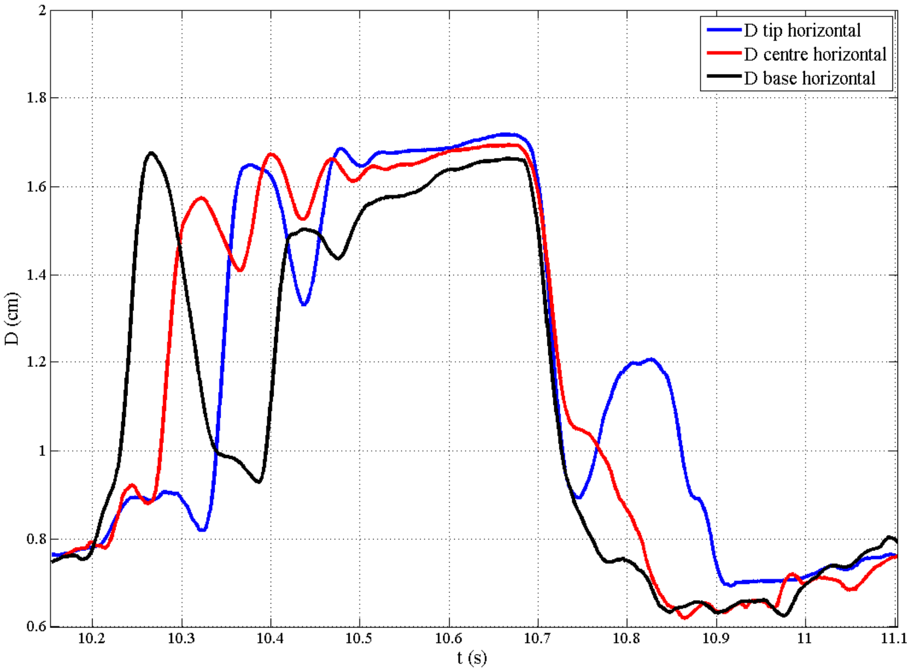

Figure 7-3: *IAB movement imposed for counterpulsation in case of the cylindrical model (black line) and of high-speed camera recordings model (red line – base, green line – centre, blue line - tip).*

To highlight the differences in the movement of the whole balloon a comparison between a model with IAB wall tracked movement at a horizontal position and a model with IAB wall tracked movement at an angled position is shown in Figure 7-4. The comparison shows the three-dimensional model of the balloon at different times during its counterpulsation cycle, underlying the differences between the three models.

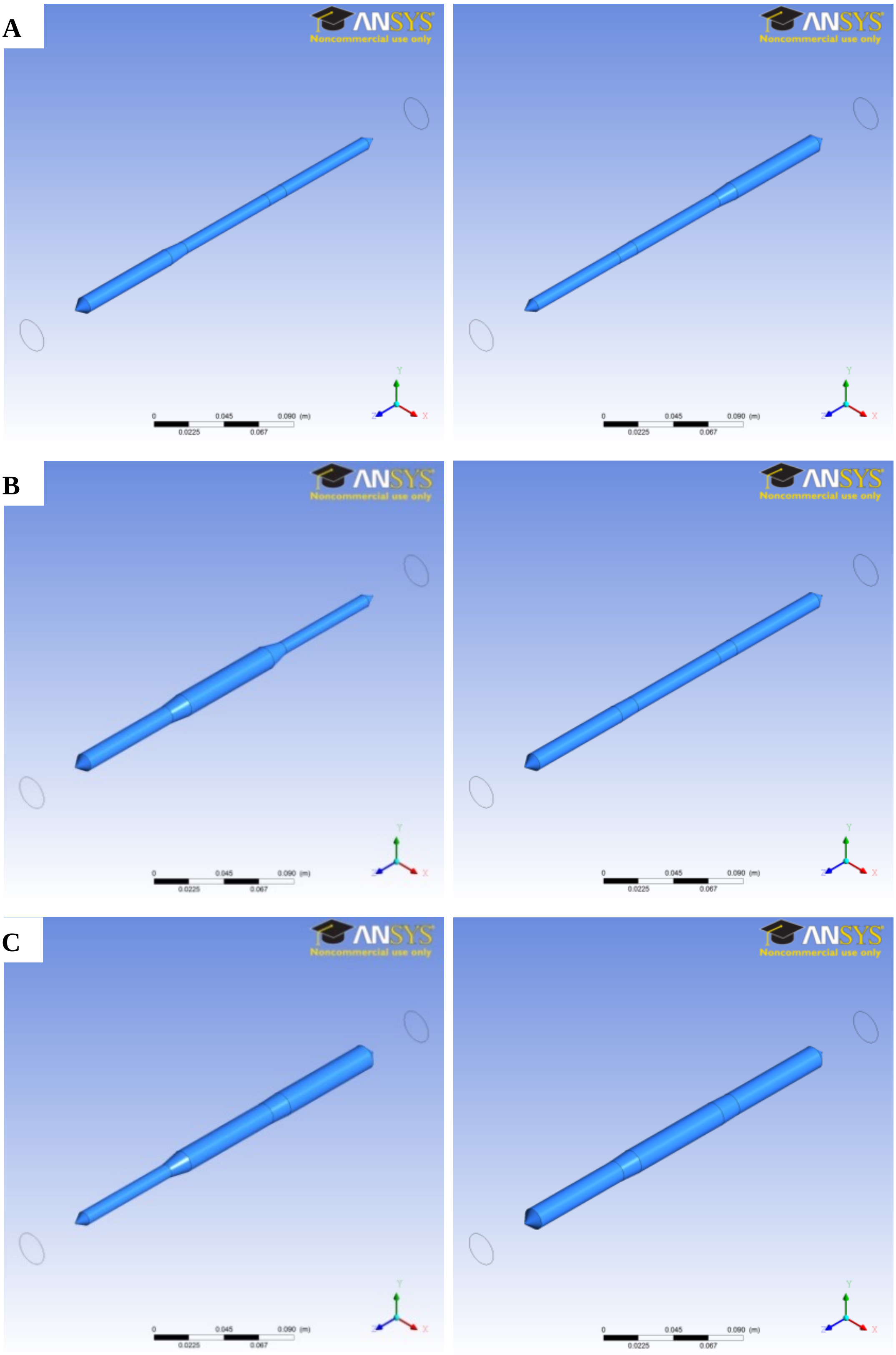

To be continued

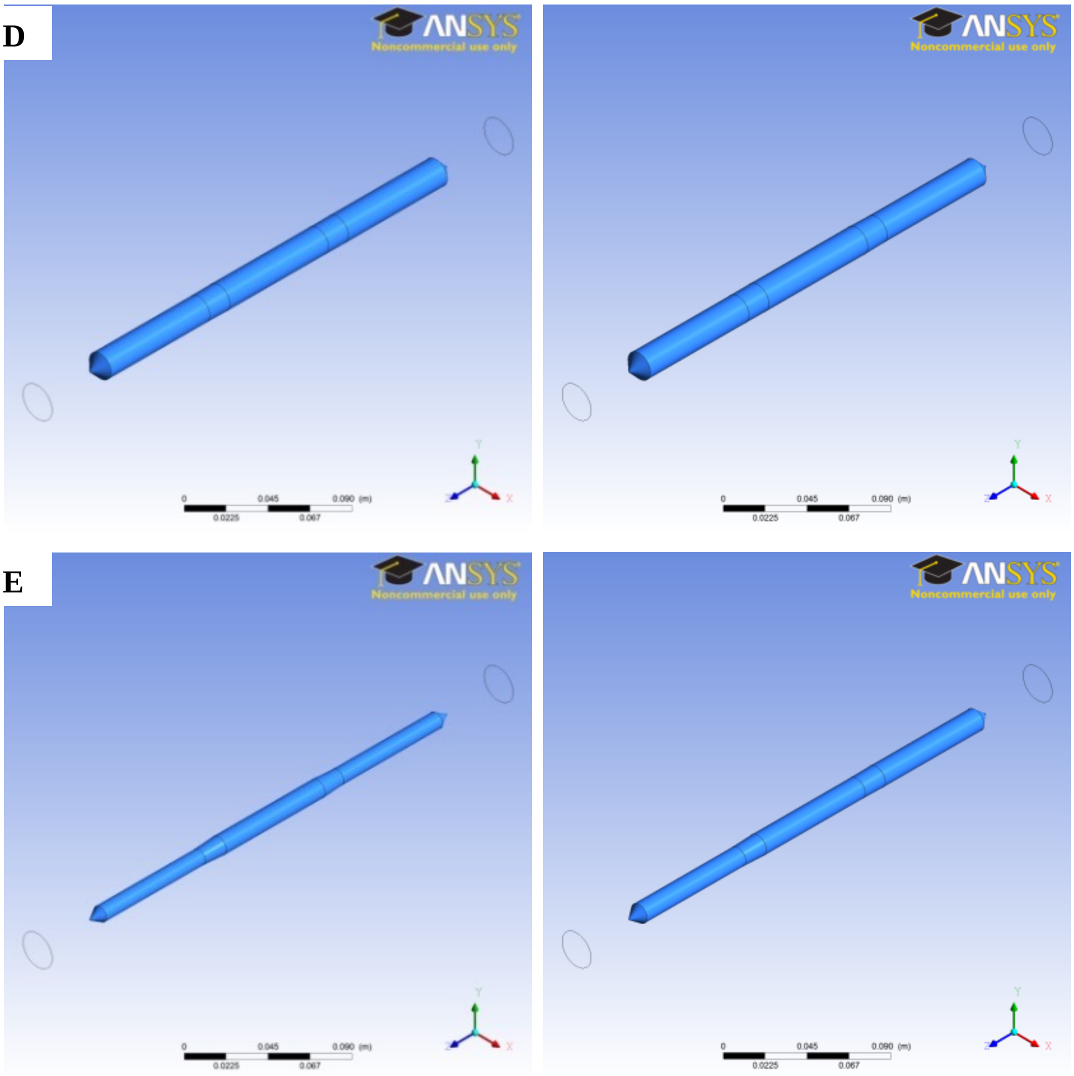

Figure 7-4*: Movement of the balloon within the thoracic aorta during its inflation (A, B, C), while IAB is fully inflated (D), and during deflation (E). The motion is indicated in case of high speed camera recordings at a horizontal position (left) and at an angle of 45° position (right). It is clear that, especially during inflation, the movement defined through function is more linear than in the other two cases, involving the movement of three different parts of the IAB.*

7.4.1.2 Mesh and solver characteristics

The mesh used consisted of 119,104 hexahedral elements, concentric and built as an “O grid” geometry mesh. This geometry was chosen to avoid distortion during compression. During IAB counterpulsation a mesh deformation exponential function was used, based on the change in size of the mesh elements related to their volumes, with higher volume cells being associated to a higher deformation compared to the smaller volume cells. The model geometry underwent mesh sensitivity analysis, as described in paragraph 7.5.4.

The 3D ANSYS CFX simulation was a transient with a cycle duration of 1 s and with a time step size, called 3D ts size, of 1 ms, corresponding to the time step size used after time step size sensitivity analysis in the 0-D model, called 0D ts size, also of 1 ms (described in the paragraph 7.4.1), imposing the boundary conditions to the 3-D fluid domain. One-dimensional Courant number was calculated according to equation 7.2 to verify the convergence of the solution in the 3D domain:

$$C = \frac{v_{peak} * \Delta t}{\Delta u} \qquad \textbf{(Eq.7.2)}$$

where is the peak velocity in longitudinal direction, assumed of 0.66 m/s, is the 3D ts size, 1 ms, and is the element size in the longitudinal direction, 0.0035 m. Courant number resulted in 0.1886, below the critical value of 1.

ANSYS CFX is a finite element based finite volume software, hence the discretization characterizing the model is based on the integration of the variables in integration points located between the centre of each element face and the connecting line between the element nodes. The high resolution discretization scheme for the advection term and standard discretization scheme (2^{nd} order approximation) for mass and momentum conservation and pressure equations were selected. High resolution scheme was used as it is less likely to induce diffusive discretization errors in case of steep spatial gradients. With velocity and pressure values data being stored at each element node, shape functions are used by ANSYS CFX to approximate the variables value at the integration points within each element constituting the mesh. Segregated algorithm was used for pressure-velocity coupling, based on a momentum-like equation on each integration point.

The transient scheme, or time integration technique, used to solve the Navier-Stokes equations for the three-dimensional domain was set to the second order implicit backward Euler method. The maximum number of iterations, called 3D iterations, was set to 50, and was stopped in case of RMS (root mean square) residuals (normalized values of equation residuals) from the momentum and mass conservation and pressure equations smaller than $10e^{-5}$.

Specifically, the raw residuals represent, for each variable, the difference between the solution of the variable equation between the 3D iteration steps n and n+1. RMS residuals are then obtained through normalization of raw residuals for each monitored variable, for the purpose of solution monitoring. In ANSYS CFX this happens through calculating, for each solution variable φ, the normalized residual, as in equation 7.3:

$$\hat{r}_{\varphi} = \frac{r_{\varphi}}{a_{p} * \Delta\varphi} \qquad \textbf{(Eq.7.3)}$$

where is the raw residual control volume imbalance, is a coefficient representative of the control volume size, and is a representative range of the variable in the domain.

This target was reached during most of the simulation. The most critical periods were the starting of the cycle and the time of IABP activation and steepest motion. In these cases the residuals were higher $10e^{-5}$ after 50 cycles 3D iterations, although still smaller than $10e^{-3}$. However this situation characterized only a small portion of the overall cycle, and was due to the steep change in velocity against time.

The following conditions were set in the 3-D domain:

- Input functions:
    1. Upstream plane (aortic side close to aortic arch): transient upstream pressure;
    2. Downstream plane (aortic side close to femoral bifurcation): transient downstream pressure;
    3. Motion: it contains the values of the balloon motion in the radial direction during a cardiac cycle. This is imposed in the different balloon portions (A, B, C, D, E, F and G in Figure 7-1).
- Boundary conditions:
    1. Upstream: this domain refers to the upstream thoracic aorta plane, closer to the aortic root, and the boundary condition is imposed by the Main Inlet function, described later in the chapter; mesh motion has

been prohibited by imposing a stationary condition at the upstream plane;

2. Downstream: this domain refers to the downstream thoracic aorta plane and the boundary condition is imposed by Main Outlet function, described later in the chapter; mesh motion has been prohibited by imposing stationary option on boundary details;

- Aortic wall: this domain corresponds to the thoracic aorta wall, a no slip wall condition was used; mesh motion has been prohibited by imposing stationary;
- Fluid domain: this domain represents the fluid flowing within the thoracic aorta; blood characteristics have been imported assuming it is a Newtonian fluid;
- Balloon wall: mesh deformation imposed to this domain followed a displacement in the radial direction according to the values imposed through the motion function;
- Upstream and downstream balloon wall: these domains refer to the balloon tip and base planes, respectively; no slip wall condition was associated to these domains.

When simulating the IAB counter-pulsating at angle of 45°, a buoyancy model was added to the simulation, in which the gravity ($g = 9.81$ m/s^2) was acting on the fluid field at an angle of 45°.

7.4.2 3D upstream and downstream boundary conditions: 0-D compartmental model of the systemic circulation

The 3-D model upstream and downstream pressure boundary conditions, on both sides of thoracic aorta the 3D model, defined in the above paragraph as Main Inlet and Main Outlet functions, are imposed through solution of ODEs characterizing a compartmental model described in detail in the following section. As already mentioned the systemic circulation imposing the boundary conditions on the 3-D domain was treated as a system constituted by a total of 54 vessels. The connections between the vessels are modelled according to the structure of the arterial system.

The main compartments were modelled as a three elements Windkessel model, constituted by the following electrical compounds: conductor **C**, representing vessel compliance, resistance **R,** representing vessel hydraulic resistance, inductance **L**, and representing blood flow inertia. For the terminal branches a 2-element Windkessel circuit constituted by one resistance and one inductance has been used. The electrical expressions associating each parameter to tension and current are indicated in the Eq. 7.4, Eq. 7.5, Eq. 7.6, and refer to Figure 7-5.

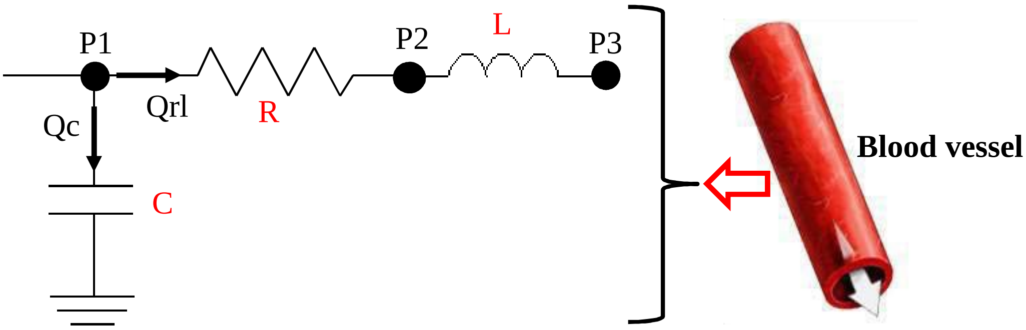

Figure 7-5*: Electronic circuit equivalent to a major blood artery vessel. This structure has been used in the 0-D model to resemble each main compartment in the arterial tree.*

$$P1(t) - P2(t) = R * Qrl(t) \quad \textbf{(Eq.7.4)}$$

$$Qc(t) = C * \frac{dP1(t)}{dt} \quad \textbf{(Eq.7.5)}$$

$$P2(t) - P3(t) = L * \frac{dQrl(t)}{dt} \quad \textbf{(Eq.7.6)}$$

The analogy is derived by treating the Navier-Stokes equations as already discussed by previous studies [108]. Blood flow in arteries can be modelled as a one-dimensional axisymmetric flow of an incompressible and Newtonian fluid, for which the Navier-Stokes equations simplify to[108]:

$$\rho\frac{\partial u}{\partial t} + \frac{\partial P}{\partial x} = \frac{\mu}{r}\frac{\partial}{\partial r}\left(r\frac{\partial u}{\partial r}\right) \quad \textbf{(Eq.7.7)}$$

in which ρ is the blood density, μ is the blood viscosity, u is the axial velocity, P is the blood pressure and r is the radius of the vessel.

The flow is considered laminar, provided that the Reynolds number Re is below the critical value of 2000 [108]. This might not be true in vessels characterized by diameter above 1.5 cm, such as the aorta, especially in case a device like the Intra-aortic balloon is activated. Hence it has been decided to separate this vessel from the systemic circulation and to model it three-dimensionally.

In case of vessels with a diameter < 0.2 cm and Re close to 10 (Eq.7.7) can be simplified to the following expression:

$$q(t) \approx \frac{\pi R^4 P(t)}{8\mu L} \qquad \textbf{(Eq.7.8)}$$

in which q is the volumetric flow, R is the radius of the vessel and L its length.

By associating (Eq.7.8) to the governing equation of an electric circuit with a resistance the following is obtained

$$P(t) = \mathbf{R} * q(t) \qquad \textbf{(Eq.7.9)}$$

in which **R** is the electric resistance, P is the potential across the resistance and q is the current flowing through it, the value of the resistance assumes the following expression, which is referred to as resistance in a Poiseulle flow [108]:

$$\mathbf{R} = \frac{8\mu L}{\pi R^4} \qquad \textbf{(Eq.7.10)}$$

In case of vessels with a diameter higher than 0.2 cm the inertial forces should be taken into account and the solution of (Eq.7.7) can be represented by the following expression

$$\frac{\lambda R^2 \rho}{\mu}\frac{dq(t)}{dt} + q(t) = \frac{\pi R^4}{8\mu L}P(t) \qquad \textbf{(Eq.7.11)}$$

in which λ = 0.1729 can be interpreted as the relaxation time index.

Considering a circuit with a resistance **R** and an inductance **L**, the governing equation

$$\frac{\mathbf{L}}{\mathbf{R}}\frac{dq(t)}{dt} + q(t) = \frac{1}{\mathbf{R}}P(t) \qquad \textbf{(Eq.7.12)}$$

by association with (Eq.7.11), will provide the expression of the resistance **R** and inductance **L**, as following:

$$\mathbf{R} = \frac{8\mu L}{\pi R^4} \quad \mathbf{L} = \frac{8\lambda\rho L}{\pi R^2} \qquad \textbf{(Eq.7.13)}$$

The formulation (Eq.7.11) can represent the flow in vessels up to 1.5 cm in radius.

It is important to mention that (Eq.7.7) refers to flow in rigid vessels. Blood vessels in the arterial tree present properties of elasticity which highly influence flow and pressure waveforms during the cardiac cycle and should be represented in the 0-D model. The addition of a lumped compliance would take this diversity into account. Hence the circuit was changed through adding a capacitor, which can represent the storage of fluid in the vessel in case of increase in pressure.

The whole arterial tree was divided into 54 segments. The compliance in the terminal branches was neglected, and these branches were modelled by a resistance and an inductance. The values associated to these parameters, for each compartment, are calculated based on physiological dimensions provided by Westerhof [70].

The inputs to the 0-D model were the flow in the aortic root and the capillaries pressure of 15mmHg. The model provides as output the pressure and flow in each compartment. A schematic representation of the modelled system is in Figure 7-6 (the main modelled compartments are here represented).

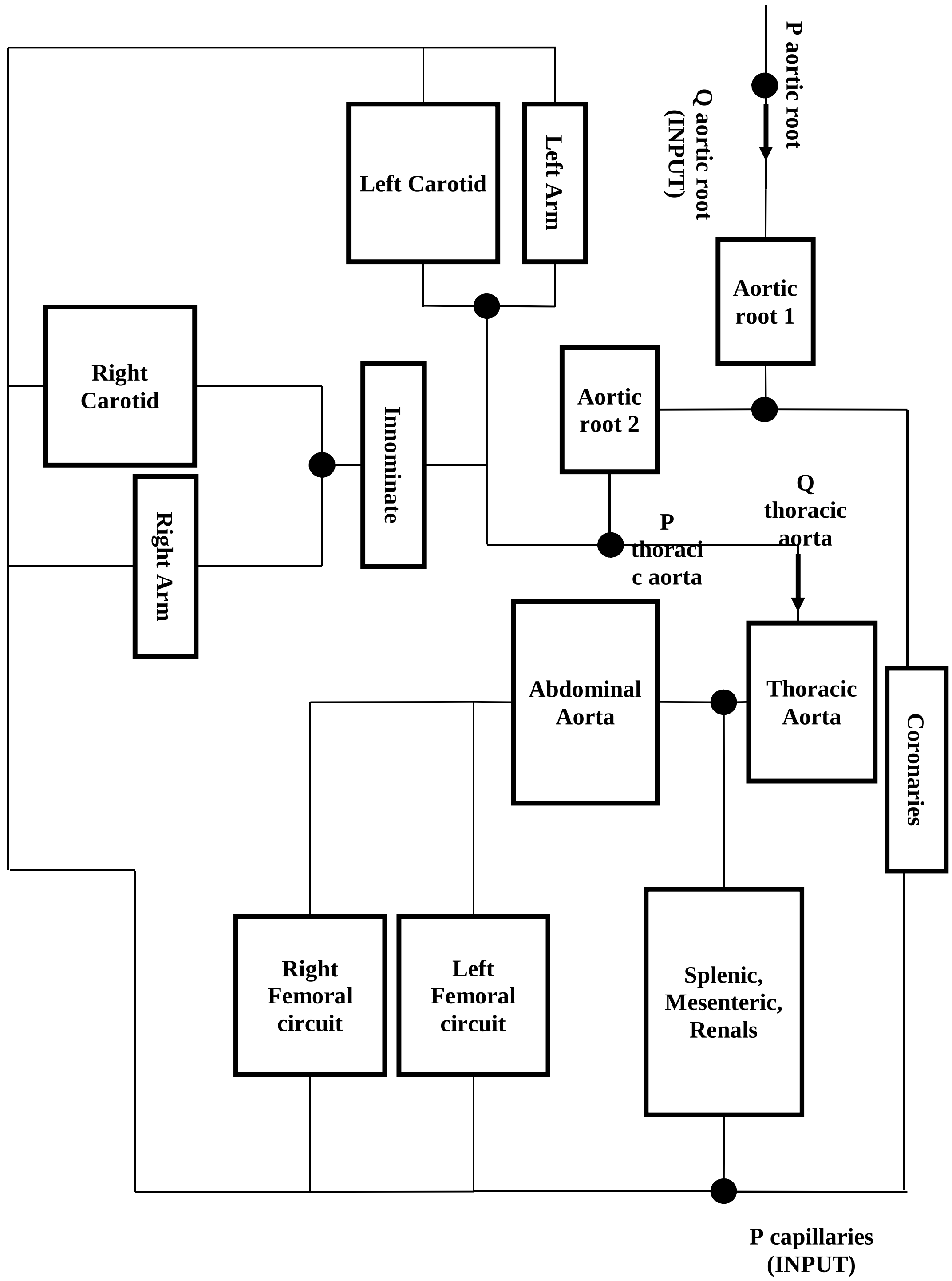

Figure 7-6*: Main compartments into which the systemic circulation was divided. As indicated the inputs to the system are the pressure on the capillaries and the flow in aortic root, and the outputs are pressure and flow on all the modelled branches.*

7.4.2.1 Implementation

The solution to the ordinary differential equations characterizing the flow and pressure on each compartment were obtained through the forward Euler method. Previous studies used this method in lumped parameter models of blood circulation [107].

For each compartment n, depicted in Figure 7-6, flow and pressure at the following time step (i + 1) are found through the solution of the following equations:

$$\frac{\Delta t}{C_n} * Qc_n(i+1) - P1_n(i+1) = -P1_n(i) \quad \textbf{(Eq.7.14)}$$

$$\frac{\Delta t}{L_n} * P2_n(i+1) + \left(\frac{\Delta t * R_n}{L_n} + 1\right) * Qrl_n(i+1) - \frac{\Delta t}{L_n} * P1_n(i+1) = Qrl_n(i)$$

(Eq.7.15)

$$Qtot_n(i+1) - Qrl(i+1) - Qc_n(i+1) = 0 \quad \textbf{(Eq.7.16)}$$

Where is the 0D ts size, $Qtot_n$ the total flow into the department n, Qc_n and Qrl_n the flows through the compliance and resistance, respectively, in the department n, $P1_n$ and $P2_n$ the pressures before resistance and inductance, respectively, for the department n, and Cn, Rn and Ln the compliance, resistance and inductance, respectively, of the department n. These equations establish the flow and pressure distribution throughout the modelled compartment and can be written in the form of a matrix product as follows:

$$A * x = b \quad \textbf{(Eq.7.17)}$$

in which x is a vector containing all unknown variable (, and), b is a vector containing the results of the equations and A is the matrix including the coefficient of the unknown variables in all equations.

As already described in the previous paragraphs the boundary conditions on the 3-D domain are established through solving the described ODEs through forward Euler method in the 0-D model, determining impedance on the two sides of the thoracic aorta, proximally and distally to the heart.

After a 0D ts size sensitivity analysis, in which a different 0D ts size was applied on the system until convergence was reached, and then changed in order to identify the effect on the model results, a 0D ts size of 1 ms was defined and initial values for pressure and flow established. The code was implemented in Matlab (Version 7.1.0.246 (R14), The MathWorks Inc., Natick, Massachusetts, USA).

7.4.2.2 0-D model verification

Pressure results in the aortic root, thoracic aorta and femoral artery are presented and compared with ‘in vivo’ measurements presented by Avolio et al. [109] in Figure 7-7. Aortic flow (input function) and flow in the descending aorta are also shown in Figure 7-7, and again compared with ‘in vivo’ results by Avolio et al. [109] and Mills et al.[110].

The presence of the dicrotic notch is clearly visible in the waveforms of the thoracic aorta and aortic root, immediately after the aortic flow reaches 0 l/min. The amplitude of the pressure pulse increases with increasing distance from the heart, as expected, confirming ‘in vivo’ measurements. The phase of the pressure pulse also changes and moves forward with increasing distance from the heart, finding confirmation from the already discussed measurements. The flow waveform shows a similar behaviour to that measured ‘in vivo’, although the amplitude of the second peak is bigger than the measured one.

Subsequently the input aortic flow was modified. ‘In vivo’ measurements from dog data have been taken and adjusted for the volume to equal 25 cc. The resulting pressure and flow waveforms are shown in Figure 7-8.

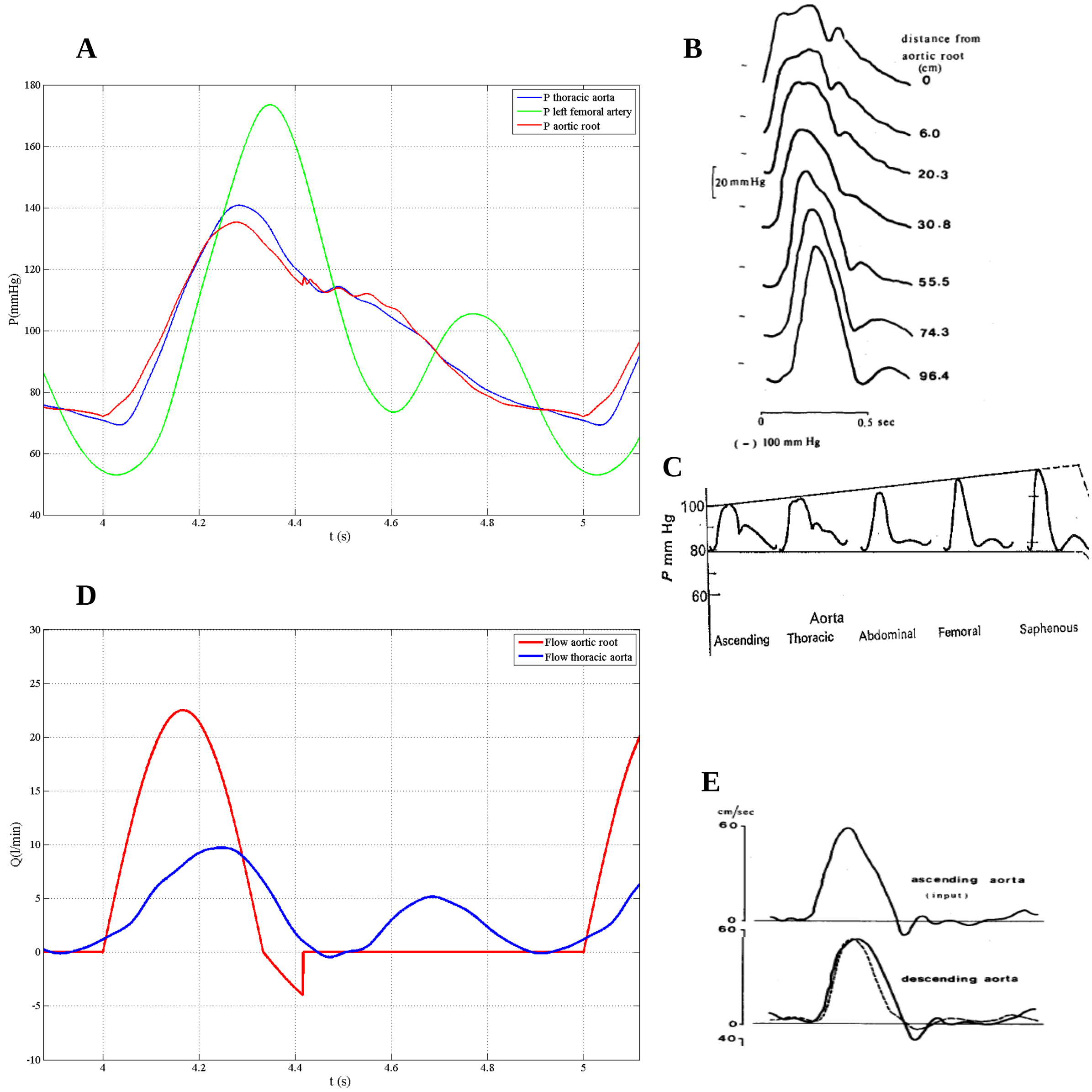

***Figure 7-7**: The above figures report the calculated pressure waveforms on aortic root, thoracic aorta and left femoral artery (A); 'in vivo' measured pressure waveform on aorta with increasing distance from the heart by Avolio et al. [109] (B); measured pressure waveform on ascending, thoracic and abdominal aorta, femoral and saphenous artery by McDonald's et al. [111] (C); calculated flow waveform on aortic root and thoracic aorta 'in vivo' (D); 'in vivo' measured flow waveform on ascending and descending aorta by Avolio et al. [109] (solid lines) and Mills et al. [110] (dashed line) (E).*

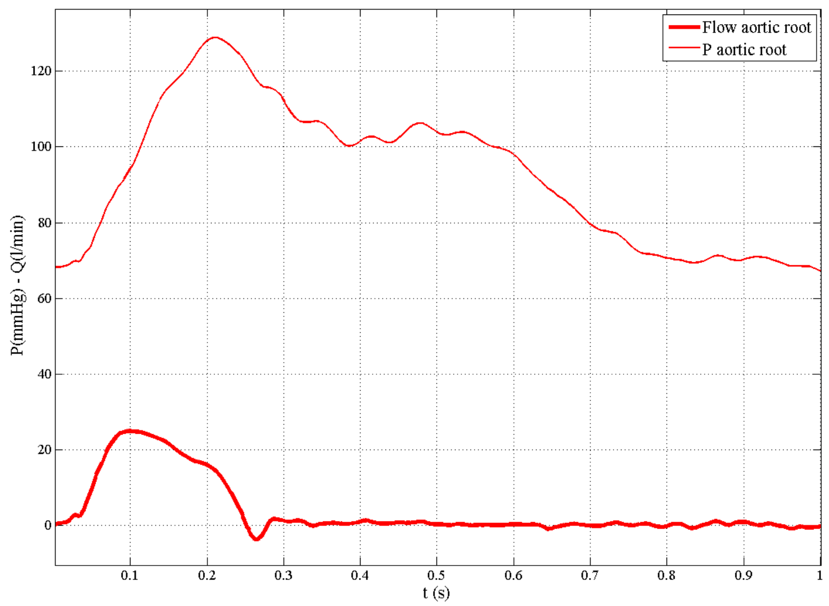

Figure 7-8: *Calculated pressure waveform in the aortic root, used in the second model of aortic flow waveform input.*

7.4.3 Interactions between 0D model and 3D model

The compartments in the 0-D model were connected to the upstream and downstream sections of the 3-D domain. Compared to the described 0-D model, a modified one, lacking of the compartment corresponding to the thoracic aorta, was used to iteratively obtain pressure and flow values in each compartment of the human body. The amended 0-D model is shown schematically in Figure 7-9. The original model, depicted in Figure 7-6, is instead used for the calculation of new values of pressure on upstream and downstream of thoracic aorta, boundary conditions on 3-D domain. The 0-D model had as further inputs the flow in the thoracic aorta upstream and downstream, together with the aortic root flow and capillaries pressure.

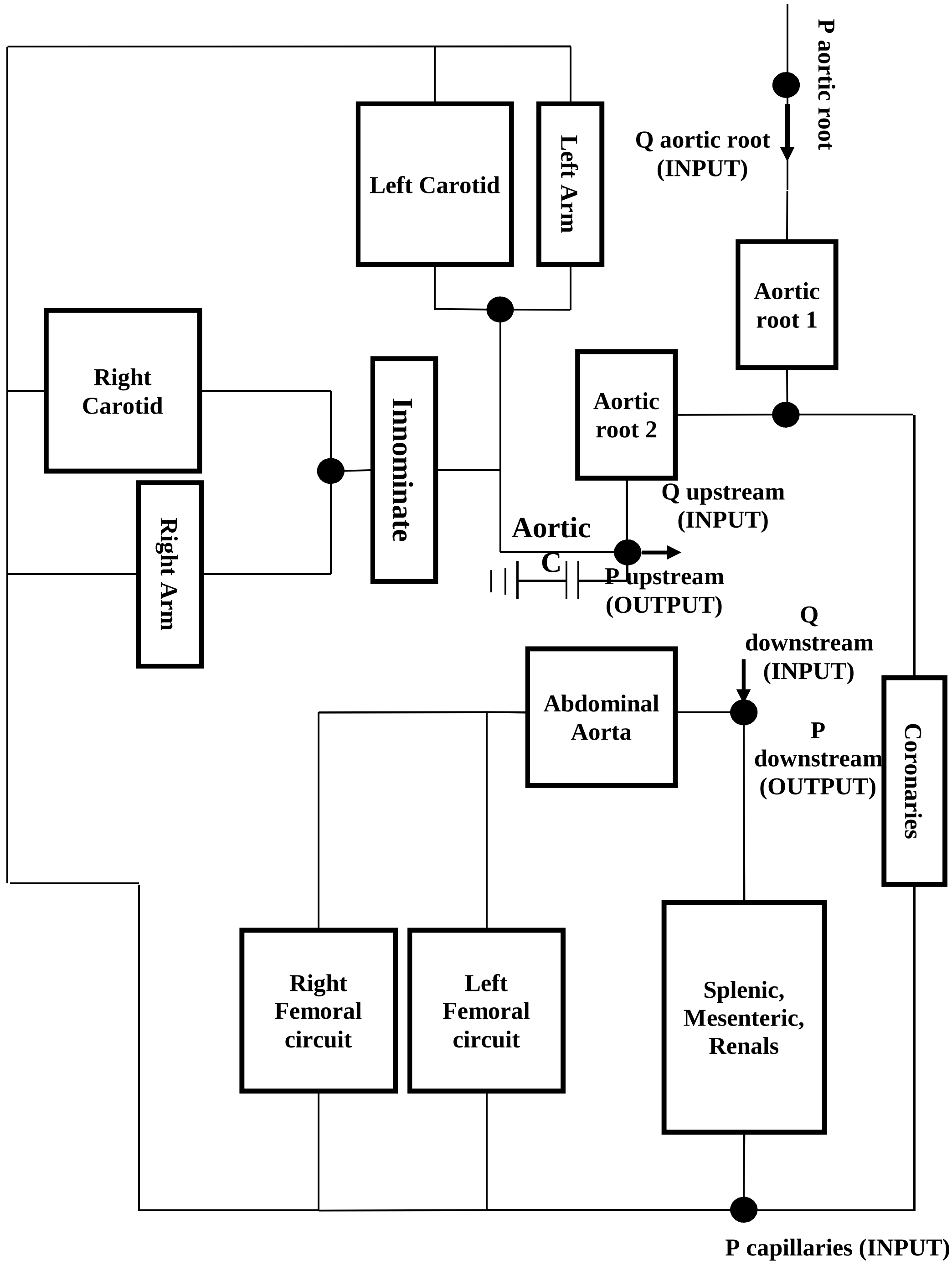

Figure 7-9: *The amended compartment model used for modelling the systemic circulation, without the thoracic aorta compartment. As indicated the inputs to the system are the pressure on the capillaries (indicated in the figure as INPUT), the flow on aortic root and the one on thoracic aorta upstream and downstream, and the outputs are pressure and flow on all the modelled branches.*

The 0D ts and 3D ts sizes are both 1 ms, with a cycle duration of 1 s. Since the information transfer between 0D and 3D simulation was done manually, it could be time consuming if coupling information between 0D and 3D model were exchanged at each 0D/3D ts (1 ms). To save the overall simulation time, results of more 0D/3D ts were transferred between 0D and 3D models. In the final setting, a total of 20 ms (or 20 0D/3D ts) data were transferred between the 0D and 3D models. This will be called iteration time step size, and abbreviated ts_i size.

At each ts_i the values of pressures on thoracic aorta upstream and downstream, obtained from 0-D model, were the inputs of the 3-D model. The value of the pressure on 3-D domain upstream and downstream were applied uniformly throughout the upstream and downstream surfaces, respectively. The outputs of the 3-D model at each ts_i were the averaged flow rates over the cross sectional area of the thoracic aorta upstream and downstream planes, which were the input parameters for the 0-D model with the thoracic aorta removed. About 3 iterations of this data transfer, called 0D-3D iterations, were done to ensure the convergence of the coupling. A schematic blocks-diagram for the clarification of the above described procedure is shown in Figure 7-10.

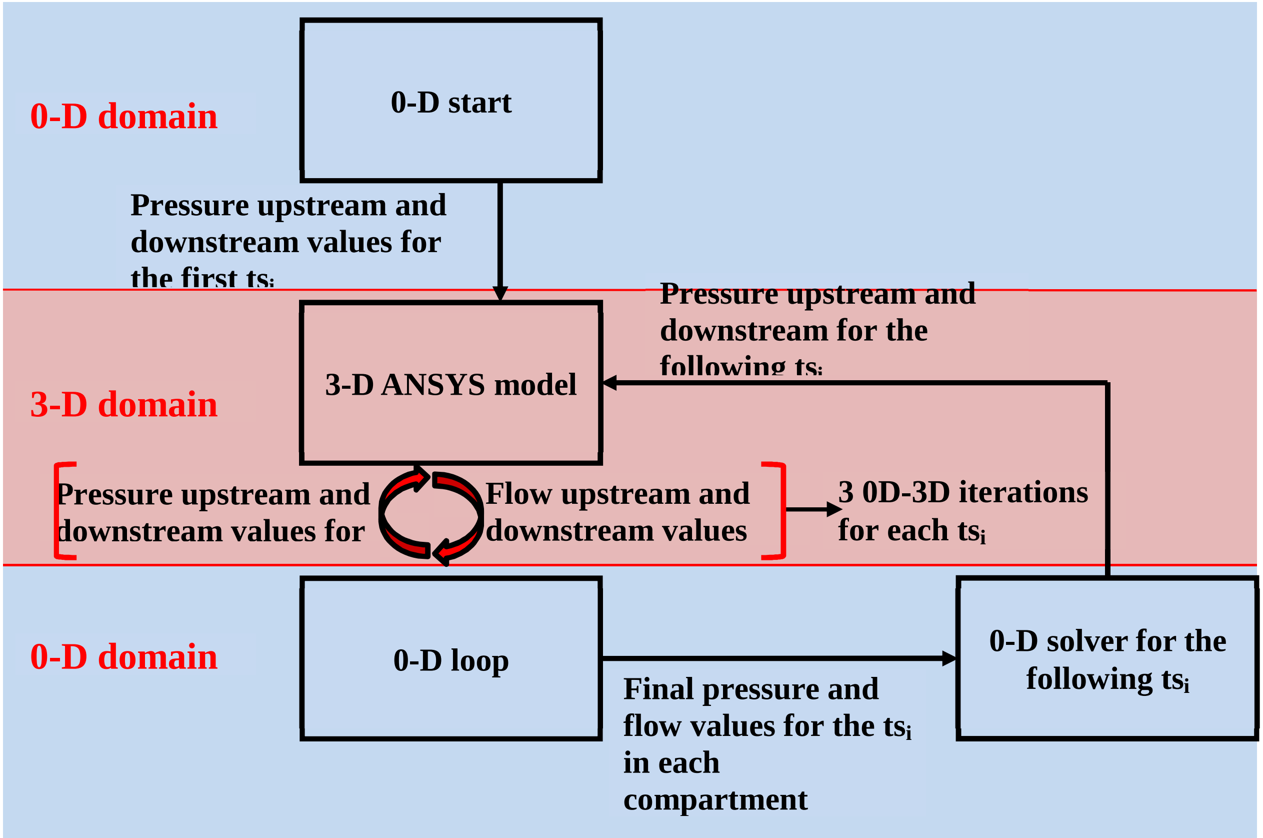

Figure 7-10: *block representation of the interactions and coupling of the 3-D and compartment models, with parameters involved in each step. The red arrows indicate multiple 0D-3D iterations between 3-D and '0-D loop' models.*

7.5 Simulation accuracy tests of the overall procedure

The following section presents all model accuracy considerations addressing the model reproducibility:

- 0D-3D iterations sensitivity test
- 0-D-3-D models interactions convergence test
- Cycle to cycle reproducibility test
- 3D model Mesh sensitivity analysis
- Model test for results differences between different 3-D model entrance lengths
- Laminar and turbulent flow considerations
- Conservation of mass on 0-D-3-D interface test

7.5.1 0D-3D iterations sensitivity test

As already explained in paragraph 7.4.2 the 0D and 3D ts sizes were set to 1 ms, while the ts_i size characterizing the variables exchange in order to solve 3-D and 0-D domains equations was set to 20 ms, and was selected after an investigation of ts_i size influence on upstream and downstream pressure waveforms. In paragraph 7.4.1.1 was explained that 1 ms 0D ts size was applied on the 0-D model of the systemic circulation after different 0D ts sizes were applied on the system to verify the 0D ts size value ensuring the convergence of the 0D model alone.

In addition the influence of ts_i size on the model was investigated and the model showed different results for different ts_i sizes. This test was conducted on a simple cylindrical model of the counter-pulsating IAB. The difference between the use of a 50 ms ts_i size and 15 ms ts_i size is shown in Figure 7-11, reporting the calculated upstream pressure in the two cases during 150 ms following IAB counterpulsation.

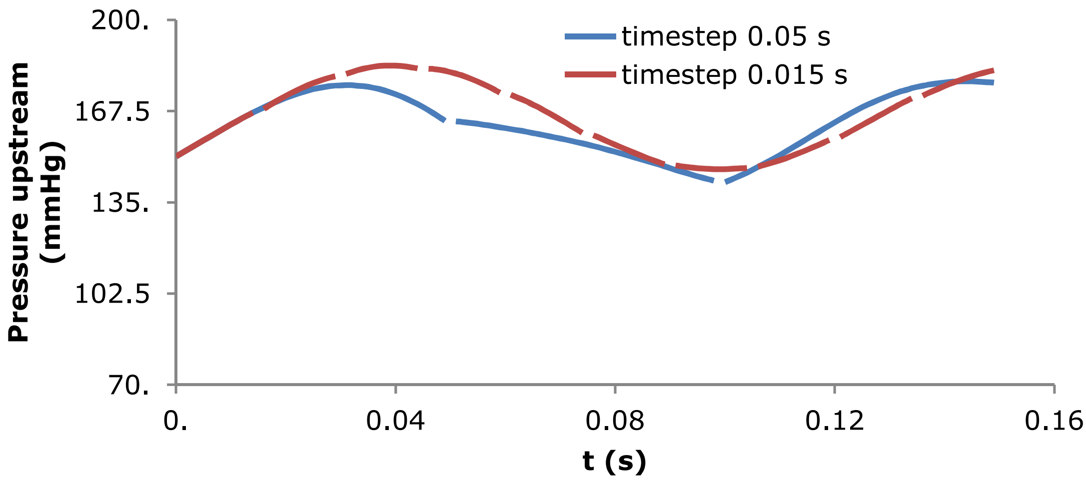

***Figure 7-11**: upstream pressure obtained through simulating the first 150 ms after IAB counterpulsation with a ts_i size of 15 ms (red line) and 50 ms (blue line). The maximum difference was found to be 10% and, although the behaviour of the two curves follow a similar pattern, with a ts_i size of 15 ms the waveform is more linear compared to the one characterized by a ts_i size of 50 ms.*

The maximum difference shown is 10%, with the waveform presented changing consistently with a reduced ts_i size. In fact it can be noticed that the waveform obtained with a ts_i size of 15 ms presents a linear behaviour compared to the one characterizing the waveform obtained with a ts_i size of 50 ms.

This analysis was conducted for 150 ms in order to optimize the time for achieving the characterization of ts_i size to be applied in the model. In fact, if conducted for the whole cycle, the analysis would be extremely time demanding, as it should be carried on for two different ts_i sizes. The difference associated to the use of two ts_i sizes can be obtained through the analysis of the most critical period during the whole cycle (steepest change in velocity and pressure), which corresponds to the starting of IAB inflation. Looking at Figure 7-13 is clear that the steepest change in pressure (increase and decrease) is found in the 150 ms following the starting of IAB inflation.

Initially ts_i size of 15 ms was selected as a linear behaviour of pressure curve can be evidenced with this ts_i size, and number of 0D-3D iterations selection is presented in the following paragraph. Although for the results presented in the last part of this chapter the ts_i size used was 20 ms, as no difference was highlighted between the two ts_i sizes.

7.5.2 Convergence test between 0-D and 3-D interactions

The ts_i size analysis presented in the above section was obtained with the number of 0D-3D iterations being selected through a pressure threshold convergence criteria. Upstream and downstream pressure values were visualized for different 0D-3D iteration numbers. The number of 0D-3D iterations was established when the difference between pressure values at two consecutive 0D-3D iterations was found to have a value smaller than the threshold value of 0.5 mmHg (≈ 65 Pa). This verification was made at the first ts_i of the cardiac cycle and at the first ts_i of the IAB counterpulsation, and a 0D-3D iterations number of 3 was then set. The values of the pressure for the checked ts_i, at the beginning of IAB counter-pulsating, are shown in Figure 7-12. It is possible to see the convergence of the values with the differences in pressure values falling below the threshold from 0D-3D iteration number two to three, for both upstream and downstream pressures.

Also in this case, as per the analysis of the ts_i size, the periods analysed for the selection of the 0D-3D iteration number were the ones corresponding to steepest change in velocity and pressure, hence the beginning of the cardiac cycle and the starting of the IAB inflation.

However a convergence loop number of three was also used by other researchers [118] in transient simulations of blood flow in the arterial bed, in combination with a time step ts_i size of 10 ms and a convergence target of $10e^{-5}$, also performed using Ansys CFX.

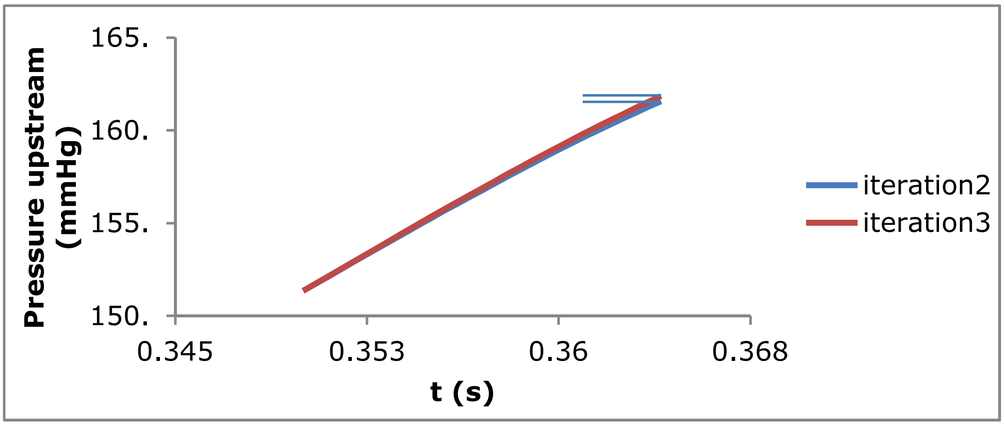

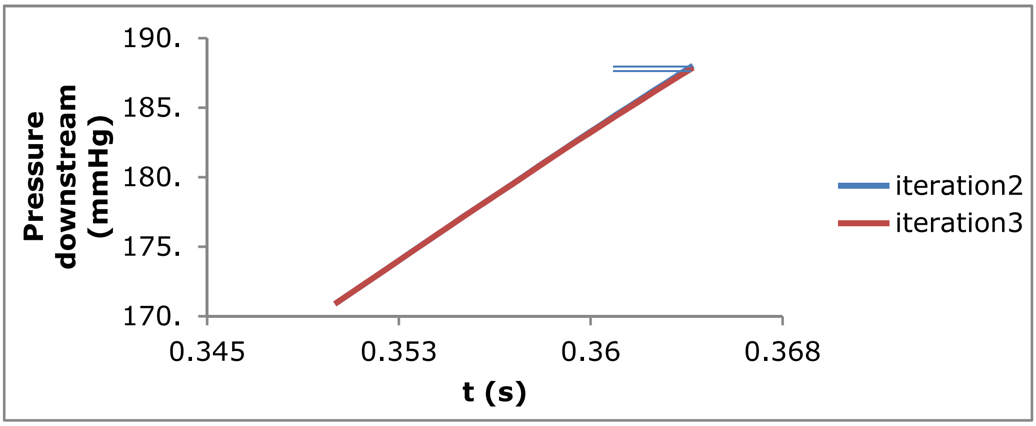

Figure 7-12: *pressure values at upstream (A) and downstream (B) of 3-D domain, after two (blue line) and three (red line) 0D-3D iterations, revealing maximum difference in pressure value (at the end of the ts_i) smaller than the threshold of 0.5 mmHg.*

7.5.3 Cycle to cycle variation and reproducibility

Two cycles were simulated at a verification level with the aim of verifying the solution of the model to be cycle independent, hence validating the values of pressure calculated through the simulation and investigating the inter cycle reproducibility. As shown in Figure 7-13, the difference in the end diastolic pressure, at the end of the cycle, between the 1st and the 2nd cycle is minimal: within 0,5 mmHg. This value was also used as a threshold value for establishing the convergence of the 0-D - 3-D model coupling, and addresses the reproducibility of the model, especially considering that this pressure difference value was reached after the initial difference in end diastolic pressure between the 1st and 2nd cycle. In the figure is also underlined the difference between the pressure values at the beginning of systole after 1st and 2nd beats, indicated as ΔP_2, and the one at the beginning of the 1st cycle, indicated as ΔP_1.

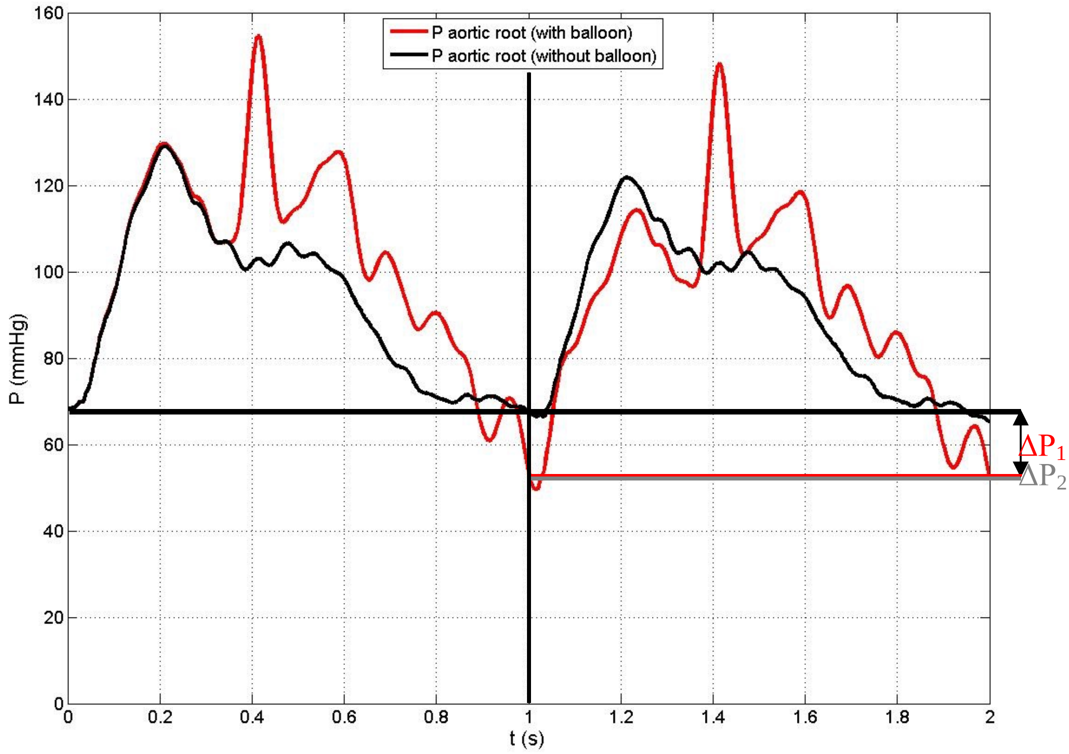

***Figure 7-13**: 2 cycles simulation of heart beat without counter-pulsating IAB, black line, and with IAB pumping, red line. The pressure waveform associated to counter-pulsating IAB reveals a minimal difference in end diastolic pressure between the 1st and the 2nd cycle.*

The waveform associated to the pressure influence by IABP counterpulsation (red line in Figure 7-13) shows similar behaviour between the 1st and 2nd beats, although the starting point has a different value because of the different hemodynamic in the beginning of systole.

In fact the pressure value at the beginning of the simulation was close to 70 mmHg, close to the physiological end diastolic pressure. Instead in case of balloon active deflation the pressure at the beginning of systole, for both 2nd and 3rd cycles, is close to 50 mmHg, similarly to values measured in vivo.

The figure also highlights that the difference shown between the beginning of the 1st and the beginning of the 2nd cycle (black line and red line, respectively, and ΔP_1 indicated in red) disappears when looking at the beginning of the 2nd and of the 3rd cycles (red line and grey line, respectively, and ΔP_2 indicated in grey). This is due to the different hemodynamic at the beginning of each cycle: at the starting of the simulation (t = 0) the balloon is in deflated configuration and the hemodynamic values, influenced exclusively by the activity of the heart, are within physiological value; on the other hand at the end of 1st and 2nd cycles the hemodynamic values depend on heart pulsation as well as IAB counterpulsation, and hence pressure results are the same between the end of 1st and 2nd cycles, but different from the starting of the simulation. In fact the difference between the two cycles end diastolic pressure is within 0.5 mmHg. As previously stated, this is in line with the value used, as already described in paragraph 7.5.2, as threshold value for establishing the number of 0D-3D iterations of pressure and flow exchange between 0-D and 3-D models.

The verification was interrupted at this point because the aortic end diastolic pressure results showed the aortic pressure starting point in the 3rd simulated cycle to have a value close to the aortic pressure starting point of the 2nd simulated cycle. In addition the pressure pulse was shown to be reproducible between the two cycles: the calculated systolic pressure pulse was 60 mmHg for both 1st and 2nd cycles, and the calculated pressure pulse induced by IAB inflation was 50 mmHg in both cycles. It is reasonable to assume that these will be maintained also in the 3rd cycle, and, as the hemodynamic and pressure at the beginning of 2nd cycle and at the beginning of 3rd cycle is reproduced, the 3rd cycle will be expected to have pressure values against time comparable with the ones of the 2nd cycle.

7.5.4 Mesh sensitivity analysis 3D model

For the use of this mesh a sensitivity test was conducted through studying the effect of a change in number of mesh elements on aortic root pressure and flow waveforms in case a simple cylinder increasing and decreasing in diameter was used to simulate IAB counterpulsation. The test first compared the mesh, represented in Figure 7-14 and constituted by 119,104 elements, used with one constituted by 486,794 elements. The increase in elements constituting the model did not induce a marked change on the pressure and flow waveforms, as it is possible to see from the comparison of aortic root pressure and flow in Figure 7-15.

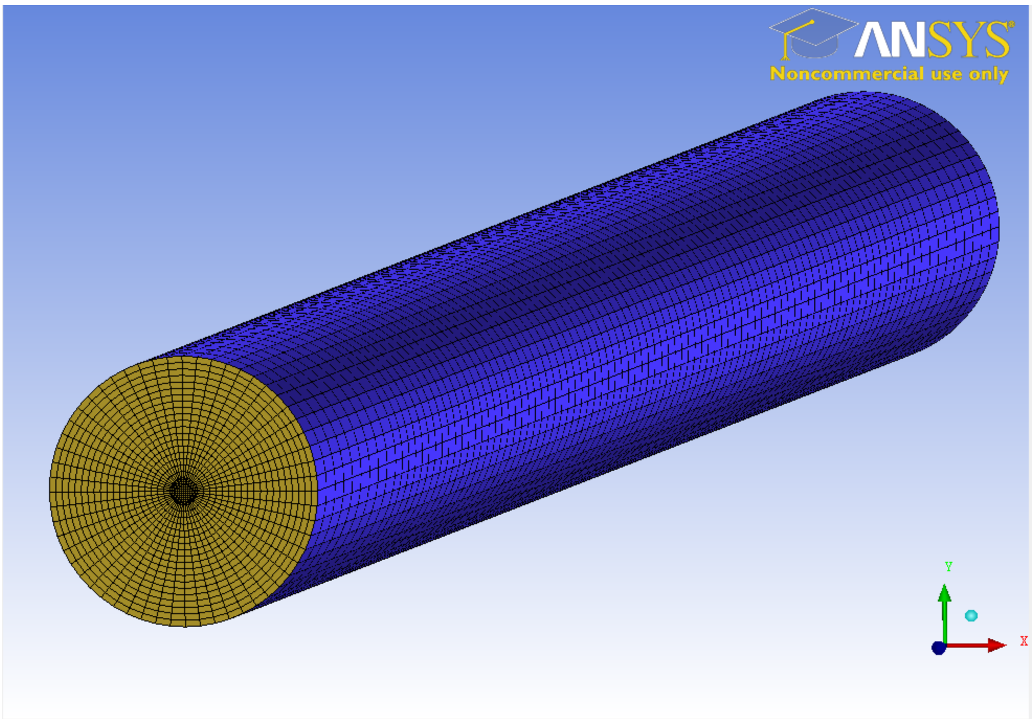

Figure 7-14: *the image show the mesh used in the three-dimensional model of the thoracic aorta and IAB. The two sides of the three-dimensional domain, highlighting the cross-sectional distribution of elements, will be the areas in which average flow is calculated and input onto the 0-D compartmental model.*

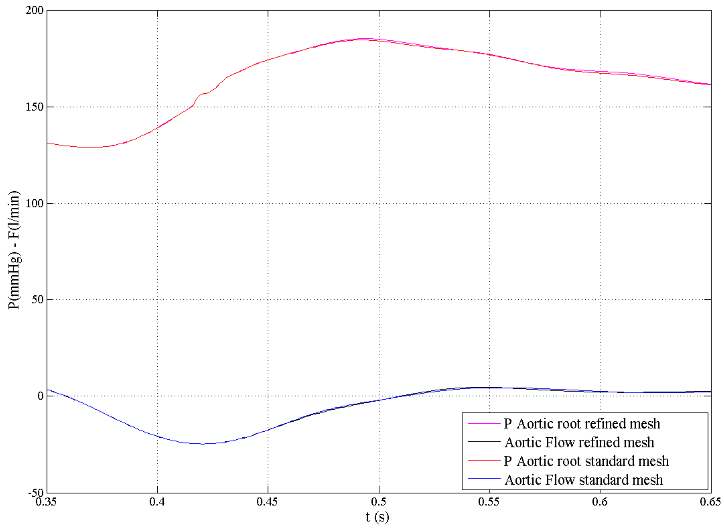

Figure 7-15: *Pressure on aortic root and flow on thoracic aorta, during inflation, obtained through simulation with standard mesh and refined mesh. As shown, no marked influence is noticed when the mesh elements number is increased.*

In this case there was no change in geometrical distribution of elements within the 3D domain, but just finer mesh and smaller elements size. Afterwards a model constituted by 257,810 elements and presenting a non-uniform distribution of mesh elements, in which finer meshes were close to balloon and aortic wall and larger elements were in the middle between the two walls, was also tested for simulating IAB counterpulsation. A representation of the cross-section for this case is indicated in Figure 7-16. Also in this case the final results do not differ from the ones of the standard model, as noticeable by looking at Figure 7-17.

Although it should be noticed that the variation in elements size between the elements close to the walls and the ones between the vessel wall and IAB wall is large and not gradual. This represents a disadvantage as errors due to discretization of the space could increase compared to a volume characterized by same number of elements changing in volume gradually from the walls towards the inner ring. However the steepest change in velocity is expected close to the vessel and IAB wall, and velocity is expected not to change largely in the area characterized by a coarser mesh. ANSYS solver also showed that a variation in mesh elements distribution and size did not induce a big change in convergence, as the RMS of residuals was kept the same ($10e^{-5}$), and it was reached after a comparable number of 3D iterations.

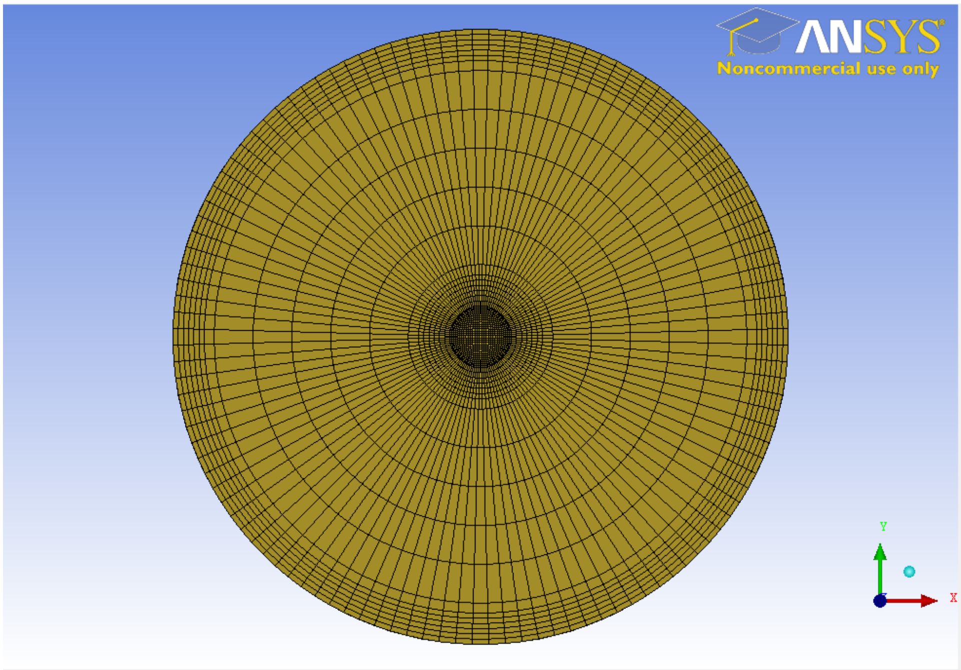

Figure 7-16: *the above image shows the alternative mesh used for the three-dimensional model of thoracic aorta and IAB, following a non-linear distribution. The decreased dimension of elements size close to the IAB and aortic walls aims at better modelling the boundary layer characterizing the flow on the two surfaces.*

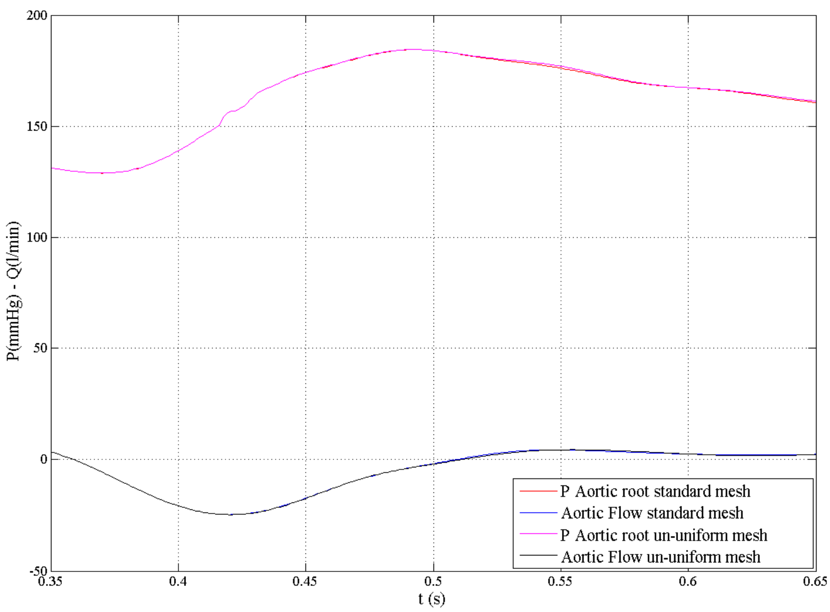

Figure 7-17: *Pressure on aortic root and flow on thoracic aorta, during inflation, obtained through simulation with standard mesh and un-uniform distribution mesh. Also in this case there is no marked influence when using the refined mesh on the final results.*

7.5.5 Considerations about flow development on upstream and downstream thoracic aorta boundaries

All results in the following section were obtained imposing a feedback between 3-D and 0-D models at 4 cm (2 x aortic diameter) away from both sides of the IAB (corresponding to the geometrical irregularities). Hence the domain is interrupted in an area in which irregularities or backward flow might characterize the flow field and a consistent amount of information might be lost inducing an incorrect estimation of velocity and pressure close to the boundaries and, consequently, on the rest of the fluid domain. Furthermore the pressure imposed in the boundaries assumed the flow to be developed on the upstream and downstream surfaces, even though this might not be true, due to geometrical variation in the domain close to the boundaries.

In order to establish whether this setting induces a consistent error on the calculation of pressure and flow on upstream and downstream planes, as well as on the flow distribution within the thoracic aorta, a longer 3-D model of thoracic aorta including IAB, with 3-D domain interrupted at 10 cm (5 x aortic diameter) away from both IAB sides, has been tested and the results are compared with the ones obtained using the standard 3-D model developed. Figure 7-18 A compares the upstream and downstream flow obtained from the two models, together with the one associated to the 0-D model alone.

The flow rate waveform is, as expected, slightly different in case the thoracic aorta is resembled as a longer tube, compared to the other two situations. Also upstream and downstream pressure resulting from the coupling of the 0-D model with the amended 3-D model vary sensibly, as noticeable by looking at Figure 7-18 B, and specifically a higher difference between the two pressures is obtained during systolic phase, even though being associated to a lower flow running through the thoracic aorta. The difference found on the systolic flow, with no IAB movement, is due to the difference in modeling the thoracic aorta tract between 0-D and 3-D, since in the 0-D calculation the tract was not modelled 3-dimensionally.

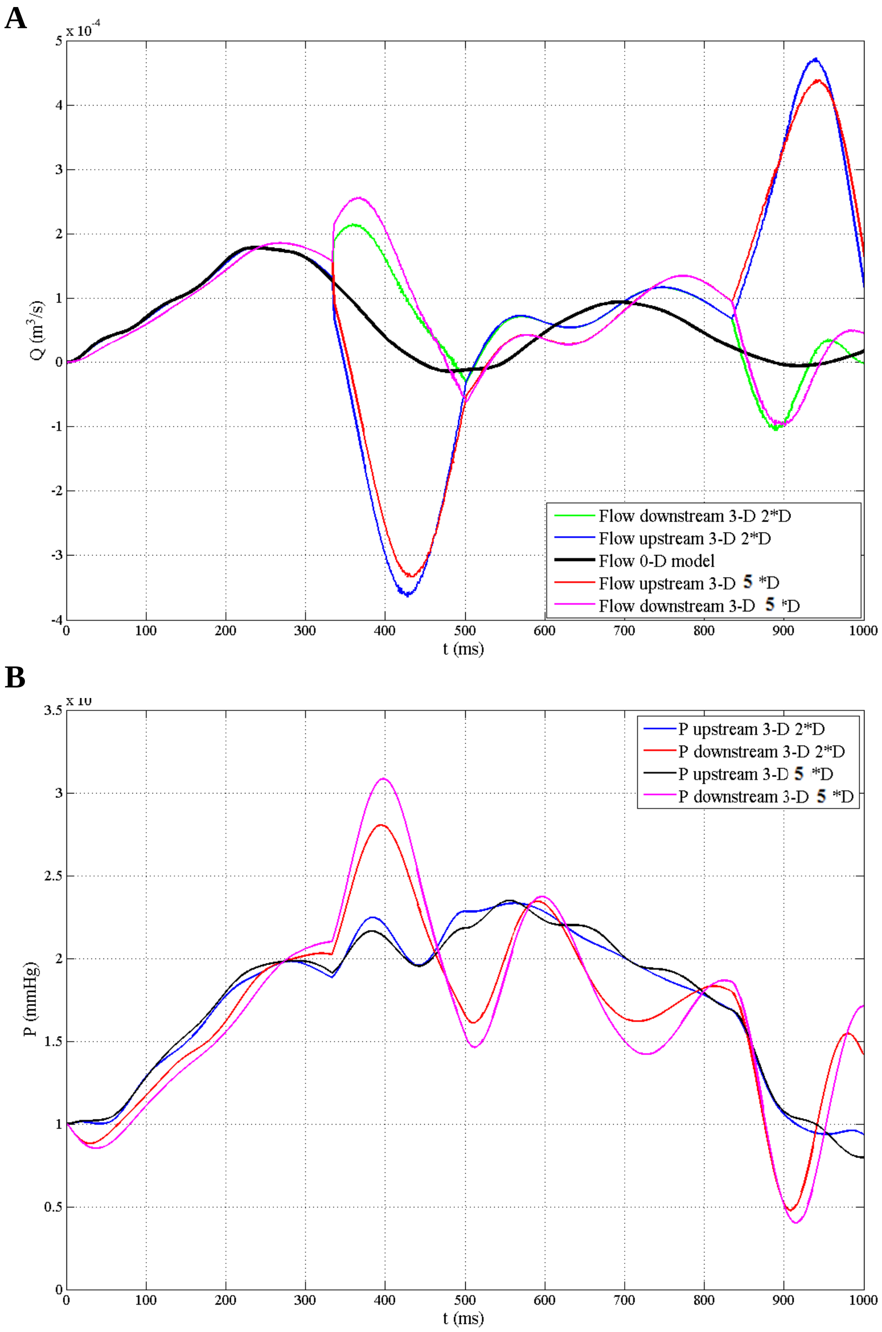

Figure 7-18: *The above pictures show flow waveforms (A) and pressure waveforms (B) for both standard and long thoracic aorta. A shows the flow in the thoracic aorta for 0-D model alone (black line), the flow displaced upstream for both models (red and blue) and the flow displaced downstream for both models (green and magenta). B shows instead the upstream (blue and black) and downstream (red and magenta) pressure waveforms for both models.*

Also important differences can be found in the fluid-dynamics within the aorta. Plotting the velocity field on the longitudinal plane inside the thoracic aorta (Figure 7-19), for both long and 'physiological' models, different velocity distribution in the gap between aortic and balloon walls and in the surrounding of the IAB is noticed. The main differences between the two models are due to the distance between the areas associated to a pressure equally distributed throughout the area (upstream and downstream boundaries) and the edge of the IAB, though the values of the velocity are reasonably similar. This would explain why the areas of backward velocity due to the presence of the IAB, close to the balloon edges, are wider in case of longer aorta (Figure 7-19). However, it is important to note that the effect induced by changing the 3-D model of thoracic aorta on the ascending aorta pressure is contained (Figure 7-20): systolic peak decreases by 2.2% and diastolic augmentation due to IAB inflation increases by 8%.

In conclusion, the standard model of IAB was better resembling the physiological environment, but the inclusion of further elements on both sides of the thoracic aorta model provides a more correct evaluation of flow field in IAB surrounding and in the flow displaced upstream and downstream. In the second case, though, it should be taken into account that the flow calculated in the 3-D model varied from the one resulting from the use of the 0-D model alone also because of a different estimation of the impedance associated to the added aortic tract. The values of flow displaced upstream and downstream changed also because of the value of fluid flowing through the thoracic aorta when the IAB starts inflating, which was different in case the thoracic aorta was modeled with physiological dimensions compared to when it was modeled with added aortic tracts. It should be noted that, however, the volumes displaced upstream and downstream did not change considerably (< 3%) and corresponded to the volume change associated to the IAB between its deflated and inflated configurations.

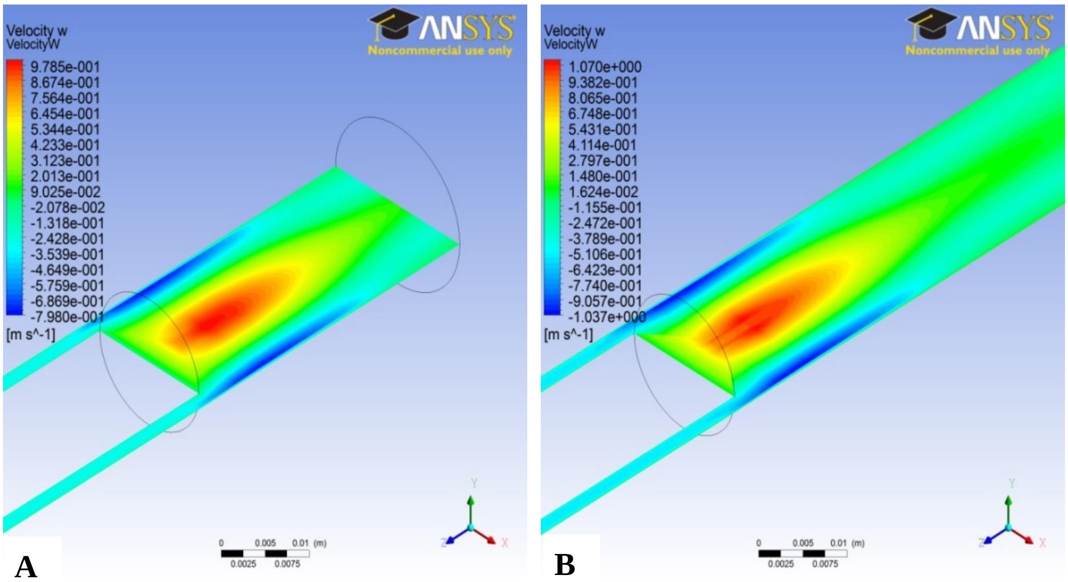

Figure 7-19*: The longitudinal velocity field is represented for the standard (A) and long (B) aorta.*

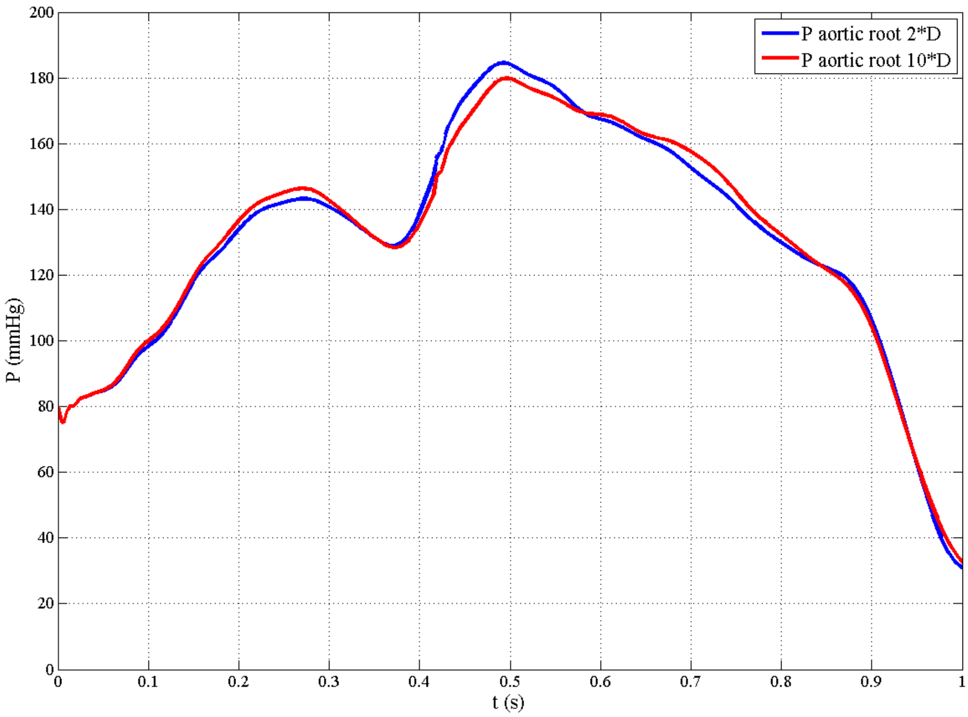

Figure 7-20*: Above the pressure waveform calculated in the aortic root is shown for both models of thoracic aorta, standard (blue line) and long (red line). The difference between the two model is contained within 8%.*

7.5.6 Hemodynamic model

Although several researches have been conducted in regards of the fluid dynamics of blood in the aorta, it is still not clear to which extend turbulence and mixed regimes are characterizing the blood flow in the aortic branch. An important study aiming at characterizing the velocity profile during the cardiac cycle in the ascending and descending aorta, through a hot-film probe used in anesthetized dogs, was lead by Nerem et al. in 1972 [105]. The study [105] is presented in following paragraphs, and this method will be used for the calculation of the critical Reynolds number associated to this model. The results are expressed in terms of arterial velocity waveforms and instantaneous and time-averaged velocity profiles in the thoracic aorta of dogs. In the study the occurrence of flow disturbances and turbulence was shown to be related to peak Reynolds number and the frequency parameter α, depending on heart-rate and size of the aorta.

The truthfulness of the measured peak systolic velocity measured in the axis of the ascending aorta was verified through the calculation of the velocity itself using measured pressure and wave speed of 500 cm/s. The result calculated was close to the one measured. However, three different types of velocity waveforms were reported, divided into undisturbed, with absence of high frequency components, disturbed, presenting high frequency components indicating presence of turbulence at the peak of systole, and highly disturbed, with signs of turbulence throughout the decelerating part of systole. The three examples are shown in Figure 7-21.

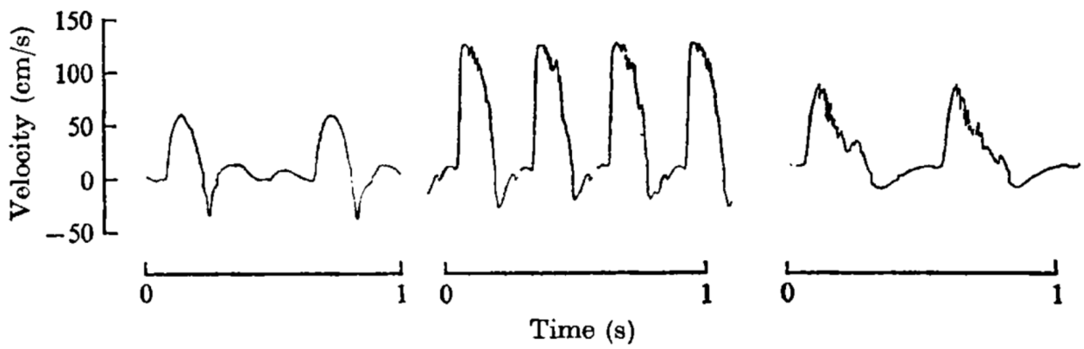

***Figure 7-21**: from left to right, velocity profile measured by Nerem et al. and characterized by no disturbances, disturbances in systolic peak and disturbances in the decelerating phase of systolic phase.*

The graphs show that turbulence does not depend on Reynolds number alone, but also on the heart rate characterizing the cardiac cycle. An important graph aiming at involving all main parameters is shown in Figure 7-22, and relates the Reynolds number characterizing the flow, the frequency parameter α and the level of disturbance. A general trend was noticed: by increasing the Reynolds number and decreasing α leads to a more disturbed condition, and a line can be traced which discriminates the disturbed or highly disturbed conditions from the undisturbed one, characterized by equation 7.18.

$$Re_c = 250\,\alpha \qquad \textbf{(Eq.7.18)}$$

where Re_c corresponds to the critical Reynolds number characterizing a transition between laminar flow and mixed flow and α is the frequency parameter, calculated as in equation 7.19.

$$\alpha = R_{ao} \times \sqrt{\frac{2\pi f}{\sigma}} \qquad \textbf{(Eq.7.19)}$$

where R_{ao} is the radius of the aorta, f is the heart rate frequency, σ is kinematic viscosity (defined as blood dynamic viscosity over its density) [106]. This parameter defines dynamic behaviors and similarities between different flow systems, whose flow is characterized by the Navier-Stokes equations simplified into the equations of motion presented by Womersley (pressure and flow equations according to Womersley hypothesis).

From a physical point of view the meaning of the equation is clear: with increasing α, the time between a cardiac cycle and the other decreases, and for turbulence to develop a higher Reynolds number is required. In our case the frequency parameter α has a value of 12.9, and hence critical Reynolds number equals 3225.

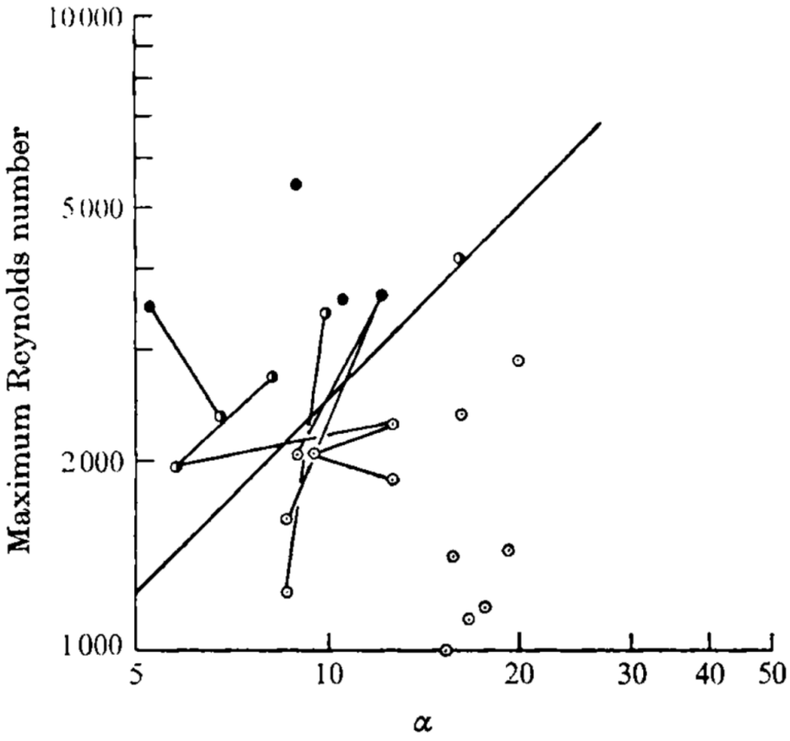

Figure 7-22*: The graph, taken from Nerem et al., shows, reported in function of frequency α and Reynolds number, 1) white dots, measured points of undisturbed flow, 2) black and white dots, points of disturbed flow, and 3) black dots, points of highly disturbed flow. A relation can be drawn: disturbed and highly disturbed flow, presenting turbulence, can be found for smaller Reynolds number at small frequencies and for higher Reynolds number at higher frequencies.*

The Reynolds number for which instabilities inducing turbulent flow arise, for flow within a duct, has a value of around 2000 [113], although this does not take into account the cardiac cycle length. In the thoracic aorta peak Reynolds number Re can be estimated as following:

$$Re = \frac{\rho * v * D}{\mu} = 3180 \qquad \textbf{(Eq.7.20)}$$

in which ρ is the blood density, 1060 Kg/m^3 [112], v is the maximum velocity in the thoracic aorta, assumed to be 0.6 m/s [111], D is the hydraulic diameter of the thoracic aorta, 0.02 m, and μ is the viscosity of the blood, 0.004 Pa*s. If turbulent flow is considered the calculated peak velocity in the descending aorta has a value of 0.56 m/s and Reynolds number would then be 2968. In both cases the value of Reynolds number is close to the critical values for transition to turbulent suggested by the literature [113] and close to the critical value of 3225, taking into consideration also cardiac frequency and aorta diameter, previously calculated. The flow model used for the simulation was the turbulence k-ε. However, also in this case, a simulation assuming fully laminar flow on the 3-D thoracic aorta has been set up with IAB modelled as a simple cylinder in order to compare the outcome on the results due to the different assumption.

For a comparison with the used model, the velocity distribution in the thoracic aorta with counter-pulsating IAB was calculated with a simple cylindrical model of IAB counter-pulsating in the 3-D domain, for both laminar and turbulent flow models. Even though upstream and downstream pressure are most likely to be different in case of laminar flow, an insight on the changes induced by the different assumption on the flow model can be provided by using the same pressure on the boundaries. By imposing a laminar flow in the 3-D fluid domain the velocity and velocity distribution obtained during cardiac systole present thicker boundary layers close to the walls and a different velocity field induced by IAB counterpulsation.

Specifically Figure 7-23 shows the differences between the two fluid models, laminar and turbulent, at different times during counterpulsation. As expected, in the case where a laminar flow model is imposed the velocity change in the boundary layer is different, compared to the condition of turbulent flow, because of the higher influence of the viscous forces. This results in the velocity to have both positive and negative values along the profile on the gap between thoracic aorta and balloon, in case of laminar flow, in certain periods during inflation and deflation.

Given the Reynolds numbers previously calculated, 2968/3180, a fully laminar flow is unlikely to characterize the fluid-dynamic of the aortic tract and a mixture of laminar and turbulent flow is expected to characterize the fluid-dynamics within the thoracic aorta. Blood was treated as Newtonian fluid (density 1060 kg/m^3 and viscosity 0.004 Pa*s).

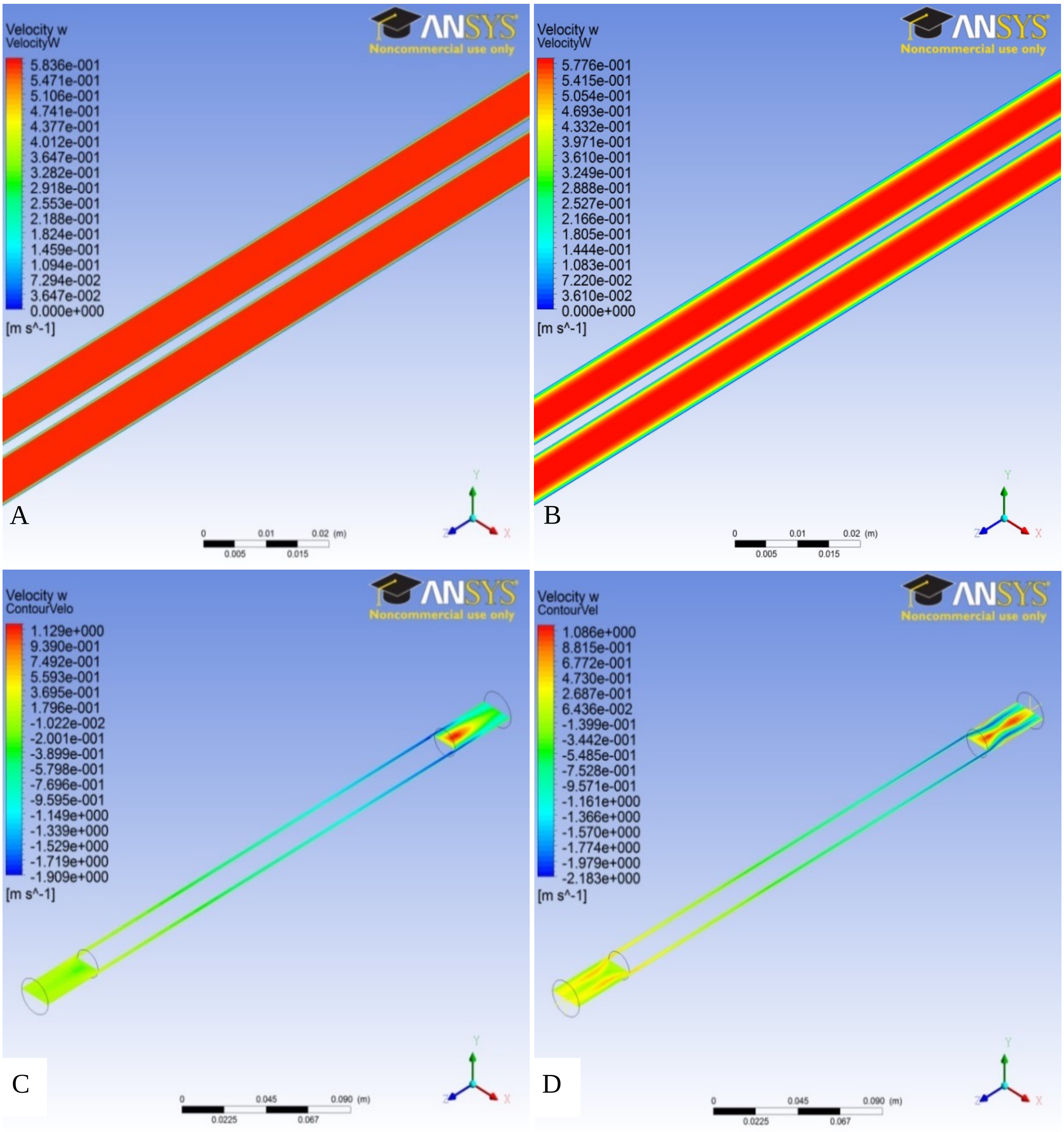

***Figure 7-23**: The longitudinal velocity field is shown for both turbulent flow (A, systolic peak, and C, IAB at the end of inflation) and laminar flow (B, systolic peak, and D, IAB at the end of inflation) assumptions.*

7.5.7 Verification on conservation of mass

Verification of the conservation of mass on the 3-D/0-D interface on the thoracic aorta sides was also performed: the change in volume of the cylindrical model of the balloon, from deflated to inflated, should equal the total flow displaced upstream and downstream, integrated throughout the time of inflation movement of the IAB, measured on the boundaries of the 3-D domain.

The IAB volume is:

$$V = L\pi({R_b}^2 - {r_b}^2) = 5.34 * 10^{-5}\ m^3 \qquad \textbf{(Eq.7.21)}$$

where V is IAB volume difference between inflated and deflated configurations, L is IAB length, R_b is IAB radius when inflated and r_b when deflated.

The integration of the flow displaced upstream and downstream during the time of inflation motion of the IAB, obtained from the two flow waveforms, resulted in a volume equal to that obtained from Eq.7.21, hence confirming the conservation of mass on the boundaries of the 3-D model of thoracic aorta and IAB. The integration was performed using the "poly-area" algorithm, in Matlab, calculating the volume included between the flow displaced upstream and flow displaced downstream curves. In fact the undisturbed aortic flow waveform would be between the upstream and downstream waveforms after IAB inflation, and variation in flow towards upstream and downstream can both refer to the reference line provided by the undisturbed flow waveform. This volume is represented in Figure 7-24.

It should be furthermore noted that the flow represented is calculated from the calculated velocity on the upstream and downstream boundaries, which was averaged throughout the upstream and downstream sections through the "areaAve" ANSYS CFX algorithm which calculated the area-weighted average of the variable, taking into account the different element size.

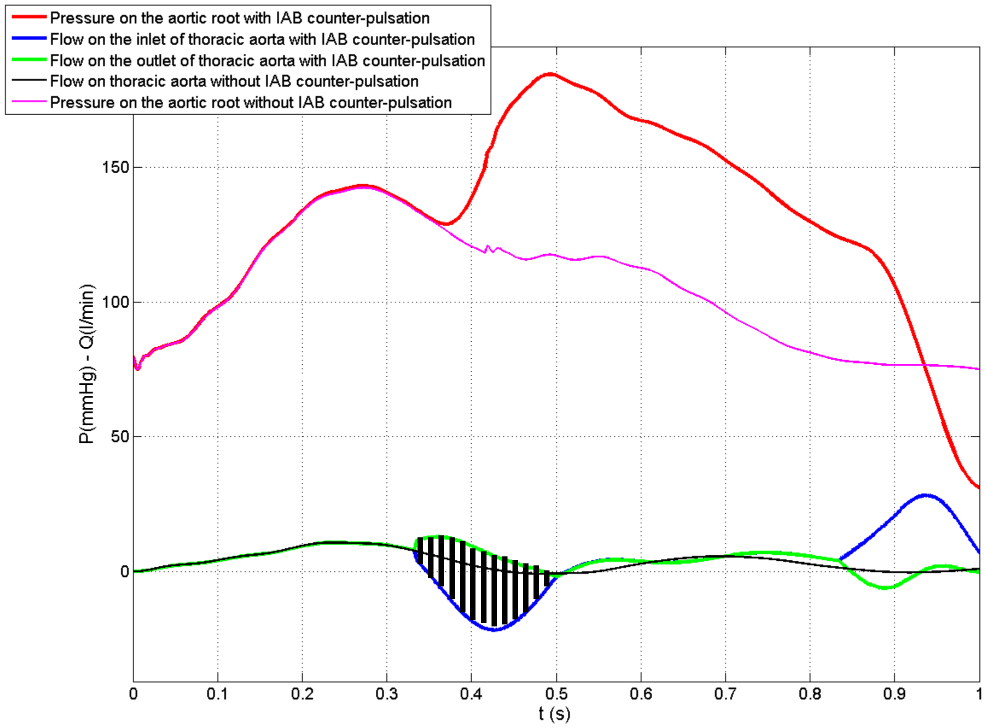

Figure 7-24*: The above image shows the waveforms of pressure and flow in case of 0-D model, without IAB, and 3-D model with active balloon counterpulsation. The picture is addressed to indicate the volume integrated to verify that conservation of mass is maintained.*

7.6 Results and discussion

7.6.1 IAB and thoracic aorta placed horizontally

The pressure waveform obtained in the aortic root and flow waveforms on upstream and downstream of the thoracic aorta, both with and without counterpulsation are shown in Figure 7-25. Figure 7-26 presents the comparison of the pressure waveform measured above the tip of the IAB when counter-pulsating in the experimental set-up presented in Chapter 4.

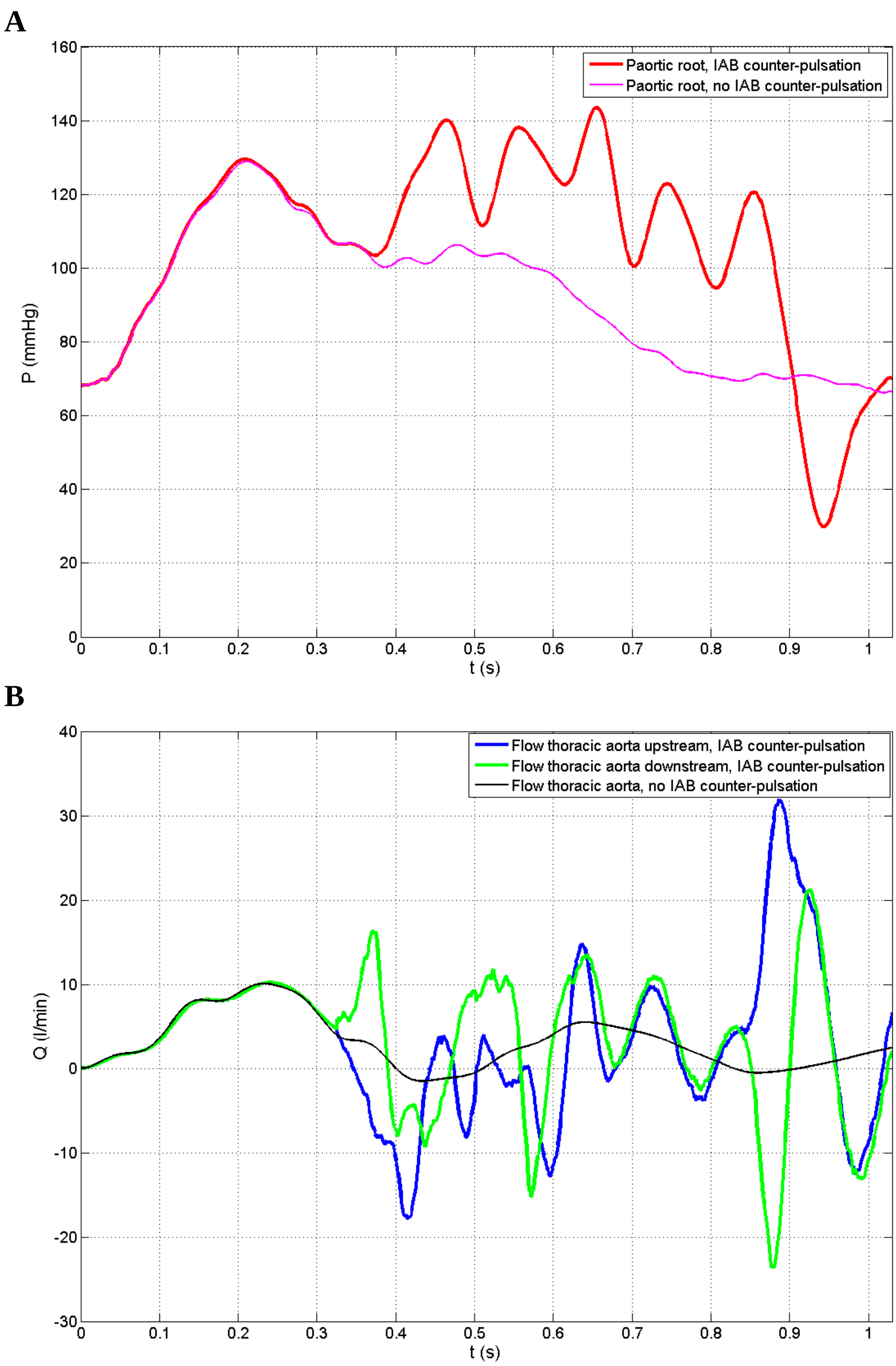

Figure 7-25: *Comparison of pressure and flow between 0-D model and 3-D model with the active balloon. The pressure waveforms (A) shown are the ones calculated in the aortic root (magenta for model without IAB and red for counter-pulsating IAB) and the flow waveforms (B) are the ones calculated in the thoracic aorta (black for model without IAB, green for downstream flow with counter-pulsating IAB and blue for upstream flow with counter-pulsating IAB).*

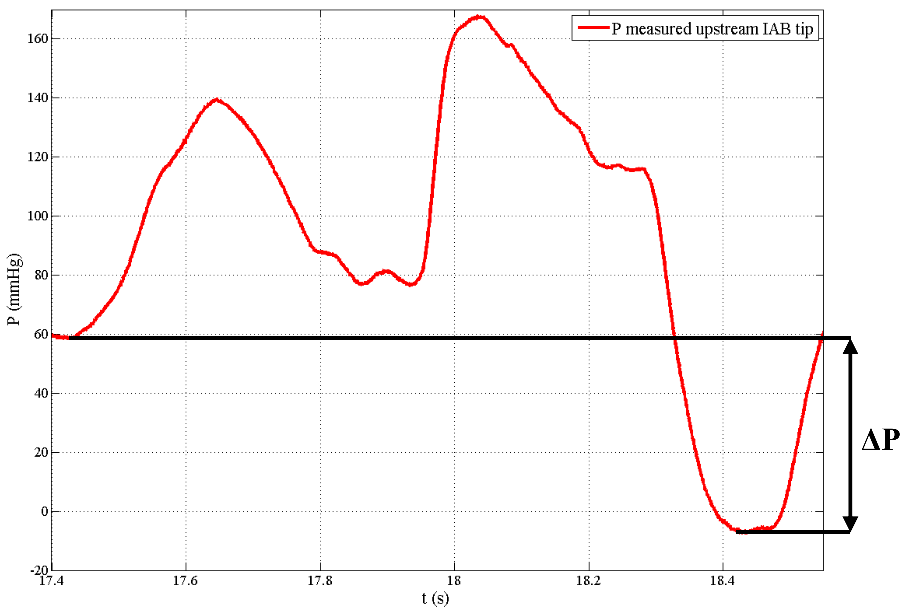

Figure 7-26: *The pressure waveform measured experimentally from the set-up presented in Chapter 4. End diastolic pressure presented a lower value and diastolic pressure lacks of oscillations, if compared to the results of the simulation.*

Diastolic pressure lacks the oscillations characterizing the pressure waveform obtained computationally, and this is probably a result of the different mechanical characteristics associated to the tube accommodating the balloon, which is elastic in the experimental model and stiff in the computational model. Also the minimum pressure value presents a relevant difference, but it should be underlined that in the computational model the whole systemic tree was modelled, while the test-bed was not constituted by mock branches simulating the impedances of the main compartments in the arterial tree. Again, it is important to underline that the aortic pressure waveform in both cases, computational simulation (Figure 7-25) and experimental study (Figure 7-26), shows different values in the beginning of the 1st cycle, where IABP starts counter-pulsating, and in the beginning of the second cycle (end of represented waveform in both Figures).

In this simulation, balloon inflation resulted in an increase in maximum pressure above the tip (pressure on upstream plane) and below the base (pressure on downstream plane) of the balloon by 41% and 60%, respectively. However, IAB inflation translates to a 9% increase in maximum pressure in the aortic root, while mean diastolic pressure during balloon inflation was calculated as 120 mmHg.

Although the minimum pressure on the aortic root, following IAB deflation, decreased by 55%, the end diastolic pressure, just before systolic phase, is decreased by just 5.5%. This is related to the movement of IAB wall, shown in the graph in Figure 7-3. IAB wall movement is characterized by marked oscillations, especially on the balloon base, and the result is a pressure waveform on the aortic root characterized by a damped increase in pressure and oscillations throughout diastolic phase. Furthermore, also the experimental measurements, as the computational simulation, the pressure value at the end of the 1^{st} cycle, when the balloon was deflated but did not counter-pulsate, is different from the pressure value at the end of the 1^{st} beat characterized by the balloon activity (highlighted by the arrow in Figure 7-26).

In this case, one single cycle was calculated: this type of analysis presents the limitation of reproducibility, as the second beat was not analysed. However the paragraph 7.5.3 presents the analysis of the model for more beats, and, although the model was changed in terms of IAB base, tip and centre movement against time, there was no difference in time steps size, 0D/3D ts and ts_i, maximum number of iterations and residuals target. In addition geometry of modelled aorta and mesh characteristics and size were maintained.

The volume displaced towards the aortic root during inflation, calculated above the tip of thoracic aorta, corresponds to 61% of the total balloon volume. The values are comparable with what was found by Biglino et al[71] while testing the IAB in a physiological set-up characterized by physiological pressure and flow waveforms. However the waveforms of the flow displaced both upstream and downstream varied markedly, as could be expected from a continuous movement of the IAB throughout the inflation process. In fact the flow displaced upstream is related to the movement of IAB tip and base: specifically Figure 7-27 shows the flow calculated on the upstream of thoracic aorta together with the difference between IAB wall movement on its tip and the one on its base, underlying that especially during the first phase of inflation the flow towards the upstream circulation is proportional to the difference in diameter between IAB tip and bottom.

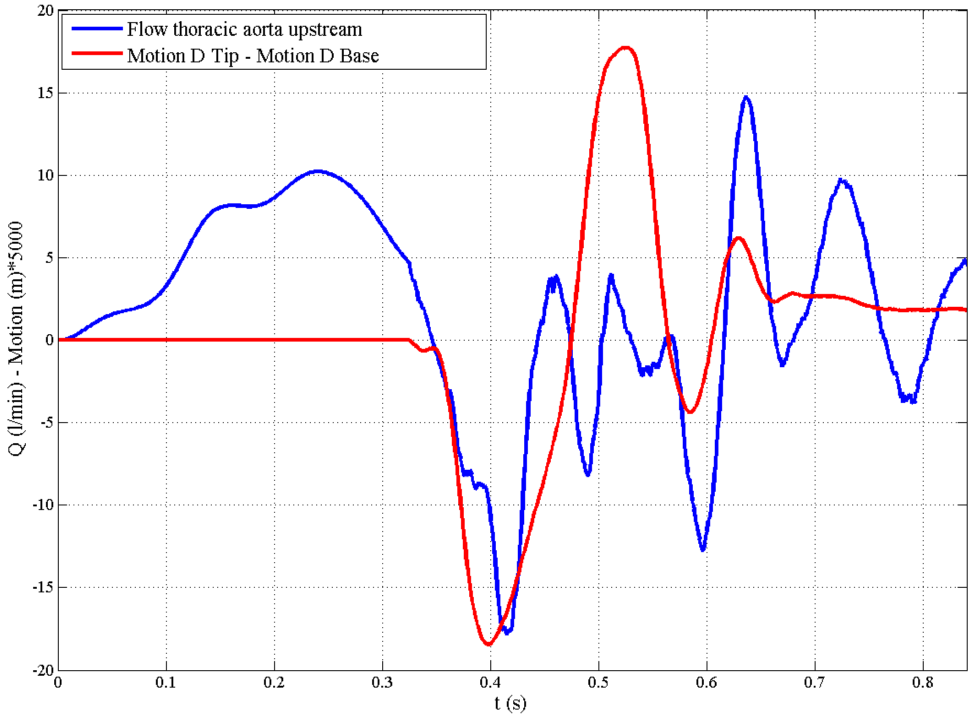

Figure 7-27*: Flow displaced upstream (blue line) and the difference between the movement of balloon tip and the one of balloon base. The first portion of the inflation phase reveals a direct proportion between the flow and the increase in IAB base diameter compared to tip.*

Figure 7-28 shows coloured plots of the longitudinal velocity on the central longitudinal section of the thoracic aorta, in the gap between balloon and aortic walls during the counterpulsation cycle. Note that the velocity scale is different for each image, aiming at optimizing the representation of the whole range of longitudinal velocity values within the thoracic aorta. The velocity profile has also been reported by Natan et al.[64] in their study based on the analysis of three dimensional blood flow associated with intra-aortic balloon counterpulsation. It should be noted, although, that their study has been conducted without taking into consideration the effect of impedance or compliance distally from the balloon on the flow field.

When the IAB is deflated, during the systolic phase, the longitudinal velocity is almost constant along the length of the thoracic aorta, except for the region adjacent to IAB end, close to downstream surface, characterized by a smaller velocity due to the presence of the balloon (Figure 7-28 A). IAB movement during inflation phase shows that initially its base is characterized by a bigger diameter compared to its tip, and the velocity field in the thoracic aorta is indicated in Figure 7-28 B. Following this phase the IAB presents a decrease in diameter at the bottom and a simultaneous increase in diameter at the tip, resulting in a higher impedance on this area of the thoracic aorta, and hence in a decrease of flow towards the upstream circulation (Figure 7-28 C). Further flow upstream is then generated when the balloon again inflates on its base while deflating on the tip, probably as an effect of the reflection of Helium within the IAB chamber (Figure 7-28 D). Deflation is characterized by a fast, simultaneous decrease in diameter throughout the balloon (Figure 7-28 E), and this results in high velocity from the system towards the thoracic aorta from both upstream and downstream circulation, around 2 m/s and 1 m/s, respectively.

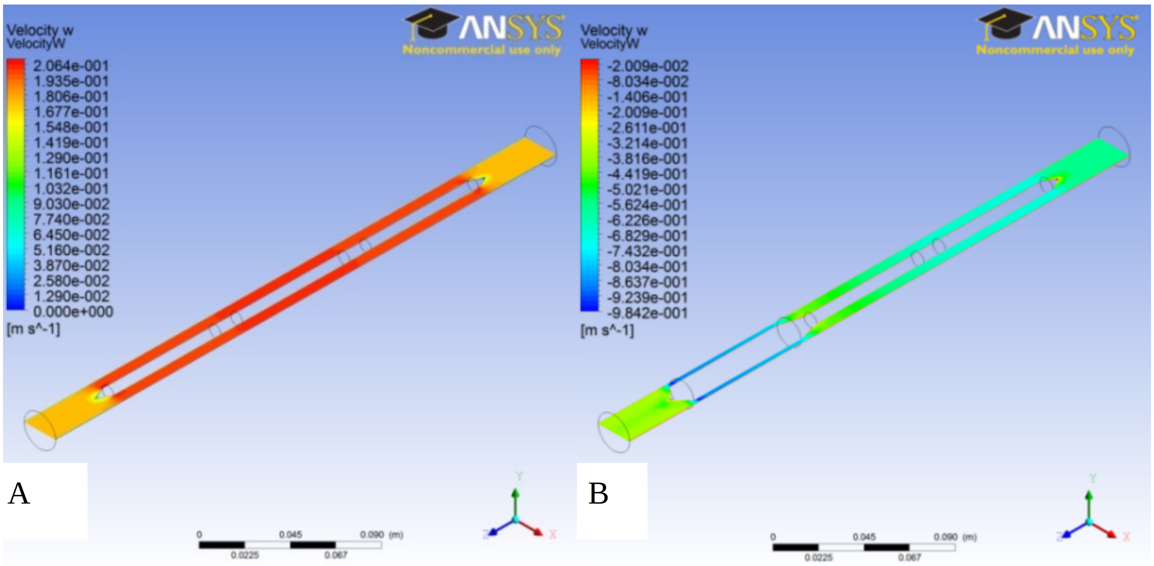

To be continued

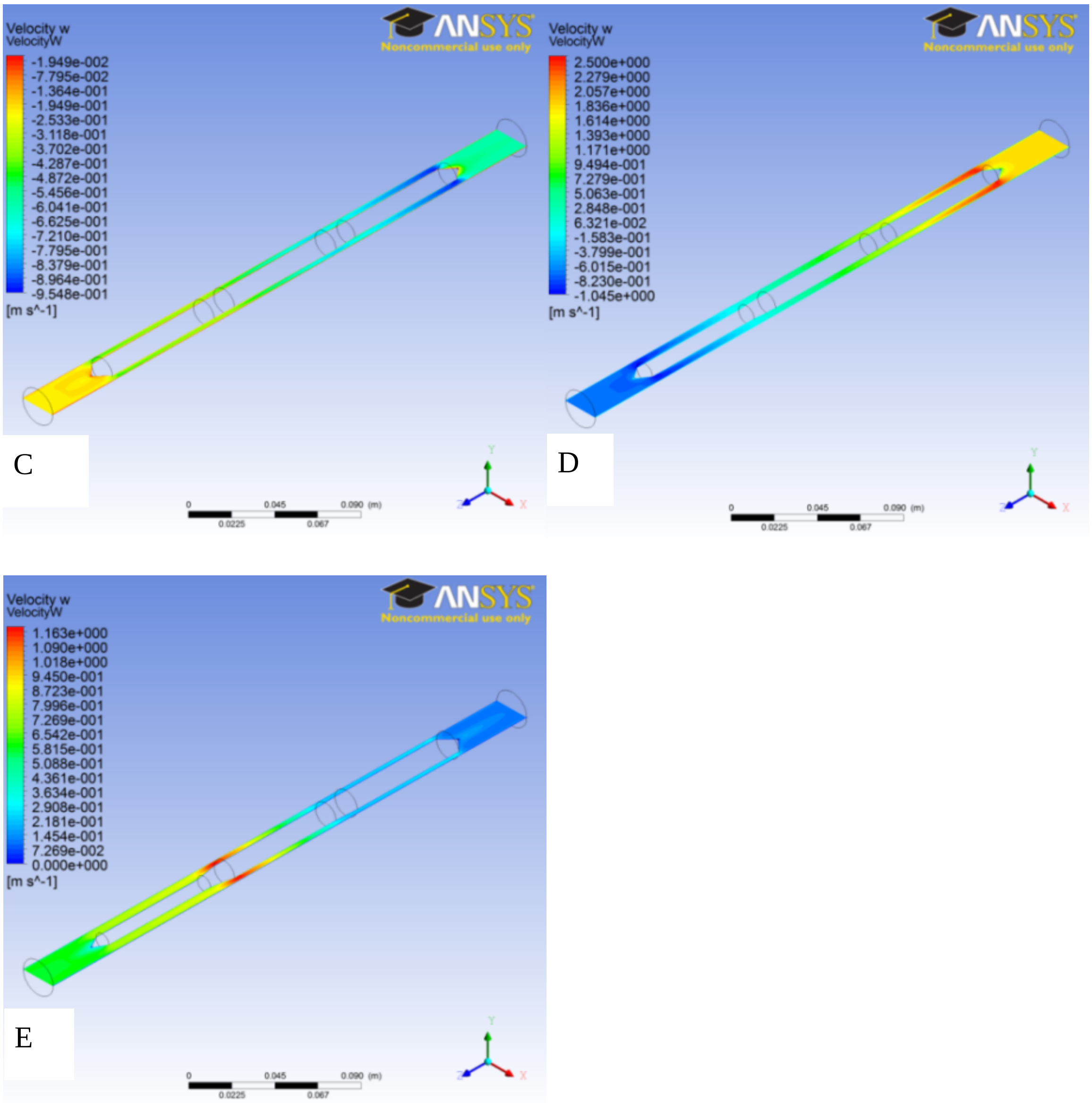

Figure 7-28: *Velocity field in correspondence of the systolic peak (A). Afterward the balloon starts inflating (B) till inflation reaches the centre and tip, obstructing the flow towards upstream (C) and finally inflates again within the base generating further volume displacement towards the upstream of thoracic aorta (D). Deflation starts simultaneously throughout the balloon (E).*

7.6.2 IAB and thoracic aorta placed at a 45° angled position

A further computational model resulted from the use of counter-pulsating IAB diameter waveforms obtained through high-speed camera recordings of the balloon activity at an angle of 45°. The aim was to simulate the balloon counterpulsation at an angle to the horizontal. As a result the waveforms characterizing pressure and flow on the aortic root and thoracic aorta were different from the ones obtained at the horizontal position. As already explained previously, in this case, the simulation featured a buoyancy model in which the gravity (g = 9.81 m/s^2) acting on the fluid field, at an angle of 45°, was taken into account.

Figure 7-29 shows the waveforms of pressure on the aortic root, with and without counterpulsation, flow on thoracic aorta without counterpulsation, and flow on upstream and downstream of thoracic aorta with counter-pulsating IAB. Figure 7-30 presents the pressure waveform measured above the tip of the IAB when counter-pulsating in the experimental set-up presented in Chapter 4 at an angle of 45 degrees. Also at an angled position it should be noticed that the aortic pressure waveform, for the computational simulation (Figure 7-29) and experimental study (Figure 7-30), is different between the start of the first cycle presenting IABP counterpulsation is and the start of the second cycle, once the balloon has completed its deflation phase.

This comparison reveals also two main differences: measured diastolic pressure lacks the oscillations characterizing the pressure waveform obtained computationally, and, as for the horizontal position, this might be the result of the different mechanical characteristics associated to the tube accommodating the balloon, elastic in case of the experimental test and stiff in the computational model; the minimum pressure value is different between experiment and simulation, and this could be related to the difference between computational model, in which the whole systemic tree was modelled, and the test-bed, which did not present mock branches simulating the impedances of the main compartments in the arterial tree. Although it should be underlined that both experimentally and computationally the minimum pressure due to IAB deflation is higher for the angled position.

In presence of an angle the balloon inflation produced an increase in maximum pressure above the tip (pressure on upstream surface) and below the base (pressure on downstream surface) of the balloon by 43% and 73%, respectively. The increase in maximum pressure on the aortic root was instead 18%, and mean diastolic pressure during balloon inflation was found to be 124 mmHg. Although the pressure values are generally similar or higher than the ones associated to the simulated IAB counterpulsation at a horizontal position, the volume displaced upstream calculated above the tip of the thoracic aorta was found to decrease from 61% of total balloon volume to 49%.

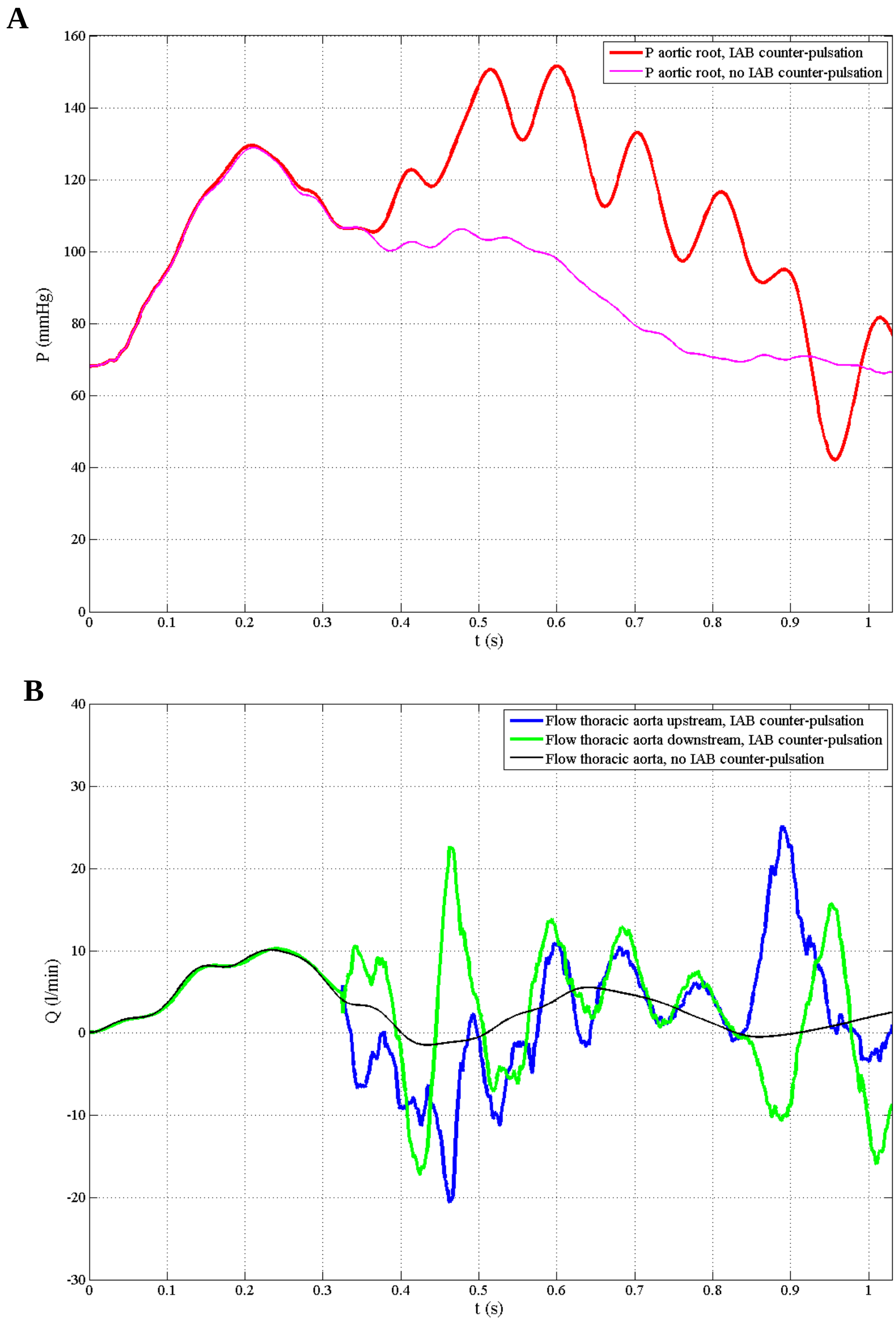

***Figure 7-29**: Comparison of pressure and flow between 0-D model and 3-D model with balloon counter-pulsating at a tilted position. The pressure waveforms shown are the ones calculated in the aortic root (magenta for model without IAB and red for counter-pulsating IAB) and the flow waveforms are the ones calculated in the thoracic aorta (black for model without IAB, green for downstream flow with counter-pulsating IAB and blue for flow displaced upstream with counter-pulsating IAB).*

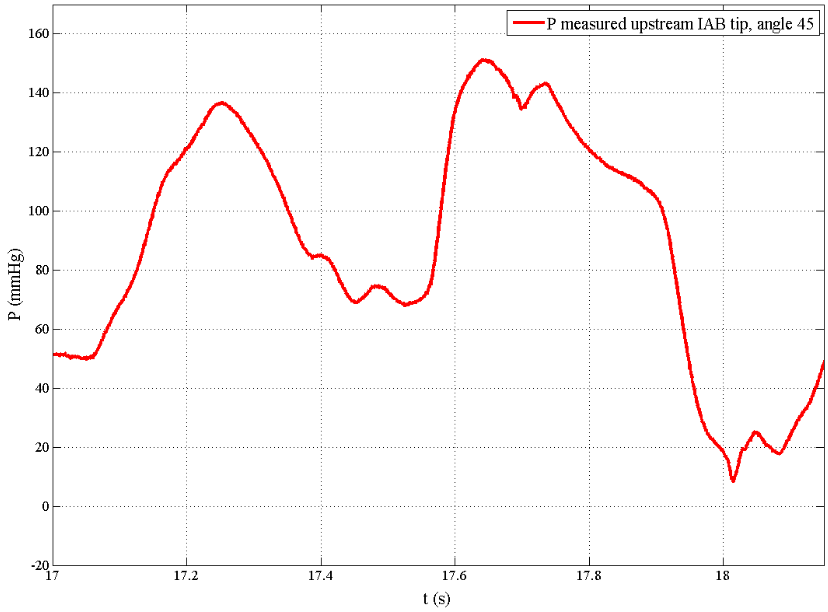

Figure 7-30: *Pressure waveform measured experimentally from the set-up presented in Chapter 4, at an angle of 45 degrees. Also in this case end diastolic pressure presented a lower pressure value and diastolic pressure lacks of oscillations, if compared to the results of the simulation.*

Figure 7-31 indicates the relation between the flow towards the upstream circulation and the difference between the diameter at the tip of the balloon and the one at the base. After the starting of inflation the tip of the IAB increases before its base, and the result is a fast change in flow above the upstream of thoracic aorta which is then reduced (0.34 s) due to the high resistance of the tip portion of the device, which is already inflated, against the flow towards the upstream circulation.

The comparison of the flow waveforms obtained in both horizontal and angled conditions reveals a marked difference in flow, induced by the different movement of the IAB, especially in the beginning of inflation (Figure 7-32). Explanation to this difference can also be exacerbated through plotting the velocity field for both horizontal and angulated positions, at the same instant during early inflation: Figure 7-33 A shows the velocity field and shape of balloon at 0.37 s at 45°, while Figure 7-33 B shows velocity field and IAB shape, at 0.37 s, at a horizontal position.

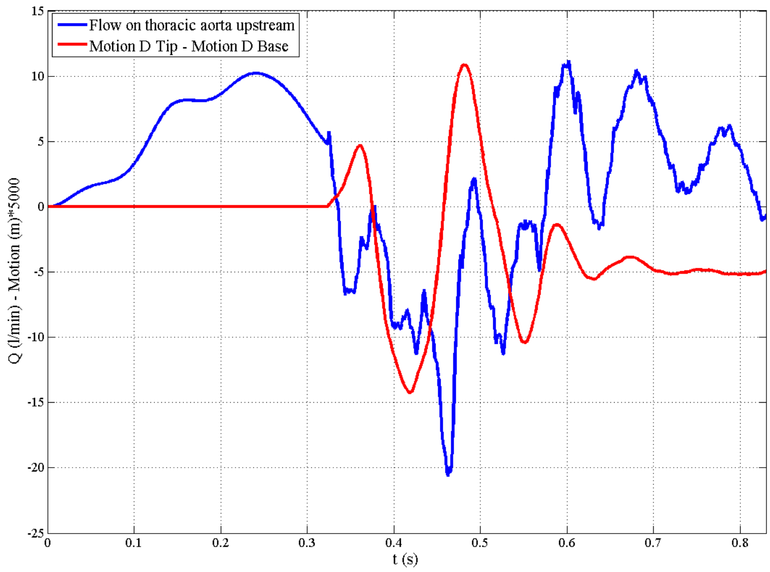

Figure 7-31*: Shows the flow displaced upstream (blue line) and the difference between the motion at balloon tip and the one at balloon base, when IAB counterpulsation at an angle of 45 degrees is simulated. The graph underlines the effect of the first inflation of the tip part of the balloon, inducing the flow towards upstream circulation to decelerate in the beginning of inflation (0.34 – 0.37 s).*

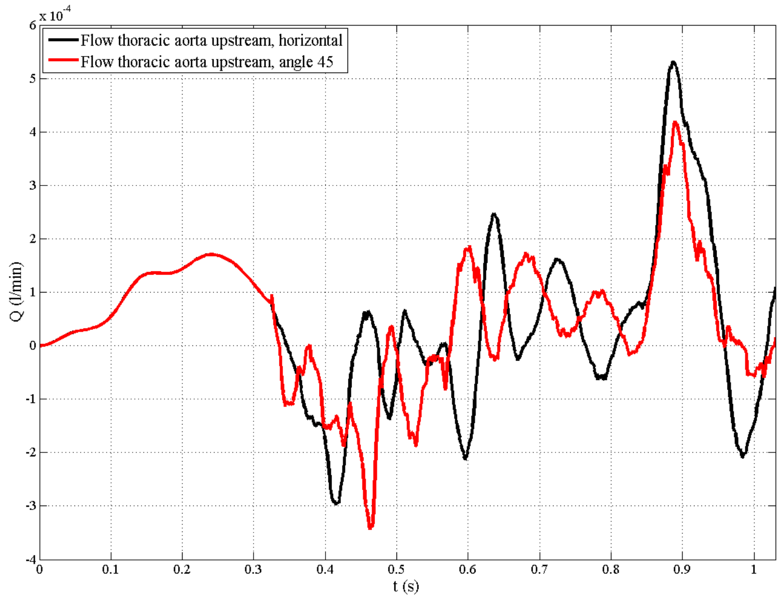

Figure 7-32*: Flow calculated on the tip of thoracic aorta at a horizontal position (red line) and angle of 45 degrees (black line). The two waveforms are radically different once balloon inflation starts, as a consequence of the different wall movement imposed to the 3-D model of the balloon.*

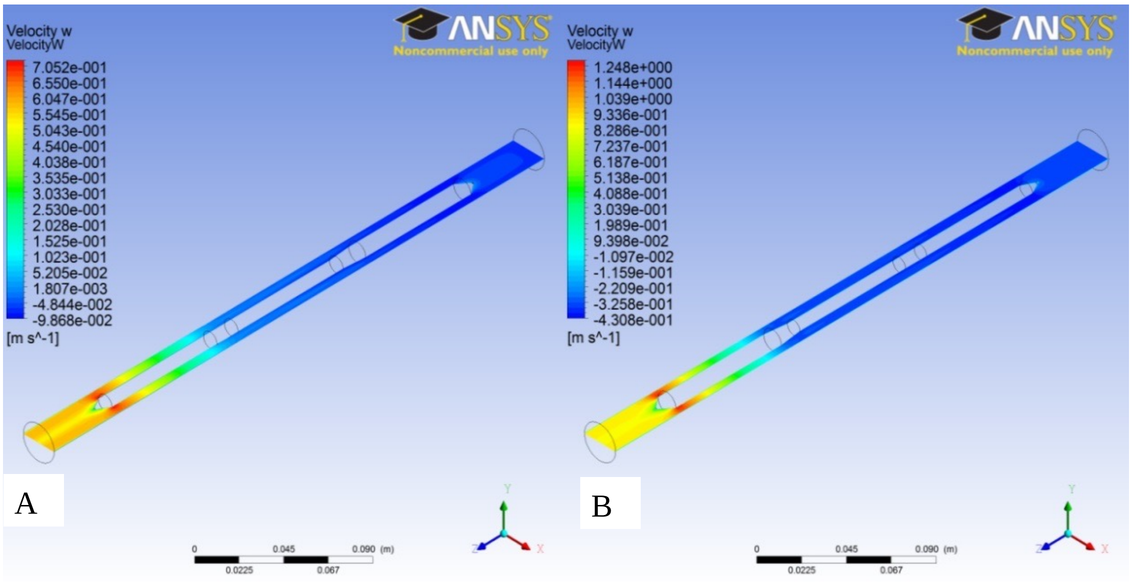

Figure 7-33*: The figure shows the velocity field on the longitudinal plane of the thoracic aorta, at the beginning of IAB inflation, comparing angled position (A) to horizontal one (B). The small velocity at the upstream of thoracic aorta at an angled position is related to the large diameter at the tip of the balloon, which does not characterize IAB inflation at a horizontal position, resulting in values of velocity close to 0.3 m/s.*

At an angled position the diameter at the tip of the IAB is larger than anywhere else, and the longitudinal velocity upstream of the thoracic aorta was close to zero; at a horizontal position, instead, the bigger diameter was found at the base of the balloon and the velocity calculated on the upstream of thoracic aorta was around 0.3 m/s. The deflation phase is also affected by the different movement of IAB wall at an angled position. Indeed the minimum pressure calculated on the aortic root, following IAB deflation, decreased by 36% instead of 55% (horizontal position), and the end diastolic pressure, just before systolic phase, is increased by 13% rather than decreased by 5.5%. These data confirm a non-negligible influence that angulation has on the benefit of IAB deflation for the ventricular afterload, highlighting the importance of correct IAB deflation movement for the optimization of the device benefit.

Also this simulation has the limitation of reproducibility: one single cycle was calculated, and Figures 7-13, 7-25 and 7-29 show that flow and pressure calculated are associated to different values between the beginning and the end of the cycle. Experimentally recorded pressure, in figure 7-25, and the simulation for the model verification, presented in paragraph 7.5.3, also present a different pressure value between starting and end of the first cycle, but reproducibility was addressed through the calculation of a second beat. The model for an angulation presents different IAB base, tip and centre movement against time, as well as the addition of a buoyancy model, but there was no difference in time steps size, 0D/3D ts and ts_i, maximum number of iterations, residuals target, geometry of modelled aorta and mesh characteristics and size.

The images in Figure 7-34 represent the velocity field in the surrounding of the IAB during deflation (0.92 s) at an angle of 45 degrees (Figure 7-34 A) and at a horizontal position (Figure 7-34 B). The velocity computed resulted to be much smaller in case of angulation rather than at a horizontal position, close to 0.1 m/s and 0.4 m/s, respectively. Again the main difference between the two models is in the diameter waveforms, which consists in the tip of the balloon to be larger in case of tilted IAB rather than at a horizontal position, as visible in Figure 7-34.

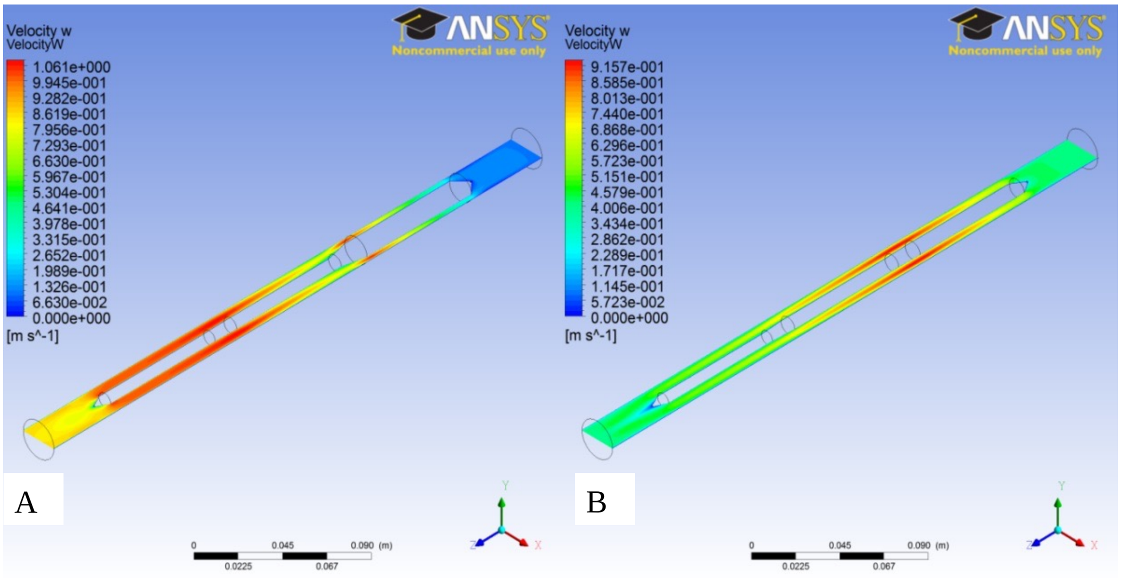

Figure 7-34*: Velocity field on the longitudinal plane of the thoracic aorta, during IAB deflation, comparing angled position (A) to horizontal one (B). Due to the different size of balloon diameter on its tip the velocity characterizing the flow from the system towards the thoracic aorta is much higher for the horizontal position (around 0.4 m/s) rather than for 45° (around 0.1 m/s).*

The differences in pressure and volume displaced upstream between the two positions, horizontal and semi-recumbent, resembled through different settings on the computational model, are representative of what was previously measured through experimental tests. Both volume displaced upstream, calculated above the tip of thoracic aorta, and deflation pressure pulse at the aortic root were found to decrease, by 20% and 26.5 mmHg, respectively, when changing position from horizontal to 45°, decrement close to the ones measured in the IAB shape comparison experiment designed by Khir and Bruti[68] (-24% and – 22 mmHg, $p<0.05$), and to the ones measured when comparing IAB shapes in a left ventricular simulator endued set-up (see Chapter 4) (-23% and -34 mmHg, $p<0.005$). In both studies, computational and experimental, inflation pressure pulse was not as compromised as the deflation pressure pulse, and the maximum change was found to be 6 mmHg.

7.7 Conclusions

The model presented in the chapter can reproduce pressure and flow waveforms at the tip of IAB and thoracic aortic root similar to those measured in vivo. Furthermore a different balloon movement resembling its counterpulsation at an angle to the horizontal could induce pressure and displaced volume variations comparable to the ones measured experimentally, both in the works presented in this thesis and in previous works from our group [68,113], for one cardiac cycle.

This model can be used for simulating balloon activity at an angled position, resembling patients being nursed at the hospital, and, as a future work, to study the effect of changes in IAB design on the benefits of this therapy in case of semi-recumbent position. Moreover the 0-D model parameters can be adjusted to re-create conditions of diseases or patient-specific models and consequently study the effect of these changes on the effectiveness of IABP counterpulsation therapy.

7.8 Limitations

The significance of the results of the simulation is limited by the following assumptions:

- The 3D thoracic aorta is resembled as a rigid tube with no pressure-dependent deformations; in addition this aortic tract is cylindrical and no physiological taper was modelled. This can result in different IAB volume displaced upstream/volume displaced downstream ratio;
- In the ascending aorta and aortic root, velocity radial components are assumed negligible, while the flow in this tract is strongly influenced by centrifugal force. However it is beyond the purpose of this work to accurately represent the velocity field in the aortic root and arch, as instead the aim is to estimate the pressure influenced by IABP counterpulsation;
- The interactions between the outside pressure and the balloon wall are not modelled, even though external pressure changes influences the IAB trans-mural pressure, hence affecting balloon inflation and deflation timings and magnitude;
- Reynolds number smaller than 2000 has been assumed to characterize the vessels modelled zero-dimensionally;
- The blood is treated as homogenous incompressible and Newtonian fluid;
- Reproducibility of calculated cycle was investigated just on the first two beats of the computational model, just at a validation stage and exclusively in terms of aortic pressure; a variable such as shear rate would provide a more accurate estimate of the variability between each simulated cycle;
- Convergence between 0D and 3D models results was just verified on two time windows, beginning of cycle and IAB inflation starting: although these are the most critical periods, convergence should have been verified throughout the simulated cycle.

Additional limitations associated to the 3D CFX model are due to the simulation time, and specifically to the manual information transfer between 0D and 3D domains. This drawback influenced not only the ts_i size sensitivity test, but also the number of simulated cycles. As already pointed out, to show full inter-beat reproducibility of the developed model three or more cycles would have been necessary to ensure that, after IABP activation, no beat to beat changes would be perceived throughout the simulation.

However the second beat simulated at the verification stage highlighted that end diastolic pressure reached was in line with the one associated to the first beat. In addition in the simulated cardiac beat pressure changes during cardiac systole and IABP counterpulsation did not vary between the first two cycles: this information can extend the reproducibility shown by the two end-diastolic pressure values to the whole simulated cardiac cycle.

In the results paragraph horizontal and angled situation were presented, which differed from the model analysed at a verification stage to investigate the issue of reproducibility, through simulation of two cardiac beats. In the cases presented in the results one single cardiac beat was simulated, hence the issue of reproducibility was not investigated. This should in fact be confirmed through the simulation of more consecutive beats, strengthening the significance of the data obtained in paragraphs 7.6.1 and 7.6.2.

The model presented is a preliminary model which aims at providing results valuable for following steps. The most relevant results are indeed presented at a verification stage, where reproducibility of cardiac cycle is better addressed and the developed model presents encouraging results, which suggests its useful application on a variety of cases for the development and optimization of IABP therapy.

7.9 Future works

The aim of this work was to develop a basic model of IABP counterpulsation in the thoracic aorta, and related changes into the cardiovascular bed. The model should be improved by adding more complexity such as fluid-structure interaction between fluid and balloon wall, Helium and balloon wall and fluid and aortic wall. Nevertheless, with the described model it will be possible to impose an established deformation to the aortic wall to mimic its elasticity and pressure damping effect. However these improvements should follow an automation of the 0D-3D interactions, which can result in reduced ts_i size and increased number of simulated cycles associated to a greatly reduced operator time.

The first results of the model are encouraging and, most importantly, they vary sensibly according to the movement characterizing IAB counterpulsation, partially replicating the results which were found experimentally. The model enables the investigation of the balloon movement effect on all the major compartments and the distribution of velocity and pressure in the surrounding of the IAB.

Chapter 8 General discussions

8.1 Chapter outlook

The experimental works presented in this thesis on the IABP deal with important clinical issues related to the performance of this cardiac assist device. Investigations on IABP therapy effectiveness and solutions to clinical problems are presented by testing the standard IAB, newly designed shapes and by comparing different pumps and IABs currently available on the market. Moreover, a pilot computational multi-dimensional model of the cardiovascular system with the IAB was developed to have an understanding of the fluid-dynamics in the surrounding of the balloon during its counterpulsation. The model could also be used to further develop different IAB designs and technologies.

In this chapter the main findings of the work will be summarized, categorized under the following interrelated novelties:

- IABP performance decreases in case of semi-recumbent position: scientific explanation through wall tracking and measurements of pressure and flow (Chapter 3);
- Novel IAB designs to overcome the negative impact of the semi-recumbent position: theoretical rationale, experimental results and clinical benefits (Chapter 4 and 5);
- Pump efficiency comparison showed differences in benefits between IABPs and their settings, addressing the use of different setting according to patient pathological conditions (Chapter 6);
- Computational model provides a first platform for the 3-D analysis of fluid-dynamic field within thoracic aorta and for future studies on different balloon shapes (Chapter 7).

8.2 IABP decrease in performance in case of semi-recumbent position: scientific explanation through wall tracking and pressure and flow measurements

As stated previously (Introduction, Chapter 1), it is common practice in intensive care units that patients are nursed at a semi-recumbent position, often at an angle between 30 and 45° [58,59].

Previous tests [63,66,67,71] showed that operating the Intra-aortic balloon at an angle affects its mechanics of inflation and deflation, hence possibly compromising the clinical benefits associated to the use of the device, and provided a scientific rationale to support the decrease in IAB performance. However, the influence of the angle on inflation and deflation mechanics had not been investigated adequately and detailed evidence on the phenomenon was not provided. Simultaneous measurements of balloon diameter and pressure during its activity in a silicone rubber tube, on different sites along the device, at both horizontal and angled positions, could address concrete explanations to the change in inflation and deflation mechanics in case of angle (Chapter 3).

Previous studies already aimed at the recording of IAB activity with high-speed camera [63,65], but balloon wall tracking was not performed. Furthermore, the set-up used for accommodating the device consisted of a stiff tube with mechanical properties consistently different from those of a physiological aorta.

The recording of the balloon at a horizontal position in a compliant tube pointed out one difference in inflation mechanics compared to previous studies: the balloon starts inflating from the base and, following, in the centre and tip, while according to previous works on rigid tubes the IAB would commence its inflation on both, tip and base, and progress towards the centre, generating the so called 'trapping phenomenon' [65]. The study hence indicates that if the device is activated in a compliant tube the mechanics of inflation can differ from the one in a rigid system.

In addition, the analysis of measured diameter revealed the presence of waves when the balloon is inflating and deflating, due to Helium bouncing while filling up (inflation) and emptying (deflation) the IAB chamber. The evaluation of the distances between the peaks on the diameter waveforms provided an estimation of the speed of travelling of Helium within the balloon chamber, quantified as 3.92 m/s and 4.12 m/s at a horizontal and angle of 45° positions respectively.

The most important and clinically relevant finding is the scientific evidence of decreased performance of balloon deflation in case of angle: diameter measurements showed that the tip of the IAB remains almost fully inflated till approximately 0.1 s before following inflation onset, while centre and base are deflated. This effect could be associated to a slower Helium flow towards the pump and also a lower volume sucked from the upstream circulation because of the higher impedance constituted by the tip of the balloon. The hydrostatic pressure difference between balloon base and tip at an angled position is the main reason for this behaviour, since it was demonstrated that the base deflates before the rest of the balloon. Simultaneous pressure measurements showed a related IAB deflation pressure pulse decreased by 14.2%. Furthermore, by calculating pressure difference between the base and the tip of the balloon, no discontinuity is monitored when the balloon deflates at a horizontal position, while a difference (tip pressure higher than base one) is shown when the IAB deflates at an angled position, revealing that the pressure at the base of the balloon starts decreasing before the one at the tip.

8.3 Novel IAB designs to overcome the negative impact of the semi-recumbent position: theoretical rationale, experimental results and clinical benefits

Based on the arguments reported above, a modification on IABP technology aiming at dealing with the negative effects that the angulation induces on the balloon inflation and deflation mechanisms is recommended and highly desirable. For this purpose new designs of IAB were developed and compared to the standard cylindrical balloon (Chapter 4 and 5). The changes between the differently shaped balloons relies on the IAB tapered configuration when IAB is inflated: the standard cylindrical balloon is associated with a uniform distribution of volume and diameter throughout its central portion, while the tapered balloons present a volume and diameter distribution higher on one side to influence the inflation and deflation mechanics; the tip for the tapered increasing in diameter (TID) set and the base for the tapered decreasing in diameter (TDD) set.

Regarding TDD the modification on shape was designed to induce an enhanced benefit on both inflation and deflation phases. During inflation the modified IAB might displace a higher volume towards the upstream circulation (coronaries) at both horizontal and angled position, because a lower resistance (estimated in Chapter 4) at the upper portion of the balloon is related to the lower diameter. This concept was also explained through theoretical approach (Chapter 4). During deflation, in case of angulation, the decrease in deflation pressure pulse (measured in Chapter 3) could be reduced because of the higher concentration of the volume on the balloon’s base; being this the first part to deflate, most of the volume would flow from the IAB towards the pump in the beginning of the deflation phase, differently from the standard cylindrical balloon.

TID shape was designed with the aim of increasing the performance of the balloon during inflation. The augmentation of the portion of volume corresponding to the balloon tip could reduce, in case of angulation, the decrease in volume displaced towards the upstream circulation. This could happen since, although the high resistance associated with the tip of the TID IABs, a smaller portion of IAB volume would be displaced after the tip compared to a standard cylindrical balloon.

Aiming at discovering the effects on the fluid-dynamics induced by the differently designed balloons, and at verifying to which extent the above described assumptions are correct, the tapered balloons were tested together with the cylindrical balloon.

Two different tests have been conducted for exploiting the potential benefits of the TDD and TID balloons: firstly, two totally tapered balloons, were tested while counter-pulsating in a compliant tube, and compared with the standard balloon, focusing on the influence of angulation on both volume displaced upstream, during inflation, and deflation pressure pulse, during deflation (Chapter 4); afterword, 3 TDDs, 3 TIDs, each constituted by a cylindrical portion (2/3, 1/2 or 1/3) and a tapered one (1/3, 1/2 or 2/3), and a standard balloon, were studied while counter-pulsating with a left ventricular simulator (LVS) at different inclinations to the horizontal, in order to investigate the performances of the differently shaped balloons in case of physiological pressure and flow waveforms (Chapter 5), and in the attempt of extending the results into clinical outcome. In the second study the design of the balloons underwent modifications in order to 1) fit the physiological space and 2) investigate the effect of a different portion of tapered/cylindrical shape on pressure and flow during cardiac cycle.

8.3.1 Inflation

8.3.1.1 Volume displaced towards upstream circulation

As extensively explained, one of the benefits associated to IABP inflation consists of the hypothetical [32] increased provision of oxygen to the heart through augmented coronary flow, depending on the amount of volume displaced towards upstream circulation by the IAB. However, this volume can decrease in presence of angulation, as shown by previous tests [62,66,68,71] and confirmed by the studies conducted: the loss in volume displaced towards coronary circulation over total balloon volume (VUTVi), changing position from horizontal to angle 45°, was close to 25% (both with and without the use of LVS).

The use of tapered balloons without LVS induced an improved benefit in case the system was tilted: TID and TDD resulted in a VUTVi unaffected and increased by around 11%, respectively, when the position was changed from 0 to 45° (Chapter 4). Some of the differently shaped balloons tested in a system provided with LVS confirmed the encouraging results obtained by using TDD and TID balloons: TDD 1/2 induced an increase of 13% in VUTVi in case of change in position from 0 to 45°, and none of the tested TID showed a decrease in VUTVi (Chapter 5).

8.3.1.2 Pressure pulse

The inflation pressure pulse has shown to be influenced by the inclination (Chapter 4 and 5). In all the balloons the pressure difference between tip and base decreased or became negative when the operating position of the IAB was angulated. This effect though could be related to the influence of the hydrostatic pressure difference on the tube accommodating the IAB rather than on the balloon itself. Indeed experiments (Chapter 5) showed that the inflation pulse of the balloon increases with increasing pressure in a silicone rubber tube, due to decreasing the tube compliance, while slightly decreases in a rigid glass tube. This effect could explain why the inflation pulse on the bottom area of the balloon, falling under higher hydrostatic pressure at an angle, is equal or bigger compared to horizontal position, while it decreases at the IAB tip.

8.3.2 IAB shape influences pressure distribution along the balloon

For investigating the effect of differently shaped IABs on the balloon counterpulsation the difference between the tip and the base measured pressure has been calculated and plotted during one cycle for cylindrical, TDD 1/3 and TID 1/3 balloons. At the horizontal position the main difference among the balloons was noticed during inflation: TID 1/3 is associated to smaller oscillations compared to the other two balloons, revealing a more simultaneous inflation of the IAB. At 45°, the main difference between the IABs was found at the onset of deflation: TDD 1/3 presents the highest pressure difference increase among the balloons tested, which translates into pressure at the base decreasing more than that at the tip in the beginning of deflation (Chapter 5). This effect is related to the higher volume concentration at the base of TDD 1/3 balloon, which is the first part to deflate when the balloon is tilted.

8.3.3 Deflation

The balloon deflation phase has not been extensively studied in the literature, and less information is available compared to the inflation mechanism. Nonetheless the beneficial effect of deflation is crucial for the operating condition of the dysfunctional heart. Indeed the benefit of IAB deflation is the decrease in end diastolic aortic pressure, which translates into a smaller ventricular afterload. In fact Cheung et al. [69], amongst others, indicated this effect as the main advantage of the counterpulsation therapy on failing heart.

As previously presented and explained (Chapter 1 and 3) the presence of an angulation induces a drastic decrease in IAB deflation performance. This was confirmed on both studies comparing the standard balloon to the differently shaped ones (Chapter 4 and 5): tilting the system from 0 to 45° in case of IAB activated without the use of LVS the decrease in deflation pulse was 22 mmHg, while in case of counterpulsation with LVS the end diastolic pressure (EDP) increased by 34 mmHg. TID set of balloon are also associated to a consistent loss in deflation pulse in both experimental set-ups. Differently all TDD balloons showed encouraging results, containing the deflation pulse loss with increasing angle from 0 to 45° within a maximum of 10 mmHg.

The reduced EDP shown by tapered balloons compared to the standard one, by 20 mmHg, is associated to a reduced EDP point in the PV loop. Although it was not possible to construct an accurate PV loop based on the experimental system, as the left ventricular pulsation was simulated through a mechanical system activating a piston pump and based on the piston displacement control, the literature [121] showed how a reduction in EDP influences the stroke volume and left ventricular end-diastolic pressure and volume, and highlighted that the most immediate and beneficial effect of IABP therapy was the reduction in end diastolic pressure.

The decrease in deflation pulse is closely related to the reduced volume sucked from upstream over total balloon volume (VUTVd): all TDDs balloons performed better than TIDs and cylindrical (Chapter 4). TDD 2/3 resulted, at an angle of 45°, in a VUTVd 33% higher than that produced by the cylindrical balloon.

8.3.4 Final considerations

At a first stage the results obtained from the experiment testing TDD, TID and cylindrical balloons without LVS underlined the potential benefit of using TDD on both inflation and deflation, and of using TID for inflation. The results presented in this Chapter were supported by a simple theoretical approach based on the use of Poiseulle formulation for describing flow in a conduct (Chapter 4).

Later on the IAB design was further modified, in order to investigate the effect of a different portion of tapered design and for fitting physiological space, and compared to the standard IAB in a physiological set-up providing physiological pressure and flow waveforms with the use of a LVS (Chapter 5). Testing the balloons in a more physiological environment confirmed the advantages of using differently shaped IABs. Even though this study showed a similar trend with increasing angle among TDD balloons in regards of the end diastolic pressure (EDP), always lower compared to cylindrical and TID balloons, the measured VUTVi resulted markedly different. Specifically among TDD series, TDD 1/2 was the only balloon whose VUTVi was not negatively affected by an increase in angulation of the system.

The use of TID series of balloons negatively affected the EDP with increasing angle. Nevertheless it should be reminded that this IAB was designed for bringing an advantage in inflation performance. The cylindrical balloon showed to induce the highest VUTVi at a horizontal position, but on the other hand VUTVi associated to TID balloons was not negatively affected by a change in position from 0 to 45°.

8.4 Pump efficiency comparison showed differences between IABPs and their settings, addressing the use of different setting according to patients with different pathological conditions

Other than the balloon design, IABP inflation and deflation onsets are dramatically influencing the fluid-dynamics in the cardiovascular system and the effective delivery of IABP therapy benefits to the dysfunctional left ventricle [79]. Even though the IABP counterpulsation can be set for the optimization of inflation and deflation timings, irregular ECG or high heart rate can result in the pump to miss some of the heartbeats or to miscalculate the onset of inflation and deflation [83].

Consequently, different algorithms have been developed for the maximization of IABP benefits and for avoiding critical time delays or intra- and inter-operator variability [83], [91], [85], [86].

A comparison between the two main companies producing IABPs, Teleflex and Datascope, and between different settings available on the two systems, has been carried out with the aim of investigating the influence of each configuration (pump and setting) on the main parameters characterizing the pressure waveform amended by the IAB (Chapter 6). The indices of interest consisted of the time between systolic peak and starting of inflation (RpIs), the duration of inflation (DoI) and the ratio between missed beats and total number of heartbeats (Ratio). A balloon was placed in a mock aorta and physiologic aortic pressure waveform was generated through a valve system which was connected to a compressed air source and controlled by ECG waveforms.

The settings used on each pump varied in terms of source signal for triggering (ECG, pressure transducer or fibre optic sensor could be selected as trigger signals, the first one delivering the ECG waveform and the others transmitting the pressure signal) and of operation mode, determining the level of operator's freedom of intervention (automatic or semi-automatic on Datascope). Most configurations were affected by high heart rate and irregular ECG, and this suggests that different settings should be used according to the patient specific conditions to maximize the IABP therapy benefit. Overall it was not possible to determine one configuration or setting which performed better than the others for all indices, but important observations could be extrapolated from the analysis of the results.

The use of a fibre optic sensor as trigger signal in the Teleflex pump resulted in a shorter RpIs, revealing a faster response to the signal by IAB. When this technology is applied by Datascope pump, instead, the advantage to the pressure transducer signal, in terms of RpIs, is not marked and did not perform as good as the Teleflex pump. Nevertheless, the use of this setting is not suggested in case of irregular heartbeat, since it showed to miss and not trigger a high number of beats, resulting in missed inflation after systolic peak or, more critical, missed deflation before the systolic phase.

The meaning of DoI index should be discussed further. Indeed a high value of DoI index reveals a positive outcome of IAB therapy in terms of assistance to left ventricle due to the inflation assisting a long portion of the diastolic phase and a higher mean diastolic pressure. Nonetheless, high DoI might also indicate a critical onset of deflation, triggered in proximity of systolic starting and resulting in a non-optimal end diastolic pressure decrease. To exploit the advantage of this index Teleflex machine, when triggering with ECG signal, selects a different algorithm according to the nature of the signal itself: the algorithm targets DoI maximization when the ECG is regular, while it ensures IAB deflation when ECG is irregular triggering it in concomitance with R-peak. On the other hand, it was shown that the Datascope machine aims at a safe IAB deflation in every case, triggering the balloon deflation onset in all types of ECGs, and hence generally producing a longer DoI.

The index Ratio indicates the actual efficiency of the IABP therapy, and reveals the assistance of the pump to the left ventricle compared to the total number of analysed heart beats. In this case, Teleflex pump showed an exceptional performance if set on ECG trigger, resulting in triggering all heartbeats of all regular and irregular ECGs. Secondly, Datascope pump on semi-automatic setting and ECG as a trigger, showed a good performance with an average of 0.08% missed beats throughout tested ECGs and settings.

In conclusion, the IABP setting should be selected according to the patient condition, evaluating the degree and nature of irregularities (Chapter 6). In case of regular or slightly irregular ECG, the configuration providing the best indices was Teleflex pump on automatic mode using fibre optic sensor technology. In case of highly irregular heartbeats, a common condition for patients treated with IABP therapy, Teleflex pump on automatic mode and ECG triggering was the safest and most advantageous configuration, inducing an excellent value of Ratio index (100% of analysed beats were triggered) and a safe deflation of the IAB. Moreover, the analysis showed that Datascope pump performs better in case semi-automatic setting is selected compared to the automatic one, inducing a higher value of Ratio index and an optimal DoI.

8.5 Computational model provided a platform for the 3-D analysis of fluid-dynamic field within thoracic aorta and for future studies on different balloon shapes

The experimental studies aiming at the analysis of changes induced by the Intra-aortic balloon different shapes can provide useful information on the potential benefits, which could be translated 'in vivo', associated to special designed IABs. The novel designs discussed were developed with the aim of contrasting the highlighted and discussed critical drawbacks introduced by the semi-recumbent position at which the IAB generally operates in the ICUs.

On the other hand, it would not be possible to access 3-D information characterizing the flow field in the surrounding of the balloon, useful for the optimization of the design of the device. Furthermore, the different experimental set-ups used for accommodating the standard and differently designed balloons did not resemble well the physiological environment, characterized by different branches and compartments.

For these reasons a computational model (Chapter 7) was developed aiming at the study of 1) IAB counterpulsation effects on the surrounding of the balloon and on the main branches of the systemic circulation 2) the distribution of the flow displaced by the balloon on both sides. Furthermore, it would be possible to analyze the effect of changes in the design of the IAB on the fluid-dynamic field in the thoracic aorta and in the systemic circulation as well as to target the development of additional amendments which could enhance the benefits associated to the counterpulsation therapy. Nevertheless, the model can be used for analyzing hemodynamic changes associated to an angulation in the system on both thoracic aorta and arterial system, and also for the study of the effect of modifying the arterial tree compartments distal impedance on the fluid-dynamics characterizing the counterpulsation.

For this purpose the system was modelled as a multi-dimensional computational model constituted by a compartmental model of the systemic circulation connected to a three-dimensional model of thoracic aorta with a counter-pulsating IAB. This structure would enable in-detail analysis of the flow field within the thoracic aorta, on the surrounding of the IAB, together with information on the flow and pressure waveforms on different compartments of the arterial tree.

8.5.1 IAB movements at a horizontal position

Diameter waveforms as recorded through high-speed camera (Chapter 3) were used for controlling the movement of IAB wall (Chapter 7). The increase in maximum pressure on aortic root, due to IAB inflation, was calculated as 9%, whilst the decrease in pressure due to IAB deflation calculated on the aortic root at the starting of systole was calculated as 5.5%. The volume displaced upstream calculated above the tip of thoracic aorta reached 61% of total balloon volume, slightly different from the volume measured by Biglino et al. [71,113] in the physiological experiment mentioned in the above paragraph (75%).

This model revealed that the flow displaced towards the upstream circulation is strongly regulated by the inflation process characterizing the balloon: in fact when the diameter at the base of the IAB was larger than that at the tip, the volume displaced upstream increased, and oppositely when the tip was bigger than the base it decreased.

Another important observation enhancing the usefulness of the model comes from the possibility of accessing three-dimensional information in the proximity of the balloon wall. Indeed the plotting of the velocity field on the longitudinal direction of thoracic aorta shows small re-circulation areas characterizing the model of IAB featuring tapering of the two edges. These phenomena should be observed when defining the shape of a balloon or when assessing the performance of an already existing design.

8.5.2 IAB movements from high-speed camera recordings, angled position

The simulation of the IAB counter-pulsating at a semi-recumbent position also underlined the potential of the pilot model, confirming what was previously measured experimentally: the benefits of the IAB at an angled position are compromised in terms of volume displaced upstream, towards the coronary circulation, and deflation pressure pulse (Chapter 7).

Indeed the volume displaced upstream calculated above the tip of the thoracic aorta was found to decrease from 61% of total balloon volume to 49%, resulting in a 20% decrease close to the one measured experimentally both without and with left ventricular simulator acting on the set-up (-25% and -23%, respectively, $p<0.05$).

The deflation pressure pulse calculated on aortic root at an angle, following IAB deflation, resulted 27 mmHg smaller than in case of horizontal position, and this outcome also does not differ from what measured experimentally without and with the use of left ventricular simulator (-22 and -34 mmHg, respectively, $p<0.05$).

The analysis of the fluid-dynamics inside the thoracic aorta confirmed that both volume displaced and sucked from upstream are dependent on the direction of inflation and deflation waves while filling up and emptying the balloon chamber, since high diameter on balloon tip induced a deceleration of flow towards upstream circulation, during inflation, and of flow from the system towards the aorta, during deflation.

8.5.3 Final considerations

The developed multi-dimensional model of IAB with arterial system can reproduce the physiological activity of the device with related modified pressure and flow waveforms. The amended aortic pressure waveform is comparable with the one measured ‘in vivo’. Furthermore the value of the calculated volume displaced upstream is close to the one experimentally measured by Biglino et al. [71,113].

Accessible information about the changes in velocity field on the balloon edges while the balloon is inflating are essential and should be taken into account in case of further modifications of the balloon shape, targeting the maximization of both volume displaced upstream and decrease in end diastolic aortic root pressure.

Indeed the model can be very useful for studying different angulations of balloon walls on both tip and bottom sides, together with the influence of the balloon diameter value on the hemodynamic parameters, aiming at improving the benefits related to both inflation, (increase in coronary artery flow) and deflation (decrease in end diastolic pressure and left ventricular afterload).

Furthermore, the model allows the modification of the resistance associated to different compartments in the arterial system in order to study their influence on the distribution of flow displaced by the balloon and to characterize the physiological bed according to patient specific features and anatomy.

8.6 Limitations

The presented works address a concrete possibility of improvement for the design and functionality of the Intra-aortic balloon pump counterpulsation therapy, through relating important results obtained experimentally to clinical advantages. Nevertheless, a number of limitations characterizes each experimental study: further investigations will be needed to strengthen the association between experimental investigations outcome and clinical benefits.

Cross-linking limitations throughout experimental studies consist in:

- The arterial tree anatomy-physiology was not resembled, although the main aim throughout experiments was to better understand the mechanics of inflation and deflation of standard and differently designed IABs and their effects on flow and pressure distribution in a symmetrical set-up;
- Water has been used instead of blood or of a liquid characterized by similar rheology with blood (generally 30% – 70% of glycerin - water solution is used [114]), hence both inertial and viscous forces assume a different value compared to the physiological situation, due to different viscosity. This could have an implication on the relationship between pressure and flow waveforms. Future tests on both standard and differently designed balloons on animals will be carried out in order to underline to which extent the conclusions drawn from the experiments in this work can be associated to clinical benefits.

The developed pilot computational model also includes a number of restrictions:

- The aorta has been considered a straight rigid tube, hence did not represent the elastic properties of a physiological aorta. As a consequence, the pressure inside the aortic branch was influenced by the balloon inflation and deflation with no changes in the aortic diameter, resulting in omitting the damping effect due to compliance. However, the model geometry was similar to that of the aorta and the compliance was resembled by including a lumped component in the 0-D model;
- The interactions between the thoracic aorta pressure and the balloon wall are not modelled, even though they can play an important role in the regulation of balloon's inflation and deflation mechanisms;
- Wave reflection is neglected, but it might play an important role in the

distribution of volume displaced towards upstream and downstream circulation. However, pressure and flow distribution on the compartmental model was similar to the physiological one, highlighting the reliability of the 0-D model as a method for establishing boundary conditions on 3-D thoracic aorta;

- Cycle to cycle reproducibility of the model is only partially addressed, as a maximum of two cycles have been calculated, and as variability was checked on pressure instead than on a more sensitive variable such as the shear rate. However, the two cycles present the same end diastolic pressure and the pressure waveforms and magnitude of pressure pulses suggest that the third cycle will have the same characteristics and values as the second cycle;
- 0D and 3D models convergence was verified on two periods, beginning of cardiac cycle and IAB inflation starting, which are the most critical periods throughout the simulated cycle. However convergence should have been verified throughout the simulation.

The model introduced suggests a novel method of analysis of Intra-aortic balloon pump effectiveness and can be used also for the analysis of other cardiac assist devices. It should be highlighted that the aim was to develop a basic model which could afterwards be improved by adding more components such as fluid-structure interaction between fluid and balloon wall, Helium and balloon wall as well as fluid and aortic wall.

Chapter 9 Conclusion and future steps

9.1 Conclusions

Although introduced for the first time into clinical practice more than 40 years ago the Intra-Aortic Balloon Pump (IABP) did not undergo relevant changes in design. Several amendments on IAB designs have been developed and studied [46,47,51,52], but eventually not introduced into clinical practice. Earlier studies conducted on this cardiac device did not completely address questions involved with its mechanism of inflation and deflation or with the fluid-dynamics in the thoracic aorta, where the IAB is placed. An in depth experimental analysis of these two phases is needed because of their importance in providing increased coronary flow (during inflation) and reduced ventricular afterload (during deflation), and because both of them seem to loose effectiveness at an angulation [63,65-67,71], often corresponding to the patient position when operating with IABP.

From the experimental studies important conclusions can be derived for a successful development of IABP therapy:

1. Operating the balloon at an angle induces decrease of both inflation and deflation effectiveness, and can compromise IAB clinical benefit. Particularly during deflation phase, the waveforms of the measured diameter during IAB counterpulsation confirmed, at an angle, a delayed deflation at the tip of the balloon, while at base and centre the IAB was collapsed. This un-uniform and slower deflation process, related to the hydrostatic pressure difference between balloon base and tip in case of angled position, is associated to a decreased deflation pulse (Chapter 3).
2. The influence of angle on balloon deflation effectiveness was shown to decrease in case a differently designed balloon, tapered from the base towards the tip (TDD) in order to influence the inflation and deflation mechanics, and to contain the negative impact of the semi-recumbent position. In addition a change in the shape of the balloon showed to introduce important benefits to the inflation phase when IAB operated at an angle from the horizontal: specifically a differently designed balloon, TDD 1/2, characterized by half cylindrical portion and half tapered towards the tip, was associated to an almost unaffected volume displaced upstream in case the balloon was tilted (Chapter 4 and 5).

3. The performance of TDD IABs in maintaining low EDP throughout angulations at which IABP operated, demonstrated in case of balloon counterpulsation with an LVAD, can be translated into a key clinical benefit of the IABP, highlighted through the use of the PV loop diagram and addressed by previous researchers [121, 36, 96, 69].
4. Improvements during balloon inflation at semi-recumbent position were noticed when a different tapered balloon, tapered from the tip towards the base (TID), was tested together with TDD and cylindrical balloons. Volume displaced upstream indeed was not decremented in case of angulation in conditions of static pressure as well as in conditions of aortic pressure waveform characterized by systolic and diastolic pressure phases (Chapter 3 and 4).
5. In addition to the IAB design, IABP setting and mode can be crucial in defining this therapy clinical effectiveness, according to the regularity of the ECG and the patient pathological conditions:
    - The Teleflex pump featuring the new technology introduced through fibre optic sensor, placed on the tip of the balloon, resulted in the fastest response following systolic peak compared to other technologies and pumps in 93% of the cases. This setting was related to an improved efficacy compared to other settings especially in cases of regular or slightly irregular ECGs;
    - The Teleflex pump and Datascope pump on semi-automatic and ECG triggering mode resulted in the ratio between number of assisted beats and total number of heartbeats, a key index establishing the reliability of the IABP, relevantly lower than all other configurations especially in situations of arrhythmia or high heartbeat, enhancing the importance of targeted setting of the IABP in these situations;
    - The Datascope pump on semi-automatic and ECG triggering mode is associated to the longest duration of inflation in most of the cases, although this index does not indicate a specific benefit of counterpulsation on ventricular recovery, since, although indicating a higher mean diastolic pressure, it might be associated to a late deflation and compromise the reduced left ventricular afterload.

Moreover, through the use of the developed pilot computational model it will be possible to analyse specifically the changes in hemodynamic induced by variation in specific parameters on the balloon geometry in case of horizontal or semi-recumbent position, to optimize the potential benefit of counterpulsation therapy during its practice in ICUs. An important feature of the computational model consists in the possibility of varying impedances in different compartments on the systemic circulation, for instance simulating conditions of vessel disease (g.e. arteriosclerosis or atherosclerosis) or characterizing the model to meet patient-specific characteristics.

9.2 Future works

Several paths can be followed to extend experimental conclusions to the clinical environment:

- Differently designed balloons should be tested, with the standard cylindrical one, in a system resembling the physiological one, constituted by a mock tapered thoracic aorta and main arterial branches. This would enable the analysis of the benefits of each IAB in a physiological environment;
- Comparison between the different manufacturers of IABPs on the market focused on the balloons, by using one singular pump on a fixed mode and different IABs. This study could address the differences between balloons in terms of material and shape of inflated balloon and internal catheter;
- An experimental model of the coronary perfusion can be added to the mock physiological aorta with branches, including a representation of coronary flow during systole and diastole. This can then be tested together with IABP in order to investigate the device benefits directly on coronary flow;
- Visualization study on tapered balloons, investigating, through IAB wall tracking, the mechanics of inflation and deflation of the differently designed balloons;

Also the computational work presents possibilities for further development and studies:

- Cycle to cycle variability of results should be investigated for a higher number of cycles, and on variables other than pressure alone: shear rate variations between each cycle would more accurately address the reproducibility of the model;
- The data obtained with the above cited visualization study on tapered balloons can be used for investigating the IABs performance in the computational model. Furthermore, it would be possible to study other amended designs of the balloon and optimize the IAB shape in order to maximize volume displaced towards coronary circulation and minimize end diastolic pressure.

References

1. Bundkirchen A, Schwinger RHG. Epidemiology and economic burden of chronic heart failure. *European Heart Journal, Supplement*. 2004;6(D):D57-D60.

2. Tortora GJ, Grabowski SR, eds. *Principles of anatomy and physiology*. Seventh Edition ed. New York, NY 10022: Harper Collins College publishers; 1993. Farrell T. R., ed.

3. Martini FH, ed. *Fundamentals of anatomy and physiology*. Fifth ed. New Jersey: Prentice Hall; 2001.

4. GREGG DE. Physiology of the coronary circulation. *Ann N Y Acad Sci*. 1960;90:145-155.

5. USA National Health and Nutrition. Examination survey. .

6. De Souza CF, De Souza Brito F, De Lima VC, De Camargo Carvalho AC. Percutaneous mechanical assistance for the failing heart. *J Interv Cardiol*. 2010;23(2):195-202.

7. Ueno A, Tomizawa Y. Cardiac rehabilitation and artificial heart devices. *Journal of Artificial Organs*. 2009;12(2):90-97.

8. Lee MS, Makkar RR. Percutaneous left ventricular support devices. *Cardiol Clin*. 2006;24(2):265-275.

9. Papaioannou TG, Stefanadis C. Basic principles of the intraaortic balloon pump and mechanisms affecting its performance. *ASAIO Journal*. 2005;51(3):296-300.

10. Swalen MJP, Konig CS, Sayma AI, Khir AW. Blade design and modelling of bi-directional axial flow pump: The basis of a novel left ventricular assist device.

11. Lemos PA, Cummins P, Lee C-, et al. Usefulness of percutaneous left ventricular assistance to support high-risk percutaneous coronary interventions. *Am J Cardiol*. 2003;91(4):479-481.

12. Gaitan BD, Thunberg CA, Stansbury LG, et al. Development, current status, and anesthetic management of the implanted artificial heart. *J Cardiothorac Vasc Anesth*. 2011;25(6):1179-1192.

13. Gray Jr. NA, Selzman CH. Current status of the total artificial heart. *Am Heart J*. 2006;152(1):4-10.

14. Copeland JG, Arabia FA, Tsau PH, et al. Total artificial hearts: Bridge to transplantation. *Cardiol Clin*. 2003;21(1):101-113.

15. Ng R, Yeghiazarians Y. Post myocardial infarction cardiogenic shock: A review of current therapies. *J Intensive Care Med*. 2013;28(3):151-165.

16. Dowling RD, Gray Jr. LA, Etoch SW, et al. The AbioCor implantable replacement heart. *Ann Thorac Surg*. 2003;75(6 SUPPL.):S93-S99.

17. Kantrowitz A, Tjonneland S, Freed PS, Phillips SJ, Butner AN, Sherman Jr. JL. Initial clinical experience with intraaortic balloon pumping in cardiogenic shock. *J Am Med Assoc*. 1968;203(2):113-118.

18. Moulopoulos SD, Topaz S, Kolff WJ. Diastolic balloon pumping (with carbon dioxide) in the aorta-A mechanical assistance to the failing circulation. *Am Heart J*. 1962;63(5):669-675.

19. Bregman D. A new percutaneous intra-aortic balloon. *Trans Am Soc Artif Intern Organs*. 1980;26:8-11.

20. Stavarski DH. Complications of intra-aortic balloon pumping. preventable or not preventable? *Crit Care Nurs Clin North Am*. 1996;8(4):409-421.

21. Ohman EM, George BS, White CJ, et al. Use of aortic counterpulsation to improve sustained coronary artery patency during acute myocardial infarction: Results of a randomized trial. *Circulation*. 1994;90(2):792-799.

22. Ishihara M, Sato H, Tateishi H, et al. Intraaortic balloon pumping as adjunctive therapy to rescue coronary angioplasty after failed thrombolysis in anterior wall acute myocardial infarction. *Am J Cardiol*. 1995;76(1):73-75.

23. Kaul U, Sahay DMS, Bahl VK, Sharma DMS, Wasir HS, Venugopal P. Coronary angioplasty in high risk patients: Comparison of elective intraaortic balloon pump and percutaneous cardiopulmonary bypass support-A randomized study. *J Interv Cardiol*. 1995;8(2):199-205.

24. Armstrong B, Zidar JP, Ohman EM. The use of intraaortic balloon counterpulsation in acute myocardial infarction and high risk coronary angioplasty. *J Interv Cardiol*. 1995;8(2):185-191.

25. Perler BA, McCabe CJ, Abbott WM, Buckley MJ. Vascular complications of intra-aortic balloon counterpulsation. *Archives of Surgery*. 1983;118(8):957-962.

26. Bauriedel G, Schwaiblmair M, Kreuzer E, Werdan K. Percutaneous intraaortic counterpulsation as a therapeutic option in cardiogenic shock. *Dtsch Med Wochenschr*. 1995;120(23):834-838.

27. Makhoul RG, Cole CW, McCann RL. Vascular complications of the intra-aortic balloon pump: An analysis of 436 patients. *Am Surg*. 1993;59(9):564-568.

28. Trost JC, Hillis LD. Intra-aortic balloon counterpulsation. *Am J Cardiol*. 2006;97(9):1391-1398.

29. Windecker S. Percutaneous left ventricular assist devices for treatment of patients with cardiogenic shock. *Curr Opin Crit Care*. 2007;13(5):521-527.

30. Tatar H, Cicek S, Demirkilic U, et al. Vascular complications of intraaortic balloon pumping: Unsheathed versus sheathed insertion. *Ann Thorac Surg*. 1993;55(6):1518-1521.

31. Weil KM. On guard for intra-aortic balloon pump problems. *Nursing*. 2007;37(7):28.

32. Santa-Cruz RA, Cohen MG, Ohman EM. Aortic counterpulsation: A review of the hemodynamic effects and indications for use. *Catheterization and Cardiovascular Interventions*. 2006;67(1):68-77.

33. Quaal SJ, ed. *Comprehensive intraaortic balloon counterpulsation.* Missouri: Mosby; 1993. Furgason C., ed.

34. Ducas J, Grech ED. ABC of interventional cardiology: Percutaneous coronary intervention: Cardiogenic shock. *Br Med J*. 2003;326(7404):1450-1452.

35. Plummer PM. Biomedical engineering fundamentals of the intra-aortic balloon pump. *Biomedical Instrumentation and Technology*. 1989;23(6):452-459.

36. Barnea O, Smith BT, Dubin S, Moore TW, Jaron D. Optimal controller for intraaortic balloon pumping. *IEEE Transactions on Biomedical Engineering*. 1992;39(6):629-634.

37. Khir AW. The balancing act of timing the intra-aortic balloon pump. *Artif Organs*. 2013;37(10):848-850.

38. Schreuder JJ, Maisano F, Donelli A, et al. Beat-to-beat effects of intraaortic balloon pump timing on left ventricular performance in patients with low ejection fraction. *Ann Thorac Surg*. 2005;79(3):872-880.

39. Skinner D. A single unit with multiple modes of support for the patient in cardiogenic shock. *Texas Heart Institute Journal*. May 1972.

40. Brown BG, Gundel WD, McGinnis GE, Selinger SL, Topaz SR, Gott VL. Improved intraaortic balloon diastolic augmentation with a double-balloon catheter in the ascending and the descending thoracic aorta. *Ann Thorac Surg*. 1968;6(2):127-136.

41. Brown BG, Goldfarb D, Topaz SR, Gott VL. Diastolic augmentation by intra-aortic balloon. circulatory hemodynamics and treatment of severe, acute left ventricular failure in dogs. *J Thorac Cardiovasc Surg*. 1967;53(6):789-804.

42. JONES RT. FLUID DYNAMICS OF HEART ASSIST DEVICES. . 1970.

43. Buckley MJ, Laird JD, Madras PN, Jones RT, Kantrowitz AR, Austen WG. Left heart assist system: Intra-aortic balloom pump. *Surg Clin North Am*. 1969;49(3):505-511.

44. Bregman D, Kripke DC, Goetz RH. The effect of synchronous unidirectional intra-aortic balloon pumping on hemodynamics and coronary blood flow in cardiogenic shock. *Trans Am Soc Artif Intern Organs*. 1970;16:439-446.

45. Bregman D, Goetz RH. Clinical experience with a new cardiac assist device. the dual-chambered intra-aortic balloon assist. *J Thorac Cardiovasc Surg*. 1971;62(4):577-591.

46. Bai J, Lin H, Yang Z, Zhou X. A study of optimal configuration and control of a multi-chamber balloon for intraaortic balloon pumping. *Ann Biomed Eng*. 1994;22(5):524-531.

47. Anstadt GL, Schiff P. Umbrella balloon for maximum unloading during intra-aortic balloon pumping. *Trans Am Soc Artif Intern Organs*. 1981;27:461-466.

48. Nanas JN, Nanas SN, Charitos CE, et al. Hemodynamic effects of a counterpulsation device implanted on the ascending aorta in severe cardiogenic shock. *ASAIO Transactions*. 1988;34(3):229-233.

49. Lazar HL, Matsuura H, Rivers S, Shemin RJ. Reduction of myocardial necrosis by positioning the intra-aortic balloon pump in the ascending aorta. *Cardiovascular Surgery*. 1994;2(5):634-638.

50. Gitter R, Cate CM, Smart K, Jett GK. Influence of ascending versus descending balloon counterpulsation on bypass graft blood flow. *Ann Thorac Surg*. 1998;65(2):365-370.

51. Meyns BP, Nishimura Y, Jashari R, Racz R, Leunens VH, Flameng WJ. Ascending versus descending aortic balloon pumping: Organ and myocardial perfusion during ischemia. *Ann Thorac Surg*. 2000;70(4):1264-1269.

52. Bian X, Downey HF. Enhanced intra-aortic balloon pump: Markedly improved systemic hemodynamics and cardiac function in canines with severe, acute left ventricular failure. *Artif Organs*. 2002;26(8):727-733.

53. Thiele H, Sick P, Boudriot E, et al. Randomized comparison of intra-aortic balloon support with a percutaneous left ventricular assist device in patients with revascularized acute myocardial infarction complicated by cardiogenic shock. *Eur Heart J*. 2005;26(13):1276-1283.

54. Williams SG, Cooke GA, Wright DJ, et al. Peak exercise cardiac power output: A direct indicator of cardiac function strongly predictive of prognosis in chronic heart failure. *Eur Heart J*. 2001;22(16):1496-1503.

55. Burkhoff D, Cohen H, Brunckhorst C, O'Neill WW. A randomized multicenter clinical study to evaluate the safety and efficacy of the TandemHeart percutaneous ventricular assist device versus conventional therapy with intraaortic balloon pumping for treatment of cardiogenic shock. *Am Heart J*. 2006;152(3):469.e1-469.e8.

56. Seyfarth M, Sibbing D, Bauer I, et al. A randomized clinical trial to evaluate the safety and efficacy of a percutaneous left ventricular assist device versus intra-aortic balloon pumping for treatment of cardiogenic shock caused by myocardial infarction. *J Am Coll Cardiol*. 2008;52(19):1584-1588.

57. O'Neill WW, Kleiman NS, Moses J, et al. A prospective, randomized clinical trial of hemodynamic support with impella 2.5 versus intra-aortic balloon pump in patients undergoing high-risk percutaneous coronary intervention: The PROTECT II study. *Circulation*. 2012;126(14):1717-1727.

58. Kollef MH. Prevention of hospital-associated pneumonia and ventilator-associated pneumonia. *Crit Care Med*. 2004;32(6):1396-1405.

59. Lorente L, Blot S, Rello J. Evidence on measures for the prevention of ventilator-associated pneumonia. *European Respiratory Journal*. 2007;30(6):1193-1207.

60. Nichols A.B., Pohost G.M., Gold H.K., Leinbach R.C., Beller G.A., McKusick K.A., Strauss H.W., Buckley M.J.. Left ventricular function during intra-aortic balloon pumping assessed by multigated cardiac blood pool imaging. *Circulation.* September 1978;58(3 Pt 2): I176-I183.

61. Kolyva C, Pantalos GM, Pepper JR, Khir AW. How much of the intraaortic balloon volume is displaced toward the coronary circulation? *J Thorac Cardiovasc Surg*. 2010;140(1):110-116.

62. Biglino G, Kolyva C, Whitehorne M, Pepper JR, Khir AW. Variations in aortic pressure affect the mechanics of the intra-aortic balloon: An in vitro investigation. *Artif Organs*. 2010;34(7):546-553.

63. Khir AW, Price S, Hale C, Young DA, Parker KH, Pepper JR. Intra-aortic balloon pumping: Does posture matter? *Artif Organs*. 2005;29(1):36-40.

64. Natan TE, Hung T-, Borovetz HS. Three-dimensional blood flows associated with intra-aortic balloon counterpulsation. *Mechanics Computing in 1990's and Beyond*. 1991:539-543.

65. Bleifeld W, Meyer-Hartwig K, Irnich W, Bussmann WD, Meyer J. Dynamics of balloons in intraaortic counterpulsation. *Am J Roentgenol Radium Ther Nucl Med*. 1972;116(1):155-164.

66. Biglino G, Whitehorne M, Pepper JR, Khir AW. Pressure and flow-volume distribution associated with intra-aortic balloon inflation: An in vitro study. *Artif Organs*. 2008;32(1):19-27.

67. Khir AW. What is it with patient's posture during intra aortic balloon pump therapy? *Artif Organs*. 2010;34(12):1077-1081.

68. Khir AW, Bruti G. Intra-aortic balloon shape change: Effects on volume displacement during inflation and deflation. *Artif Organs*. 2013.

69. Cheung AT, Savino JS, Weiss SJ. Beat-to-beat augmentation of left ventricular function by intraaortic counterpulsation. *Anesthesiology*. 1996;84(3):545-554.

70. Westerhof N, Bosman F, De Vries CJ, Noordergraaf A. Analog studies of the human systemic arterial tree. *J Biomech*. 1969;2(2):121-143.

71. Biglino G. *Experimental study of the mechanics of the intra-aortic balloon.* [Doctor of Philosophy]. Brunel Institute for Bioengineering, Brunel University; 2009.

72. Cohen M, Fasseas P, Singh VP, McBride R, Orford JL, Kussmaul III WG. Impact of intra-aortic balloon counterpulsation with different balloon volumes on cardiac performance in humans. *Catheter Cardiovasc Interventions*. 2002;57(2):199-204.

73. Nishida H, Koyanagi H, Abe T, et al. Comparative study of five types of IABP balloons in terms of incidence of balloon rupture and other complications: A multi-institutional study. *Artif Organs*. 1994;18(10):746-751.

74. Li TST, Joynt GM, So HY, Gomersall CD, Yap FHY. Semi-recumbent position in ICU. *Critical Care and Shock*. 2008;11(2):61-66.

75. Thomas PJ, Paratz JD, Stanton WR, Deans R, Lipman J. Positioning practices for ventilated intensive care patients: Current practice, indications and contraindications. *Australian Critical Care*. 2006;19(4):122-132.

76. Bird RB, ed. *Transport phenomena.* 2nd ed. Wiley; 2001.

77. Charitos CE, Nanas JN, Kontoyiannis DA, et al. The efficacy of the high volume counterpulsation technique at very low levels of aortic pressure. *J Cardiovasc Surg*. 1998;39(5):625-632.

78. Moulopoulos SD. The limits of counterpulsation. *Int J Artif Organs*. 1993;16(12):803-805.

79. Zelano JA, Li JK, Welkowitz W. A closed-loop control scheme for intraaortic balloon pumping. *IEEE Transactions on Biomedical Engineering*. 1990;37(2):182.

80. Hanlon-Pena PM, Quaal SJ. Intra-aortic balloon pump timing: Review of evidence supporting current practice. *American Journal of Critical Care*. 2011;20(4):323-334.

81. Schreuder JJ, Maisano F, Donelli A, et al. Beat-to-beat effects of intraaortic balloon pump timing on left ventricular performance in patients with low ejection fraction. *Ann Thorac Surg*. 2005;79(3):872-880.

82. Reesink KD, Van Der Nagel T, Bovelander J, Jansen JRC, Van Der Veen FH, Schreuder JJ. Feasibility study of a fiber-optic system for invasive blood pressure measurements. *Catheterization and Cardiovascular Interventions*. 2002;57(2):272-276.

83. Bakker EWM, Visser K, Van Der Wal A, Kuiper MA, Koopmans M, Breedveld R. Inflation and deflation timing of the AutoCAT 2 WAVE intra-aortic balloon pump using the autoPilot mode in a clinical setting. *Perfusion (United Kingdom)*. 2012;27(5):393-398.

84. Schreuder JJ, Castiglioni A, Donelli A, et al. Automatic intraaortic balloon pump timing using an intrabeat dicrotic notch prediction algorithm. *Ann Thorac Surg*. 2005;79(3):1017-1022.

85. Wesseling KH, Jansen JRC, Settels JJ, Schreuder JJ. Computation of aortic flow from pressure in humans using a nonlinear, three-element model. *J Appl Physiol*. 1993;74(5):2566-2573.

86. Donelli A, Jansen JRC, Hoeksel B, et al. Performance of a real-time dicrotic notch detection and prediction algorithm in arrhythmic human aortic pressure signals. *J Clin Monit Comput*. 2002;17(3-4):181-185.

87. Pantalos GM, LuAnn Minich L, Tani LY, McGouch EC, Hawkins JA. Estimation of timing errors for the intraaortic balloon pump use in pediatric patients. *ASAIO Journal*. 1999;45(3):166-171.

88. Pantalos GM, Koenig SC, Gillars KJ, Haugh GS, Dowling RD, Gray Jr. LA. Intraaortic balloon pump timing discrepancies in adult patients. *Artif Organs*. 2011;35(9):857-866.

89. Kresh JY, Kerkhof PL, Goldman SM, Brockman SK. Heart-mechanical assist device interaction. *ASAIO Trans*. 1986;32(1):437-443.

90. Kantrowitz A, Freed PS, Cardona RR, et al. Initial clinical trial of a closed loop, fully automatic intra-aortic balloon pump. *ASAIO Journal*. 1992;38(3):M617-M621.

91. Schreuder JJ, Castiglioni A, Donelli A, et al. Automatic intraaortic balloon pump timing using an intrabeat dicrotic notch prediction algorithm. *Ann Thorac Surg*. 2005;79(3):1017-1022.

92. Weber KT, Janicki JS, Walker AA. Intra-aortic balloon pumping: An analysis of several variables affecting balloon performance. *Trans Am Soc Artif Intern Organs*. 1972;18(0):486-492.

93. Barnea O, Moore TW, Dubin SE, Jaron D. Cardiac energy considerations during intraaortic balloon pumping. *IEEE Transactions on Biomedical Engineering*. 1990;37(2):170.

94. Zehetgruber M, Mundigler G, Christ G, et al. Relation of hemodynamic variables to augmentation of left anterior descending coronary flow by intraaortic balloon pulsation in coronary artery disease. *Am J Cardiol*. 1997;80(7):951-954.

95. Kern MJ, Aguirre FV, Caracciolo EA, et al. Hemodynamic effects of new intra-aortic balloon counterpulsation timing methods in patients: A multicenter evaluation. *Am Heart J*. 1999;137(6):1129-1136.

96. Croston RC, Fitzjerrell DG. CARDIOVASCULAR MODEL FOR THE SIMULATION OF EXERCISE, LOWER BODY NEGATIVE PRESSURE, AND TILT EXPERIMENTS. . 1974:471-476.

97. Shi Y, Lawford PV, Hose DR. Numerical modeling of hemodynamics with pulsatile impeller pump support. *Ann Biomed Eng*. 2010;38(8):2621-2634.

98. Pennati G, Bellotti M, Fumero R. Mathematical modelling of the human foetal cardiovascular system based on doppler ultrasound data. *Medical Engineering and Physics*. 1997;19(4):327-335.

99. Burattini R, Natalucci S. Complex and frequency-dependent compliance of viscoelastic windkessel resolves contradictions in elastic windkessels. *Medical Engineering and Physics*. 1998;20(7):502-514.

100. Stergiopulos N, Young DF, Rogge TR. Computer simulation of arterial flow with applications to arterial and aortic stenoses. *J Biomech*. 1992;25(12):1477-1488.

101. Stergiopulos N, Young DF, Rogge TR. Numerical study of pressure and flow propagation in arteries. *Biomed Sci Instrum*. 1991;27:93-104.

102. Abdolrazaghi M, Navidbakhsh M, Hassani K. Mathematical modelling of intra-aortic balloon pump. *Comput Methods Biomech Biomed Engin*. 2010;13(5):567-576.

103. Hung T-. Forcing functions in navier-stockes equations. *Journal of the Engineering Mechanics Division, ASCE*. 1981;107(EM3, Proc. Paper, 16344):643-648.

104. Ferrari G, Khir AW, Fresiello L, di Molfetta A, Kozarski M. Hybrid model analysis of intra-aortic balloon pump performance as a function of ventricular and circulatory parameters. *Artif Organs*. 2011;35(9):902-911.

105. Nerem RM, Seed WA, Wood NB. An experimental study of the velocity distribution and transition to turbulence in the aorta. *Journal of Fluid Mech*. 1972;52(1): 137-160.

106. Yellin EL. Laminar-turbulent transition process in pulsatile flow. *Circulation Res*. 1966;19:791-804.

107. Pennati G, Corsini C, Cosentino D, Hsia T-Y, Luisi VS, Dubini G, Migliavacca F. Boundary conditions of patient specific fluid dynamics modelling of cavopulmonary connections: possible adaptation of pulmonary resistances results in a critical issue for a virtual surgical planning. Interface Focus. 2011;1:297-307.

108. Olufsen MS, Nadim A. On deriving lumped models for blood flow and pressure in the systemic arteries. *Math Biosci Eng*. 2004;1(1):61-80.

109. Avolio AP. Multi-branched model of the human arterial system. *Medical and Biological Engineering and Computing*. 1980;18(6):709-718.

110. Mills CJ, Gabe IT, Gault JH, et al. Pressure-flow relationships and vascular impedance in man. *Cardiovasc Res*. 1970;4(4):405-417.

111. McDonald DA. Blood flow in arteries. *EDWARD ARNOLD PUBL*. 1974;?12.-.

112. Cutnell, John & Johnson, Kenneth, ed. *Physics.* 4th ed. Wiley; 1998.

113. Dubini G. Notes of biofluid dynamics. . 2009.

114. Quaal SJ, ed. *Comprehensive intraaortic balloon counterpulsation.* Second Edition ed. USA: Alison Miller; 1993. Furgason C., ed.

115. Papaioannou TG, Mathioulakis DS, Nanas JN, Tsangaris SG, Stamatelopoulos SF, Moulopoulos SD. Arterial compliance is a main variable determining the effectiveness of intra-aortic balloon counterpulsation: Quantitative data from an in vitro study. *Med Eng Phys*. 2002;24(4):279-284.

116. Kolyva C, Biglino G, Pepper JR, Khir AW. A mock circulatory system with physiological distribution of terminal resistance and compliance: Application for testing the intra-aortic balloon pump. *Artif Organs*. 2010:no-no.

117. Cheung Y-, Cheng C-, Chao C, et al. Microfluid as a mean for piezoresistive strain measurement-A mixture of glycerin with salt water. *3rd IEEE International Conference on Nano/Micro Engineered and Molecular Systems, NEMS*. 2008:480-484.

118. Neidlin M., Stenseifer U., Kaufmann T.A.S.. A multiscale 0-D/3-D approach to patient-specific adaptation of a cerebral auto-regulation model for computational fluid dynamics studies of cardiopulmonary bypass. *Journal of Biomechanics*. 2014;47:1777-1783.

119. Sagawa K.., Maughan L., Suga H., Sunagawa K… Cardiac contraction and the pressure-volume relationship. *Oxford University Press edition*. 1988.

120. Kirkman E.. Mechanical events and the pressure-volume relationships. *Anaesthesia and intensive care medicine*. August 2009;10(8):373-376.

121. Schreuder J.J., Maisano F., Donelli A., Jansen J.R., Hanlon P., Bovelander J., Alfieri O.. Beat-to-beat effects of intraaortic balloon pump timing on left ventricular performance in patients with low ejection fraction. *Annuals of thoracic surgery*. March 2005;79(3):872-880.

122. Dunkman W.B., Leinbach R.C., Buckley M.J., Mundth E.D., Kantrowitz A.R., Austen W.G., Sanders C.A.. Clinical and hemodynamic results of intraaortic balloon pumping and surgery for cardiogenic shock. *Circulation*. September 1972;46(3):465-477.